Role of the prefrontal-brainstem pathway in mediating avoidance behavior

Suzana Khoder

Ecole doctorale des sciences
de la vie et de la santé

Thèse présentée par :

SUZANA KHODER

Soutenue le:

30 Novembre 2018

Afin d'obtenir le grade de :

DOCTEUR EN NEUROSCIENCES

Rôle de la projection cortex préfrontal-tronc cérébral dans les réponses d'évitement de peur

Role of the prefrontal-brainstem pathway in mediating avoidance behavior

Membres du jury :

Pr. Andreas Lüthi	FMI-Basel	Président
Pr. Nadine Gogolla	MPIN-Munich	Rapporteur
Pr. Philip Tovote	ICN-Würzburg	Rapporteur
Dr. Yann Humeau	CNRS-Bordeaux	Examinateur
Dr. François Georges	CNRS-Bordeaux	Examinateur
Dr. Cyril Herry	INSERM-Bordeaux	Directeur de thèse

ACKNOWLEDGMENTS

Firstly, I would like to address my sincere and enormous gratitude to the director of my thesis *Cyril Herry*. *Cyril* I would like first to thank you for believing in me and giving me the opportunity to work on this challenging project during my PhD. Also I would like to thank you for the person you are, your patience, your support, your trust, your kindness and your modesty. You helped me in acquiring a knowledge of the state of the art in neurosciences starting from my internships during my masters and all along my PhD years. Also, thank you for your patience in reviewing and correcting the several versions of this manuscript. You are a person I admire a lot and will never be thankful enough for all the opportunities you gave to me.

Besides my thesis director, I address my big gratitude to all my thesis committee members. Professor *Andreas Lüthi*, thank you for accepting to be the director of this jury. You are one of the pillars in neurosciences, thank you for accomplishing so elegant studies that helped us to understand more what our amygdala can possibly do during fear. Many of your recent and less recent works gave me the base to elaborate my PhD project.

Thank you Dr. *Nadine Gogolla* and Dr. *Philip Tovote* for accepting to be the reporters of this work. Thank you for taking the time to read my thesis and evaluate it and also thank you for all your comments/ suggestions.

Thank you to Dr. *Yann Humeau* and Dr. *François Georges* for examining this work. Thank you for each one of you for accepting to be part of this jury, for examining my work and for all your comments/ suggestions on my project during our lab meetings.

I would also like to address my gratitude to all the “François Magendie Institute” members starting from the director of the institute *Stéphane Oliet* and including all people who contributed directly or indirectly to this work.

I would also like to particularly address a thank you to *Juliette Viellard* who spent a year and a half working side by side with me on this project. Thank you for sharing this fantastic ‘’FZAA’’ experience, I hope that you enjoyed co-working with me as much as I did with you. One of the keys, I feel, to our successful lab-partnership is the fact that we were complementary. Indeed, I would like to thank you for your calmness, your positive attitude and your constant smile which made co-working with you a pure pleasure and helped in successfully advancing this project.

I would also like to address my gratitude to *Yann Humeau* and *Harang Kim* for accepting to perform *in-vitro* patch-clamp recordings on mice, me and *Juliette*

injected for them. Collaborating with you was a pleasure, thank you for your exceptional expertise in this field which was of a big importance to complement our *in-vivo* electrophysiological data. *Yann* thank you for your patience, your expertise and your pedagogy in transmitting and explaining a small part of your big expertise in *in-vitro* electrophysiology. I enjoyed discussing and working with you.

Thank you very much, to *Robert Rozeske*, who had a big contribution to my formation in optogenetics and electrophysiological recordings. Thank you for your guidance, your mentorship, your organizational skills and encouragements which allowed me to learn, during my masters' internships, the techniques and tools I afterwards used all along my thesis. Thank you Rob, for sharing your knowledge.

Thank you to all the actual and former members of the *Herry*'s lab and particularly I would like to thank people I directly interacted with namely *Hélène Wurtz, Fabrice Chaudun, Nikolas Karalis, Julien Courtin, Delphine Girard, Maiena Aincy, Harang Kim, Stéphane Valerio, Cyril Dejean* and many others. Thank you for the discussions, the help, and the fun moments I shared with each one of you.

Also, thank you to all the friends *Maria*, *Farah*, *Hasan*, *Jamil*, *Ali*, *Samar* and *Dayana* who supported me and with whom I spent unforgettable moments during those 4 years of thesis.

I also need to express my enormous gratitude to *de Chassey* family who welcomed me in their home for many years since my arrival to France. Thank you for sharing with me the French culture, for your constant help and guidance in daily life issues and for being my French adoptive family. I will never forget all you did for me.

In this last part, I would like to address my gratitude to several people who mean the world to me. First, I would like to address a big thank you to my sister who will also defend her thesis in a couple of days. *Natalia* thank you for your constant encouragements, for being there when I most needed and for always being you. For me (and many others I am sure) you are and always will be perfect. I am sure your defense will be at the same perfection level as all the efforts and sacrifices you did during the whole thesis and especially the last month.

I would also like to address my sincere gratitude to a person who physically was there for me all the time. Rami, thank you for sticking there during my rainy and stormy days, thank you for all the help (especially in coding and trying to understand Matlab!), love and patience you offered to me. You were one of the main reasons of my positive attitude that propelled me in advancing in this thesis.

Finally, I would like to address my enormous gratitude to the people that count for me the most, my beloved parents. You were the shoulder that supported, encouraged and cheered me up all along this experience, on a daily basis despite your preoccupations and the miles between us. Thank you for always being there and caring for me despite my moody temperament. I love you and hope that I made you proud with the thesis I dedicate for you and for all the people that worked on it, discussed it and contributed in its' progression.

I can't forget to address this thesis also to a star shining bright up in the sky, I will never forget all the things you transmitted to me and all the moments we shared. I hope that today you are proud of me. Odpoczywaj w pokoju babuniu, kocham cie na zawsze.

ABSTRACT

Mammals, including rodents, show a broad range of defensive behaviors as a mean of coping with threatful stimuli including freezing and avoidance behaviors. Several studies emphasized the role of the dorsal medial prefrontal cortex (dmPFC) in encoding the acquisition as well as the expression of freezing behavior. However the role of this structure in processing avoidance behavior and the contribution of distinct prefrontal circuits to both freezing and avoidance responses are largely unknown. To further investigate the role of dmPFC circuits in encoding passive and active fear-coping strategies, we developed in the laboratory a novel behavioral paradigm in which a mouse has the possibility to either passively freeze to an aversive stimulus or to actively avoid it as a function of contextual contingencies. Using this behavioral paradigm we investigated whether the same circuits mediate freezing and avoidance behaviors or if distinct neuronal circuits are involved. To address this question, we used a combination of behavioral, neuronal tracing, immunochemistry, single-unit, patch-clamp recordings and optogenetic approaches. Our results indicate that (i) dmPFC and dorsolateral and lateral periaqueductal grey (dl/lPAG) sub-regions are activated during avoidance behavior, (ii) a subpopulation of dmPFC neurons encode avoidance but not freezing behavior, (iii) this neuronal population project to the dl/lPAG, (iv) the optogenetic activation or inhibition of this pathway promoted and blocked the acquisition of conditioned avoidance and (v) avoidance learning was associated with the development of plasticity at dmPFC to dl/lPAG synapses. Together, these data demonstrate for the first time that activity-dependent plasticity in a subpopulation of dmPFC cells projecting to the dl/lPAG pathway controls avoidance learning.

Résumé

Les mammifères, comme par exemple les rongeurs, soumis à des expériences aversives présentent des réponses comportementales de peur caractéristiques notamment une réponse d'immobilisation (freezing) ou d'évitement. Alors que le rôle du cortex préfrontal dorso-médian (CPFdm) dans l'acquisition ainsi que l'expression du freezing a déjà été expérimentalement établi, son implication dans l'encodage des réponses d'évitement de peur ainsi que l'interaction entre les circuits neuronaux préfrontaux impliqués dans le freezing et/ou l'évitement restent mal compris. Afin de répondre à ces questions, nous avons développé au laboratoire un paradigme expérimental permettant à une souris d'acquérir et d'exprimer le freezing ou l'évitement lors de la présentation d'un même stimulus aversif et ceci en fonction du contexte environnant. Ainsi, nous avons pu déterminer si les mêmes circuits neuronaux dans le cortex préfrontal dorso-médian encodent les deux réponses de peur, le freezing et l'évitement. Nous avons mis en œuvre au cours de ce travail des approches comportementales, de traçage neuroanatomique, d'immunohistochimie, d'enregistrements extracellulaires *in vivo* et intracellulaires *in vitro* ainsi que des approches optogénétiques. Nos résultats indiquent que (i) le CPFdm et les régions dorsales de la substance grise périaqueducale sont activés pendant le comportement d'évitement, (ii) une sous population de neurones du CPFdm encode le comportement d'évitement mais pas le freezing, (iii) cette population neuronale projette sur le dl/lPAG, (iv) l'activation et l'inhibition optogénétique de cette projection induit et bloque l'apprentissage de l'évitement, respectivement et (v) l'apprentissage de l'évitement est associé à la mise en place d'une plasticité des afférences préfrontales sur le dl/lPAG. Dans leur ensemble ces résultats démontrent pour la première fois que la plasticité dépendante de l'activité des neurones du CPFdm projetant sur le dl/lPAG contrôle l'apprentissage de l'évitement de peur.

Table of Contents

Abbreviations

5-HT: serotonin
AAV: adeno-associated virus
ACC: anterior cingulate cortex
Ach: acetylcholine
AHN: anterior hypothalamic nucleus
AP5 or APV: 2R-amino-5-phosphonovaleric acid
BA: basal nucleus of amygdala
BA: brodmann areas
BDNF: brain-derived neurotrophic factor
BLA: basolateral nucleus of amygdala
BM: basomedial nucleus of amygdala
BNST: basal nucleus of the stria terminalis
CB: calbindin
CCK: cholecystokinin
CeA: central nucleus of amygdala
CeL: centrolateral nucleus of amygdala
CeM: centromedial nucleus of amygdala
CGRP: calcitonin gene-related peptide
CNF: cuneiform nucleus
CR: calretinin
CRF: corticotropine release factor
CS: conditioned stimulus
dHPC: dorsal hippocampus
DL: dorsolateral
dlPAG: dorsolateral periaqueductal gray
dlPFC: dorsolateral
DLS: dorsolateral striatum
DM: dorsomedial
dmPAG: dorsomedial periaqueductal gray
dmPFC: dorsomedial prefrontal cortex
DMS: dorsomedial striatum
DREADD: designer receptors exclusively activated by designer drugs
DS: dorsal striatum
DSM-V: diagnostic and statistical manual of mental disorders 5th edition
e.g.: example
EAA: Excitatory Amino acids
EC: entorhinal cortex
FACS: facial action coding system
FS: fast-spiking
GABA: gamma aminobutyric acid
GAD: glutamic acid decarboxylase
hM4Di: Gi-coupled human M4 muscarinic DREADD receptor
IEG: immediate early genes
IL: infralimbic cortex
IN: interneuron
ITC: intercalated cells
L: lateral

LA: lateral nucleus of amygdala
LH: lateral hypothalamus
lPAG: lateral periaqueductal gray
LTM: long-term memory
LTP: long-term potentiation
MD: mediodorsal nucleus of the thalamus
MDTB: mouse defense test battery
mGluR: metabotropic glutamatergic receptors
mPFC: medial prefrontal cortex
MSN: medium spiny neurons
Nac: nucleus accumbens
NacC: nucleus accumbens core
NacS: nucleus accumbens shell
NADPH: nicotinamide adenine dinucleotide phosphate hydrogen
NO: nitric oxide
NPY: neuropeptide Y
NR: nucleus reuniens of the thalamus
NTS: nucleus of the solitary tract
OCD: obsessive compulsive disorder
OFC: orbital prefrontal cortex
PAG: Periaqueductal gray
PBN: parabrachial nucleus
PFC: prefrontal cortex
PKC-Δ: protein kinase delta
PL: prelimbic cortex
PN: pyramidal neurons
PrCm: medial precentral cortex
PTSD: post-traumatic stress disorder
PV: parvalbumin
RA: risk assessment
REM sleep: rapid eye movement sleep
RS: regular spiking
RVM: Rostral Ventromedial Medulla
SD: Sprague Dawley
SNc: substantia nigra pars compacta
SP: substance P
SSDR: species-specific defense reaction
STM: short-term memory
TNC: caudal trigeminal nucleus
TRP2: Tryptophane-Hydroxylase 2
TTX: tetrodoxin
UR: unconditioned response
US: unconditioned stimulus
VGCC: voltage-gated calcium channels
VGLUT: Glutamate
vHPC: ventral hippocampus
VIP: vasoactive intestinal peptide
VL: ventrolateral
VLM: ventrolateral medulla
vlPAG: ventrolateral periaqueductal gray

vlPFC: ventrolateral prefrontal cortex
VMH: ventromedial hypothalamic nucleus
vmPFC: ventromedial
vmPFC: ventromedial prefrontal cortex
VS: ventral striatum
VTA: ventral tegmental area
WHO: World Health Organization

I. Introduction

One of the most influent theories of experimental neurosciences in the 20th century was behaviorism. Behaviorists' main field of interest was to understand the behaviors of humans and animals (Watson, 1913; Skinner, 1938). Behaviorists' theory postulated that all our behaviors consist in specific responses to environmental stimuli without any contribution or influence of emotions. This idea was opposed by Darwin who first described emotions not only in humans but also in animals in line with his theory of evolution (Darwin, 1872). Darwin explored the expression of emotions in humans but also dogs, cats, birds and horses and reported that the expression of basic emotions is a process allowing a species survival. Darwin was criticised by scientists of his epoque because animals can not show how they feel, and he was accused of attributing human thoughts and feelings to animals (antropomorphism).

Today, it is well established that emotions shape our everyday life. They play an essential role in rational decision-making, perception, learning and a variety of other cognitive processes. Emotions are defined as being the conscious expression of the internal subjective state of an organism. The expression of emotions can be split into three components: physiological (hormones levels, blood pressure, heart rate), behavioral (immobilization, escape, crying, screaming, laughing) and psychological (feelings). All of these components can be quantified in humans. However, in animals, exploring the psychological component of emotions remain controversial since they can not express it verbally. Paul Ekman is one of the pioneers who identified 6 universal emotions in humans based on their internationally recognized facial expression: fear, disgust, surprise, happiness, sadness, anger (Ekman, et al., 1969). Ekman and Friensen used the Facial Action Coding System (FACS) (Ekman and Friensen, 1978) to taxonomize human facial expression. The FACS is a system developed by an anatomist (Hjorztsjö, 1969) allowing to recognize any human emotion based on their anatomical facial expressions.

Among all of the cited above emotions, fear is the main one promoting survival. Across evolution, people and animals who feared the right things survived and passed their genes. Fear is also one of the emotions presenting a clear physiological signature associated with a specific behavioral state of the body (Steenland and Zhuo, 2009; Karalis, et.al, 2016) which makes the fearful state easy to capture and to

quantify through behavioral and physiological studies. Fear is indeed one of our emotional repertoire defined as an unpleasant feeling linked to an anticipatory reaction to something that threaten one's security or safety. Fear should not be counfonded with anxiety which is also triggered in response to threat, but is a general state of distress, that is longer lasting than fear emotion and that is elicited by a subjective state and not a specific stimulus like in the case of fear (Lang, et al., 2000; Tovote, et al., 2016; Felix-Ortiz, et al., 2016). Neuroscientists have demonstrated that fear is an innate emotion, existing instinctively and demonstrated it through several experiments. Freedman (Freedman, 1964), argued that facial expressions of emotions such as smiling and laughing are innate because they are expressed at a very young age in children in a period that is too early for imitation or learning to have taken place. He also showed that deaf-blind children, who are not able to learn smiling and laughing through imitation of audible and visual stimuli (Freedman, 1964) can still express happiness emotion by smiling, supporting the innateness of emotions. Waller and colleagues (Waller, et al., 2008) added that even though facial musculature varies greatly in individuals, the same basic facial musculature recruited for the expression of emotions is conserved for all of the 6 basic emotions. Fear can also be mediated by learning processes widely studied in neurosciences using associative learning paradigms mainly classical Pavlovian conditioning paradigms. During Pavlovian classical conditioning, an organism learns to associate a previously neutral stimulus (conditioned stimulus, CS, typically a sound or light) with an aversive stimulus (unconditioned stimulus, US, typically a mild footshock). Following training, the organism presents a broad range of conditioned fear responses to the CS presented alone including freezing, an innate immobilization reaction, that has been one of the most studied behavioral expressions of fear in animals given the simplicity and the robustness of classical fear paradigms. Nevertheless, other conditioned fear responses are also expressed upon exposure to fearful stimuli, mainly fight and avoidance behaviors. During my thesis I was interested in investigating the neural underpinnings of avoidance behavior and the dynamical interaction of freezing and avoidance defensive behaviors in terms of neuronal brain circuits. In the first part of my thesis, I will introduce avoidance learning theories and the dynamical interaction between freezing and avoidance based on animal studies. I will also highlight some clinical studies adressing the pathological aspect of fear emotions in humans. Then I will review the gross anatomy and functions of brain structures known to be involved

in both avoidance and freezing behaviors and the ones reported to be controlling exclusively avoidance behavior. Finally, I will introduce the main questions, the hypothesis of my work and the techniques we used to adress it during my thesis.

II. Fear defensive strategies

Depending on the environment, animals present a repertoire of defensive behaviors related to their species-specific survival needs. Indeed, animals adopt defensive strategies to protect themselves and/or their conspecifics against environmental dangers. The most salient observable expression of a frightened animal is freezing defined as the cessation of all movements except the ones related to respiration and which usually occurs in a crouching posture next to the corners of an object or a chamber: the so called thigmotaxis (Telonis, 2015). Freezing should not be confounded with catatonia characterized by muscles' rigidity (Pot and Lejoyeux, 2015) because freezing behavior is associated with a state of high alertness with a considerable muscle tone. Freezing animals show also a potentiated startle response (Leaton, 1985). Freezing behavior is adopted as a defensive strategy when a route of escape is not offered to the animal. Nevertheless, when the danger is escapable more active defensive behaviors such as avoidance, escape and flight are adopted (Gabriel, et al., 1991; Ramirez, et al., 2015). An index of activation of those active and passive defensive responses is the various autonomic changes (heart rate, blood pressure,...) which enables the animal, by redirecting the blood flow to the muscles, to provide muscles with the energy and nutrients essential for the defensive action. Both passive (freezing) and active (avoidance, escape, flight) behaviors will be defined and the main theories about the acquisition and the expression of mainly active avoidance behavior will be presented and discussed in the following parts. See (Blanchard and Blanchard, 1969; Hofmann and Aleena, 2018) for a more detailed view of the dominant theories of passive fear reactions.

1) Avoidance: Definitions and characteristics of avoidance learning

Animals or humans exposed to a threat or an unpleasant stimulus develop predictable goal-directed behaviors, motivated by negative reinforcement meaning the removal of the aversive stimulus source of distress (see below the reinforcement

concepts developed in *theories of avoidance* section). There are two main categories of behaviors learned under negative reinforcement: escape behavior and avoidance behavior.

Escape behavior is a motor action performed by the animal to terminate an ongoing aversive stimulus. This behavior is negatively reinforced by the elimination of the unpleasant stimulus. For instance, a rat standing on a platform will jump into the water when the platform is electrified. Jumping to stop the shock is an escape behavior.

As for avoidance behavior, it is a motor action that would keep an individual from experiencing aversive events. Escape behavior is converted into avoidance behavior by giving a signal before the aversive stimulus starts. For example, if a tone is presented just before the platform is electrified for several trials, rats would learn to jump into the water during the signal (tone), avoiding by this action the shock delivery.

Avoidance learning is nowadays studied in species starting from invertebrates: crayfish (Nobuyuki, et al., 2004), earthworms (Wilson, et al., 2014) which turn off an aversive white light by increasing their movement (avoidance behavior) as compared to controls after only 12 pairings between the light and an aversive shock. Avoidance behavior can be also learned and quantified in vertebrates such as zebrafish (Xu, et al., 2007), rabbits (Grabiel, et al., 1991; Poremba and Grabiel, 1999), dogs (Wynne and Solomon, 1955; Solomon and Turner, 1962), rodents including rats, mice and hamsters (Babbini and Davis, 1967; Burton, 1973; Ramirez, et al., 2015; Bravo-Rivera, et al., 2015) and finally humans (Low, et al., 2015; Schlund, et al., 2015).

It is also important to note that some gender and animal's strain diffences have been reported as to avoidance behavior acquisition and expression. It has been shown mainly that female rats acquire avoidance behavior quicker and to a higher degree (Avcu, et al., 2014) as compared to male rats from the same strain (Sprague Dawley (SD)). Female also respond with a lower latency as compared to male rats.

Another characteristic of avoidance learning is that it is very resistant to extinction; a process through which a behavior that is no longer reinforced get weakened and disppears with time (Herry, et al., 2006; Jiao, et al., 2011; Bravo-Rivera, et al., 2014). Indeed, once avoidance behavior is acquired and stabilized, it is very hard to decrease it even though the aversive stimulus (for instance a shock) is no longer present. One technique used to promote avoidance extinction is flooding. One way of

administering flooding involves not allowing the animal to perform avoidance response to the conditioned cue, or allowing it to avoid the CS but not stopping it after avoidance is performed; the contingency between avoidance and CS removal is then broken and avoidance extinction process is accelerated.

Given that avoidance following extensive training is resistant to extinction, one should not confound goal-directed and habitual avoidance. Indeed, with significant training, avoidance behavior becomes habitual (Gillan, et al., 2014; Dickinson, 1980; Wood and Neal, 2007), allowing it to persist even if it becomes disconnected from it's reinforcing consequences. Habitual avoidance learning occurs when avoidance response switches from being conscious, goal-directed behavior to automated behavior (Thorn, et al., 2010), unconsciously triggered by the CS. To disentangle both goal-directed and habitual avoidance behaviors, devaluation experiments are performed given that habitual responses lack of sensitivity to devaluation (Dickinson, 1985; Gillan, et al., 2014).

While avoidance represents complexe motor actions learned by repetitive trials of conditioning paradigms, other motor actions representing innate bursts of motor activity to a present or imminent danger are studied and labelled flight behavior (Clarke, 1972). Ethobehavioral studies pointed out that under natural conditions (Blanchard, et al., 2003; Dielenberg, et al., 2001), for instance the exposure to a cat or to pyrazine analogues; a compound found in wolf urine (Osada, et al., 2013), a rodent presents unlearned fear responses namely flight behavior expressed starting from the first presentation of the predator or the predator odor. Choi and colleagues (Choi and Kim, 2010) studied defensive flight in mice when confronted with a predator-like moving object each time the animal emerges from it's nest foraging for food. One characteristic of flight behavior is that the initiation of the movement is very sensitive to the distance separating the animal from the potential threat. It has been for instant described that, in different species for instance birds and lezards, the initiation of flight behavior is affected by the distance between the predator and the prey; the closer they are the quicker flight is initiated (Cooper, 2005). Recently, a Pavlovian conditioning paradigm inducing flight behavior was developed by Fadok and colleagues (Fadok, et al., 2017) . They used a serial compound stimulus consisting of a pure tone followed by a white noise associated with a footshock. With conditioning, mice learned to freeze during the pure tone and to express flight behavior during the white noise. This paradigm is interesting because it allows the

study of the neural underpinnings underlying the switch between two behavioral defensive behaviors, freezing and flight.

2) Paradigms of avoidance learning

Given the complexity of avoidance behavior, it is studied nowadays using a multitude of paradigms depending on which characteristic of the behavior scientists want to adress. First, avoidance behavior is classically studied using avoidance conditioning through which an organism learns to avoid unpleasant or punishing stimuli (the unconditioned stimulus (US)) by the production of anticipatory responses. The US administered can be of different natures, the most commonly used ones are mild electrical shocks both in humans (Low, et al., 2015) and rodents (Bravo-Rivera, et al., 2015; LeDoux, et al., 2017). In avoidance conditioning paradigms using footshocks in rodents, it has been reported that the stronger the shock (high intensity) the quicker avoidance is acquired and stabilized (Kimmel, et al., 1969). Researchers also use less aversive US such as corneal air-puff resulting in eyeblink conditioning or eyelid response (Allen, et al., 2014). This kind of aversive conditioning is now widely used in virtual reality studies (Rajasethupathy, et al., 2015; Lin, et al., 2016), in which a mouse is placed on a spherical ball treadmill and performs behavioral tasks in a virtual space. In these studies, the shock can not be delivered through the spherical ball treadmill the mouse is moving one, therefore air-puff conditioning is used as a US.

Using avoidance conditioning different forms af avoidance behavior can be promoted. The most general distinction is made between passive and active avoidance. Passive avoidance also labelled inhibitory avoidance refers to abstaining from a particular response in order to not get an aversive stimulus (LeDoux, et al., 2017).

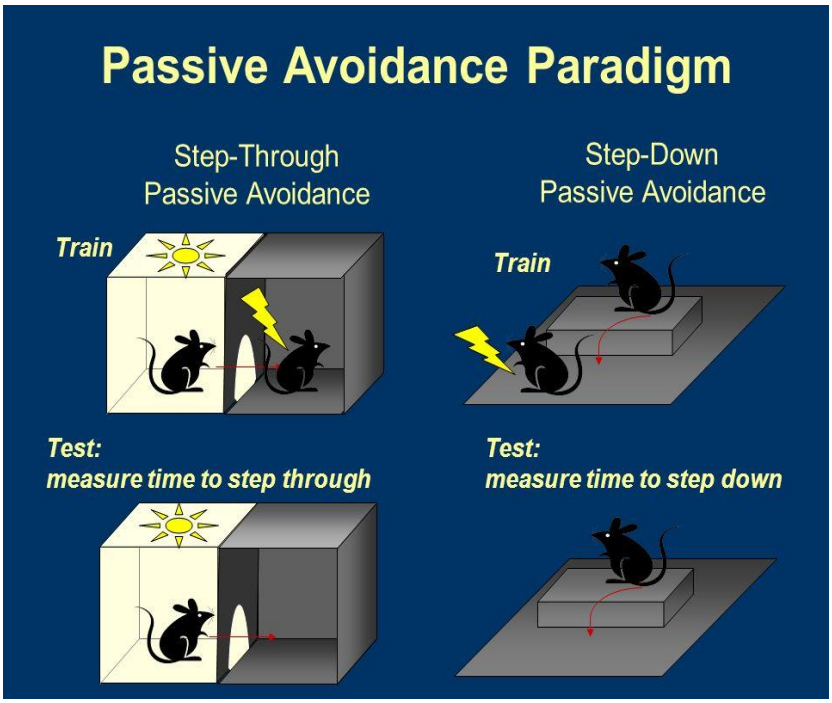

Figure 1. Passive avoidance paradigm

Left panel. In the step-through passive avoidance paradigms**,** during a training phase, the rodent learns to associate the light-compartment with no-shock and the dark-compartment with a shock presentation. During the test shock-free phase the time to step from the light to the dark compartment is measured. **Right panel.** In the step-down passive avoidance paradigms, the rodent during a training phase learns that stepping down from an elevated platform is associated with a shock presentation. At the test session, the time to step down from the platform is quantified.

Passive avoidance can be implemented by using a two-compartment behavior apparatus (Ambrogi Lorenzini, et al., 1999), one of which the rodents' prefer: a dark compartment **(Figure 1, left panel)**. The prefered compartment is associated with an inescapable footshock and the latency to enter the prefered compartment (dark) is measured. At the test session (no shock), rodents present high latency of entrance in the prefered compartment reflecting passive avoidance learning. Other paradigms to study passive avoidance have also been used consisting on withholding the behavior of stepping down from an elevated plateform, passively avoiding to get a footshock **(Figure 1, right panel)**. Passive avoidance studies are of a strong importance to investigate the neural circuits underlying the learning of ''what not to do''. Indeed, in some individuals passive avoidance can be maladaptive and results in avoiding taking decisions or postponing them motivated by the fear of the negative consequences that it might engender (Anderson, 2003).

Another form of avoidance is active avoidance, which consists on taking action to prevent harm. It is often studied using one-way active or two-way active avoidance paradigms. In one-way active avoidance paradigms, only one of the two chambers of a shuttle-box is aversive (Gebhardt, et al., 2013) and associated with a shock

presentation. In two-way active avoidance, both chambers can be aversive, therefore two-way active avoidance behavior is less context dependent as compared to one-way avoidance paradigms. Two-way active avoidance can be either signaled by a stimulus such as a tone or a light, or unsignaled (Servatius, et al., 2016). Unsignaled avoidance also named Sidman avoidance conditioning (Sidman, 1953) is a type of learning in which an organism receives an aversive stimulus at fixed intervals, without any warning signal, unless it performs an avoidance response. Each avoidance response reseting the timer to zero. Due to the absence of any signal warning that a shock will be delivered, unsignaled active-avoidance is very difficult to acquire in rodents which is the reason why a majority of studies prefer signaled two-way active avoidance paradigms. In the latter type of learning paradigms, shuttle-boxes are separated into two compartments by a door or a hurdle, that the animal learns to cross during the warning signal to anticipate the delivery of the unconditioned stimulus (US) (Lichtenberg, et al., 2014; Ramirez, et al., 2015; Yasuno, et al., 2017; Kirkerud, et al., 2017). Other research studies use behavioral boxes in which the instrumental learning is more prominent, namely pressing a lever (Tsutsui-Kimura, et al., 2017) or stepping into a wheel (Gabriel, et al.,1991) to avoid shock delivery.

3) Theories of avoidance: A historical overview

Several theories have been proposed to highlight the type(s) of learning occurring before having high and stable expression of avoidance behavior. I will present and discuss the main theories of avoidance learning in the present sections.

Avoidance: Pavlovian learning

Early theories of avoidance learning were elaborated by behaviorists. They stipulated that all behaviors (including avoidance), no matter how complex, are elicited in a reflex-fashion by a prior stimulus and therefore are learned through interaction with the environment (Watson, 1913). They introduced the classical conditioning concept also called Pavlovian conditioning (Pavlov, 1927), which refers to a learning procedure through which an association between two stimuli is formed and results in a learned behavior. Two behaviorists in the early 19's, Bekhterev (1913) and Pavlov (1927), performed experiments on dogs in a mean to produce Pavlovian associative learning. Bekhterev (Bekhterev, 1913) quantified dog's leg flexion after the presentation of a stimulus that was previously paired with a shock. As to Pavlov's

dogs (Pavlov, 1927), they would salivate upon the presentation of a stimulus (bell ring) previously reinforced by food administration. However both behaviors, which were considered to be acquired through Pavlovian associative learning, differed at several points. After learning the association between the bell ring and the food presentation, Pavlov's dogs salivate independently of the unconditioned stimulus (US) delivery. The US (food) being the stimulus which would induce by itself before conditioning the unconditioned response (UR), salivation. However, in Bekhterev's experiment the US delivery (shock) is dependent on the dog's response; the animal's leg flexion (avoidance response) cancels or prevents the US delivery (Herrnstein, 1969). In addition, the dog's leg flexion is a voluntary controlled avoidance response (not a reflex) whereas the dog's salivation is based on the autonomic nervous system controlling involuntary functions.

Avoidance: Instrumental learning

Skinner one of the most influential behaviorists introduced the concept of operant conditioning (Skinner, 1938), which is a form of associative learning between a voluntary behavior and a consequence. He postulated that reinforcers, which can be positive or negative stimuli, increase the probability of a behavior being repeated. Positive reinforcing stimuli for example food or water would increase the rat's bar pressing behavior in Skinner box to get water or food (Skinner, 1938). In contrast, negative reinforcement occurs when the rat learns that pressing the bar would have as a consequence to avoid or switch off an aversive footshock. Therefore, in the first half of the 20th century, psychologists interested in avoidance behavior studies were more likely to use aversive instrumental tasks (Miller, 1948; Mowrer, 1946).

Avoidance: Two-factor theory

Mowrer proposed the two-factor theory (Mowrer, 1947) of avoidance learning which combined both classical and instrumental conditioning. He postulated that avoidance learning occurs in two phases. In a first phase, through Pavlovian associative learning processes **(Figure 2)**, a neutral stimulus (e.g. tone) paired with a fearful stimulus (e.g. shock) becomes a CS and triggers an emotional negative state. In a second phase, to reduce the fearful state and unpleasant emotions engendered by the CS, avoidance response to the CS are performed and reinforced with time. This second phase of learning implies an instrumental learning during which avoidance

behavior is reinforced through negative reinforcement (the omission of an unpleasant US).

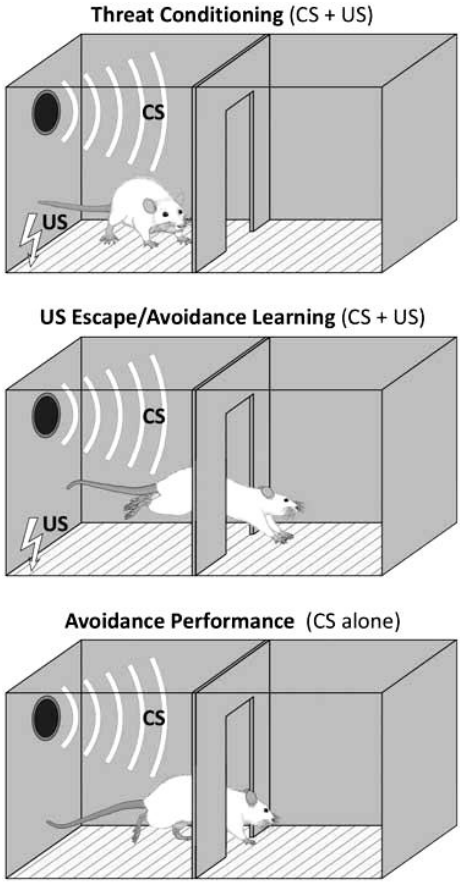

Figure 2. Adapted from (LeDoux, 2017). Avoidance learning phases in a shuttle-box

Top panel. A rat associates the presentation of a tone (CS) with a footshock (US). Following several pairings, the presentation of the tone evokes a fearful state through Pavlovian associative learning mechanisms. **Middle panel**. The rat learns that the US following CS presentations can be switched off by shuttling to another compartment of the shuttle-box: escape learning. It also learns with time that the CS itself can be stopped and the shock not delivered if it shuttles during the CS: avoid learning. **Bottom panel.** In late phases of training avoidance trials are reinforced, rats still avoid to the CS despite the fact that the US is not delivered.

Critisism of the two-factor theory

Despite the fact that Mowrer's two-factor theory was one of the most influential in avoidance studies it was deeply discussed notably on the psychological processes underlying avoidance behavior. The first concern adressed was linked to extinction process in avoidance. In avoidance learning, avoidance responses are thought to be reinforced by the fearful state provoked by the US. However the US, which is delivered at early trials after CS presentation, is almost inexistant at late trials when the animal has learned that the avoidance response prevents the shock delivery. Therefore the fearful state engendered by the US following the CS presentation is supposed to be extinguished with learning. Nevertheless, avoidance responses persist and are resistant to extinction (Annau and Kamin, 1961; Starr and Mineka,

1977). At advanced learning stages the avoidance expression and it's persistance can not be explained by negative reinforcement which is thought to motivate avoidance behavior since the negative stimulus (typically a shock) is almost never delivered.

Another argument against the two-factor theory was the extent to which Pavlovian and instrumental learning are necessary for the acquisition of avoidance. Bolles (1970) proposed a theory of avoidance, the species-specific defense reaction (SSDR) hypothesis (Bolles, 1970), which minimizes the role of reinforcement in the acquisition of avoidance behavior and stipulated that learning of avoidance responses can be facilitated if it is choosen to be one of the innate defensive reactions. In other words, avoidance was defined by Bolles as CS-elicited flight acquired through Pavlovian conditioning. Therefore from Bolles' point of view Pavlovian learning processes can explain avoidance behaviors without the involvement of goal-directed processes. Bolles concerns were driven by researchers such as D'Amato and Schiff (D'Amato and Schiff, 1964; Domjan, 2008) who trained rats to press a bar to avoid shock. They observed that only 3 of their 24 rats attained a modest level of proficiency even after 1000 trials. To explain this lack of avoidance learning, Bolles stipulated that in an aversive situation, the organism's repertoire is severely limited to a set of instinctive species-specific defensive responses (SSDR) with fleeing being the dominant avoidance response if there is a potential route of escape. Indeed rats readily learn to avoid aversive stimulation if the instrumental response is running in a wheel, jumping out of a shock box, or remaining still (Maatsch, 1959; Bolles, 1969; Brener and Goesling, 1970). However, they have difficulty learning to rear or press a lever to avoid shock (Bolles, 1969; Domjan, 2008). Bolles was one of many criticizing the instrumentality of avoidance learning and the arguments accumulated against the two-factor theory of avoidance learning without coming to a satisfiying resolution led to a decay in avoidance research field starting from the 1980's.

4) The dynamics of defensive behaviors

Humans, like other animals, in order to survive and perpetuate their species have to adapt to situations, environmental changes, and also types of threats that endanger their existence (Darwin, 1859). Adaptation includes selecting the apropriate defensive

strategy taking into account it's costs, the threat that elicits it and the context in which it occurs. As described above, avoidance is one defensive strategy adopted when an individual is exposed to harm. However, under certain circumstances, for instance inescapable threat, individuals eventually adopt other defensive strategies. Exciting fields of research have been developed to study the selection of individual's defense responses in rodents placed in groups, in seminaturalistic habitats, to predict which defensive behavior would be selected with different contextual and stimuli changes. An example of this grouping of tasks is the Mouse Defense Test Battery MDTB (Blanchard, et al., 2003; Blanchard, 2017) in which numerous defensive responses in rodents exposed to threatful situations have been observed: flight, hiding, freezing, attack and risk assessment. An example of MDTB tests, is a long oval runaway permitting to quantify escape behavior that can be modified and transformed to an unescapable arena to study the switch to freezing strategy. Indeed, apart from avoidance, freezing has been one of the most studied defensive behaviors. While some studies describe freezing as being a passive tonic immobilization excepting the respiration movements (Blanchard and Blanchard, 1972; LeDoux, 2000) other researchers argue that freezing is an active preparation state during which the organism gets ready to flight, avoid or fight (Bovin, et al., 2008; Gladwin, et al., 2016). Choosing the most adapted defensive strategy or switching between strategies depends on the threat imminence (Kim, et al., 2013 ; Low, et al., 2015). The threat imminence theory stipulates that an organism in a ''post-encounter'' with danger phase, during which the threat has been detected but is still far, would more lickely freeze to ''hide''. During the ''circa-strike stage'' when the threat is most imminent, defensive behavior switches from passive (freezing) to active (flight, avoid), or fight if a confrontation is engaged. Based on this theory, paradigms with looming visual stimuli that simulates an approaching threat for e.g. dark circles that keep getting bigger with time, have been developed to explore innate flight and freezing behavior (Yilmaz and Meister, 2013 ; Temizer, et al., 2015). Nevertheless work still need to be done in this field to compare learned active behavior and freezing in terms of brain circuits and behavioral selection.

Another process enabling an organism to screen the environment to detect potential threat, analyze it and prepare to adequate defensive behavior is risk assessment (RA). It involves postures the animal adopts to investigate the source of danger e.g. low-back posture of mice and stretched-approach pattern while approaching the

potential danger (Blanchard, et al., 2010). RA also involves the animal exploration of the environment to detect routes of possible hiding or escape (Ellard and Eller, 2009).

5) Avoidance and freezing-like defensive behaviors studies in humans

As described so far in animals, avoidance is an adaptive defensive behavior used when an escape route is available. In humans, avoidance is also used as an adaptive strategy to actively cope with a threatful situation. Several research studies highlighted in humans, mainly imaging studies, the neuronal correlates of adaptive avoidance. For instance, in demand-selection tasks, humans avoid options associated with higher cognitive demands in which the ratio costs over benefits is too high (Rattel, et al., 2017 ; Mitsuto, et al., 2018). Also computer tasks have been developed to explore for e.g. human's actively avoiding getting a shock by moving between virtual game board (Collins, et al., 2014). It has been also reported, that individuals having the possibility to actively cope with threatfull stimuli by avoiding them, have improved fear extinction and decreased spontaneous recovery of fear as compared to unescapable stressors (Hartley, et al., 2014). Knowing that extinguished fear reemerges with time (spontaneous recovery), adaptive active avoidance have been shown in humans to be a ''proactive coping'' behavior more effective than extinction learning to persistently decrease threat responses (Boeke, et al., 2017).

In line with animals studies, it has been reported that, also in humans, threat imminence is applied to selecting the most adapted defensive behaviors (Blanchard, 2017). Indeed, dynamically approaching spiders, snakes, a gun-directed toward the observer pictures elicited more freezing-like behaviors in participants: reduced body sway (Bastos, et al., 2016), increased skin-condutance, bradycardia and a potentiated startle behavior (Sagliano, et al., 2014 ; Gladwin, et al., 2016), whereas when the participants were given the opportunity to actively avoid approaching threat by for e.g. getting exposed to a gun picture directed-away from the observer, increased body sway, tachycardia as well as startle inhibition were measured (Bastos, et al., 2016 ; Low, et al., 2015; Wendt, et al., 2017).

However, when individuals show a bias in excessively expressing avoidance behavior in daily situations following a trauma, it becomes a maladaptive behavior. In fact, avoidance is a core symptom of a multitude of anxiety disorders such as post-traumatic stress disorder (PTSD) (DSM-V), obsessive compulsive disorder (OCD), agrophobia and others. According to the World Health Organization (WHO) the

prevalence of anxiety disorders is approximately 30%. It has been documented that genetic factors could predispose some individuals exposed to a trauma to develop avoidance PTSD's symptoms. For instance, a study done on women who underwent a deadly earthquake in China in 2008 (Cao, et al., 2014) and lost their children suggests that their expression of a biomarker: a certain allele of Tryptophane-Hydroxylase 2 (TRP2) enzyme was associated with a development of more severe avoidance symptoms.

Other studies highlighted the necessity to considere gender as a potential determinant of developing maladaptive avoidance. Indeed some studies showed that women are more prone to be affected by avoidance symptoms than men in workplace violence traumas (Geoffrion, et al., 2018) or war conditions (Sheynin, et al., 2017).

One proposed treatment of avoidance is extinction. However as shown in rodents (Rodriguez-Romaguera, et al., 2016), it was demonstrated in humans that avoidance behavior persists even after extinction process and the availability of avoidant behavior can renew fear (Vervliet and Indekeu, 2015). Nevertheless therapies have been developed to promote extinction, namely exposure-therapies which consisted on encouraging patients to refrain avoidant behavior by administring anxiolytics, however as expected, patients often relapse following exposure therapies (Treanor and Barry, 2017).

Maladaptive expression of other defensive behaviors mainly freezing-like behaviors have been also described in humans. A condition called tonic immobility which is counfonded with freezing but is different in the sense that it is a state of unresponsiveness, catatonic-like immobile posture, parkinsonian-like tremors, suppressed vocal behavior when a person is present in an inescapable threatful context or simply feeling entraped (Marx, et al., 2008). Those symptoms have been described mainly in patients suffering from sexual traumas (Kalaf, et al., 2017). Tonic immobility is also correlated with PTSD severity and poor response to treatments (Lima, et al., 2010). For a more detailed overview of the subject, the reader could check the following research and review papers (Sienaert, et al., 2014; Wijemanne and Jankovic, 2015; Pease-Raissi and Chan, 2018).

A field of research that is still poorly understood in humans is the neural underpinnings and the biological markers allowing the selection of a specific defensive response. Studies on rodents have shown that rats adopting passive

defensive strategies present an enhanced activity of a key enzyme of serotonin-biosynthesis in the striatum, increased serotonin levels in the midbrain and a decreased sensitivity of postsynaptic serotonin receptors (Popova, 2004). Those kind of questions need to be addressed in humans to evaluate whether in anxious patients there is a shift to avoidance strategies correlated with the expression of specific biomarkers in certain brain regions.

III. The prefrontal cortex: an encoder of both avoidance and freezing

As already discussed earlier, avoidance learning relies on several cognitive processes including associative learning, instrumental learning, and attention processes. Encoding such complex functions would for sure rely on neural computations in cortical structures receiving information from sensory systems and sending connections to motor effectors serving the acquisition and execution of defensive behaviors. A hub structure receiving connections from a multitude of cortical and subcortical regions and sending projections to a wide range of brain regions is the prefrontal cortex (PFC). Also there are a number of studies implicating the prefrontal cortex in both avoidance and freezing defensive behaviors (Bravo-Rivera, et al., 2015; Karalis, et al., 2016; Franklin, et al., 2017). In this section, I will develop the anatomical characteristics as well as the connectivity of the prefrontal cortex to other brain regions across species and introduce experimental studies investigating the role of the different subregions of the PFC in both avoidance and freezing defensive behaviors.

1) mPFC neuronal elements

a) Historical evolution of the mPFC definition across species

Before even the term ‘’prefrontal’’ cortex was used to study the regions we call today prefrontal, lesional experiments were first done on this region in dogs (Ferrier, 1886). The first description of the regions we consider today as prefrontal cortex was made by Brodmann who based his definition on cytoarchitectural properties of the frontal lobe in primates. Based on interspecies comparative studies he observed the presence of a granular layer IV exclusively in primates whereas in other species it is

very poorly developed or absent (Brodmann, 1909). Brodmann's view was an influential one since many studies referred to, the granular frontal region described by him, as the granular frontal or prefrontal (Preuss, 1995). However defining prefrontal cortex as the granular frontal region means that only primate have a brain region called prefrontal cortex. Nevertheless, the fact that primates have a part of prefrontal cortex (the granular prefrontal) lacking homology in other species still persists today. In an attempt to find a common evolutionary origin allowing a common definition of the mPFC applied across species, Rose and Woolsey (Rose and Woolsey, 1948), based on interspecies structural connectivity studies made on rabbits, sheep and cats defined the mPFC as being the part of the cerebral cortex that receives projections from the mediodorsal nucleus of the thalamus (MD). It was also demonstrated in primates (the granular frontal cortex), rats and mice (Markowitsch and Pritzel, 1979; Guldin, et al., 1981; Uylings, et al., 2003). However, it has been demonstrated that the MD projects to other cortical areas in addition to the mPFC (Markowitsch and Pritzel, 1979; Guldin, et al., 1981; Uylings, et al., 2003), which renders the definition of the mPFC solely based on the MD projection not accurate. It is difficult if not impossible to adopt a universal definition of the mPFC based on the homology of this structure between species. Indeed nowadays to consider structural homologies across species one have to consider a complexity of factors including the embryological development, the functional properties, pattern, and density of specific connections, and the presence and distribution of neuroactive substances and receptors (Uylings, et al., 2003). Therefore, scientists did not agree to date on a single criterion to define the mPFC across species (Carlén, 2017).

b) mPFC subregions definitions and terminologies across species

i) Humans and monkeys mPFC

The mPFC is subdivided into subregions based on cytoarchitectural, connectivity and functional characteristics which could differ between species. In humans and macaque monkeys, efforts have been made to have a common Brodmann's cortical definition and cytoarchitectural numbers (Petrides, et al., 2012). The Brodmann areas (BAs) traditionally defined as prefrontal in humans are BA8 to 14 and BA44 to 47 **(Figure 3)**. These areas correspond roughly to the granular part of the prefrontal

cortex defined in monkeys. Nevertheless the granular mPFC in humans display changes in the laminar structure and is therefore subdivided into granular, dysgranular, agranular and thin lightly granular layer IV cortical types **(Figure 3)**. The anterior cingulate cortex (ACC) is also a part of the prefrontal cortex in humans since it also receives MD projections. Based on neuroimaging studies in humans, the human mPFC have been subdivided into several regions specific to different functions (Kolb, 2015) mainly: the dorsolateral (dlPFC), dorsomedial (dmPFC), ventromedial (vmPFC), and orbital prefrontal cortex (OFC) **(Figure 3)**. The vmPFC being involved in complex cognitive processing of avoidance and risk assessment for instance (Mobbs and Kim, 2015; Qi, et al., 2018) while the dlPFC (Wang, et al., 2018; Nitschke, et al., 2006; Ueda, et al., 2003) as well as the ACC (García-Cabezas and Barbas, 2017; Fleming, et al., 2012) being associated with emotional computations.

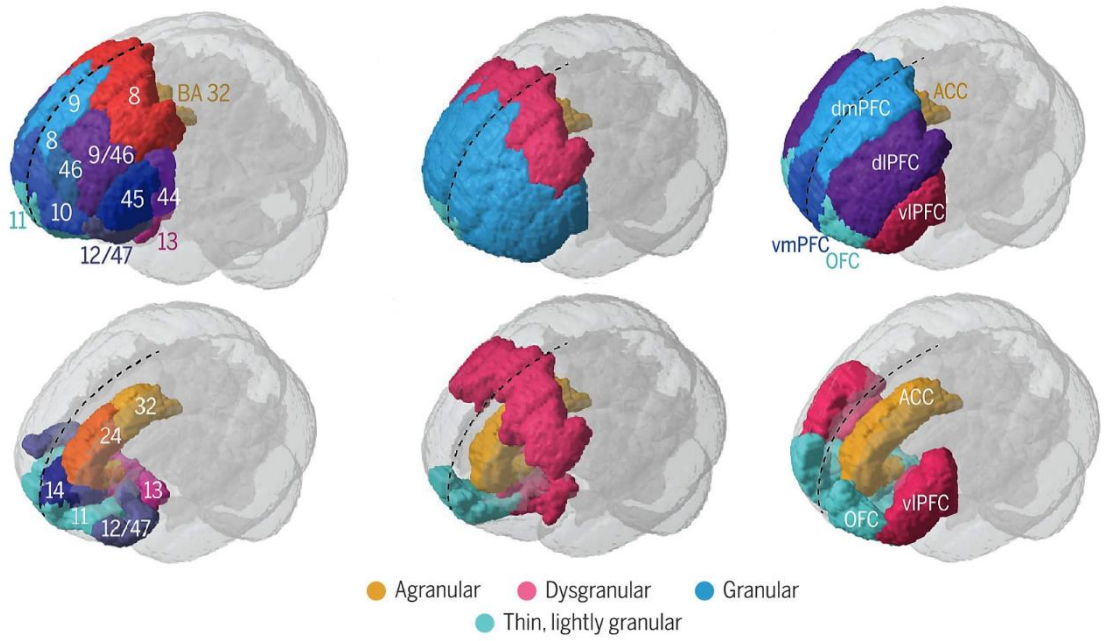

Figure 3. Adapted from (Carlén, 2017). Representation of the human prefrontal cortex
Right: Frontal view of the human prefrontal Brodmann areas (BA) in the PFC. Middle: Frontal view of the four cortical types in the prefrontal cortex. Left: Frontal view of the human PFC with the different functional delimitations: dmPFC, dorsomedial prefrontal cortex; dlPFC: dorsolateral prefrontal cortex; vmPFC, ventromedial prefrontal cortex; vlPFC, ventrolateral prefrontal cortex; OFC, orbito frontal cortex; ACC: anterior cingulate cortex. The dashed line indicates the sagittal midline.

ii) The mPFC in rodents

Nowadays it is accepted that mPFC in rodents can be functionally divided into four regions: the medial precentral cortex (PrCm) and the anterior cingulate cortex (ACC) areas, which regulate various motor behaviors, and the prelimbic (PL) and infralimbic

(IL) areas which are implicated in emotional, mnemonic, and cognitive processes (Heidbreder and Groenewegen, 2003). Furthermore, based on their differing target structures, the PL has been involved in emotional regulation and cognitive processes whereas the IL functions were linked to the regulation of visceral and autonomic functions (Vertes, 2006). PL and IL can be also separated based on a cytoarchitectural criterion: the width of layer II, which is a characteristic of the IL subregion (Van Eden and Uylings, 1985; Ray and Price, 1992). Indeed the PFC is part of the cortex, which presents a particular cytoarchitectural laminar organization. The cortex has a paralleled laminar organization (in laminaes or layers) defined by different numbers of layers, with each layer having characteristic cell types and patterns of intra-cortical and inter-cortical connectivity. The granular cortex is defined by six layers ordered from the farthest (layer 1) to the closest (layer 6) to the brain's white matter.

The layer 1, labeled 'molecular layer', is a thin layer located at the surface, below the pia, and is characterized by a low number of neurons and the presence of axons organized parallel to the surface and dendrites coming from deeper layers.

Layers 2 and 3, represent the external granular layer and the external pyramidal layer, respectively. In most cortices there is no clear anatomical segregation between these two layers since both are composed of densely concentrated neurons with a pyramidal shaped cell body. They are composed of vertically oriented cells that connect to other local cells or project to other brain areas and that are all excitatory in the cortical midbrain: the pyramidal neurons (PN).

The layer 4, labeled the internal granular layer, is lacking in the rodent's PFC which gives it the characteristic nomenclature of agranular PFC as opposed to the granular PFC in primates. Indeed, in the granular cortex in which layer 4 is a characteristic one, granule cells (highly concentrated and small sized cells) are excitatory spiny stellate neurons that amplify and distribute thalamo-cortical inputs throughout the cortex.

The layer 5 or the internal pyramidal layer is mostly composed of sparse and large PN vertically oriented.

The last layer 6, called the polymorph layer, contains various neuronal types with no specific organization. These six layers have distinct extrinsic connectivity. In particular, layers 2/3 support the cortico-cortical connections, layers 1 and 4 receive thalamic inputs and layers 5 and 6 are respectively the main sources of thalamic and

subthalamic projections **(Figure 4)** (Thomson and Lamy, 2007; Harris and Shepherd, 2015).

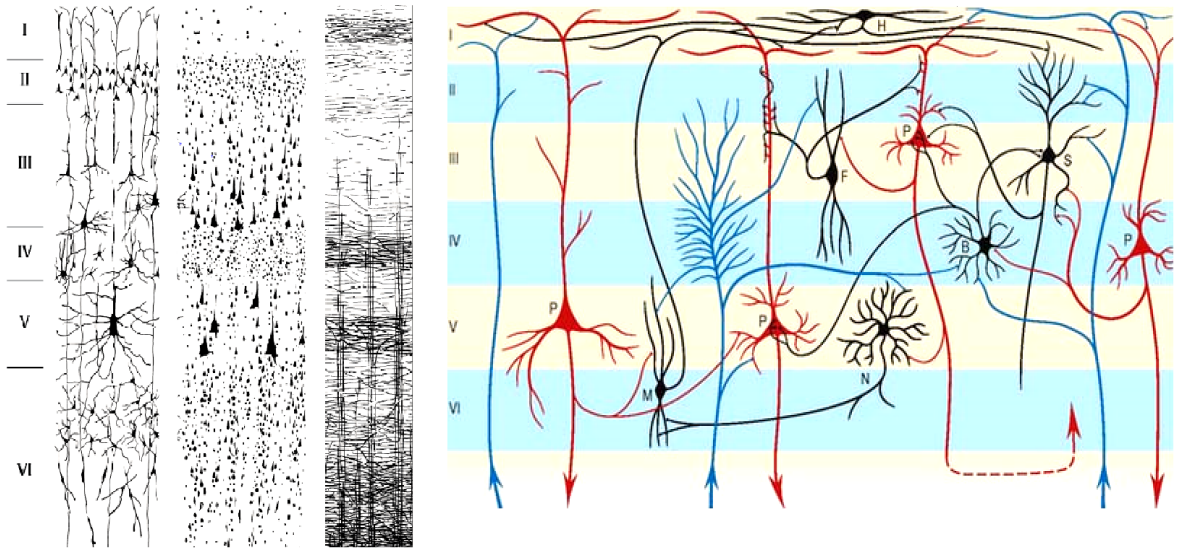

Figure 4. Schematic representation of layers of the cerebral cortex and cortical projections
Left: The three vertical columns represent the disposition of cellular elements as revealed by (from left to right column) Golgi staining (impregnating whole neurons), Nissl (staining cell bodies) and Weigert (staining nerve fibres). **Right:** Cortical neuronal connectivity scheme. Basket (B), Fusiform (F), Horizontal (H), Martinotti (M), Neurogliaform (N), Pyramidal (P), Stellate (S) neuronal shapes distributed in the 6 cortical layers. Afferent fibers are represented in blue and efferent fibers in red. (Adapted from Basic medical Key engine, chapter 23, Cerebral hemisphere).

Across all these layers, the cortex essentially consists of three neuronal cell types based on their size and shape: the pyramidal neurons (PN), the non-pyramidal spiny and non-spiny neurons **(Figure 4)**. The most abundant are pyramidal cells (PN) (80%), which have a flask-shaped or triangular cell body ranging from 10 to 80 µm in diameter. The soma gives rise to a single thick apical dendrite and multiple basal dendrites. The apical dendrite ascends towards the cortical surface, and branches with the most superficial lamina, the molecular layer. From the basal surface of the cell body, dendrites spread more horizontally, for distances up to 1 mm for the largest pyramidal cells. All PN dendrites are studded with a myriad of dendritic spines. These become more numerous as distance from the parent cell soma increases. A single axon arises from the axon hillock, which is usually situated on the basal surface of the PN. Ultimately, PN axon leaves the grey matter to enter the white matter, thus PN are known to be projection neurons. They all use an excitatory amino acid, glutamate, as their neurotransmitter and can be located in all six layers except layer 1 (Spruston, 2008; DeFelipe and Farinas, 1992).

Non-pyramidal cells, also called stellate or granule cells, are divided into spiny and non-spiny neurons. Spiny stellate cells are the second most numerous cell types in

the cortex and for the most part occupy lamina IV (absent in rodents). They have small multipolar cell bodies, commonly 6 to 10 μm in diameter and several primary dendrites, abundantly covered in spines. Their axons ramify within the grey matter predominantly in the vertical plane.

The smallest group (~ 20%) comprises the heterogeneous non-spiny or sparsely spinous stellate cortical cells. All are GABAergic inhibitory neurons, and until recently it was thought that their axons are confined to the grey matter, they only communicate with other cells locally: interneurons (Letinic, et al., 2002). Nevertheless, long-range GABAergic inhibitory projection neurons have been described in several cortical and subcortical regions (Melzer, et al., 2012; Seo, et al., 2016; Melzer, et al., 2017) including the prefrontal cortex (Lee, et al., 2014). Morphologically, GABAergic cortical neurons have a multitude of different aspects **(Figure 4)**, including basket, chandelier, double bouquet, neurogliaform, bipolar/fusiform and horizontal cells (Markram, et al., 2004). The principal neurotransmitter of cortical interneurons and inhibitory projection neurons is GABA. However, some $GABA^+$ neurons are also characterized by the coexistence of one or more neuropeptides, including neuropeptide Y (NYP), vasoactive intestinal polypeptide (VIP), cholecystokinin (CCK), somatostatin (SST), or calcium binding proteins such as calretinin (CR), parvalbumin (PV), calbindin (CB). Cortical IN are also defined based on their electrophysiological properties: fast spiking, irregular spiking, burst firing, accelerating spiking, adapting, non-fast-spiking non-adaptative cells (Ascoli, et al., 2008). In mice the two major IN types are PV and SST making up to ~ 50% and 30% respectively of cortical GABAergic interneurons (Xu, et al., 2010; Rudy, et al., 2011). These two groups have unique electrophysiological properties and form distinct synaptic connections with pyramidal cells of the cortex. PV INs exhibit somatic action potentials that are short in duration and are often referred to as fast-spiking (FS) INs. FS interneurons are typically basket or chandelier GABAergic cell types, and their axons target the proximal dendrites, somata, and axon initial segments of nearby pyramidal cells (McCormick, et al., 1985; Ascoli, et al., 2008; Hu and Jonas, 2014).

SST-expressing INs, which are typically Martinotti cells, show regular spiking (RS) activity patterns with broad action potentials. In contrast with FS cells, SST-expressing INs target the distal portions of pyramidal cell dendrites (Wang, et al., 2004; Halabisky, et al., 2006; McGarry, et al., 2010).

FS interneurons are capable of generating high-frequency (>300 Hz) trains of relatively short duration (e.g., < 0.5 ms at half amplitude) action potentials with little spike frequency adaptation, as recorded from their somata (McCormick, et al., 1985; Wang, et al., 2002; Nowak, 2003; Hu and Jonas, 2014). In contrast, SST INs are typically characterized by a RS somatic electrophysiological signature consisting of relatively broad action potentials (> 0.5 ms at half amplitude), spike frequency adaptation, and maximal firing rates of < 200 Hz (Xu, et al., 2006; Halabisky, et al., 2006; Ma, et al., 2006; McGarry, et al., 2010).

Given the big variety of neurotransmitters' expression, electrophysiological and brain layers' specific expression of INs, it is evident that INs underlie several functions ranging from regulating the activity of PN through PN-IN circuitry preventing brain's hyper-excitability to the successful processing of sensory information and the generation of rhythmic activity in the brain (Batista-Brito, et al., 2018; Ferguson and Gao, 2018; Dienel and Lewis, 2018). There is growing evidence that the specialization of INs in regulating certain functions relies on their genetic profile. Those studies have been made possible using a combination of physics and biological tools allowing the emergence of optogenetics allowing a precise control over neuronal microcircuits' activity as well as the identification of neuronal subpopulations (Deisseroth, 2015).

In fear studies, it has been documented that VIP INs in the prefrontal cortex are excited during both reward and punishment in go-no go tasks and mediate disinhibition of PN, a mechanism consisting on IN-IN interactions. Indeed, VIP INs through their inhibition of SST and PV INs decrease the inhibition of PN in the prefrontal cortex (Garcia-Junco-Clemente, et al., 2017; Pi, et al., 2013).

As for PV INs, they are key actors in fear expression. Courtin and colleagues (Courtin, et al., 2014) have shown that optogenetic inhibition of prefrontal PV-INs selectively disinhibit PN projecting to the basolateral amygdala and induce freezing behavior. SST INs mediate the suppression of visual responses (Taniguchi, et al., 2013) and some subtypes of SST can also mediate disinhibition in the cortex (Xu, et al., 2013).

GABAergic INs are also the source of generation and/or transmission of oscillations: they are thought to coordinate the precise timing of PN activation. Numerous elegant studies were performed, on anaesthetised animals in which recordings in the hippocampus from targeted INs have been used to correlate their firing to network

oscillations (Varga, et al., 2012; Klausberger, et al., 2003; Klausberger, et al., 2004; Tukker, et al., 2007). These studies revealed that some interneurons' subtypes coordinate the activity of pyramidal cell ensembles. Indeed, it has been shown in the hippocampus that distinct interneuronal subtypes fire during different rhythms (for example, theta, gamma and ripple) and with distinct phase relationships, suggesting that they differentially contribute to network dynamics (Buzsáki and Draguhn, 2004; Varga, et al., 2012).

2) mPFC connectivity: afferents and efferents

a) Afferent projections to the mPFC

Each division of the mPFC receives a unique set of afferent/efferent projections driven by the functional differences. Indeed, there is a dorso-ventral shift along the mPFC from predominantly sensorimotor inputs to the dorsal mPFC (dorsal ACC) to primarily 'limbic' inputs to the ventral parts of the mPFC (PL and IL). The dorsal ACC receives afferent projections from widespread areas of the cortex (and associated thalamic nuclei) representing all sensory modalities. As for the MD thalamic nucleus, the medial segments of the MD preferentially contact the IL and PL, whereas its lateral segments more often contact the ACC and PrCm (Groenewegen, 1988 ; Uylings and Van Eden, 1990). Therefore the sensory information coming through thalamic inputs is integrated at the dorsal mPFC in goal-directed actions. In contrast, with the dorsal mPFC, the ventral mPFC receives significantly less cortical inputs overall and more afferents from limbic structures as opposed to sensorimotor regions of the cortex (Hoover and Vertes, 2007; Conde, et al., 1995).

The main sources of afferent projections to PL/IL are from the orbitomedial prefrontal, agranular insular, perirhinal and entorhinal cortices, the hippocampus (the vHPC (CA1 region and subiculum)) is the main source of inputs while sparse inputs come from the dorsal hippocampus dHPC (Cenquizca and Swanson, 2007; Hoover and Vertes, 2007), the claustrum, the medial basal forebrain, the basal nuclei of amygdala, the midline thalamus and monoaminergic nuclei of the brainstem. With a few exceptions, there are few projections from the hypothalamus to the dorsal or ventral mPFC. Accordingly, subcortical limbic information mainly reaches the mPFC

via the midline thalamus and basal nuclei of amygdala: BLA and LA (Mcdonald, 1991). In addition, afferents from the basal ganglia have been described; the dorsal striatum projecting preferentially to the dorsal mPFC and ventral striatum projects more to the PL and IL (Gabbott, et al., 2005). Also the dorsal and lateral periaqueductal gray as well as the ventral tegmental area (VTA) send projections to the mPFC (Gabbott, et al., 2005).

b) Efferent projections from the mPFC

Dorsal and ventral mPFC project to distinct anatomical targets linked to their differentiation in functionality. The dorsal mPFC mainly the PrCm projects to sensorimotor effectors including motor and somatosensory cortices, dorsal striatum, ventral and lateral nuclei of thalamus, tectum/pretectum and the brainstem reticular formation, but essentially avoids 'limbic' regions of the forebrain and hindbrain (Guandalini, 1998; Reep and Corwin, 1999; Voorn, et al., 2004; Gabbott, et al., 2005).

In contrast to motor-associated properties of the dorsal mPFC (ACC), IL and PL have been functionally linked to the limbic system. The IL influences visceral/ autonomic activity; it's stimulation produced changes in heart rate, blood pressure, respiration rate (Burns and Vyss, 1985; Verberne, et al., 1987) while the PL is implicated in cognitive processes. PL lesions produce deficits in delayed-response tasks for instance (Ragozzino, et al., 1998; Dalley, et al., 2004). PL and IL projections distribute differentially throughout the brain; their different projections are summarized in **Figure 5**. Interestingly, IL projections to the amygdala contact essentially the lateral capsular subdivision of the central nucleus (the hub of ITC cells) and the lateral nucleus LA and are more widespread than PL's which projects mainly to the basal nucleus of the amygdala BA (McDonald, et al. 1996; McDonald, 1991; Shinonaga, et al., 1994; Hoover and Vertes, 2007).

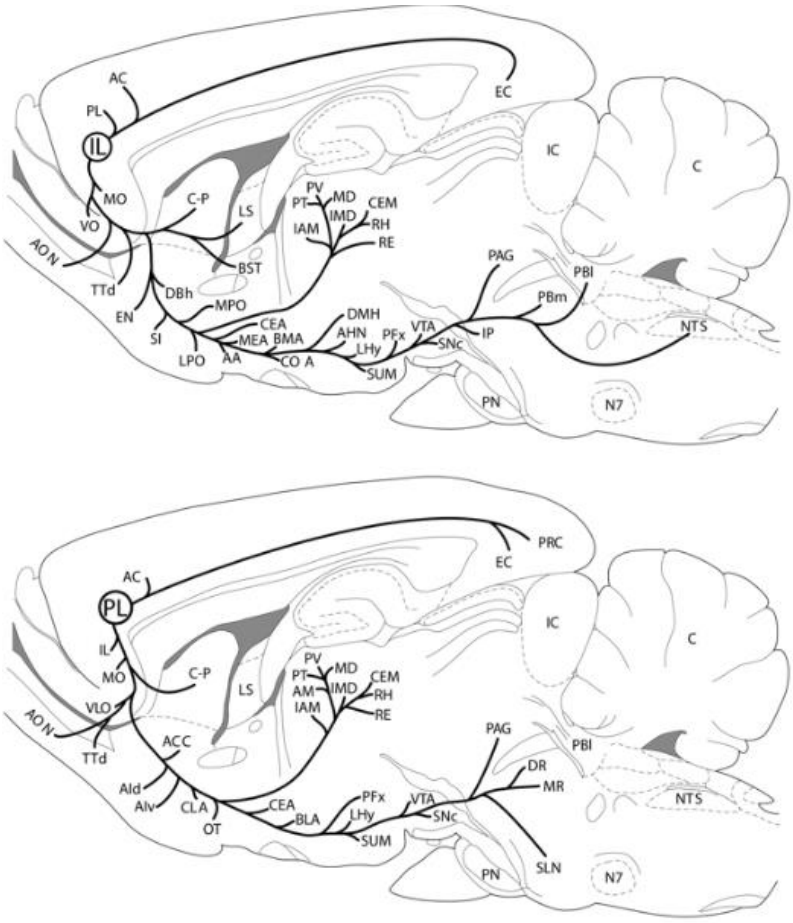

<u>Figure 5.</u> Schematic sagittal sections summarizing the main projection sites of the IL (Up) and PL (Bottom) in rats Sections are modified from the rat atlas of Paxinos and Franklin (Paxinos and Franklin, 2008)

Note that IL projections are much more widespread than PL projections, particularly to the basal forebrain, amygdala and hypothalamus. Abbreviations: AA, anterior area of amygdala; AHN, anterior nucleus of hypothalamus; AI,d,v, agranular insular cortex, dorsal, ventral divisions; AM, anteromedial nucleus of thalamus; AON, anterior olfactory nucleus; BMA, basomedial nucleus of amygdala; C, cerebellum; CEM, central medial nucleus of thalamus; CLA, claustrum; COA, cortical nucleus of amygdala; C-P, caudate/putamen; DBh, nucleus of the diagonal band, horizontal limb; DMH, dorsomedial nucleus of hypothalamus; DR, dorsal raphe nucleus; EN, endopiriform nucleus; IAM, interanteromedial nucleus of thalamus; IC, inferior colliculus; IMD, intermediodorsal nucleus of thalamus; IP, interpeduncular nucleus; LHy, lateral hypothalamic area; LPO, lateral preoptic area; LS, lateral septal nucleus; MEA, medial nucleus of amygdala; MO, medial orbital cortex; MPO, medial preoptic area; MR, median raphe nucleus; N7, facial nucleus; OT, olfactory tubercle; PBm,l, parabrachial nucleus, medial and lateral divisions; PFx, perifornical region of hypothalamus; PN, nucleus of pons; PRC, Reuniens nucleus; RE, perirhinal cortex; RH, rhomboid nucleus of thalamus; SI, substantia innominata; SLN, supralemniscal nucleus (B9); SUM, supramammillary nucleus; TTd, taenia tecta, dorsal part; VLO, ventral lateral orbital cortex; VO, ventral orbital cortex. Reprinted from Vertes (2004).

PL and IL project reciprocally to the dlPAG and lPAG (Gabbott, et al., 2005). Both of PL and IL do not project directly to the hippocampus but regulate HPC's activity indirectly via their projections to the nucleus reuniens of the thalamus (NR), a major source of thalamic inputs to the HPC (Vertes, et al., 2007; Varela, et al., 2014).

As for the ACC, it is a structure having connections with both cognitive and emotional regions. The anterior as well as the posterior parts of the ACC, project to cortical

structures (intracingulate, retrosplenial and parietal associative cortex), the non-cortical basal forebrain, (dorsal striatum (caudate putamen mainly), septum, claustrum, basolateral amygdala), the hypothalamus (anterior, lateral, posterior), the thalamus (anterior, laterodorsal, ventral, mediodorsal, midline and intralaminar nuclei), the brainstem (periaqueductal gray, superior colliculus, pontomesencephalic reticular formation, pontine nuclei, tegmental nuclei) and the spinal cord (Fillinger, et al., 2018). Interestingly, it has been shown in mice that the ACC projects to defined subregions of the PAG: the dorsolateral and lateral PAG (dlPAG/lPAG) exclusively; a pathway that potentially could be important in mediating defensive behaviors (Vargas, et al., 2000). The ACC reciprocal connections to mainly the anterior BLA are thought to encode working memory and decision making processes (Heidbreder and Groenewegen, 2003), although there is some evidence about its involvement in the regulation of fear behavior (Bissière, et al., 2008). The ACC is the only mPFC subregion projecting directly to the dorsal hippocampus (Rajasethupathy, et al., 2015).

In a comparison between rodents and primates, PL is positioned to serve a direct role in cognitive functions homologous to dlPFC of primates, whereas IL appears to represent a visceromotor center homologous to the OFC of primates.

3) mPFC functions in conditioned fear behaviors: freezing and avoidance

a) Lesional/ stimulation studies

i) Conditioned avoidance

It is thought that lesions of the mPFC (ACC, IL and PL) disrupt the acquisition but not the expression of goal-directed behaviors (Ostlund and Balleine, 2005). Indeed in avoidance studies it was reported that lesions of the mPFC act on the amount of avoidance responses and/or the latency it takes the animal to avoid the aversive stimulus (Fritts, et al., 1998; Blancoa, et al., 2009 ;Beck, et al., 2014). For instance, pre-training ibotenic acid lesions of the ACC in rabbits led to a retardation of avoidance acquisition consisting in stepping in an activity wheel in response to a 0.5 seconds tone (CS^+) (Gabriel, 1991). In most of the studies lesions were made prior to

training therefore most of them did not investigate the effect of post-training lesions on expression of avoidance behavior.

Given the variation in the paradigms used to study avoidance, lesions of mPFC could differentially impact the type of avoidance learned. Indeed, it was shown that lesions of dmPFC in adult rats prior to training impaired avoidance acquisition in rats undergoing a two-way active avoidance training but not rats passing through a passive avoidance training (Brennan, et al., 1977).

An important factor to control in lesioned animals is the extent and the location of the lesion in mPFC subregions, which seem to be crucial for the behavioral outcome. On one hand, some papers postulate that large mPFC lesions are needed to impair avoidance acquisition. For instance, in a passive avoidance task (Blancoa, et al., 2009) the lesion of the entire mPFC impaired avoidance behavior. Interestingly, some lesional studies limited to PL alone or IL alone or extended to PL+IL failed to reveal a robust effect on the acquisition or expression of avoidance in a lever-press avoidance paradigm (Beck, et al., 2014). In this task a combined lesion of the PL and IL slightly slowed but did not impair avoidance acquisition and expression behaviors. On the other hand, several lines of evidence demonstrate that lesions targeting specific areas of the mPFC perturbed avoidance acquisition. Indeed, small targeted lesions of the PL in rats done prior to a step-through passive avoidance test impaired fear memory by decreasing the latency to enter the dark, shock compartment at the retention test (Maaswinkel, et al., 1996). Several lines of evidence, point-out the PL as the essential structure for avoidance acquistion. It was reported for instance that PL stimulation with effective current intensities 50 and 100 µA improve avoidance memory by prolonging the delay of entering the dark chamber in rats submitted to a passive avoidance task (Mehdipour, et al., 2015). Also electric stimulation of the posterior part of the cingulate cortex in cats facilitate the process of active avoidance acquisition in a two-way active avoidance paradigm (Eckersdorf, 1905).

However depending on the avoidance learning paradigm, PL seems to be more or less involved in encoding avoidance acquisition. For instance, it was shown that pharmacological ibotenic acid lesions of both PL and IL prior to training impaired slightly lever-press avoidance acquisition, whereas lesions limited to PL only slowed avoidance responses (Beck, et al., 2014). In contrast to the previous findings, some other studies suggested, based on lesional experiments, that the PL is not essential for avoidance acquisition and that the IL is the key structure driving avoidance

acquisition. It was shown that rats with small mPFC lesions sparing the PL present impaired avoidance learning whereas rats with the mPFC lesioned entirely (dorsal and ventral regions) or with only the PL lesioned do not present impaired avoidance learning (Fritts, et al., 1998). Also, electrolytical lesions of the IL but not PL showed impaired step-down passive avoidance learning (Jinks and McGregor, 1997) and impaired two-way active avoidance (Moscarello and LeDoux, 2013). The IL is thought to play a role in inhibiting the behaviors associated with negative outcomes, therefore it is essential in avoidance acquisition when instrumental learning is required to acquire avoidance behavior. In addition in a recent paper, it was suggested that the IL regulates approach to appetitive stimuli rather than avoidance of aversive ones. This study based on recordings demonstrated that vmPFC cells responding to cues predicting reward fire more often and more robustly than cells modulated by cues preceding avoidable shocks (Gentry, et al., 2018).

As for extinction of avoidance learning, defined as the decline in avoidance conditioned fear responses (CR) following non-reinforced exposure to the conditioned stimulus (CS), there is evidence of the implication of dorsal mPFC regions as lesions can disrupt avoidance extinction learning in one-way avoidance paradigms (Brennan, 1982). Also, pharmacological ibotenic acid lesions of PL prior to training, do not impact lever-press avoidance acquisition but promote extinction-resistant avoidance behavior in rats (Fragale, et al., 2016). To explain this effect it is suggested that BLA to PL projections regulate avoidance extinction learning since in a lever-press avoidance task, impaired plasticity in BLA-PL pathway (marked by the lack of LTP of BLA-evoked responses in the PL cortex) is thought to contribute to extinction-resistant avoidance process (Fragale, et al., 2016).

Therefore, lesional studies linked to avoidance behavior suggested that the mPFC drives avoidance behavior. Nevertheless, to determine the precise mPFC subregional implication in avoidance behavior, additional approaches are required

ii) Freezing Behavior

In several studies, the PL has been associated with fear expression whereas the IL was associated with fear extinction (Sotres-Bayon, et al., 2004). Based on electric

stimulation studies, PL microstimulation, but not PrCm nor ACC, concomitant with a conditioned tone onset increases fear expression (freezing) whereas IL microstimulation reduces conditioned freezing expression (Vidal-Gonzalez, et al., 2006). Using electrophysiological recordings, it was shown that PL neurons are not only activated to conditioned stimuli but also sustain their activity during freezing behavior (Burgos-Robles, et al., 2009; Corcoran and Quirk, 2007). In our laboratory, Courtin and colleagues (Courtin, et al., 2014) have unraveled a mechanism underlying fear expression namely the inhibition of PV interneurons in the PL disinhibiting PL projection pyramidal neurons driving fear expression. We also showed that freezing expression is concomitant with the synchronization of PL neurons projecting to the BLA on 4Hz oscillatory rhythm (Karalis, et al., 2016). More specifically, freezing behavior is coincident with the activation of neuronal assemblies in the PL in the ascending phase of 4 Hz oscillations (Dejean, et al., 2016). The PL underlies also contextual fear expression. Indeed, PL post-training lesions disrupted contextual freezing expression (Kim, et al., 2013).

Consistently, some lesional studies showed that IL lesions impair the extinction of fear responses (Morgan, et al., 1993) and attenuate the recall of fear extinction (Quirk, et al., 2000). More specifically, several groups demonstrated that pre-training vmPFC lesions blocked the consolidation but not the original formation of fear extinction memories (Quirk, et al., 2000; Lebron, et al., 2004; Tian, et al., 2011). Consistent with this, an eletrophysiological signature of the consolidation of freezing extinction was identified in the IL through high-frequency bursting of IL neurons immediately after extinction training (Burgos-Robles, et al., 2007).

As for the ACC it has been documented that this mPFC subregion underly fear acquisition since pre-training lesion of ACC impair fear acquisition (Bissière, et al., 2008).

However, there is still some controversial data about the involvement of specific mPFC subregions during conditioned freezing acquisition, expression and extinction. Indeed, it has been shown that lesions of the mPFC including both the PL and IL, either pre-conditioning or post-extinction, is not required for the acquisition, expression or the retention of extinction (Garcia, et al., 2006; Gewirtz, et al., 1997; Lebron, et al., 2004). Morgan et al. (Morgan, et al., 1993) demonstrated that pre-conditioning mPFC lesions (ACC, PL, and IL) did not affect fear acquisition or fear

expression during either context or cued fear conditioning. However, these animals took longer to reach extinction criterion, suggesting that mPFC neural activity plays a role in extinction learning. In a follow up study, selective PL lesions produced a general increase in both cued and context fear during acquisition and extinction phases, suggesting that the dmPFC lesions yield a general increase in fear (Morgan and LeDoux, 1995). The authors suggested that these findings revealed a differential contribution of PL vs. IL in the expression of conditioned fear. However, based on the extent of the lesions presented in each study, an alternative interpretation is that behavioral differences reflected gross differences in functions mediated by the dorsal-ventral axis of mPFC and not specifically PL vs. IL. In support of this, some studies have reported decreased freezing and differential cardiovascular responses to the CS as a function of the dorsal-ventral extent of mPFC lesions, suggesting that the functional contribution of mPFC may differ along this axis rather than being exclusively confined to PL vs. IL (Frysztak and Neasfey, 1991).

Finally, animals' strain might influence the effect of IL lesion on the consolidation of extinction learning as IL lesions impaired the retention of extinction in Sprague Dawley, but not Long Evans rats in an auditory fear conditioning paradigm (Chang and Maren, 2010).

To summarize, lesion studies pinpoint a clear role of the mPFC in conditioned fear learning processes with the ACC sustaining the acquisition, PL the expression and IL the consolidation of extinction. The dorso-ventral axis of the mPFC, the extent of the lesion as well as the strain of rodents are factors, which could add controversy to this general view. Therefore, to assess the specific role of mPFC subregions in fear learning phases more subtle technical approaches are required.

iii) Freezing assessed in avoidance paradigm

In avoidance learning paradigms, according to the two-factors theory, in early-training phases, learning depends on Pavlovian associative processes and lead to increased fear expressed in terms of freezing. In a second step, avoidance responses are developed depending on instrumental associative processes to ultimately reduce the negative state generated by the CS presentation. In several avoidance studies both freezing and avoidance are quantified allowing to assess the effect of lesional studies on both freezing and avoidance behaviors in the same paradigm (Bravo-Rivera, et

al., 2014; Boeke, et al., 2017; Diehl, et al., 2018). Pre-training lesions of the IL region increased freezing expression and disrupted two-way active avoidance learning (Moscarello and LeDoux, 2013). According to Moscarello and colleagues, the expression of passive freezing behavior and active avoidance are inversely correlated and depends on a balance of activity between IL and amygdala *(see amygada section)*. IL is thought to mediate avoidance responses by inhibiting CeA which activation drives freezing responses.

b) Pharmacological inactivation studies

i) Avoidance behavior

Acquisition and expression of avoidance learning

Paradigm-dependent contradictory data have been reported on the implication of mPFC subregions in the acquisition and expression phases of avoidance behavior. Moscarello and LeDoux (Moscarello and LeDoux, 2013) reported that IL but not PL is relevant for both the acquisition and expression phases of a signaled active avoidance task. Pre-training injection of muscimol, or anisomycin (a protein synthesis inhibitory) in the IL induced a significant decrease in avoidance responses across 5 daily training sessions indicating the necessity of IL to acquire avoidance behavior. Muscimol-induced IL inhibition had also a slight but significant decrease in avoidance expression (Moscarello and LeDoux, 2013). In contrast, using a platform avoidance task, Bravo-Rivera and colleagues (Bravo-Rivera, et al., 2014), showed that muscimol inactivation of the PL but not IL impaired the expression of avoidance behavior.

Recently, Svoboda and colleagues (Svoboda, et al., 2017) reported that muscimol-induced ACC inactivation disrupt fast-moving robot avoidance expression when administered at pre-ultimate training session, suggesting that the ACC is crucial in robot-avoidance behavior expression.

An important point to note is that varying the amount of training (the intensity and the amount of the shocks per session) may have important consequences on memory processes and partially explain the discrepancies described above.

For instance, when learning occurs through intense training (high intensity shock), memory formation is preserved against amnestic treatments. It has been for instance reported that interfering with serotonergic activity impairs both acquisition and

retention of active avoidance after training with relatively low foot-shock intensities, but not when training was done using higher foot-shock intensities (Galindo, et al., 2008). Pre-training PL inactivation, by TTX infusion, impairs memory consolidation of passive avoidance in the 1.0 mA group, while no effect on consolidation was produced in the 3.0 mA group (Torres-García, et al., 2017). Intense training is thought to cancel potential deficiencies produced by such inactivation.

Consolidation of avoidance behavior

Several papers pinpoint that the ACC, PL and IL are all crucial for consolidation processes during avoidance learning. Indeed, PL and IL are also thought to be crucial for memory consolidation in avoidance tasks, since their TTX-mediated inactivation perturbed memory retention in a passive avoidance task (Torres-García, et al., 2017). PL inactivation using lidocaine infusion, immediately after a passive avoidance training, impaired the retention process (Yang and Liang, 2014). As for the ACC, several lines of evidence indicate that pre-training and post-training infusion of scopolamine, a cholinergic antagonist, impaired memory consolidation of a passive avoidance task (Riekkinen, et al., 1995). Consistently, infusion of the cholinergic agonist oxotremorine into ACC immediately after training improved memory (Malin and McGough, 2006). More precisely, the ACC has been shown to be crucial for retrieval of long-term passive avoidance memory but not for short-term retrieval. Pre-retrieval inactivation of the ACC by locally infusing muscimol, produced a severe deficit in 7-day, 4-day and 1-day retrieval memories, with no effect on 2-h and 6-h memories.

Nevertheless, other papers argue that ACC is not essential for CS-US consolidation during avoidance learning. TTX-inactivation of ACC with intense (3 mA) or less intense (1 mA) training (Torres-García, et al., 2017), or post-training intra-ACC administration of muscimol and AP5 (Mello e Souza, et al., 1999) did not interfere with memory consolidation of a passive avoidance task.

Extinction of avoidance behavior

Several studies agreed on the exclusive implication of IL in avoidance extinction processes. Chemogenetic inactivation with designer receptors exclusively activated by designer drugs (DREADDs) or micro-injections of GABA agonists into the IL but

not ACC or PL, blocked the extinction of avoidance of a pain-predictive cue (Schwartz, et al., 2017). In addition, Bravo-Rivera and colleagues (Bravo-Rivera, et al., 2014) showed that IL is crucial for retrieval of extinction in a platform-based avoidance paradigm. Muscimol inactivation of IL but not PL impaired between but not within extinction sessions.

In summary, ACC, PL and IL seem to be differentially encoding acquisition, consolidation and expression of avoidance behavior depending of the task used. Moreover, strong evidence support that IL is crucial for retrieval of avoidance extinction.

ii) Freezing behavior

Just as for avoidance behavior, the use of local, reversible, pharmacological inactivation also yielded contrasting results as inactivation of both ventral PL and IL impaired between session extinction, prevented discrimination of a non-conditioned tone, increased, decreased, or did not change fear expression during a post-extinction retrieval test (Resstel, et al., 2006; Sierra-Mercado, et al., 2006; Lee and Choi, 2012; Morawska and Fendt, 2012).

However, restricted pre-training or post-training inactivation of ACC, PL or IL provided more consistent results. Indeed, pre-training inactivation of the ACC via lidocaine, TTX or muscimol infusions blocked fear acquisition (Sacchetti, et al., 2002; Bissière, et al., 2008; Tang, et al., 2005). Furthermore targeted pre-training activation of the ACC using mGluR agonist (trans-(±)-1-amino-(1S, 3R) cyclopentanedicarboxylic acid) or $GABA_A$ receptor antagonist (bicuculline) induced an enhancement of fear behavior, suggesting an involvement of the ACC in the acquisition of fear behavior (Bissière, et al., 2008; Tang, et al., 2005).

As for PL, it has been demonstrated that muscimol injection prior to extinction training impairs fear expression. However, this manipulation has no long-term effects on extinction recall, suggesting that the PL inactivation does not interfere with the acquisition of extinction but rather with the expression of freezing (Corcoran and Quirk, 2007; Sierra-Mercado, et al., 2011; Stevenson, 2011). In contrast, when inactivation was restricted to the IL, the same manipulations have no effect on fear expression but impaired within session extinction. Nonetheless, one study reported a facilitating effect on extinction (Akirav, et al., 2006). Interestingly, post-training

activation of the IL using the $GABA_A$ receptor antagonist picrotoxin (Thompson, et al., 2010; Chang and Maren, 2011) facilitates between session extinction of fear, further supporting a role of IL in retrieval of fear extinction memory.

In summary, these studies indicated that inactivation of overlapping mPFC regions lead to inconsistent results whereas more delimited manipulations of ACC, PL and IL have produced consistent and specific effects. In particular, these data strongly suggest that ACC plays a key role in the acquisition of conditioned freezing behavior, PL in freezing expression and IL in the retrieval of freezing extinction.

c) Immediate-early genes activation studies

Immediate early genes (IEGs), are used in behavioral neuroscience as a marker of neuronal activation to depict, most of the time, activity related to the expression of a certain behavior. IEGs comprise a diverse group of factors encoding for a wide variety of functions namely transcriptional factors, growth factor receptors and receptors-associated binding proteins, secreted and membrane proteins, tyrosine phosphatases, coagulation proteins, and many other factors. One major category is transcription factors including the well-known c-fos, c-jun, jun-B, and zif268. IEG expression is induced inside nerve cells by stimuli such as activity-induced changes in synaptic efficacy and plasticity producing an up-regulation of the expression of IEGs. The c-fos expression is linked for instance to neuronal excitability (O'Donnell, et al., 2012). It is largely the most used IEG in neuroscience and its' expression peaks 30-60 minutes after stimulation (cell-extrinsic or cell-intrinsic signals) (Greenberg and Ziff, 1984).

i) Avoidance behavior

Acquisition and expression of avoidance learning

IEGs expression in the mPFC correlates with avoidance expression in several avoidance tasks. Asymptotic expression of lever-press avoidance, consisting on pressing a lever when the CS^+ is played to avoid a shock delivery, in Spargue Dawley (SD) rats was associated with an increased expression of ΔFosB in the mPFC (Perrotti, et al., 2013). In a two-way active avoidance task avoidance behavior was also correlated with a c-fos up-regulation in the mPFC (Martinez, et al., 2013).

Some studies, went further and identified the type of neurons activated in the mPFC during avoidance. Lever-press avoidance was shown to be associated with an increased c-fos expression in inhibitory PV^+ cells (Jiao, et al., 2015) at late acquisition phase in all three mPFC subregions: ACC, PL and IL, as compared to early acquisition. This study suggests that lever-press avoidance expression is associated with an inhibitory activity in the mPFC.

Also, Bravo-Rivera et al., in accordance with their pharmacological inactivation results (Bravo-Rivera, et al., 2015), demonstrated that IEG up-regulation occurs in the PL but not the IL during persistent avoidance expression. Indeed, they showed that rats submitted to a platform-based avoidance paradigm, present a c-fos higher expression in the PL but not the IL (Bravo-Rivera, et al., 2015).

Consolidation of avoidance behavior

Consolidation of avoidance memories has been mainly investigated in passive avoidance paradigms. A main requirement of avoidance memories consolidation is the induction and the expression of IEGs in the prefrontal cortex. The up-regulation of c-fos and Arc (Zhang, et al., 2011) were induced after passive avoidance training in the PL and IL and Arc expression was also increased after training in the ACC (Zhang, et al., 2011). Anisomycin, a protein synthesis inhibitor, infused into the ACC or the PL/IL directly after training, blocked avoidance suggesting that the mPFC is crucial for consolidation of avoidance memory. Another study confirmed that passive avoidance consolidation is associated with increased c-fos in the ACC. Interestingly, avoidance extinction in this paradigm has been also associated with increased c-fos in the ACC (Huanga, et al., 2013). Altogether, these data suggest that the consolidation of avoidance memories seems to involve the ACC, PL and IL regions.

Extinction of avoidance behavior

Jiao et al. (Jiao, et al., 2015) showed that c-fos expression is higher in the mPFC PV^+ neurons during extinction of a lever-press avoidance task than after acquisition suggesting that the transition from acquisition to extinction is associated with a greater activity of inhibitory circuits in the mPFC (PL and IL).

Also consistently with pharmacological inactivation studies, successful extinction of avoidance behavior using two-way active avoidance has been shown to be

associated with an increased c-fos activation in the IL (Tapias-Espinosa, et al., 2018). Therefore the implication of the mPFC subregions in the extinction of avoidance behavior seems to be directly linked to the task used.

ii) Conditioned freezing

Conditioned freezing has been shown to be associated with an increase in IEG expression particularly in the mPFC. Smith and colleagues associated the re-exposure to a CS previously paired with a footshock with an increase in c-fos expression in the ACC (Smith, et al., 1992). However, subsequent studies have also shown that both PL and IL exhibit an increase in IEG expression following fear conditioning when freezing was used as a fear readout (Morrow, et al., 1999; Herry and Mons, 2004).

Freezing assessed in an aversive conditioning context was reported to be associated with an increased c-fos expression in both ACC and IL (Reis, et al., 2016).

As for extinction, several IEGs-based studies emphasized the implication of IL in the consolidation of extinction. Using the activity marker c-fos, it was shown that IL activity is increased in rodents that successfully retrieved (or consolidate) extinction (Knapska and Maren, 2009), but not in strains that are extinction-deficient (Hefner, et al., 2008).

In addition, IEG expression assessed during renewal of fear behavior was increased in the PL suggesting its' involvement in modulating fear expression in a context-dependent manner (Knapska and Maren, 2009).

IEG expression data, support the idea of a differential regulation of freezing behavior operated by the mPFC, with the dmPFC involved in the expression of freezing behavior and the vmPFC mediating consolidation of fear extinction.

iii) Freezing assessed in avoidance paradigm

The expression of c-fos correlated to freezing and avoidance in an avoidance task has also been quantified in several studies. In an unsignaled two-way active avoidance task, two groups of rats were categorized: good avoiders and bad avoiders. Freezing behavior was negatively correlated with IL activity while avoidance behavior was positively correlated with IL activity. More precisely, bad avoiders

presenting high freezing and low avoidance exhibited low IL activation, while good avoiders exhibiting high avoidance and low freezing presented high IL activation. Freezing persistence after chronic aversive exposure is associated with a low IL activity while avoidance expression is associated with a high avoidance expression (Martinez, et al., 2013).

Nevertheless, in the platform-based avoidance paradigm (Bravo-Rivera, et al., 2015) rats showing an increase in c-fos activity in PL but not IL during avoidance expression, also express very low levels of freezing responses. Hence, in this paradigm PL activity is associated with a high avoidance expression and low freezing expression after a chronic aversive avoidance paradigm.

IV. Periaqueductal gray matter

Being at the interface between the forebrain and the brainstem, the PAG is perfectly situated to receive and process sensory and mnemonic information from cortical and subcortical structures. It is also perfectly situated to control the activity of output brainstem structures regulating the organism's behavioral response. The PAG has been indeed described as regulating several key functions including emotional coping: defensive reactions namely freezing and avoidance (Fanselow, 1991; Carrive, 1993; Lovick, 1993; Vianna, et al., 2001; Vianna and Brandao, 2003; Mottaa, et al., 2017), analgesia (Behbehani, 1995 ; Zanoto De Luca-Vinhas, et al., 2006; Martins, et al., 2008; Heinricher, et al., 2009; Albutaihi, et al., 2004), autonomic activation and suppression such as changes in blood pressure and heart rate (Carrive and Bandler, 1991), vocalizations (Jurgens and Pratt, 1979; Gruber-Dujardin, 2010), maternal behavior (Behbehani, 1995 ; Klein, et al., 2014) as well as reward seeking (Mota-Ortiz, et al., 2009; Sobieraj, et al., 2016; Mottaa, et al., 2017). In this section, I will first review the gross anatomy of the PAG, its connections with main brain regions and then discuss the functional implications of this structure mainly in defensive behaviors.

1) PAG neuronal elements

The periaqueductal gray refers to the portion of the ventricular gray matter, which surrounds the midbrain aqueduct of Sylvius. Rostrally, the PAG is continuous with the periventricular gray matter surrounding the third ventricle while caudally it is in

continuity with the borders of the fourth ventricle. Most authors agree on a concentric organization of the PAG with an internal zone surrounding the aqueduct, and a peripheral zone containing an increased cell density. Nevertheless, there is a lack of agreement about the width of the concentric zones, and different parts have been described at the peripheral zone by several authors (Paxinos and Watson, 1986; Conti, et al., 1988; Reichling, et al., 1988). Based on its functional organization, the existence of four longitudinal columns has been suggested in the PAG, namely the dorsomedial (dmPAG), dorsolateral (dlPAG), lateral (lPAG), and ventrolateral (vlPAG) columns named relative to their position to the aqueduct (Carrive, 1993; Bandler and Shipley, 1994; Bandler and Keay, 1996). All the PAG columns are not present throughout the entire rostro-caudal axis, since the dlPAG is present throughout the rostral and intermediate part of the PAG but gradually diminishes at the caudal part of the PAG. The vlPAG neuronal column is present at the caudal half of the PAG. The columnar organization of the PAG appears to be of biological importance since it is conserved across mammalian species (Carrive and Morgan, 2012). Moreover, specific functions of the PAG also seem to be conserved in mammals. The PAG comprises diverse heterogeneous subpopulations of neurons with distinct neurochemical properties that regulate excitatory and inhibitory neurotransmission. Glutamate and aspartate play a critical role as the main excitatory neurotransmitters in the PAG, and their effects are mediated by the activation of ionotropic and metabotropic receptors (Nakanishi, et al., 1998). Glutamate and aspartate-expressing neurons are mainly present at the periphery of the PAG throughout the rostro-caudal axis as shown with immunoreactivity staining of glutamate, glutaminase, aspartate and aspartate amino-transferase in the PAG (Beitz and Williams, 1991). Very low proportions of immunoreactive neurons were found near the mesencephalic aqueduct. Electronic microscopy studies also showed that 95.2% of neurons expressing glutamate co-localize with aspartate throughout the rostro-caudal extent of the PAG in the cell body as well as the synaptic terminals suggesting that those two neurotransmitters can be possibly co-released (Beitz and Williams, 1991). Inhibitory control in the PAG is mainly ensured by GABAergic and glycinergic interneurons (Min, et al., 1996). Glycine inhibitory action in mature neurons is mediated by activating strychnine-sensitive glycine receptors and the opening of Cl^- channels, which results in hyperpolarization of postsynaptic neurons (Lynch, 2004). As for γ-Aminobutyric acid (GABA) inhibitory control in the PAG, it's

mediated through the activation of ionotropic $GABA_A$ and/or metabotropic $GABA_B$ receptors (Li, et al., 2017). Immunocytochemical detection of GAD (glutamic acid decarboxylase), an enzyme allowing the biosynthesis of the GABA molecule, revealed labeled cell bodies throughout the rostro-caudal axis of rats, rabbits and opossum PAG (Penny, et al., 1984; Mugnaini and Oertel, 1985; Barbaresi and Manfrini, 1988). The dmPAG, dlPAG as well as the vlPAG concentrate up to 50% of $GABA^+$ population, lPAG being relatively poor in GAD-immunoreactive cell bodies (Mugnaini and Oertel, 1985). Neurons in the PAG have been shown to express a wide variety of other neurotransmitters and peptides including dopamine (DA), acetylcholine (Ach), serotonin (5-HT), parvalbumin (PV), somatostation (SST), vasoactive intestinal polypeptide (VIP), Substance P, cholecystokinin, neuropeptide Y (NPY), calcitonin gene-related peptide, enkephalin, and galanin (Smith, et al., 1994). The PAG has been demonstrated to be reactive to opioids, cytokines and cannabinoids (Heinisch, 2011; Palazzo, 2010; Wilson-Poe, 2013). The PAG is therefore the substrate of action of some opioids (morphine, fentanyl) through the activation of mu-opioid receptors in the PAG inducing an anti-nociceptive effect (Morgan, et al., 2014). The PAG subdivisions also display some chemical specificity. For instance, the dlPAG contains neurons that express NADPH-diaphorase and synthesize nitric oxide (NO) (Onstott, et al., 1993), whereas the vlPAG contains a group of dopaminergic neurons (Lu, et al., 2006). In terms of morphology, comparative studies in rats, cats and monkeys revealed that the PAG is composed of five different cell types with somatas' diameter ranging from 10 µm to 45 µm. These studies described the presence of (i) fusiform neurons with one or several dendrites, (ii) multipolar neurons with a very large dendritic arborization, (iii) stellate cells, (iv) pyramidal cells with a very diffuse dendritic arborization and (v) ependymal cells at the border of the cerebral aqueduct (Hamilton, 1973; Mantyh, 1982; Beitz and Shephard, 1985).

2) PAG connectivity: afferents and efferents

a) Afferent projections to the PAG

The PAG receives afferents from the forebrain, brainstem, and sensory neurons of the dorsal horn and trigeminal nucleus; these inputs have a distinct pattern of connectivity in different PAG columns.

Indeed, the PAG receives afferent projections from numerous brainstem regions namely the nucleus reticularis lateralis, the nucleus raphe magnus, pallidus and obscurus, the nucleus reticularis pontis oralis and caudalis, the paralemniscal nucleus and the dorsal and ventral parabrachial nuclei (Marchand and Hagino, 1983). It receives a dense network of noradrenergic and adrenergic fibers originating in the ventrolateral (A1 and C1 groups) and dorsomedial (A2 and C3 groups) medulla (Herbert and Saper, 1992). Neurons of lamina I of the superficial dorsal horn and caudal trigeminal nucleus provide nociceptive information to the contralateral PAG. These projections target the lPAG and vlPAG columns and are somatotopically organized; trigeminal projections terminate in the rostral PAG, and cervical and lumbar spinal projections at progressively more caudal levels. Those afferents could be involved in the relay of sensory ascending information from the brainstem to the PAG allowing the initiation of the behaviors controlled by the PAG (Marchand and Hagino, 1983).

Another major source of projections to the PAG is the hypothalamus. Indeed, tracing experiments revealed that the PAG receives dense innervation from hypothalamic nuclei, more specifically the anterior hypothalamic nucleus (AHN), the ventromedial hypothalamic nucleus (VMH) and the dorsal premammillary nucleus (PMD). More precisely, the AHN contacts strongly all PAG subdivisions, whereas VMH and PMD inputs contact massively only the posterior part of dlPAG. Those connections are thought to be important in regulating motor autonomic responses (Canteras, et al., 1994; Wang, et al., 2015). Interestingly, a recent paper describes an inhibitory GABAergic lateral hypothalamus (LH) to lPAG and vlPAG projections driving predatory attack or fight behavior (Li, et al., 2018). This set of data is an evidence of long-range inhibitory projections received by the PAG region.

The amygdala projects directly to the PAG via the CeA, which sends direct GABAergic afferents preferentially to the vlPAG (Rizvi, et al., 1991; Oka, et al., 2008). Those GABAergic projections are thought to be a forebrain source of corticotropine

release factor (CRF), neurotensin, somatostatin, and substance P terminals in the vlPAG (Gray and Magnuson, 1992). A recent study revealed that direct projections from from CeL SST neurons to vlPAG drive fear responses (Penzo, et al., 2014).

The PAG also receives projections from different thalamic nuclei such as the medial and intralaminar nuclei (Krout and Loewy, 2000), which are involved in nociceptive transmission to higher cortical structures.

The main forebrain afferents to the PAG come from the lateral septum and mPFC (Marchand and Hagino, 1983; Beart, et al., 1990; Floyd, et al., 2000). In particular, the PL and ACC send a massive projection to the lPAG and dlPAG whereas projections from the vmPFC reach mostly the dlPAG and vlPAG. Also depending on the ACC rostro-caudal level, differential projections to the PAG are sent. It has been recently reported in mice that rostral ACC send dense projections to the dlPAG and the lPAG (Fillinger, et al., 2018) as compared to more caudal ACC. As for the ACC projections to the vlPAG, rostral ACC send moderate projections to the vlPAG whereas no anterogradely labeled projections have been detected from the caudal ACC to the vlPAG (Fillinger, et al., 2018).

Interestingly there is a segregation of the populations of cortical cells projecting to PAG and amygdala. The mPFC to PAG projecting cell bodies are located in deep cortical layers 5 and 6 as compared to the mPFC to BLA projectors located in non-overlapping superficial cortical layers (Harris and Shepherd, 2015; Rozeske and Herry, 2018) suggesting that these populations are more likely to modulate distinct fear responses or distinct fear-coding mechanisms, a field that still need to be investigated.

b) Efferent PAG projections

The PAG projections can be subdivided into ascending projections to the cortical and subcortical regions and descending projections to the brainstem and spinal cord. The PAG ascending projections target mainly the thalamus and hypothalamus (Cameron, et al., 1995). The dlPAG preferentially innervates the centrolateral and paraventricular thalamic nuclei whereas the vlPAG projects to the parafascicular and central medial thalamus (Cameron, et al., 1995). The dlPAG and the vlPAG projects preferentially to the anterior hypothalamus nucleus AHN and lateral hypothalamus LH respectively. Projections to cortical regions have not been identified to date.

As for the descending pathway originating from the PAG, with the exception of the dorsolateral column (dlPAG), all PAG columns project to the lower brainstem. The dlPAG neurons do not project directly to the medulla, but innervate densely the cuneiform nucleus (CNF), which is connected with the spinal cord (Mitchell, et al., 1988, Redgrave, et al., 1988). The dlPAG projects preferentially to the locus coeruleus (Cameron, et al., 1995), the principal center of noradrenergic synthesis in the brain located in the pons (dorsal pontine tegmentum). All other PAG columns project densely to the Barrington nucleus (pontine micturition center), the motor nuclei of the pontomedullary reticular formation, the parabrachial nucleus, and the nucleus retroambiguus, the rostral and caudal ventrolateral medulla (VLM), the rostral ventromedial medulla (RVM), including the nucleus raphe magnus (serotoninergic nucleus preferentially supplied by the vlPAG), and the nucleus raphe pallidus (Mantyh, 1983; Benarroch, 2012). Most of these targets are premotor centers that in turn project to sensory, motor, or autonomic nuclei of the brainstem and spinal cord (Holstege, et al., 1996).

Even if a clear anatomical dissection of the connections between the PAG and other brain areas have been already done, it is still not fully understood how nociceptive and passive/active fear responses pathways from the PAG to the medulla are segregated. A recent work from Tovote and colleagues (Tovote, et al., 2016), showed that excitatory vlPAG neurons projecting to the magnocellular nucleus of the medulla and receiving CeA inhibitory projections are disinhibited during freezing behavior. Nevertheless, additional work is required to dissect PAG mediated upstream and downstream circuits underpinning the selection of avoidance versus freezing behavior.

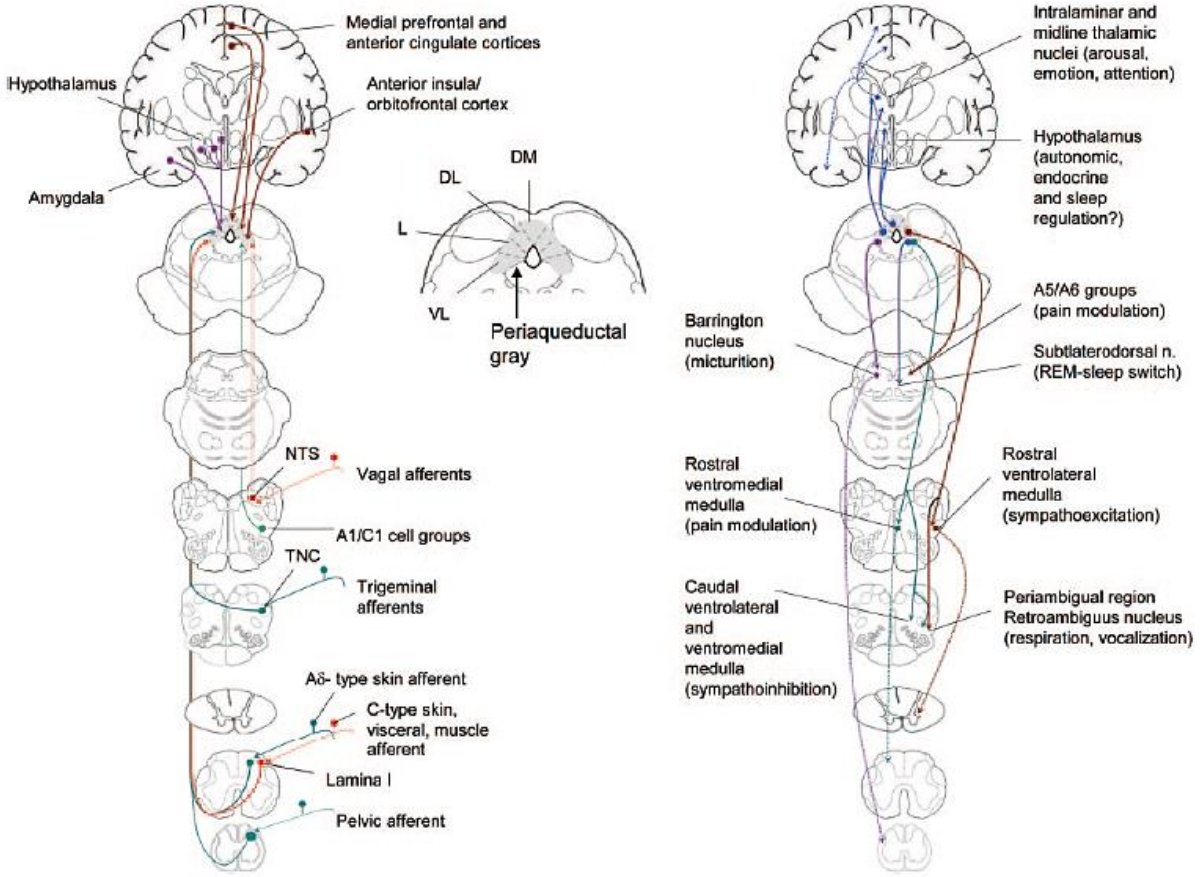

Figure 6. Schematic representation of afferents and efferents of the PAG in a human brain. Adapted from (Benarroch, 2012)

Left panel: PAG afferents. The PAG is subdivided into 4 functional columns: dorsomedial (DM), dorsolateral (DL), lateral (L), and ventrolateral (VL), which have distinct connections with other brain areas. The main forebrain sources of input to the PAG are the medial prefrontal cortex, anterior cingulate, the posterior orbitofrontal/anterior insular cortex. PAG receives inputs from the central nucleus of the amygdala; and essentially all regions of the hypothalamus. Brainstem inputs include vagal afferents relayed via the nucleus of the solitary tract (NTS) and catecholaminergic noradrenergic and adrenergic fibers originating in the A1/C1 groups of the ventrolateral medulla. Neurons of lamina I of the superficial dorsal horn and caudal trigeminal nucleus (TNC) provide nociceptive information to the contralateral PAG. **Right panel:** Forebrain projections target the intralaminar and midline nuclei of the thalamus, which serve as a gateway to the prefrontal cortex, amygdala, and basal ganglia, and several regions of the hypothalamus. Most brainstem targets of the PAG projections are premotor centers that in turn project to sensory, motor, or autonomic nuclei of the brainstem and spinal cord. These include the nucleus cuneiformis (notshown), locus coeruleus and pericoeruleus regions, Barrington nucleus (pontine micturition center), parabrachial nucleus, rostral ventromedial medulla (including the nucleus raphe magnus), rostral and caudal ventrolateral medulla, and nucleus retroambiguus. Via these projections, the PAG participates in micturition, regulation of REM sleep switch, pain modulation, cardiovascular responses to stress, and vocalization.

3) PAG-mediated effects on different behaviors

a) PAG-mediated pain modulation

Studies conducted in humans showed that the PAG is activated as an anticipation of painful stimuli (Yaguez, et al., 2005; Linnman, et al., 2011). Using fear conditioning

paradigms in humans, authors reported about PAG activation during a conditioned cue predictive of the delivery of an aversive unconditioned stimulus. Also the observation of aversive images lead to PAG activations in participants (Petrovic, et al., 2005). Indeed the different PAG columns receive inputs from nociceptive pathways. The lPAG and the dlPAG receive inputs from superficial nociceptors (primarily A-delta type), relayed by the superficial lamina of the spinal and spinal trigeminal nucleus **(Figure 6)**. In contrast, the vlPAG column receives convergent inputs from both the superficial and deep dorsal horn relaying nociceptive afferent information from visceral, muscle, and C-fiber skin nociceptors, as well as visceral inputs from the nucleus of the solitary tract and sacral spinal cord (Keay and Bandler, 2001; Lumb, 2004; Parry, et al., 2008).

Studies in rodents allowed to distinguish the contribution of the different PAG columns to pain modulation. The vlPAG is crucial in the descending control of the transmission of pain from the spinal cord dorsal horn. Several reports have indicated that electrical stimulation of the vlPAG selectively inhibits responses to noxious stimuli in a variety of pain test conditions (Reynolds, 1969; Harris, 1996). Consistent evidence has been provided for the regulation of this analgesic response by GABA, opioids, and serotonergic mechanisms (De Luca, et al., 2003). Indeed, it has been reported that injections of GABA antagonists (Fields, 2000), or the opioid antagonist naltrexone (Zanoto De Luca-Vinhas, et al., 2006), or the 5-HT2 antagonist ketanserin (Zanoto De Luca-Vinhas, et al., 2006) inhibit the analgesic effect elicited specifically by vlPAG stimulation. Electrical stimulation in the PAG (all columns) elicits analgesia (Reynolds, 1969) nevertheless only the one elicited by vlPAG stimulation is opioid-dependent (Castilho and Brandao, 2001; Castilho, et al., 2002). Indeed, the vlPAG descending direct projections to the rostral ventro-medial medulla (RVM) and the spinal cord dorsal horn is thought to be the main pathway mediating opioid-based analgesia (Loyd and Murphy, 2009). The vlPAG contains a high density of mu-opioid receptors (MOR) (Commons, et al., 2000), activated by their agonist injection, morphine, which is the most commonly prescribed opiate for persistent pain relief (Yaksh and Rudy, 1978). Also other peptides control this descending pain modulating pathway. In a recent study, Yin and colleagues, (Yin, et al., 2014) identified, a population of neurons projecting from the vlPAG to the RVM and co-expressing BDNF brain-derived neurotrophic factor and other neurotransmitters such as 5-HT, PV and substance P. It is thought that those $BDNF^{+}$ neurons participate in pain

modulation by enhancing the presynaptic release of neuroactive substances in the RVM. In summary, pain studies focused on the vlPAG since it directly projects to the medulla and seems to be the target structure for pain-related medication.

b) PAG-mediated modulation of defensive responses

The PAG is recognized as a downstream structure in neural networks specialized in the regulation of defensive behaviors mainly fight, flight/avoid and freezing behaviors. Depending on the stimulus' nature eliciting PAG activation, different columns and differential parts of those columns in the rostro-caudal axis are recruited. Indeed, a distinction should be made between (i) innate fear-elicited responses by naturalistic stimuli in ethological environments (for instance an odor, a sound or a threatening posture of a potential predator e.g. a mouse exposed to a cat or a snake in a complex labyrinth in an escapable (shelter) or non-escapable environment (Blanchard , et al., 1993; Coimbra, et al., 2017; Paschoalin-Maurin, et al., 2018) and (ii) conditioned fear-elicited responses (Moscarello and LeDoux, 2013; Bravo-Rivera, et al., 2014). Indeed both innate and conditioned threat-elicited responses include a common repertoire of behaviors namely avoidance, escape, and freezing. However, the type of stimulus used (innate versus conditioned) recruits PAG columns differentially. In the next section, I will present lesional, inactivation and IEG studies emphasizing the role of each PAG column in encoding both freezing and avoidance defensive behaviors induced by either innate or conditioned stimuli.

i) Lesional, stimulation and pharmacological studies

Following the discovery that stimulation of the PAG produces analgesia (Magoun, et al., 1937), it has been shown that the electrical stimulation of the PAG in humans evoked fearful sensations (Nashold, et al., 1969).

The dissociation of the role of PAG columns in the rostro-caudal axis in encoding passive versus active responses has been described very early. Early studies by Carrive and Bandler have shown that intra-dlPAG infusion of excitatory amino acids (EAA) induce fight-or-flight type of responses (Bandler, et al., 1985; Carrive and Bandler, 1991). Indeed EAA injections made within the rostral portions of dlPAG and lPAG columns evoke a confrontational defensive reaction, tachycardia, and hypertension (associated with decreased blood flow to limbs and viscera and increased blood flow to extracranial vascular beds). Also, electrical or chemical

stimulation of dmPAG and dlPAG produces defensive/rage like and predatory-attack behaviors that are thought to be driven by instinctive innate defensive responses to threat (Graeff, 1994; Behbehani, 1995; Zalcman and Siegel, 2006). EAA injections made within the caudal portions of the dlPAG and the lPAG evoke flight, tachycardia and hypertension (associated with decreased blood flow to visceral and extracranial vascular beds and increased blood flow to limbs). In contrast, EAA injections made within the vlPAG evoke cessation of all spontaneous activity (freezing), a decreased responsiveness to the environment (hyporeactivity), hypotension and bradycardia (Bandler and Depauli, 1991; Bandler and Carrive, 1988) **(Figure 7)**.

Nevertheless some studies reported that dlPAG lesions impact freezing behavior. More precisely, dlPAG and vlPAG lesions indicated that these two structures control opposite effects for both innate and conditioned stimuli. Indeed, it has been shown that lesions of the vlPAG strongly attenuated, whereas lesions of the dlPAG enhanced, unconditional freezing to a cat (De Oca, et al., 1998). In the same way, dlPAG lesions made before but not after fear conditioning and vlPAG lesions made before or after training respectively enhanced or impaired freezing behavior (De Oca, et al., 1998). These antagonist effects in term of freezing could be explained electrophysiologically by an inhibitory effect between both dlPAG and vlPAG as demonstrated in slice experiments (Chandler, et al., 1993).

Also a number of studies using classical fear conditioning with sound-, light- or odor-conditioned stimuli (CS) have shown that electrical or chemical stimulation of the dorsal PAG may be used as a useful US to support associative learning (Di Scala, et al., 1987; Kincheski, et al., 2012; Kim, et al., 2013). Those studies emphasized on the major role of the dPAG in the mediation of aversive associative fear learning and suggest that it is mediated via ascending projections to both the medial hypothalamic defensive circuit (Kincheski, et al., 2012) and the BLA (Kim, et al., 2013).

Also an interesting observation is that dlPAG and lPAG stimulation may evoke either freezing or escape and jumps; with low doses of NMDA producing freezing, and slightly higher doses trotting, galloping and jumping behaviors (Bittencourt, et al., 2004). Also small variations in the intensity (5–15 μA) of a sine-wave stimulus applied through a single electrode in the dlPAG or lPAG produced freezing at low magnitude and at slightly higher intensities gave rise to flight behavior (Schenberg, et al., 1990; Sudré, et al., 1993; Vargas, et al., 2000). Those data suggest that a higher intensity of stimulation is needed to induce active defensive behaviors and at low stimulation

intensities of lPAG and dlPAG passive defensive behavior is more likely to be induced. Mechanistically, this phenomenon could be linked to phasic versus tonic GABA inhibition, a hypothesis, which remains to be demonstrated.

In addition, a recent study reported that dPAG encodes both innate and learned defensive behaviors since electrical stimulation of the dPAG following fear-conditioning training produced brief bursts of activity followed by freezing whereas in a foraging task in a semi naturalistic environment, dPAG electrical stimulation evoked flight to the nest (Kim, et al., 2013).

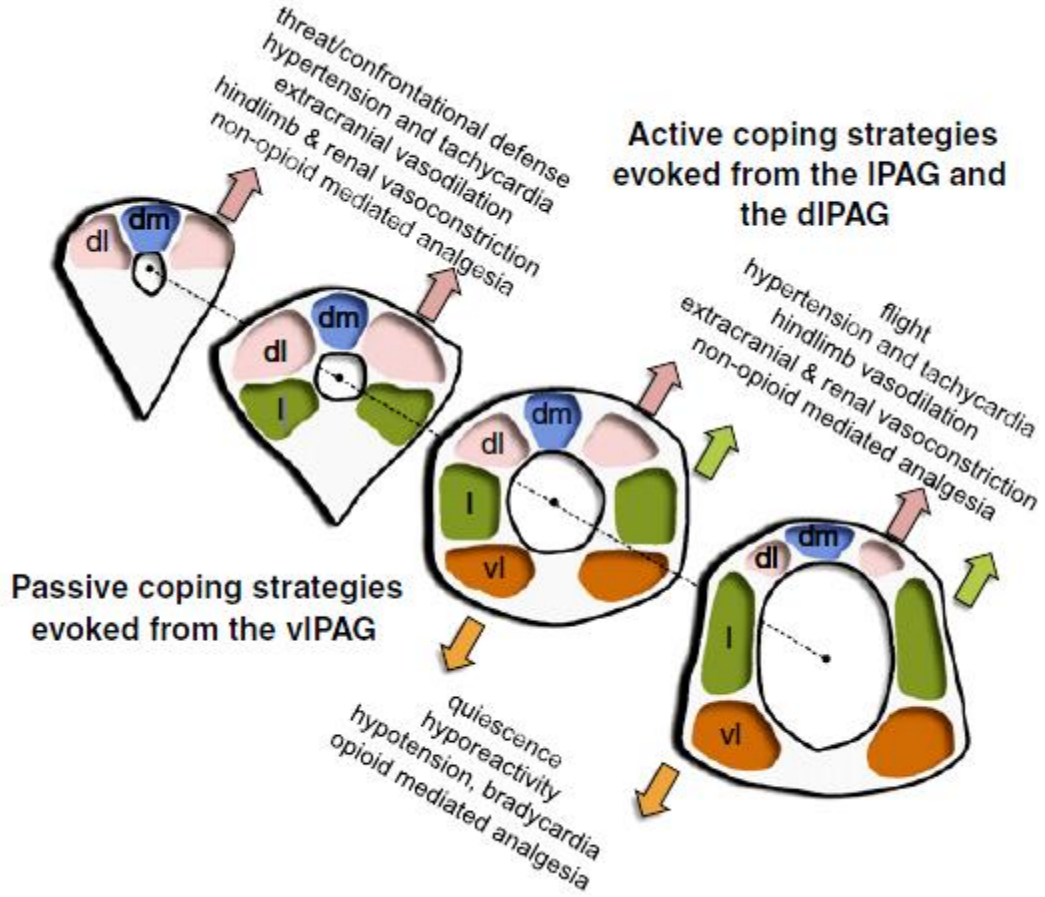

<u>Figure 7.</u> Schematic representation of the dorsomedial (blue), dorsolateral (pink), lateral (green) and ventrolateral (orange) neuronal columns within (from left to right) the rostral PAG, the intermediate PAG (two sections) and the caudal PAG

Evoked active and passive strategies, respectively, from the dl/lPAG and the vlPAG (grey color). Each of these strategies show specific somato-sensory evoked responses and differences in processing analgesia. Adapted from (Linnman, et al., 2012).

It's also interesting to note that the PAG has been shown to be implicated in driving another defensive innate behavior, which is predation. Indeed electrical stimulations in the PAG of cats induced "quit biting attacks" towards their prey (Siegel and Pott, 1988; Han, et al., 2017). It has been also reported that rostral lPAG lesions interfere

with prey hunting, leaving the animal without chasing or attacking the prey, without altering its' basal locomotion and regular feeding (Mota-Ortiz, et al., 2012).

ii) Neurotransmitters involved in encoding both active and passive defensive strategies

The PAG contains a large number of peptides and neurotransmitters. Nevertheless two candidates seem to be essential in encoding freezing and avoidance behaviors: GABA and serotonin.

GABA mediated modulation of active and passive defensive behaviors

The PAG contains a large network of GABAergic neurons (Reichling and Basbaum, 1990a; Reichling and Basbaum, 1990b) that regulate aversive defensive states. The GABA network present in all PAG columns (Behbehani, et al., 1990; Chiou, 2000) is tonically active since blockade of GABA receptors, in particular $GABA_A$ receptors by the antagonist bicuculline (Behbehani, et al., 1990), causes an increase in the firing rate of PAG neurons and produces aversive responses. Indeed, injections of the GABA antagonists bicuculline and picrotoxin into dlPAG induced flight behavior just like an electrical stimulation (Brandão, et al., 1982; Graeff, et al., 1986; Tomaz, et al., 1988). In contrast, direct stimulation of GABA receptors with locally administered GABA or the $GABA_A$ receptor agonist muscimol, raised the aversive threshold (defined as the lowest electrical current intensity inducing flight or escape behaviors) when applied to the dlPAG (Graeff, et al., 1986; Behbehani, et al., 1990). The $GABA_B$ receptor agonist baclofen was ineffective (Graeff, et al., 1986). Therefore, these evidence suggest that inhibition of the GABAergic network in the PAG could be one key mechanism for generating defensive behaviors.

Also, a broad inhibition of the PAG via infusions of the GABA agonist muscimol disrupts both Pavlovian associative fear learning and the transmission of the shock US related information to the BLA (Johansen, et al., 2010).

As for conditioned freezing expression, it has been reported that the administration of the $GABA_A$ agonist muscimol into the dlPAG reduced the expression of conditioned freezing (Reimer, et al., 2008). On the contrary, intra-dlPAG injections of glutamate or glutamatergic agonists enhanced conditioned freezing (Ferreira-Netto, et al., 2005; Reimer, et al., 2012). Freezing expression mediated by dlPAG is supported by glutamatergic dlPAG networks and freezing-mediated by dlPAG activation resulting

of NMDA-receptors activation is thought to be a preparatory response to flight (Ferreira-Netto, et al., 2005). One mechanism also described is the disinhibition of VGLUT2 neurons in the vlPAG projecting to motor centers and driving the expression of freezing. Therefore, the net effect for the expression of passive defensive behavior relies on direct projections from the vlPAG to motor effectors (Tovote, et al., 2016).

5-HT mediated modulation of active and passive defensive behaviors

An extensive early literature suggested that active and passive defensive behaviors are disrupted by interference with 5-HT function and these data are compatible with a role of 5-HT in conditioned fear (Deakin, 1983). Microinjections into the PAG of 5-HT itself, 5-methoxy dimethyltryptamine, 5-HT re-uptake blockers and the terminal autoreceptor antagonists propranolol and isomaltane have been reported to inhibit escape behavior evoked by the PAG stimulation (Kiser and Lebovitz, 1975; Schutz, et al., 1985; Audi, et al., 1988; Jenck, et al., 1989). Consistent with this idea, pharmacological elevation of serotonin levels in the PAG produces anti-aversive effects (Lovick, et al., 2000). The behavioral effects mediated by PAG's serotonin are mediated by at least two main receptors, 5-HT1A and 5-HT2 receptors (de Paula Soares and Zangrossi, 2009).

It is noteworthy that the majority of 5-HT2A labeled receptors in the PAG (90%), also show immunoreactivity to GABA (Griffiths and Lovick, 2002). These studies highlighted the implication of dPAG 5-HT in regulating anxiety and panic-related defensive responses (Zangrossi and Graeff, 2014) but not defensive avoidance behavior since all behavioral tests were made on an elevated-plus maze used to assess anxiety.

iii) Immediate-early genes studies

Following fear conditioning, several studies reported that the PAG is one of the main brain structures involved in defensive behaviors processing. Indeed, c-fos quantification following contextual fear conditioning showed an increased c-fos immunoreactivity in the vlPAG, as compared to controls, concomitant with high levels of freezing (Beck and Fibiger, 1995; Tulogdi, et al., 2012).

The $GABA_A$ receptors antagonist bicuculline infused in the dlPAG induced escape behavior whereas the glutamic-acid decarboxylase semicarbazide led to freezing

behavior. Freezing induced by chemo-disinhibited dlPAG was associated with an increase in c-fos expression in the dorsolateral nucleus of the thalamus (LD) and ventrolateral periaqueductal gray (vlPAG) whereas bicuculline-induced escape behavior was related to a widespread increase in c-fos labeling, notably in the columns of the periaqueductal gray, the hypothalamus nuclei, the CeA, the LD, the cuneiform nucleus (CnF) and the locus coeruleus (LC) (Borellia and Ferreira-Nettoa, 2005). This study supported the notion that freezing induced by dlPAG disinhibition activates only structures that are mainly involved in sensory processing, whereas escape behaviors activates structures involved in both sensory processing and motor output (Borellia and Ferreira-Nettoa, 2005). It has also been shown by the same group that freezing induced by NMDA-infusion in the dlPAG induced c-fos expression in output structures of defensive behaviors, namely the dlPAG and the cuneiform nucleus (Ferreira-Netto, et al., 2005).

C-fos studies were also used to investigate the implication of the PAG in defensive innate behaviors expressed in ethological environments when animals are confronted to predators, for example hamsters exposed to snakes (Paschoalin-Maurin, et al., 2018) or rats confronted with cats (Canteras and Got, 1999; Comoli, et al., 2003). Those studies showed that animals exhibited defensive responses such as flat back approaches, defensive freezing, and escape defensive responses that were associated with and increase c-fos immunoreactivity more pronounced in rostral divisions of the dmPAG and dlPAG compared to intermediate and caudal divisions.
All the above data suggest a dual role of the PAG in the expression of defensive fear behaviors depending on the nature of the threat. In the case of defensive responses elicited by natural predators, the rostral dmPAG/dlPAG seem to be recruited, whereas defensive responses induced by conditioned CS can recruit both vlPAG and dlPAG. The dlPAG seem to be recruited depending on the stimulation intensity during both escape and freezing behaviors while vlPAG activation is exclusively correlated with freezing expression.

iv) PAG optogenetic manipulation effects on freezing and avoidance

Using optogenetic tools several pathways connecting the PAG have been demonstrated to be causally driving defensive active and passive behaviors. Indeed,

hypothalamic nuclei afferents to the PAG have been shown to encode both active and passive defensive strategies. On one hand, optogenetic activation of a PAG-afferent originating from steroidogenic factor 1 (SF1)-expressing neurons in the dorsomedial and central parts of the ventro-medial hypothalamus VMH (VMHdm/c) projecting to the dlPAG induced freezing but not avoidance behavior supporting the role of dlPAG in encoding freezing behavior (Wang, et al., 2015).

On the other hand, predation has been demonstrated to be driven by the l/vlPAG with optogenetic experiments, confirming c-fos and lesional data. More precisely it has been shown that activating GABAergic projections from the LH to the l/vlPAG induced chasing, attacking and biting behaviors in mice chasing crickets while optogenetically inactivating this pathway blocks the predatory behavior (Li, et al., 2018).

Also l/vlPAG optogenetic activation has been demonstrated to induce innate escape behavior from a moving food-dish in mice (Li, et al., 2018). Activating glutamatergic projections from LH to l/vlPAG induced a high-speed running in the opposite direction of the moving object and occasional jumping in an open-field arena (Li, et al., 2018).

The role of CeA to PAG descending projections in encoding defensive behaviors have been recently also investigated. More particularly, a tripartite pathway has been optogenetically characterized by Tovote and colleagues (Tovote, et al., 2016). This circuit is composed of CeA inhibitory neurons projecting to the vlPAG, which through a disinhibition process activate glutamatergic descending pathway from the vlPAG to pre-motor targets in the medulla (Tovote, et al., 2016). Local projections in the PAG namely glutamatergic projections from dlPAG, which excite inhibitory vlPAG cells, are described in this paper and are hypothesized to mediate flight behavior (Tovote, et al., 2016).

To investigate the question of the neural substrates mediating the switch between active and passive fear responses, the same group (Fadok, et al., 2017), identified a population of neurons in the CeL expressing CRF. Activation of this cell population promoted flight behavior. These CRF^+ cells mediated flight behavior by inhibiting SST^+ CeL neurons mediating freezing behavior. Interestingly, CRF^+ neurons project directly to the PAG (all columns) which could be a possible descending pathway mediating the switch between avoidance and freezing behavior (Fadok, et al., 2017). One hypothesis that will deserve additional investigations suggests that CRF^+ cells project to the dlPAG and promote disinhibition of glutamatergic neurons projecting to

the vlPAG. This disinhibition would allow flight behavior as shown in Tovote et al., a study in which the authors directly manipulated this glutamergic cell population (Tovote, et al., 2016). Other descending PAG-projections, notably the ones emanating from the prefrontal cortex that could directly regulate defensive responses, have been overlooked in the past decades and will require further investigations. Nevertheless, we recently reported that PL to l/vlPAG descending projections are both necessary and sufficient in mediating contextual fear discrimination in the sense that activating this pathway in a fearful context blocks freezing whereas optogenetically inactivating it in a non-fearful context promotes freezing expression (Rozeske, et al., 2018). Nevertheless, the manipulation of this pathway did not affect avoidance behavior as tested with place-avoidance test. Therefore prefrontal projections to other columns of the PAG mainly the dlPAG known to be encoding more active defensive responses are worth to test.

V. Amygdala

The third structure reported to be crucial in managing both avoidance and freezing defensive behaviors is the amygdala. The first most convincing evidence of amygdala's role in emotional coping particularly fear coping, came from the work by Kluver and Bucy (Kluver and Bucy, 1937). They found that the bilateral removal of the medial temporal lobes in rhesus monkeys resulted in abnormal emotional behavior (Kluver and Bucy, 1937). Before the temporal lobectomy, the monkeys were fearful and withdrew from their human handlers. After the surgical procedure, however, the monkeys no longer feared human beings and did not display aggression. Importantly, they also showed interest in exploring objects in the environment (Kluver and Bucy, 1937). Because Kluver and Bucy's lesions included many brain structures such as the hippocampus, amygdala, and temporal neocortex, Weiskrantz (Weiskrantz, 1956) reexamined lesions restricted to the amygdala and observed the same pattern of behavior, especially the loss of fear. These behavioral phenomena, following amygdala lesions, have been observed in both rodents (Blanchard and Blanchard, 1972; LeDoux, et al., 1990) and humans (Adolphs, et al., 1994) revealing a strong conservation of amygdala's functions across species, most notably an impairment in the recognition of fearful stimuli in humans, and in a type of emotional learning: fear conditioning in rodents. In addition to lesion studies, it has

been reported that amygdala seizures induce fear-like behaviors (Depaulis, et al., 1997). Those early results were convincing enough to attribute to the amygdala one of its' main functions namely emotional regulation. In this section, I will first introduce the gross anatomy of the amygdala with its' main connections then I will discuss the functional roles of amygdala in encoding freezing and avoidance behaviors through mainly lesional, pharmacological, and optogenetic manipulations studies.

1) Amygdala gross anatomy

The amygdala is an almond shaped structure located in the temporal lobe. It is composed of a complex network of interconnected subnuclei mainly the basolateral complex of the amygdala (BLA) composed by the lateral (LA), basal (BA) and basomedial (BM) cell groups and the central nucleus of the amygdala (CeA) composed by a lateral (CeL) subdivision and a medial (CeM) subdivision. The BLA consists of glutamatergic principal neurons and inhibitory interneurons which makes it of a similar neuronal composition as compared to the cortex, being the reason behind its' labelling ''the cortical like amygdala''. CeA neurons are primarily GABAergic, they have the same origin as striatal neurons (Medina, et al., 2004; Garcia-Lopez, et al., 2008) and are morphologically, histochemically and electrophysiologically similar to striatal medium spiny projection neurons (Martina, et al., 1999; Schiess, et al., 1999). Several clusters of GABAergic neurons, termed the intercalated cells, are also found in the amygdala. Most of them form an interface between the BLA and the CeA, providing an important source of inhibition (Ehrlich, et al., 2009). Intercalated cells are a source of feedforward inhibition to neurons in the CeA, and are thought to play a central role in fear extinction (Likhtik, et al., 2008). For the interested reader I would propose to check the following reviews resuming the amygdalar anatomy and main functions (Gründemann et al., 2015; Janak and Tye, 2015; Yan and Wang, 2017; Fadok, et al., 2018; Krabbe, et al., 2018; Yizhar and Klavir, 2018).

a) BLA neuronal characterization

Neuronal morphology and physiology in both BLA and CeA are distinct. In the BLA two classes of neurons have been described. The first type comprises ~ 80% of the cell population (Sah, et al., 2003) and has been described as pyramidal-like or projections neurons (Mcdonald, 1982). The second category of neurons described in

the BLA are GABAergic interneurons ~ 20% of the BLA neuronal populations (Sah, et al., 2003) which axons branch several times and thus have a “cloud of axonal collaterals and terminals” near the cell body (Millhouse and Deolmos, 1983).

Interneurons in the BLA are also characterized by the expression of specific calcium binding proteins or neuropeptides. The two primary non-overlapping groups of interneurons are those that express calbindin (CB) accounting for 50% of BLA interneurons and those that express calretinin (CR) accounting for about 20% of the remaining BLA INs (Kemppainen and Pitkanen, 2000). Some CR^+ INs express vasoactive intestinal peptide (VIP) and/or cholecystokinin (CCK) with some overlap between these two subgroups (Mascagni and McDonald, 2003; McDonald and Mascagni, 2002), while CB^+ interneurons can be subdivided into non-overlapping groups that express either PV, somatostatin (SST) or CCK (McDonald and Mascagni, 2002; Mascagni and McDonald, 2003; Davila, et al., 2008). Those diverse interneurons in the BLA synapse at diverse targets. CCK^+ and PV^+ BLA interneurons synapse with the somata of BLA pyramidal cells as well as proximal dendrites, while SST^+ terminals are more often found in contact with distal dendrites (McDonald and Mascagni, 2001; Muller, et al., 2006; Muller, et al., 2007). Interneurons in the BLA also innervate other local circuit interneurons: VIP^+ INs heavily target CB^+ INs (Muller, et al., 2003) while a small percentage of SST^+ terminals target VIP^+ or PV^+ INs (Muller, et al., 2007). Each interneuronal type (VIP^+, PV^+, SST^+ and CB^+) also forms synapses with other INs within their own group (Muller, et al., 2003; Muller, et al., 2005; Muller, et al., 2007).

From an electrophysiological standpoint, within the BLA, principal cells have low resting firing rates (Pare and Gaudreau, 1996) and single interneurons can powerfully block activity in principal neurons (Woodruff and Sah, 2007). Electrophysiological analyses have identified at least 6 distinct types of firing properties of INs in the BLA (Spampanato, et al., 2011) **(Figure 8)**. Those firing properties are similar to those found in cortical INs (Ascoli, et al., 2008) but different from those of GABAergic neurons in the CeA (Dumont, et al., 2002). A subpopulation of PV^+ INs can be easily identified by their firing properties. They fire short duration action potentials with a half-width measured at ~ 0.5 ms with a frequency going up to 100 Hz (Rainnie, et al., 2006). These PV^+ IN are labelled fast-spiking INs. However, a small subtype of PV^+ INs also exhibits regular firing and accommodating phenotypes (Rainnie, et al., 2006).

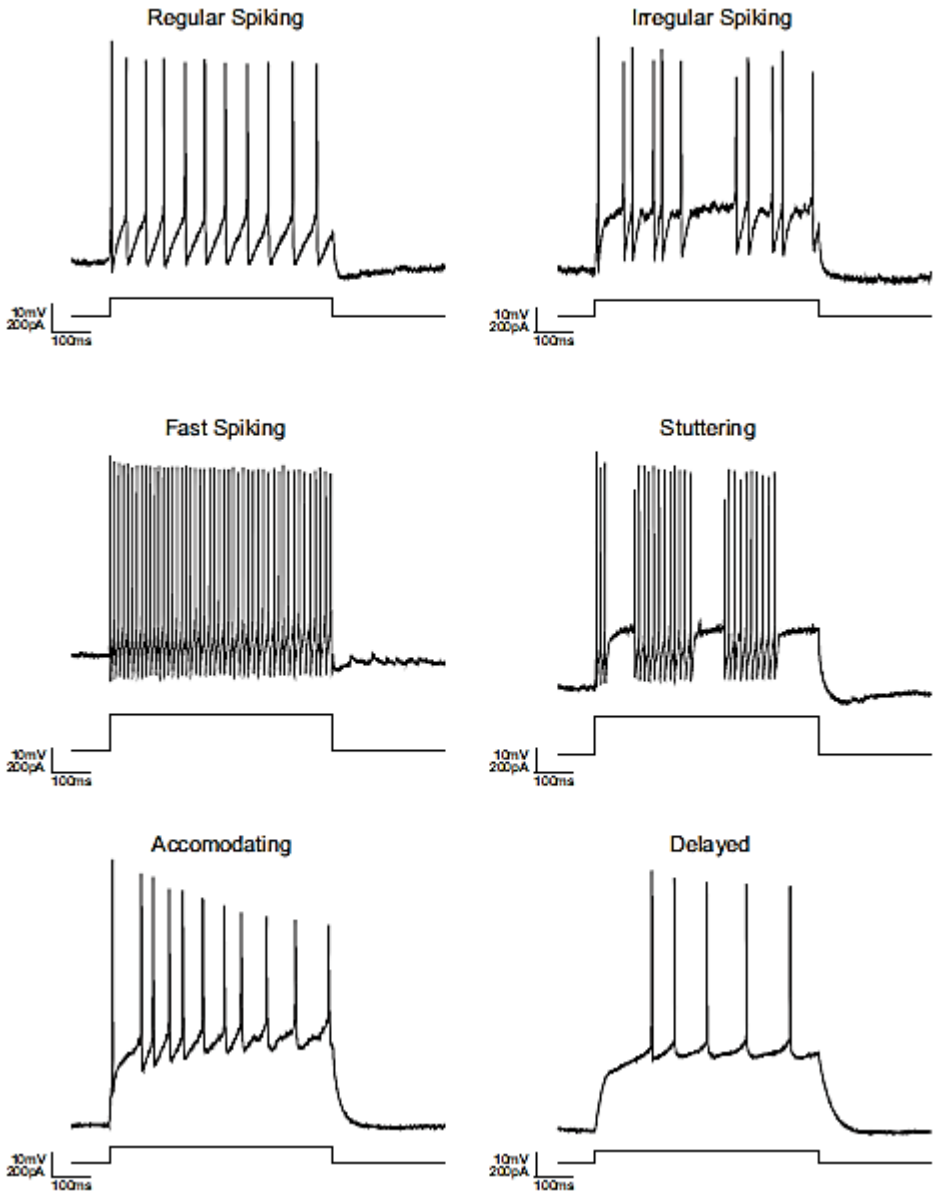

Figure 8. Adapted from (Spampanato, et al., 2011). The six main firing patterns of INs in the BLA recorded using in-vitro slices of BLA of a transgenic GAD67-EGFP mouse
Action potentials were elicited by supra-threshold square pulse current injections shown below the recording for each cell. The firing properties represented here resemble those observed in recordings from cortical IN.

PV^+ INs in the BLA are characterized by gap junctions connecting together groups of PV^+ INs with similar electrophysiological properties, allowing them to act in concert in order to modulate BLA activity. PV^+ INs synchronize the firing rate of PNs and are capable of altering the phase of this synchrony (Woodruff and Sah, 2007; Courtin, et al., 2014). As for CCK^+ BLA INs, they fire broad action potentials at low frequencies and most undergo significant spike frequency adaptation during sustained depolarizations (Jasnow, et al., 2009).

b) CeA neuronal characterization

The CeA is mainly composed of GABAergic interneurons, however there are slight differences between cells in the CeL and the CeM. The CeL contains medium-sized spine-dense neurons that branch prolifically. Neurons in the CeM have larger soma than the CeL ones, yet do not contain many dendritic spines and branch sparsely (Sah, et al., 2003).

Immunohistochemical studies have demonstrated the presence of a wide variety of peptides (enkephalin, neurotensin, corticotropin, oxytocin and vasopressin releasing hormone) and receptors expression in the CeA (Roberts, et al., 1982; Veinante, et al., 1997; Huber, et al., 2005). In addition, two distinct populations of neurons within the CeL have been identified based on the expression of the protein kinase delta (PKC-Δ). It has been demonstrated that PKC-Δ positive and PKC-Δ negative cells make reciprocal inhibitory connections with one another and that PKC-Δ positive cells project to the CeM (Ciocchi, et al., 2010; Haubensak, et al., 2010). Therefore, in the CeA the existence of inhibitory local circuits within the CeL and inhibitory projections from the CeL to the CeM have been revealed. It is important to notice that long-range projections from the CeA are predominantly GABAergic compared to the BLA projections, which are mainly glutamatergic (Davis, et al., 1994; McDonald, et al., 2012). Finally, apart from the CeL and CeM, the basal nucleus of the stria terminalis (BNST) is considered as an amygdaloid nucleus more precisely as an extension rostrally and medially of the central amygdala, called also the ‘’extended amygdala’’ (Alheid, et al., 1995). For more details about the anatomy and the functions of the extended amygdala I would suggest for the reader to check the following reviews (Stamatakis, et al., 2014; Fox, et al., 2015; Lebow and Chen, 2016; Fox and Shackman, 2017).

2) Amygdala connections

Anterograde or retrograde tracers have been injected into various amygdaloid, cortical, and subcortical regions revealing that each amygdaloid nucleus receives inputs from multiple yet distinct brain regions. Efferent projections from the amygdala are also widespread and include both cortical and subcortical regions.

a) Afferents

The amygdala receives two types of inputs: (i) the ones carrying information from sensory areas and structures related to memory systems: the cortical and thalamic inputs and (ii) the ones arising from areas involved in behavior and autonomic systems processing: hypothalamic and brainstem inputs.

The prefrontal cortex is a major source of cortical projections to the amygdala. Information from all sensory modalities critical for cognitive processes, including associative learning and decision making, converge in the prefrontal cortical areas (McDonald, 1998; Seymour and Dolan, 2008). The basal nucleus (BA) is the main target of afferents from the prefrontal cortex, although projections to the LA as well as the CeA have also been described (McDonald, et al., 1996). PFC projections to the BLA more specifically to the BA mainly arise from the ACC and PL (Cassell and Wright, 1986). The CeA and the LA were reported to receive connections mainly from the IL (McDonald, et al. 1996; McDonald , 1991; Shinonaga, et al., 1994; Hoover and Vertes, 2007). Sensory inputs terminate mainly in the LA (LeDoux, et al., 1990). Auditory inputs, which are thought to be particularly relevant during fear conditioning, reach the amygdala from association areas rather than primary cortex and target mainly the LA (Shi and Cassell, 1997). As for subcortical auditory inputs, they arise from the thalamic medial geniculate nucleus and also target the LA, which in turn receives projections from the inferior colliculus essential in processing acoustic sensory stimuli (LeDoux, et al., 1990). The CeA and the BLA also receive inputs from the thalamus mainly the thalamic paraventricular nucleus, which in turn receives massive inputs from the hypothalamus (Moga, et al., 1995). Moreover, the hippocampus, which conveys contextual information, projects to the amygdala, with the BA being the main target and other amygdaloid nuclei being sparsely innervated (Canteras and Swanson, 1992).

For brainstem inputs, the CeA is a major target for a variety of inputs from the midbrain, pons, and medulla, while the other nuclei receive few or no inputs from these areas (Pitkanen, et al., 2000).

b) Efferents

The amygdala projects to a widespread variety of structures in the forebrain, midbrain and brainstem modulating both sensory and motor processing of fear-related responses. Efferents from the BLA arise from pyramidal-like neurons and are thought to be glutamatergic (Paré, et al., 1995). The BLA projects mainly to the striatum including the nucleus accumbens and caudate putamen (McDonald, 1991), which are thought to be substantial in mediating avoidance of aversive stimuli. Direct projections from the BLA to the hypothalamus, mainly the rostral hypothalamus (including the medial preoptic and anterior hypothalamic areas), have been described and are thought to mediate the processing of innate defensive behaviors (Petrovich, et al., 2001). The BLA presents direct and indirect projections to the hippocampus. BLA projects directly to the ventral hippocampus (Petrovich, et al., 2001; Huff, et al., 2016) and indirectly through its projections to the entorhinal cortex, which in turn projects to the hippocampal formation (mainly the dentate gyrus of the dorsal hippocampus) known to be critical in contextual processing (Sparta, et al., 2014). The Basal nucleus (BA) projects also to the prefrontal cortex (ACC, PL and IL) (Sah, et al., 2003; Hoover and Vertes, 2007). Indeed, extensive direct projections to the mPFC from the BLA but not from the CeA have been described (Hoover and Vertes, 2007). These pathways are organized rostro-caudally in the sense that the anterior BLA projects preferentially to the dorsal mPFC (ACC and dorsal PL) while the posterior BLA projects more heavily to the ventral mPFC (ventral PL and IL) (Reppucci and Petrovich, 2016). More precisely, the LA is massively connected with the infralimbic cortex (IL) whereas the BA is mostly connected with the anterior cingulate cortex (ACC) and the prelimbic cortex (PL) (Hoover and Vertes, 2007).

As for the CeA, it projects extensively to a variety of extrinsic structures regulating the different components of fear behavioral outputs. The CeA projects densely to the vlPAG thought to mediate both analgesia and freezing behavior (Behbehani, 1995; Tovote, et al., 2015). It also sends direct projections to the lateral hypothalamus, which is involved in the activation of the sympathetic autonomic nervous system during fear leading to tachycardia, pupil dilatation, and blood pressure elevation (LeDoux, et al., 1988).

The CeA projects directly and indirectly to the brainstem contributing in the regulation of several responses expressed during fear. Direct projections from the CeA to the dorsal motor nucleus of the vagus, nucleus of the solitary tract and ventrolateral medulla may be involved in the regulation of heart rate and blood pressure, (Schwaber, et al., 1982). Projections to the parabrachial nucleus may be involved in respiratory as well as cardiovascular changes during fear and pain modulation (Gauriau and Bernard, 2002). Indirect projections of the CeA to the paraventricular nucleus of the thalamus (PVT) via the BNST and preoptic area may mediate the neuroendocrine responses (corticosterone release) to fearful or stressful stimuli (Davis and Whalen, 2001). Interestingly it was reported that SST^{+} cells project directly from the CeL to the PVT and that this pathway mediate fear acquisition (Li, et al., 2013).

Also, the CeA send projections to other neuroendocrine systems essential in defensive responses modulation mainly the noradrenergic locus coeruleus, the dopaminergic substantia nigra and the ventral tegmental area, the serotonergic dorsal raphe, and the cholinergic nucleus basalis in the substantia innominata (Davis and Whalen, 2001; Sah, et al., 2003).

All the described above extrinsic projections from the CeA are thought to arise from GABAergic CeM neurons (Pitkanen and Amaral, 1994; Sah, et al., 2003, Li et al, 2013). An important thing to note is that tracing studies have shown that many afferents to the CeA may also pass through the CeA to terminate in the BNST (Davis and Whalen, 2001). The postero-lateral division of the BNST has also many of the same described above hypothalamic and brainstem projections as the CeA. Therefore afferents activating the CeA and its' target structures may, by the same way, activate the BNST and its' target structures (Davis and Whalen, 2001).

c) Intra-amygdala connectivity

Several studies reported the existence of intra- and inter-nuclear connections in the amygdala. The general view is that sensory information enters the amygdala through the basolateral nuclei, is processed locally, and then flows from the CeL projecting to the CeM, which is thought to be the output nucleus of the amygdala (Pitkanen, et al., 1997).

More precisely, sensory inputs enter the LA, which sends extensive projections to the BA and the CeA (Pitkanen, et al., 1995). LA projections to the BA are reciprocal

whereas those sent to the CeA are unidirectional (Jolkkonen and Pitkanen, 1998). Most projections to and from the LA are excitatory (Savander, et al., 1997). The BA sends also direct glutamatergic projections to the CeM (Savander, et al., 1995). As for the CeA, it receives projections from all the other amygdaloid nuclei but sends back very sparce intra-amygdaloid connections (Jolkkonen and Pitkanen, 1998). It is also notable that the main inter-nuclear inputs to the CeA synapse within the CeM (Jolkkonen and Pitkanen, 1998). As for the CeL, it projects mainly to the CeM and receives very few connections from amygdaloid nuclei (Jolkkonen and Pitkanen, 1998). Nevertheless, it is important to note that the CeL also sends extrinsic reciprocal direct connections to the PVT (Li, et al., 2013; Penzo, et al., 2014; Penzo, et al., 2015) and unidirectional to the lPAG (Penzo, et al., 2014) that are thought to control defensive behaviors (Li, et al., 2013; Penzo, et al., 2015). The CeL also receives direct inputs from cortical and subcortical structures (Pitkanen, et al., 2000) suggesting that the CeL might also be an integration amygdaloid site of incoming information to the amygdala and an output amygdaloid nucleus and not only a rely site of the information coming from the BLA (Pitkanen, et al., 2000).

3) Amygdala encoding defensive behaviors

a) Acquisition and consolidation of freezing

The implication of amygdala nuclei in the acquisition of conditioned freezing behavior has been largely studied. The current model of amygdala implication in fear learning postulates that the association between the CS and the US is made in the LA which is thought to be critical for both acquisition and consolidation of fear learning. The process of associative fear memory formation in the LA is thought to be mediated by a change of the synaptic plasticity in the LA. First, functional reversible inactivation or lesions of the LA during conditioning impairs the acquisition of auditory and contextual fear conditioned passive freezing responses (Helmstetter and Bellgowan, 1994; Muller, et al., 1997; Wilensky, et al., 1999; Goosens and Maren, 2001; Koo, et al., 2004).

Johansen and colleagues (Johansen et al., 2010) assessed that optogenetic activation of pyramidal neurons in the LA along with presentation of a tone is sufficient to produce fear learning. They showed that fear memory was acquired only

when the tone CS preceded the optical stimulation US indicating that the LA is a site of the associative learning between the CS and the US (Johansen, et al., 2010). Also, optogenetic inhibition of glutamatergic projections from the BLA to the entorhinal cortex (EC) (part of the hippocampal formation) during the acquisition phase of contextual fear but not during the expression of contextual freezing impaired freezing behavior, suggesting that the BLA-to-EC glutamatergic pathway plays an important role in the acquisition of contextual fear conditioning (Sparta, et al., 2014).

The LA has been also demonstrated to be the site of Hebbian plasticity (Hebb, 1949) occurring during fear conditioning, which provides a neural mechanism for long-term memory storage. Hebb postulates that when a neutral CS is paired with a US, neurons that respond to the CS become activated simultaneously with neurons that respond to the US (Hebb, 1949). After CS-US pairings, synaptic connections between these neural populations should become stronger, thereby storing a memory for the association between the CS and the US. Hebb's requirements for plasticity to occur have been fulfilled in the LA since it has been demonstrated that auditory information conveyed by thalamic and cortical inputs and nociceptive US information project to the same neurons in the LA (Romanski, et al., 1993). Also, CS evoked neural responses in the LA are enhanced when the CS is paired with the US (Quirk, et al., 1995; Rogan, et al., 1997; Repa, et al., 2001) supporting the hypothesis by which CS and US concomitant presentation leads to the strengthening of the synaptic connections activated by the CS **(Figure 9)**.

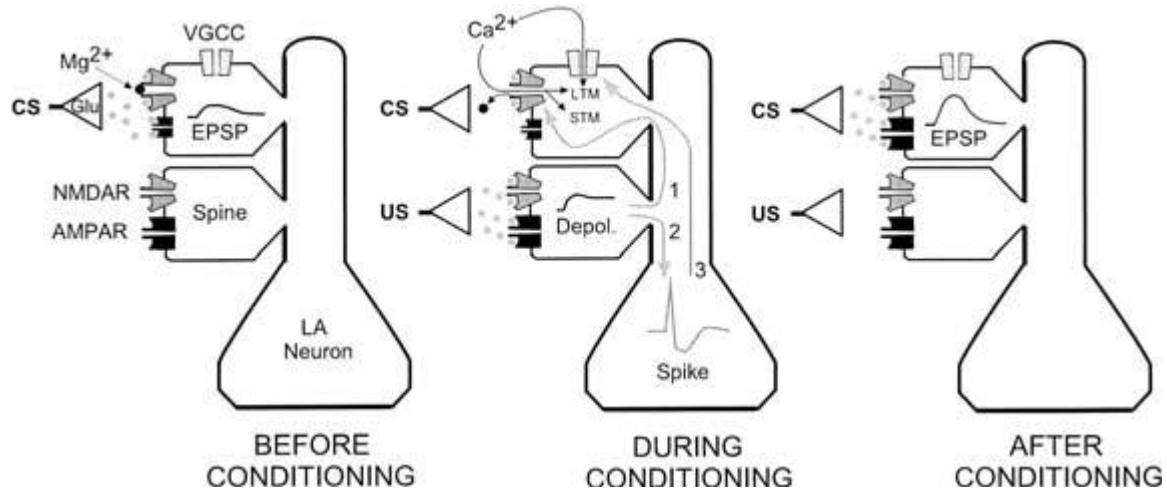

Figure 9. Postsynaptic currents in the LA eliciting plasticity during fear conditioning
Before fear conditioning, when the CS is presented alone, glutamate is released and binds onto AMPA-R and NMDA-R inducing a small excitatory postsynaptic potential (EPSP) at the postsynaptic LA neurons. During conditioning when the US is now paired to the CS, the magnesium block fixed at NMDA-R is removed allowing the influx of calcium into the synapses through NMDA-R producing a short-term memory (STM) which is stabilized into a long-term memory (LTM) by the activation of VGCC and the influx of calcium through both NMDA-R and VGCC. As a result of the LTP induced in the LA by fear conditioning, the CS alone elicits a larger EPSP.

The LA is also thought to be the site of fear memory consolidation, a process by which a short-term memory (STM) is transformed, over time, into a stable long-term memory (LTM) (Schafe, et al., 2001). Following CS–US pairing, the activation of intracellular signaling cascades allowing the transcription of genes and subsequent synthesis of the relevant proteins **(Figure 10)** leads to LTM formation (Stevens, 1994). The infusion intra-LA of inhibitors of protein and RNA synthesis disrupts the consolidation of fear conditioning implying that the LA is necessary for fear memories consolidation (Bailey, et al., 1999; Schafe and LeDoux, 2000). It has been also shown that calcium entry through both NMDARs and voltage-gated calcium channels VGCCs is required to initiate the molecular processes that consolidate synaptic changes into a long-term memory (Blair, et al., 2001).

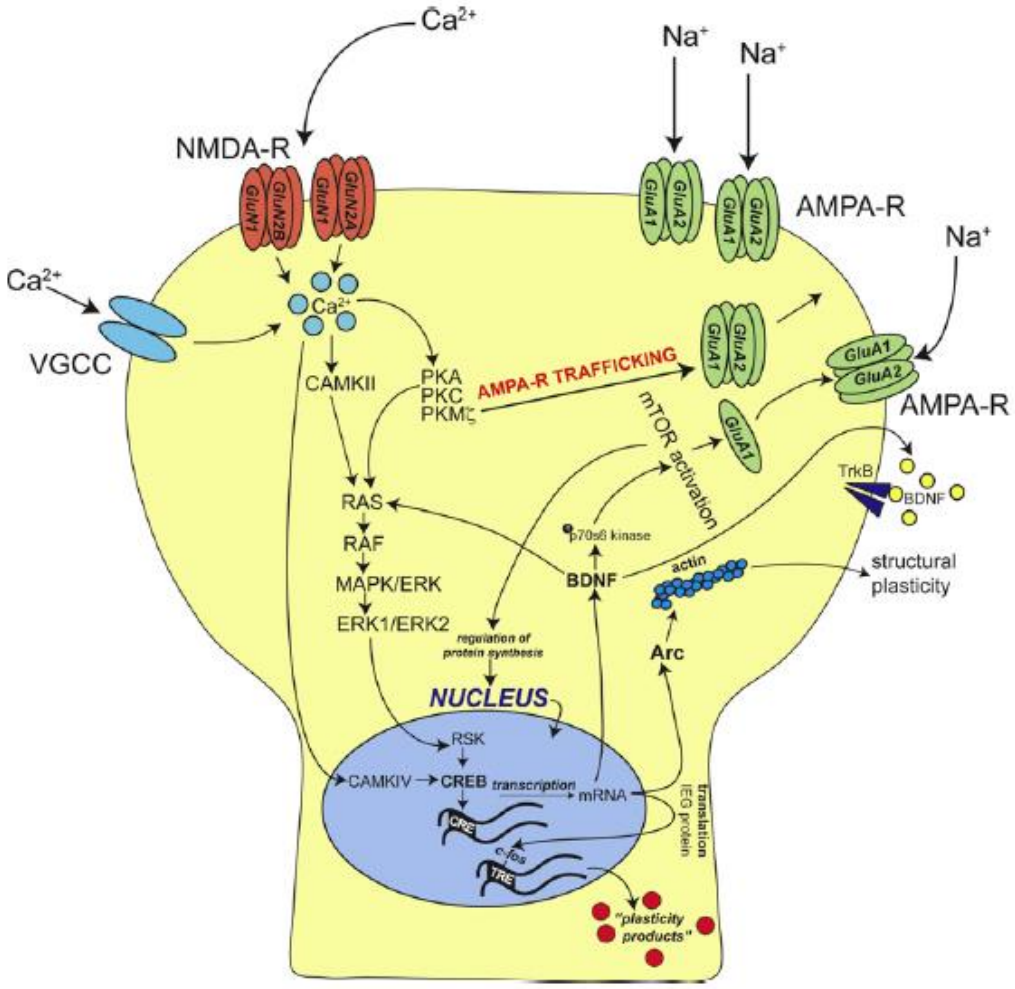

<u>Figure 10</u> Signal transduction pathways underlying synaptic plasticity occurring during fear learning.

The fixation of glutamate (not shown) on AMPA and NMDA receptors mediating postsynaptic depolarization allows the entry into the cell of calcium through NMDA receptors (NMMDA-R) and voltage gated calcium channels (VGCC). Intracellular calcium is used to several processes initiating synaptic plasticity: (i) AMPA-R trafficking allowing the increase in number of AMPA-R expressed on the membranes surface, (ii) the activation of several proteins which activity depends on the calcium availability such as kinases, (iii) the activation of cellular protein cascades such as ERK/MAPK pathway allowing the activation of transcription nuclear factors such as CREB. The activation of CREB allows mRNA transcription, which is then transduced into protein important in cellular plasticity such as brain-derived neurotrophic factor (BDNF), activity-regulated cytoskeleton-associated protein (Arc), c-fos and other plasticity products. Adapted from (Orsinia and Maren, 2012).

Using optogenetics and single-unit recordings Wolff et al. (Wolff, et al., 2014) found that PV and SST neurons in the BLA bidirectionally modulate fear acquisition. PV cells activated with ChR2 stimulation only during the CS resulted in increased freezing, while a decreased freezing was produced when the stimulation was given during the US. PV ArchT-mediated inhibition during the US presentation caused an increase in freezing during a non-stimulated test of fear retrieval the following day. In contrast, manipulation of SST^{+} neurons during the CS resulted in the opposite behavioral effects. These data suggest that within the BLA, PV and SST expressing inhibitory neurons bidirectionally control the acquisition of fear conditioning.

Another amygdala nucleus has emerged as a site of CS-US associative learning plasticity. Indeed, several evidence suggested that the CeA, rather than being a passive relay station of information coming from the BLA, it also participates to fear memory acquisition. Inactivation of the CeA (Wilensky, et al., 2006; Ciocchi, et al., 2010) or CeL alone (Ciocchi, et al., 2010) but not CeM alone (Ciocchi, et al., 2010) before fear conditioning disrupts the acquisition of fear learning. It has been also shown that rats with BLA lesions undergoing over-training are able to acquire conditional freezing, which is thought to be mediated by the CeA (Zimmerman and Maren, 2007). Thus the CeA, in parallel to the LA, can be conceived as a site of CS-US association. The plasticity in the CeA driving the acquisition of fear memory could be conceived to pass by direct monosynaptic excitatory inputs from sensory thalamus to the CeM, which exhibits NMDA-dependent LTP (Samson and Paré, 2005). Nevertheless the contribution of this LTP to the acquisition of freezing still remains to be tested. A neuropeptide that has been recently shown to be crucial for the associative memory formation in the CeL is CGRP (Han, et al., 2015). Indeed, calcitonin gene-related peptide (CGRP) expressing neurons in the parabrachial nucleus (PBN) processing nociceptive information, send direct projections to the CeL which are necessary for the acquisition of cued and contextual associations between the neutral CS and the aversive US (Han, et al., 2015).

SST expressing neurons in the CeL were also shown to be critical for the acquisition of fear memories. In transgenic SST-cre mice, CeL was inhibited using chemical-genetic (Dong, et al., 2010) manipulation that expresses hM4Di, an engineered inhibitory G protein-coupled receptor that suppresses neuronal activity. Using this tool, SST activity was suppressed before fear conditioning and resulted in impaired fear conditioning suggesting that CeL expressing SST neurons are critical for fear memory acquisition.

CeL has been also shown to control the plasticity generated during fear learning in the LA through a population of cells expressing protein kinase C-δ (PKC-Δ^+). CeL neurons expressing PKC-Δ^+ optogenetic inhibition completely abolished the fear conditioning induced synaptic plasticity onto LA neurons and impaired the acquisition of conditioned freezing. This study also highlights the role of CeA not only as an output nucleus of the amygdala controlling the generation of defensive

behaviors but also in conveying information necessary for the acquisition of associative fear learning (Yu, et al., 2017).

As for the BA, Herry et al. (Herry, et al., 2008) demonstrated the existence of one subpopulation of neurons which increases its' firing specifically during and after fear conditioning and decreased firing during extinction training. The change in frequency of those cells corresponded to the freezing behavior. Those BA cells were labeled the ''Fear'' cells encoding specifically the acquisition and expression of fear. This study demonstrated the importance of the BA nucleus in fear memory acquisition (Herry, et al., 2008).

b) Acquisition and consolidation of avoidance

A large literature also implicates the amygdala in other measures of fear namely active and passive avoidance acquisition (Takashina, et al., 1995) and consolidation. Amygdala nuclei are reported to participate differentially in avoidance acquisition. First, the LA is shown to be crucial for the acquisition of both freezing and avoidance behaviors. Indeed it has been reported that electrolytic lesions before or shortly after training of the LA but not the CeA impaired the acquisition of Sidman active avoidance behavior (Lázaro-Muñoz, et al., 2010) and signaled avoidance (Manassero, et al., 2018) in rodents. Moreover, muscimol inactivation of the BLA during pre-training impaired avoidance acquisition in rabbits (Poremba and Gabriel, 1999). Nevertheless, the LA cannot be the only site at which Pavlovian CS–US associations are stored, as lesions or inactivation of the LA produce a transitory deficit of avoidance learning acquisition at early sessions that is not apparent in the subsequent sessions (Lázaro-Muñoz, et al., 2010; Manassero, et al., 2018). Some IEG studies suggested that inhibitory neurons in the LA are more activated during late acquisition phases of a lever-press avoidance task (Jiao, et al., 2015), which would in part explain the lack of effect on avoidance at late acquisition phase with LA lesions. Some studies reported that the BA is not required for the acquisition of fear conditioning (Amorapanth, et al., 2000; Nader, et al., 2001) although other studies highlighted the importance of the anterior BA but not the posterior BA in the acquisition of Pavlovian fear conditioning (Goosens and Maren, 2001). Post-training muscimol inactivation of the BA or the LA impaired consolidation of inhibitory avoidance (Wilensky, et al., 2000). Also, a selective protein-kinase C inhibitor of

isomers (α, β I, and β II) infused post-training into the BLA, blocked the consolidation of an inhibitory avoidance task (Bonini, et al., 2005). In addition, the release of endogenous norepinephrine during inhibitory avoidance training influences memory consolidation through mechanisms involving β-adrenoceptor activation (McGaugh, 2004) and α-adrenoreceptors (Ferrya, et al., 2015) in the BLA.

As for the CeA implication in the acquisition of avoidance behavior, it has been reported that CeA lesions facilitate the acquisition of signaled active avoidance (Moscarello and LeDoux, 2013), passive avoidance (Grossman, et al., 1975) and rescues the acquisition of an unsignaled (Lázaro-Muñoz, et al., 2010) or signaled (Choi, 2010) active avoidance in ‘’bad avoiders’’ by blocking the expression of freezing behavior. The CeA is thought to hold the breaks on active avoidance acquisition by mediating the expression of an opposing behavior namely freezing (Moscarello and LeDoux, 2013).

c) Expression of freezing

In a number of studies, infusions of the NMDA non-selective antagonist APV into the LA and the BA impairs not only the acquisition of new auditory (Lee and Kim, 1998) and contextual fear responses (Fanselow and Kim, 1994) but also the expression of previously learned cued and contextual fear responses (Maren, et al., 1996; Fendt, 2001; Lee, et al., 2001). This suggests that NMDA receptors are crucial not only for synaptic plasticity important for a memory formation and consolidation, but also for synaptic transmission (Gean, et al., 1993; Weisskopf and LeDoux, 1999). However, the subunit composition of NMDA receptors classes seems to be particularly important. For instance NMDA receptors expressing the GluN2B subunit blocked using the selective antagonist ifenprodil in the LA disrupted the acquisition but not the expression of auditory fear conditioned freezing (Rodrigues, et al., 2001). NMDARs in LA that incorporate the GluN2B subunit seem to be particularly important for synaptic plasticity essential during the acquisition process of fear learning, whereas other classes of NMDARs may be more important for normal synaptic transmission allowing the expression of the learned fear behavior.

As for the BA, a recent paper described a mechanism of transmission of contextual information to the BA through double projecting hippocampal inputs to both the mPFC and the BA contributing in contextual fear expression (Kim, et al., 2017).

Electrophysiological experiments showed that the activation of double-projecting ventral CA1 neurons induces excitatory synaptic activity in both the mPFC and the amygdala, which could contribute to contextual fear expression by synchronizing the activity in both mPFC and BA, a hypothesis that will require additional investigations (Kim, et al., 2017).

Lesions of the CeA blocked the expression of conditioned fear (Blanchard and Blanchard, 1972; Hitchcock and Davis, 1986). However both CeL and CeM nuclei participate differentially in fear expression. The main CeA-mediated mechanism for encoding freezing expression relies on the activation of CeM output neurons projecting to the hypothalamus and various brainstem nuclei, which mediate-motor related aspects of fear behavior expression. Indeed, inactivation of the CeM attenuates the expression of freezing (Ciocchi, et al., 2010). The CeM being under a tonic inhibitory control of the CeL, one mechanism driving freezing expression is the disinhibition of CeM output neurons, which is thought to be mediated by neurons expressing different neuropeptides. It has been shown that CeL activity is also modulated by direct PVT projections, which activate preferentially SST^+ CeL neurons disinhibiting CeM and producing freezing expression (Penzo, et al., 2015). Also CeL neurons contain a population of cells expressing oxytocin. The activation of this population of neurons with oxytocin agonists in the CeL leads to the inhibition of CeM neurons which drives CS-evoked freezing expression through a disinhibition process (Viviani and Stoop, 2008; Viviani, et al., 2011). Disinhibition also occurs through two cell populations expressing protein kinase C delta (PKC-Δ): the CeL ON cells which are excited by the CS following fear conditioning and CeL OFF cells which, in contrast, are inhibited by the CS following fear conditioning (Ciocchi, et al., 2010; Haubensak, et al., 2010). CeL ON cells inhibit CeL OFF neurons, which in their turn disinhibit GABAergic CeM output neurons allowing freezing expression (Ciocchi, et al., 2010; Haubensak, et al., 2010). One of the possible output structures on which CeM neurons, controlling freezing expression, could act is the PAG. A recent paper (Tovote, et al., 2016) reported that inhibitory neurons in the CeA projecting to the vlPAG induce conditioned freezing expression by disinhibiting vlPAG excitatory outputs onto pre-motor cells in the magnocellular nucleus of the medulla. Nevertheless, those neurons in the CeA originate from both the CeM and the CeL which suggests a possible role of direct CeL projections to motor output structures in

encoding freezing expression. Indeed, CeL projections to the CeM might not be the only CeL projections that contribute to freezing behavior expression after fear conditioning. Some CeL neurons project directly to brainstem effector structures (Penzo, et al., 2014) in a pathway that could bypass CeM for mediating fear responses.

Although, pieces of information are still missing to a clear view of fear conditioning acquisition and expression neuronal and circuitry elements in the CeA, it is now well established that (i) both acquisition and expression of freezing relies on a dynamic interaction between the LA and CeL and that (ii) projections to multiple output structures of both CeL and CeM may regulate freezing expression.

d) Expression of avoidance

Very early studies showed that post-training amygdala stimulation disrupts inhibitory passive avoidance (Gold, et al., 1973; Izquierdo, et al., 1997) and one-way active avoidance (Handwerker, et al., 1974) in rats. Nevertheless, this effect is observed when the stimulation is given directly after the training and not long after (3 hours) (Handwerker, et al., 1974). Therefore amygdala was thought to be crucial for short-term avoidance expression but not long-term memories expression. This effect was reproduced recently in a paper which examined the role of amygdala subnuclei in long-term avoidance expression (Manassero, et al., 2018). LA lesions shortly after training impaired both freezing and avoidance expression. Nevertheless LA and CeA lesions performed four weeks after training did not impair avoidance expression, BA lesion on the contrary suppressed avoidance. Therefore BA is suggested to be crucial for long-term avoidance expression and it has been demonstrated that auditory information is sent to the BA through direct inputs from the auditory cortex namely the area Te2, a crucial cortico-BA pathway driving long-term avoidance memories expression independently from LA and CeA circuits (Manassero, et al., 2018).

In addition in unsignaled active avoidance following overtraining (Lázaro-Muñoz, et al., 2010) avoidance expression is unchanged after LA, BA or CeA lesions. The same is reported for instrumental active avoidance after BLA muscimol inactivation following overtraining in rabbits (Poremba and Gabriel, 1999). These findings suggest that once learned, avoidance behavior becomes amygdala independent and seems

to depend upon extra-amygdalar structures, presumably the cortico-striatal circuitry (Poremba and Gabriel, 1999).

As for the amygdala nuclei implications in short-term avoidance expression it has been reported that lesions of the LA blocked both freezing and avoidance (Amorapanth, et al., 2000; Choi, et al., 2010). Lesions of the BA alone or combined with the LA also blocked the expression of two-way active avoidance, while lesions of the CeA has minimal effects on active avoidance expression (Choi, et al., 2010). Also, lesions of the basolateral, but not the central nucleus blocked bar-press avoidance (Killcross, et al., 1997). Moreover, lesions of the CeA blocked freezing but not escape behavior to a tone previously paired with shock, whereas lesions of the BA have just the opposite effect (Amorapanth, et al., 2000). Disrupting BA connection to the nucleus accumbens shell but not core region impairs two-way active avoidance expression, which suggests that projections from the BA to the ventral striatum are essential for the expression of avoidance behavior (Ramirez, et al., 2015).

In conclusion, LA and BA but not CeA seem to be required for the expression of voluntary avoidance responses but play a transient, and time-limited role in the performance of avoidance responses. In contrast, CeA seems not to be required for avoidance expression using lesional and pharmacological inactivation studies. The CeA is most likely blocking avoidance expression because of its role in mediating competing Pavlovian responses such as freezing. Therefore, recently optogenetic and imaging studies gave rise to an extended view of the CeA as an inhibitory interface capable of dynamically controlling the switch between passive (freezing) and active (flight, avoidance) fear behaviors expression through the activation of specific CeA subregions, cells types, and specific projections to different output structures.

In this model, SST^+ cells in the CeL gate the behavioral output of the animal in the sense that when SST^+ cells are activated the animals' behavior is biased toward passive fear responses, namely freezing or lick suppression, whereas the inhibition of SST^+ CeL neurons allows the expression of active fear responses namely running or active avoidance (Yu, et al., 2016). Those SST^+ CeL cells are (i) activated by an auditory outcome predicting the US (Yu, et al., 2016) and (ii) receive excitatory inputs from the LA which are potentiated after fear conditioning (Li, et al., 2013) suggesting

that SST^+ CeL cells represent at least in part the described above CeL ON cells (Ciocchi, et al., 2010). Another recent paper, have showed that CeL SST^+ interact with CRF^+ CeL neurons through inhibitory connections between the two populations mediating the switch between passive and active fear responses. The activation of CeL SST^+ cells initiate passive freezing expression while CRF^+ CeL activation induced flight behavior (Fadok, et al., 2017).

In addition, a group identified a GABAergic CeM projection pathway (Han, et al., 2017) to the glutamatergic neurons of l/vlPAG controlling active pursuit behavior during hunting. Optogenetic activation of CeM inhibitory projections to the vl/lPAG promoted the expression of innate hunting behavior by shortening the latency of hunting and increasing the velocity of preys' pursue in mice.

Those CeA projections to the PAG are different from the ones identified by Tovote et al. (Tovote, et al., 2016) who showed that GABAergic CeA cells projecting to l/vlPAG control the expression of freezing by a disinhibition of glutamatergic projections from the l/vlPAG to the medulla. The dynamic switch from passive freezing to active flight behavior was demonstrated to be mediated by inputs received by GABAergic neurons in the l/vlPAG: (i) CeA inputs through inhibiting GABAergic l/vlPAG neurons and by the same way disinhibiting the output projection to the medulla mediate freezing behavior, while (ii) dlPAG glutamatergic inputs through the activation of GABAergic l/vlPAG neurons mediate flight behavior.

e) Extinction of freezing and avoidance

Over the past decade, there was also considerable interest in elucidating the neuronal circuits underlying fear extinction. A set of lesional studies examined the contribution of the BLA in fear extinction. However, because post-training BLA lesion was associated with a suppression of fear behavior it was difficult to disentangle the contribution of the BLA to fear extinction and/or fear suppression (Campeau and Davis, 1995; Cousens and Otto, 1998; Anglada-Figueroa and Quirk, 2005; Amano, et al., 2011). Reversible inactivation using the $GABA_A$ receptor agonist muscimol allowed to further investigate this question since it was reported that, inactivation restricted to the BA completely blocks acquisition of extinction (Akirav, et al., 2006; Herry, et al., 2008; Hart, et al., 2009). An important advance in the understanding of the role of the BLA in the acquisition of fear extinction was done with pharmacological

studies using either micro-infusion of protein synthesis inhibitor, or an antagonist of NMDA receptor or mitogen-activated protein kinase inhibitors. These studies demonstrated that glutamatergic plasticity in the BLA was necessary for fear memory extinction (Lu, et al., 2001; Lin, et al., 2003; Herry, et al., 2006; Sotres-Bayon, et al., 2007). Furthermore local infusion of muscimol in the BLA potentiated fear extinction when made after extinction training (Myers and Davis, 2002; Akirav, et al., 2006). Altogether, these studies demonstrated that the acquisition of extinction can be directly regulated at the level of the BLA.

Also studies using *in vivo* extracellular electrophysiology allowed a rapid growing of our knowledge related to the contribution of specific neuronal elements in fear extinction. These studies established the existence in the BLA of two types of cell populations showing opposite firing patterns during extinction learning. The first population of BLA neurons (fear neurons, 15% of BLA neurons) was selective of high fear states and displayed a reduced firing activity during extinction learning. In contrast, the second population (extinction neurons, 15% of BLA neurons) was selective of low fear states and displayed an increased firing activity during extinction learning (Herry, et al., 2008).

Furthermore it was shown that these two neuronal populations show a specific connectivity pattern with the medial prefrontal cortex (mPFC) and the ventral hippocampus (vHPC). Whereas fear neurons received inputs from the vHPC and project to the mPFC, extinction neurons were exclusively connected with the mPFC (Herry, et al., 2008; Senn, et al., 2014). More specifically, that BA neurons projecting to the PL are active during fear expression while the ones projecting to the IL displayed cell type specific plasticity related to extinction behavior (Senn, et al., 2014).

Additionally, another study established the existence in the LA of two populations encoding differentially extinction, the first group, the ‘extinction susceptible’ neurons decrease their activity during extinction, while the second population, the ‘extinction resistant’ maintain their activity all along the extinction session (An, et al., 2012).

Together those data demonstrate that specific subpopulations of BLA neurons encode the acquisition and expression of extinction learning, and that their activity can be regulated by mainly cortical inputs.

f) Extinction of avoidance

In some avoidance protocols, a major characteristic of avoidance learning is that during the extinction phase which starts with the removal of the shock, animals still perseverate to avoid despite the fact that avoidance behavior is not reinforced anymore due to the shock removal. This is a phenomenon called the perseveration of avoidance behavior despite extinction that has been reported mainly in rats (Servatius, et al., 2008). It has been demonstrated in humans that partially reinforced avoidance behaviors are less resistant to extinction and are extinguished more rapidly than avoidance allowing a highly controlled contact with an aversive event (Xia, et al., 2017). Nevertheless, the neural circuits underlying the extinction of avoidance and its' perseveration are still largely a matter of speculation. However, some data suggest the involvement of the amygdala in encoding avoidance extinction.

It has been shown using c-fos immunoreactivity that LA and BA remain active during several extinction sessions of lever-press avoidance suggesting that both structures are necessary for avoidance extinction (Jiao, et al., 2015). Also it has been shown that activation of GABAergic neurons in the BLA is important to ensure successful extinction in rats undergoing lever-press avoidance extinction learning. Therefore deficits in GABAergic activation in the BLA could be at the origin of the deficits in avoidance extinction (Jiao, et al., 2011). Indeed, increased PV immunoreactivity in the LA across extinction was found (Jiao, et al., 2015).

It is known that the BA receives afferent projections originating from the IL that could mediate successful avoidance extinction since it has been reported that IL inactivation immediately before avoidance extinction session impairs avoidance retrieval in platform-based avoidance task (Bravo-Rivera, et al., 2014) and inhibitory avoidance (Cammarota, et al., 2005). This suggests that IL activation is necessary to successfully extinguished avoidance behavior.

ITC activity increase when comparing acquisition sessions to extinction sessions of a lever-press avoidance task suggesting that ITC cells are important as well during avoidance extinction (Jiao, et al., 2015). It was hypothesized that during extinction,

increased excitatory inputs from the IL to the ITC suppress CeA activity promoting avoidance extinction.

g) Amygdala a multi-functions structure

The amygdala is also implicated in a wide variety of functions. As for aversive learning, the amygdala has been shown to be implicated in other emotional states such as anxiety as well as different aspects of reward learning and addiction (Wassum and Izquierdo, 2015).

For example BLA to CeA glutamatergic projecting neurons have been shown to drive anxiolytic-like state as optogenetic activation of this pathway increases the time rodents spend in open-arms of an elevated-plus maze, a test commonly used to assess anxiety-like behaviors (Tye, et al., 2011). On the contrary, anxiogenic-like state is provoked by selective stimulation of BLA to ventral hippocampus projections (Felix-Ortiz, et al., 2013). A recent study, demonstrated that in patients suffering from generalized anxiety state, the PFC to amygdala functional connectivity is impaired, a reason that could lead to maladaptive processing of emotional states inducing the maintenance of high anxiety and worrying state in those patients (Assaf, et al., 2018).

BLA to nucleus accumbens core (NacC) glutamatergic projections have been demonstrated to promote appetitive behavior (Stuber, et al., 2011). BLA to Nac pathway is also implicated in the consequences of maladaptive appetitive behaviors namely addiction. It has been demonstrated that BLA-Nac optogenetic inactivation reduces maladaptive cue-induced cocaine seeking (Stefanik and Kalivas, 2013).

Amygdala has also been shown to be implicated in emotional states associated with a multitude of behaviors for example maternal, eating, drinking and sexual behaviors. It also encodes the emotional modulation of a variety of cognitive functions such as attention and perception (LeDoux, et al., 2007; Janak and Tye, 2015; Fadok, et al., 2018).

VI. Striatum

Another structure worth discussing in this introduction is the striatum. I will first introduce briefly its' anatomy then I will highlight its' contribution to avoidance learning behavior.

1) Gross anatomy and connectivity of the striatum

The striatum is mainly composed of projection medium spiny neurons (MSNs), which constitute ~ 90-95% of the striatal neuronal populations. These neurons form a specific GABAergic inhibitory population constituting the striatal output (Bolam, et al., 2000). In addition to these MSNs, local interneurons (INs) form 5-10% of the striatal neuronal population. The main GABAergic INs in the striatum are well known to have calcium binding proteins namely calbinding (CB), calretinin (CR) and parvalbumin (PV) (Bae, et al., 2015). Cholinergic interneurons also contribute approximately to 2% of the total amount of striatal neurons (Graybiel, 1995).

The striatum is divided into two regions the dorsal (DS) and the ventral striatum (VS). The dorsal striatum consists of the caudate nucleus and the putamen. Striatums' functions have been mainly investigated in appetitive learning tasks. Based on appetitive learning studies, the dorsal striatum (DS) has two functionally defined subdivisions: a dorsomedial striatum (DMS) region involved in mediating goal-directed behaviors (Redgrave, et al., 2010) that requires conscious effort, and a dorsolateral striatum (DLS) region involved in the execution of habitual behaviors (Balleine and O'Doherty, 2010; Seger and Spiering, 2011).

As for the VS, it includes the nucleus accumbens (Nac) and the olfactory tubercle (Bloom, et al., 1999). The Nac is subdivided into two subterritories the Nac shell (NacS) and the Nac core (NacC).

While the VS is similar to the dorsal striatum in most respects, there are also some unique features. While both the dorsal and ventral striatum receive inputs from the cortex, thalamus, and brainstem, the VS alone also receives a dense projection from the amygdala and the hippocampus. Therefore the DS is classically associated with sensory-motor functions processed through glutamatergic afferents from motor cortex and dopaminergic afferents from substantia nigra pars compacta (SNc) (Haber, et al., 2000; Reep, et al., 2003). VS regions are rather associated with limbic ''emotional'' functions processed through glutamatergic afferents from prefrontal cortex, amygdala and hippocampus, and dopaminergic afferents from ventral tegmental area (VTA) (McGeorge and Faull, 1989; Sesack, et al., 1989; Brog, et al., 1993). Indeed, the striatum receives inputs from three main structures. The substantia nigra pars compacta (SNc), which sends projections mainly to the dorsal striatum MSNs

(Tritsch, et al., 2012) (caudate nucleus and putamen). This dopaminergic pathway forms one of the main dopaminergic pathways in the brain and is labeled the nigro-striatal pathway. The dopaminergic inputs to the VS are mainly generating from the VTA (Haber, 2011). It is particularly important in the initiation of movement, and loss of dopaminergic neurons in the SNc is one of the main pathological features of Parkinson's disease (Zeng, et al., 2018). Beside the nigrostriatal dopaminergic afferents, the striatum receives corticostriatal and thalamostriatal glutamatergic afferents, which also synapse onto the MSNs (Haber, 2011). Those afferents are common to both VS and DS. Nevertheless, the prefrontal cortex sends preferentially afferents to the VS with the IL projecting preferentially to the NacS while the ACC and the PL to the NacC (Brog, et al., 1993). The amygdala also exclusively synapse onto the VS MSNs originating mainly in the BLA, which sends glutamatergic projections controlling both NacS and NacC neural activity (Fudge and Haber, 2002; Jones, et al., 2010). In contrast to the amygdala, the hippocampus also exclusively projecting to the VS, target a more limited region of the VS confined to the NacS (Friedman, et al., 2002).

Those are important features of the VS distinguishing it from the DS but it is important to note that VS dorsal and lateral borders are continuous with the rest of the striatum, and neither cytoarchitectonic nor histochemical distinctions mark a clear boundary between the VS and the DS.

Efferent projections from the VS, like those from the dorsal striatum, project primarily to the pallidum and substantia nigra (Haber, et al., 1990). Also the NacS sends fibers caudally and medially into the lateral hypothalamus. The medial VS fibers travel to and terminate in the bed nucleus of the stria terminalis, and parts of the ventral regions of the VS terminate in the nucleus basalis in the basal forebrain, a nucleus which constitutes the main source of cholinergic fibers to the cerebral cortex and the amygdala (Haber, et al., 1990) and allows the VS to influence the cortex throughout this projection (Zaborszky and Cullinan, 1992).

I would suggest the interested reader about the anatomy and the global functions of the striatum to check the following articles/ review (Fudge and Haber, 2002; Gruber and McDonald, 2012; Haber, 2016).

2) Role of the striatum in regulating freezing and avoidance behaviors

The Nucleus accumbens (Nac) has been widely studied in reward and appetitive reinforcement (Ambroggi, et al., 2008; Corbit, et al., 2001). Nevertheless several evidence suggest that Nac neurons also process aversive information (Jensen, et al., 2003; Delgado, et al., 2008). In this section, I will present electrophysiological, imaging, lesional, pharmacological and optogenetical studies suggesting the implication of the Nac in aversive learning.

First, it has been shown via functional magnetic resonance imaging (fMRI) studies using blood oxygenation level dependent (BOLD) signals, that active avoidance increased BOLD signal within the Nac (Delgado, et al., 2009; Levita, et al., 2012), whereas inhibitory avoidance was associated with a deactivation in this region in humans (Levita, et al., 2012).

On the one hand, some reports suggested that both NacC and NacS are crucial for active avoidance. In well-trained rats, pharmacological inactivation of either the NacC or the NAcS impaired lever-press active avoidance (Piantadosi, et al., 2018). Importantly, inhibitory avoidance is disrupted by NacS but not NacC inactivation (Piantadosi, et al., 2018). On the other hand, it was shown that NacS but not NacC inactivation impaired two-way active avoidance expression and that disruption of the amygdala BA-NacS connection impairs avoidance expression (Ramirez, et al., 2015). The ventral striatum NacS has been shown to be necessary for active avoidance but not freezing expression since muscimol inactivation had no effect on the expression of conditioned freezing behavior (Amorapanth, et al., 2000; Ramirez, et al., 2015). Another pathway between the mPFC and NacS has been shown to be crucial for avoidance expression (Lee, et al., 2014). Optogenetic activation of GABAergic long-range projecting inhibitory PV neurons from the mPFC (PL and IL) to the Nac promoted avoidance behavior in a real-time place preference protocol (Lee, et al., 2014). As for the NacC, it has been reported that DA release in the NAcC increases during the presentation of an aversive CS eliciting an active avoidance response, suggesting that the NacC is crucial for predicting avoidance behavior (Gentry, et al., 2016; Oleson, et al., 2012). The source of this DA to the NacC comes mainly from the VTA, and the optogenetic activation of the VTA to NacC dopaminergic pathway enhanced lever-press avoidance acquisition. *In-vivo* microdialysis studies have also reported that DA release is proportional to avoidance learning, which supports the

hypothesis that during active avoidance learning, positive prediction errors generated when the animal do not receive an anticipated footshock cause DA release that reinforces the instrumental avoidance action (Dombrowskia, et al., 2013). It has also been reported that NacC excitotoxic lesions affect two-way active avoidance acquisition but not expression (Wendlera, et al., 2014). The same effects were observed when the DLS was lesioned suggesting its' implication in avoidance acquisition (Wendlera, et al., 2014). Therefore neuronal activity in the NacC and DLS is thought to facilitate active avoidance acquisition. It is also noteworthy that NacC lesions also reduced freezing expression (Wendlera, et al., 2014). Therefore, the implication of the NacC in encoding passive and active defensive behaviors is still controversial since it is not clear whether it contributes to avoidance acquisition or if it allows the learning of Pavlovian components which is a pre-requisite for the subsequent learning of the instrumental components.

Model of active/passive structural and neuronal correlates

In summary, the PAG is a central structure for encoding both passive defensive freezing and active defensive avoidance and flight behaviors.

On the one hand, a central circuit encoding the expression of freezing behavior has been characterized. It consists on the disinhibition of glutamatergic vlPAG neurons projecting to the medulla by the activation of inhibitory inputs arising from CeA long-range projection neurons (Penzo, et al., 2014; Tovote, et al., 2016; Fadok, et al., 2017).

On the other hand, evidence show that the main PAG subregion involved in driving active defensive behaviors (flight) is the dlPAG. Indeed, the available data suggest that the activation of glutamatergic dl/lPAG neurons, which directly project to vlPAG interneurons, inhibits vlPAG glutamatergic projections to the medulla and therefore blocks freezing behavior and facilitates active defensive behaviors expression (Tovote, et al., 2016).

The activation of glutamatergic dl/lPAG could come from multiple sources namely direct projections from the hypothalamus (Li, et al., 2018) or the prefrontal cortex (Halladay and Blair, 2015). These projections could mediate a direct excitatory activation of dl/lPAG glutamatergic neurons **(Figure 11)** or an indirect activation of these neurons through disinhibition mechanisms. Indeed, direct excitatory projections from the hypothalamus, namely the lateral hypothalamus to the lPAG, have been shown to induce flight behavior (Li, et al., 2018). As for the dmPFC to dl/lPAG projections their implication in driving avoidance/ flight responses are still not investigated, a question that we will address in this thesis.

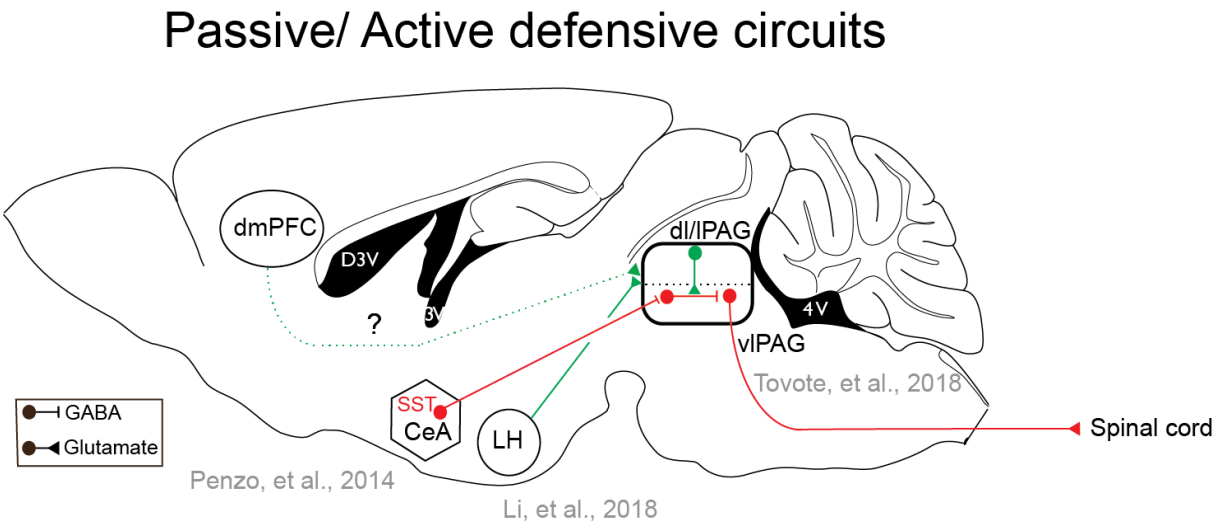

Figure 11. A model of passive and active defensive structural and neuronal interactions.
The red pathway represents freezing-described circuitry and the green pathway represents active (avoidance/ flight)-described and non-described (dashed line) circuitry. Glutamatergic vlPAG neurons projecting to the spinal cord are disinhibited by SST^{+} GABAergic long-range projections promoting freezing behavior. Active defensive behaviors are mediated by dl/lPAG inhibition of the vlPAG through dl/lPAG glutamatergic projections onto interneurons inhibiting glutamatergic vlPAG neurons. These glutamatergic dlPAG neurons could be activated either by direct projections from the hypothalamus (LH) mediating flight response or by direct dmPFC excitatory projections to the glutamatergic dl/lPAG neurons.

Hypothesis and Objectives of our study

As outlined in the general introduction, the medial prefrontal cortex (mPFC) appears as a critical structure processing both freezing and avoidance defensive behaviors. Although there is a number of lesional and inactivation studies available, it is still unclear whether those two antagonistic behaviors rely on the recruitment of the same or different pools of mPFC neurons projecting to the amygdala or the PAG. This is a challenging question as to be fully addressed it implies to monitor the changes in activity of the very same neurons during both freezing and avoidance behaviors. Moreover, the involvement of the mPFC in the acquisition versus expression of avoidance behaviors is still under debate. Anatomically, the dmPFC projects to both the PAG and BLA and could thereby directly or indirectly regulate freezing and avoidance acquisition/expression. Although the role of the dmPFC-BLA pathway in regulating freezing and avoidance expression has already been documented, there is to date very few data available on the role of the dmPFC-PAG pathway in the regulation of these two behaviors.

In this context, the main goal of this thesis was to evaluate the precise neuronal elements and circuits at the level of the dmPFC mediating freezing and avoidance behaviors.

Our main objectives were threefold:

* to develop a novel behavioral paradigm allowing to evaluate changes in the activity of dmPFC neurons during both freezing and avoidance behaviors
* to evaluate whether freezing and avoidance behaviors depend on segregated or overlapping pools of neurons
* to determine the connectivity and the causal role of dmPFC neurons mediating avoidance behavior

Materials and methods

I. Animals

Three month old male C57BL6/J mice (Janvier), VGLUT2-IRES-Cre mice, GAD-IRES-Cre mice and SST-IRES-Cre mice were individually housed for at least 7 days prior to all experiments, under a 12 hours light/dark cycle, and provided with food and water *ad libitum*. Experiments were performed during the light phase. All procedures were performed in accordance with standard ethical guidelines (European Communities Directive 86/60-EEC) and were approved by the committee of Animal Health and Care of Institut National de la Santé et de la Recherche Médicale and French Ministry of Agriculture and Forestry (authorization A3312001).

II. Behavioral paradigm and protocol

Training was performed in a shuttle-box made up of two-identical square compartments (20cm x 20cm x 20cm) separated by a 15 cm vertical sliding door which, when slided-up (door closed configuration) separated the shuttle-box into two independent contexts preventing the mouse to move between the two compartments. When the door was slided-down (door opened configuration), it offered to the animal a possibility to shuttle between the two-compartments. The floor of the two compartments was made of stainless steel rods (5 mm diameter, spaced 0.5 cm apart) that were linked to a shock delivery apparatus (Imetronic, Bordeaux). All experiments were carried on under 100 lux light illumination. The plexiglas walls as well as the floor of the shuttle-box were cleaned before and after each behavioral session using 70% ethanol solution.

Mice were trained in the shuttle-box to learn the association between a CS^+ (a tone, 7 kHz, 30 pips, 50 ms ON delivered at 1.1 Hz) and an unconditioned stimulus (US, a mild footshock, 0.6mA). A different control tone (the CS^-, white noise, 30 pips, 50 ms ON delivered at 1.1 Hz) was also used but not associated with the footshock.

During several daily sessions mice were submitted to two types of trials: door opened (DO) and door closed (DC) trials, which both started with the CS^- or the CS^+ presentation for the first 21 pips. In CS^+ DC trials, the CS was maintained for an

additional 9 pips and the door was kept raised, which prevented the US (0.6 mA intensity, 4 sec length) from being avoided. In CS^+ DO trials, 23.1 seconds after the tone onset, the door was lowered and the mice could avoid the US by initiating an avoidance response allowing animals to move to the opposite compartment. In this later type of trials, a move to the opposite compartment terminates the CS presentation. Moreover, in case the animals do not shuttle before the CS offset (after the 30^{th} played pip), a footshock was delivered but could be escaped by moving to the opposite compartment (escape trial). An error trial was scored if after the footshock delivery the animal still remains in the same compartment **(Figure 12)**. Both DO and DC trials were also initiated with the CS^- but without any footshock delivery.

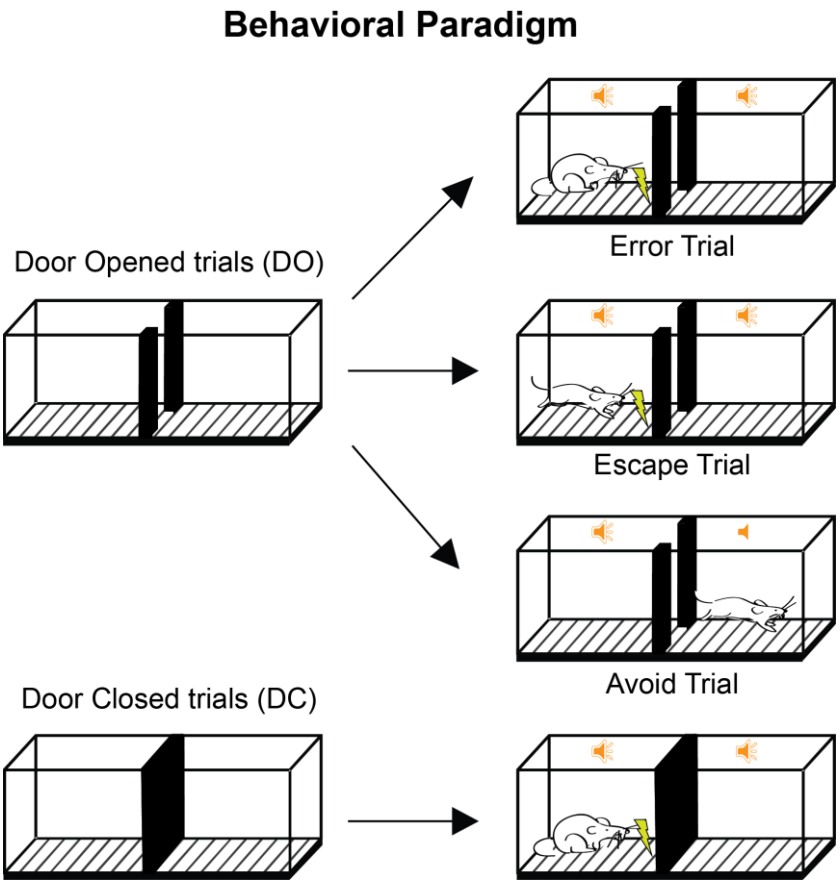

Figure 12. Behavioral paradigm

Behavioral paradigm. In the door opened trials (DO), 3 types of behavioral readouts were scored: error trials during which animals stayed during the whole CS^+ and the US delivery; escape trials during which mice crossed to the opposite compartment of a shuttle-box during the US and avoid trials during which animals crossed during the CS^+ and avoided the US. In door-closed trials (DC), freezing behavior was assessed during the sound presentation.

DC and DO trials were repeated 15 times each **(Figure 13)** in an intermingled fashion for each CS condition (15 CS^- and 15 CS^+ DO trials; and 15 CS^- and 15 CS^+ DC trials).

Training was performed over 6 days upon which mice were classified into two categories based on their avoidance scores. Mice that avoided at least on 30% of the 15 CS^+ DO trials were classified as (1) **Good avoiders** as opposed to (2) **Bad avoiders**. **Good avoiders** were also subdivided into (1.1) **Discriminators**, (that discriminated at session 6 between DO CS^- and CS^+ trials) as opposed to (1.2) **Generalizers**.

Two days before training, animals were habituated on the first habituation day to the contextual apparatus and on the second habituation day to both tones as well the door sliding-up and down. For this purpose, animals were submitted to the same protocol applied during the training sessions but with fewer trials to avoid latent inhibition (9 trials per condition instead of 15) and without any aversive pairings (during habituation both tones were not associated with footshocks). This control allowed us to assess whether animals present any freezing or locomotion differences linked to the sensory properties of the tones.

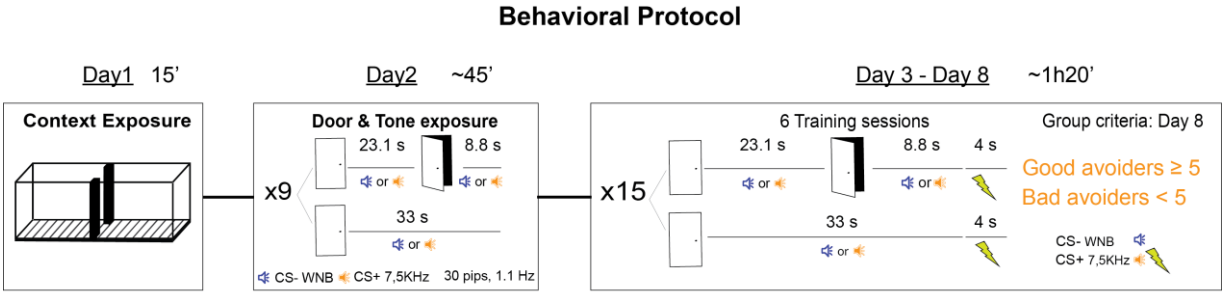

Figure 13. Behavioral protocol

Behavioral protocol. On day 1, mice were habituated during 15 min to the shuttle-box. On day 2, animals were habituated to the presentation of two sounds that were played in two contextual conditions : (i) door-closed trials (DC) during which the sound was played for 33 s , and (ii) door-opened trials (DO) during which 23.1 s following the sound's onset the door was slided-down (DO) and slided-up again 8.8 sec after. 9 trials of each of the DO and DC types of trials were played for both CS^- and CS^+ and the session lasted about 45 min. From day 3 to day 8, animals underwent 6 training sessions lasting each about 1h20min and during which the same type of trials than during day 2 were played except that the number of trials was increased to 15, and that CS^+ trials were followed by a 4 s shock in the DC condition. At day 8, animals were categorized into **Good** or **Bad avoiders** based on their behavioral avoidance scores.

III. Control test

Forced-swim test

Our behavioral paradigm resulted in **Good and Bad avoidance learners**. Although this may simply represent a phenotypic trait, we were concerned that repetitive footshock experience in DC trials might promote depressive behaviors, which could manifest by a lack of avoidance responses like in the **Bad avoiders** group. Therefore we conducted a standard test of depressive behavior: the forced swim test (FST). Following avoidance training, **Good and Bad avoiders** underwent a FST session during which each mouse was individually placed in a cylindrical tank (50 cm height and 20 cm width) filled with clean tap water (24 ± 1 °C). Mice were forced to swim during 6 minutes. The first two minutes were considered as an acclimatization time and during the last 4 minutes, Behavioral Observation Research Interactive Software (BORIS) was used to process the recorded behavioral video allowing to score the total duration of immobility. Mice were scored to show immobility when they floated without struggling and making only those movements necessary to keep their heads above the water: namely moving only their hind paws but not front paws. In the end of the FST, mice were carefully dried before being returned to their home cages.

IV. Fos: immunostaining and quantification of labeled cells

Following the 6^{th} session of training mice were divided into three groups and underwent a last 7^{th} behavioral session. The first control group received, at a 7^{th} behavioral session, only 15 CS^- trials. The second and the third groups, which were respectively classified at session 6 as **Bad** and **Good avoiders** underwent a 7^{th} behavioral session during which they received 15 trials of CS^+ presentations without footshocks. A forth group of naïve mice was also used as a control. Ninety minutes after the 6^{th} behavioral session (not for the naïve mice), mice were deeply anesthetized with sodium pentobarbital (40 mg/kg, i.p.) and perfused transcardially with a solution of 4 % paraformaldehyde in 0.1 M phosphate buffer (pH 7.4). The brains were removed and left overnight in a solution of 20% sucrose in 0.1 M phosphate buffer at 4 °C. The brains were then frozen, and 5 series of 40-µm-thick sections in the frontal plane were cut using a sliding microtome.

One series of sections was processed for immunohistochemistry. The sections were incubated with anti-Fos antiserum raised in rabbit (Ab-5; Calbiochem) at a dilution of 1:20,000. The primary antiserum was detected using a variation of the avidin–biotin complex system. In brief, the sections were incubated for 90 min at room temperature in a solution of biotinylated goat anti-rabbit IgG (Vector Laboratories) and then placed in a mixed avidin–biotin horseradish peroxidase (HRP) complex solution (ABC Elite Kit; Vector Laboratories) for 90 min. The black-blue peroxidase complex was visualized after a 5 min exposure to a chromogen solution containing 0.02% 3,3′ diaminobenzidine tetrahydrochloride (DAB; Sigma) with 0.3% nickel ammonium sulfate in 0.05 M Tris buffer (pH 7.6), followed by a 20 min incubation in a chromogen solution containing hydrogen peroxide (1:3000). The reaction was stopped using potassium phosphate-buffered saline (KPBS; pH 7.4). The sections were mounted on gelatin-coated slides, dehydrated and cover slipped using DPX mounting media (Sigma). An adjacent series of sections was stained with thionin (Nissl stain) to serve as a reference series for cytoarchitectonic purposes.

Images of the selected brain regions (PFC, PAG, amygdala) were generated using a Nikon Eclipse 80i (10 x magnification, Nikon Corporation, Chiyoda-Ku, Tokyo-To, Japan) microscope equipped with a Nikon digital camera (DXM1200F, Nikon Corporation). To quantify the density of the Fos-labeled cells, we first delineated the borders of the selected brain regions by referring to the reference (Nissl-stained) sections and the mouse brain atlas (Paxinos, 2008). Then, the Fos-labeled cells were counted. Only darkly labeled oval nuclei that fell within the borders of a region of interest were counted. The density of Fos labeling was determined by dividing the number of Fos-immunoreactive cells by the area of the region of interest. Both the cell counting and area measurements were performed with the aid of a computer program (Image-Pro Plus, version 4.5.1; Media Cybernetics, Silver Spring, MD, USA). Cell densities were obtained on both sides of the brain and were averaged for each mouse.

V. Surgery and recordings

Mice were anesthetized with isoflurane (induction 3%, maintenance 1.5%) in O2. Body temperature was maintained at 37 °C with a temperature controller system

(FHC) and eyes were hydrated with Lacrigel (Europhta Laboratories). Animals were secured in a stereotaxic frame (Kopf) and 3 stainless steel screws were attached to the skull. Following craniotomy, mice were unilaterally implanted in the left dmPFC with an optrode at the following coordinates relative to bregma (Franklin and Paxinos, 1997): +1.8 mm AP; −0.4 mm ML; and −1.15 mm DV from dura. The optrode consisted of 16 individually insulated nichrome wires (13 µm diameter, impedance 30–100 KΩ; Kanthal) fixed to a 4 mm optic fiber. The electrode bundle was attached to an 18-pin connector (Omnetics). Connectors were referenced/grounded via a silver wire (127 µm diameter, A-M Systems) placed above the cerebellum. All implants were secured using Super-Bond cement (Sun Medical). During surgery long- and short-lasting analgesic agents were injected (Metacam, Boehringer; Lurocaïne, Vetoquinol). After surgery mice were allowed to recover for at least 7 days. Electrodes were connected to a headstage (Plexon) containing sixteen unity-gain operational amplifiers. Each headstage was connected to a 16-channel PBX preamplifier (gain 1000 ×, Plexon) with bandpass filters at 300 Hz and 8 kHz. Spiking activity was digitized at 40 kHz and isolated by time-amplitude window discrimination and template matching using an Omniplex system (Plexon). At the conclusion of the experiment, electrolytic lesions were administered before transcardial perfusion to verify electrode tip location using standard histological techniques as described in the histological analysis section below.

VI. Single unit analyses

Single-unit spike sorting was performed using Offline Sorter software (Plexon) and analyzed using Neuroexplorer (Nex Technologies) and MATLAB (MathWorks) for all behavioral sessions. Waveforms were manually defined while visualizing in a three-dimensional space using principal components, timing, and voltage features of the waveforms. A single unit was defined as a cluster of waveforms that formed a discrete, isolated, cluster in the feature space, and did not contain spikes with a refractory period less than 1 ms, based upon auto-correlation analyses. Additionally, multivariate ANOVA were used to quantify separation of clusters in the principal component space. Cross-correlation analyses were performed to control that a single unit was not recorded on multiple channels. Target neurons that displayed a peak of

activity when the reference neuron fired were considered duplicates and only a single neuron was considered for analysis. For neurons that were potentially recorded throughout anesthesia and kept from the behavioral session (*see "antidromic identification" section*) a correlation coefficient was computed between the waveforms and considered as the same if the correlation coefficient was higher than 95%. Extracellularly recorded dmPFC units that met these criteria were classified into clusters based on similarities in their waveform shape based on Ward's method using three extracellular spike features: peak-to-trough, firing frequency and the area under the peak. Using those parameters, units were separated into putative inhibitory interneurons (PINs) and putative excitatory principal neurons (PPNs) using a hierarchical cluster algorithm. Briefly, the Euclidian distance was calculated between all unit pairs based on the three-dimensional space defined by each neuron's average peak-to-trough latency, firing rate, and the area under the peak of the spike waveform. An iterative agglomerative procedure was then used to combine neurons into groups based on the matrix of distances in the feature space so that the total number of groups was reduced to produce the minimal within-group sum of square deviation. Because we were interested in projection neurons and based on our knowledge that most cortical projecting cells correspond to excitatory neurons we confined our analyses to PPNs. Freezing-evoked activity of recorded neurons was calculated by comparing the firing rate during a 2 s freezing episode to the preceding 2 s non-freezing episode (bin size: 200 ms) via a *z*-score transformation. *Z*-scored values were calculated by subtracting the average baseline firing rate established over the 2 s during non- freezing episodes from individual raw values and by dividing the difference by the baseline standard deviation. A unit was considered as significantly activated during freezing episodes if at least two consecutive time bins presented *z*-score > 1.95 alternatively a unit was considered as significantly inhibited if it presented two consecutive time bins < -1.95. In order to identify the main pattern of avoidance-evoked activity among PPNs, we used an unbiased principal component analysis (PCA) based on the neuronal normalized activity evoked in the time period between the door-opening for CS^+ door opened avoid trials and the moment preceding the shock delivery (8.8 s post-door opening). The PCA was made on a group of 8 mice displaying good avoidance rate (> 30%) and CS^-/CS^+ discrimination (neural normalized activity was *z*-scored, bin size 200ms, during behavioral session 6). Only the first PC was considered (PC1) because it explained

most of the variance of our dataset observed among PPNs between door opening and avoidance, namely a sustained activation. Avoidance-activated and avoidance-inhibited dmPFC PPN were defined as respectively positively and negatively correlated with PC1 at the $P < 0.01$ significance level using Pearson's correlation table.

VII. Virus injections, implantations and optogenetics

For specific optogenetic manipulation of the dmPFC-dl/lPAG pathway during behavior we used C57BL6/J wild-type mice. Animals were bilaterally injected with glass pipettes (tip diameter 10-20 µm) connected to a picospritzer (Parker Hannifin Corporation; ~ 0.2 µL per hemisphere) with a cocktail of Cav2-Cre, HSV-Cre retrograde virus and AAV-hSyn-mCherry in the dl/lPAG at the following coordinates relative to bregma: −4.50 mm AP; ± 0.5 ML; −1.45 DV from dura. The same animals received also an injection of AAV5-EF1a-DIO-hChR2 (H134R)-EYFP or AAV9-FLEX-ArchT-GFP, or AAV5-FLEX-GFP (UNC Vector Core Facility) in the dmPFC at the following coordinates relative to bregma: +1.8 mm AP; ± 0.40 ML; −1.3 DV from dura. Following 4 weeks of recovery from injections, mice were implanted with a custom-built optrode in the left hemisphere consisting of 16-wire electrode, as described in "*Surgery and recordings*" attached to a custom-built optic fiber (diameter: 200 µm; numerical aperture: 0.39; Thorlabs) and a simple optic fiber in the right hemisphere at the following coordinates relative to bregma: +1.8 mm AP; ± 0.55 mm ML; −1.15 mm DV from dura; lowered at an angle of 10°.

To visualize dmPFC terminals into VGLUT2$^+$, GAD$^+$, SST$^+$ cells in the dl/lPAG, transgenic mice respectively VGLUT2-Cre, GAD-cre and SST-cre mice were injected into the dmPFC with unconditionally expressed GFP-tagged synaptophysin (Syn) in presynaptic terminals (AAV(2/9)/CAG-SynGFP) and a cre-dependant mcherry in the dl/lPAG. Following 4 weeks of recovery, mice were perfused and dmPFC presynaptic terminals into different specific cell types in the dlPAG were counted (*see "Histological analyses" section*).

VIII. In-vitro patch-clamp recordings

Acute slice preparation

Fresh slices were obtained from 3- to 4-month old VGLUT2-Cre, GAD-Cre and SST-Cre mice as described previously (Houbaert, et al., 2013). All recordings were performed on dlPAG-containing coronal slices (anteroposterior 3.8–4.5 mm). Briefly, mice were anesthetized by intraperitoneal injection of a mixture of ketamine (10 mg/ml)/xylazine (1 mg/ml) before an intracardiac perfusion with a refrigerated bubbled (carbogen: 95% O2/5% CO2) sucrose solution containing the following (in mM): 2.7 KCl, 26 NaHCO3, 1.25 NaH2PO4, 10 glucose, 220 sucrose, 0.2 CaCl2, and 6 MgCl2. Then, the brain was sliced (350 um thickness with a vibratome (Leica VT1200s) at 4°C in sucrose solution. Slices were then maintained for 45 min at 37°C in an interface chamber with ACSF containing the following (in mM): 124 NaCl, 2.7 KCl, 2 CaCl2, 10 MgSO47H2O, 26 NaHCO3, 1.25 NaH2PO4, 18.6 glucose, and 2.25 ascorbic acid and equilibrated with 95% O2/5% CO2. Recordings were performed with standard ACSF (Humeau, et al., 2005).

Electrophysiological recordings

Light-evoked and spontaneous excitatory synaptic activities and cellular properties of dlPAG GFP-expressing neuronal cells were recorded using classical whole-cell patch-clamp techniques as previously described (Humeau, et al., 2005; Houbaert et al., 2013). Cells were recorded in current clamp (spiking activities) or voltage-clamp mode (synaptic conductances), respectively, using K-gluconate-based (in mM as follows: 140 K-gluconate, 5 QX314-Cl, 10 HEPES, 10 phosphocreatine, 4 Mg-ATP, and 0.3 Na-GTP, pH adjusted to 7.25 with KOH, 295 mOsm) and Cs-methyl sulfonate-based (in mM as follows: 140 Cs-methyl sulfonate, 5 QX314-Cl, 10 HEPES, 10 phosphocreatine, 4 Mg-ATP, and 0.3 Na-GTP, pH adjusted to 7.25 with CsOH, 295 mOsm) intracellular recording solutions.

Optogenetic-based experiments

mPFC-dlPAG monosynaptic EPSCs were elicited by 1 ms light pulse delivered by an ultrahigh-power 460 nm LED (Prizmatix) at maximal intensity. All included cells were

recorded in dorso-lateral portion of the PAG region. As for above-mentioned experiments, data were recorded with a Multiclamp700B (Molecular Devices), filtered at 2 kHz, and digitized at 10 kHz. Data were acquired and analyzed with pClamp10.2 (Molecular Devices).

IX. In-vivo optogenetic manipulations

Wild-type C57BL6/J mice expressing either Channelrhodopsin coupled with GFP or a control GFP in neurons projecting from the dmPFC to the dl/lPAG were stimulated optogenetically using analog blue light pulses (10Hz, 10 ms pulse width, 10mw) delivered during training sessions 7 and 8. The stimulation was performed at the door opening for both CS^- and CS^+ trials until the door was slided up.

A second group of C57BL6/J mice expressing either Archeorhodopsin coupled with GFP or control GFP in dmPFC to dl/lPAG projectors neurons was stimulated with a continuous yellow light in the same conditions than the first group of mice. Following the two stimulation sessions, all groups underwent two other behavioral sessions with no light stimulation to assess the long-term effect of the optogenetic manipulation.

X. Optogenetic control tests

1) Locomotion control test

To control whether our optogenetic manipulation of dmPFC to dl/lPAG pathway influenced motor responses, all animals were exposed to a control session in the shuttle-box during 15 min. A 10 Hz blue light stimulation, or a yellow light continuous stimulation of dmPFC neurons projecting to the dl/lPAG was delivered from minute 5 to 10 of the 15 minutes test. The distance traveled in the shuttle-box as well as the number of crossings during, before and after the light stimulation were extracted.

2) Place-preference test

The place-preference test was conducted to determine whether the optogenetic activation of dmPFC to dl/lPAG pathway present any rewarding properties. If so, the optogenetic activation of the pathway would induce a preference of the animal towards the compartment in which the stimulation is delivered. This would also

introduce a bias into the dissociation between the effect of the stimulation on avoidance performance and the rewarding part of it.

During this control, animals underwent three days of tests in a two-identical compartments shuttle-box. On the first day, they were submitted to a context habituation session, during which they were able to freely explore the two compartments of the apparatus for 9 minutes. At the end of this session, the preferred compartment, in which the animal spent most of the 9 minutes test was determined. On the second day, animals underwent a second 9 min session in the same apparatus during which a 10 Hz optogenetic blue laser stimulation (10 ms pulse-width, 10 mw, 473 nm wavelength) was started each time the animal enters the non-preferred compartment. Animals were exposed to the same context for 9 min on the last third day without any stimulation. The time spent in the preferred and non-preferred compartment was scored during the three days.

3) Hot-plate test

Knowing that all columns of the PAG receive nociceptive inputs (Keay and Bandler, 2001; Lumb, 2004; Parry, et al., 2008), it is of a big importance to control whether the optogenetic manipulation of dmPFC-dl/lPAG pathway changes pain perception. To do so we used a hot-plate test during which animals underwent two days of tests. The apparatus consisted of a square arena in which the floor presented an aluminium heating plate. Two minutes after habituation to the context, the temperature was increased linearly with a rate of 6 °/min and a starting temperature of 30°C. To determine the time and temperature at which the mice displayed pain responses, we quantified hindpaw licking or jumping behaviors. On the first day of exposure, we determined the basal nociceptive temperature whereas on the second day we measured the nociceptive temperature during optogenetic stimulation of dmPFC neurons projecting to the dl/lPAG (10Hz, 10mw, 10 ms pulse width), which started 30 seconds before heating the plate. The day of the optogenetic stimulation was counterbalanced for half of the mice. During both days, we measured the nociceptive temperature as well as the latency of nociceptive responses.

XI. Antidromic identification

Following the 6th or 10th behavioral sessions, concentric stimulating electrodes (FHC) were lowered in the PAG at the following coordinates relative to bregma, −4.5 mm AP; −0.55 mm ML; −1 to −2 mm DV from dura. During electric identification the stimulation electrodes were advanced in steps of 5 µm by a motorized micromanipulator (FHC) and evoked responses were recorded in the dmPFC. Stimulation-induced and spontaneous spikes were recorded and sorted as described in *"Surgery and recordings"* and *"Single unit analyses"*. To ensure that the same neurons were recorded during the last behavioral session (6th or 10th) and during the electric identification, waveforms were averaged during behavior and anesthesia and correlated as previously described. To be classified as antidromic, evoked-responses had to meet at least two out of three criteria (Lipski, 1981): stable latency (< 0.4 ms jitter), collision with spontaneously occurring or evoked spikes, and follow high-frequency stimulation (200 Hz). At the end of the experiments, stimulating sites were marked with electrolytic lesions before perfusion, and electrode locations were verified as described in the *Histological analyses section*.

XII. Histological analyses

Mice were administered a lethal dose of isoflurane and underwent transcardial perfusions via the left ventricle with 4% paraformaldehyde (PFA) in 0.1 M phosphate buffer. Following dissection, brains were post-fixed for 24 h at 4°C in 4% PFA. Brain sections of 80 µm-thick were cut on a vibratome, mounted on gelatin-coated microscope slides, and dried. To identify electrolytic lesions, sections were stained with toluidine blue, dehydrated, mounted, and verified using conventional transmission light microscopy. Only electrodes terminating in the anterior cingulate, and prelimbic cortex were included in our analyses. For verification of viral injections and optic fiber location in dmPFC and dl/lPAG, 80 µm-thick slices containing the regions of interest were mounted in VectaShield (Vector Laboratories) and were imaged using an epifluorescence system (Leica DM 5000) fitted with a 10x dry objective. For imaging of slices at different wavelength (Figure 6A), we always started

imaging the higher wavelength (green) and then the lowest one (blue). In some cases, the microscope setting was not optimum and revealed stripes on the acquired images. The location and the extent of the injections/infections were visually controlled. Only infections accurately targeted to the dmPFC and optic fibers terminating in the anterior cingulate and prelimbic cortex were considered for behavioral and electrophysiological analyses.

To characterize the connectivity between the dmPFC and the dl/lPAG we injected transgenic mice with GFP-tagged synaptophysin (Syn) in the dmPFC and labeled dl/lPAG specific cell types by injected a Cre-dependent mCherry in VGLUT2-cre, Gad-Cre and SST-Cre mice (See *virus injections, implantations and optogenetics* section).

The quantification of synaptic inputs was performed manually on images acquired with Olympus confocal microscope (Confocal microscope SPE 2, Model Leica DM6 TCS SPE) with z-stacks of 80 µm of slice, with a step of 0.3 µm and a x10 or x40 objective. We used Imaris software allowing a 3 dimensional reconstruction of cells surface and synaptic contacts that we manually counted.

XIII. Quantification and Statistical Analysis

Analyses were performed with Matlab and Graphpad Prism. For all datasets normality was tested using the Shapiro-Wilk normality test ($\alpha < 0.05$) to determine whether parametric or non-parametric analyses were required. Parametric analyses included t. tests and one- and two-way repeated-measures ANOVA followed by Bonferroni's multiple comparison post-hoc test if a significant main effect or interaction was observed. For parametric data, correlation analyses were made using Pearson's correlation. If datasets did not meet normality assumptions non-parametric analyses were used (mainly non-parametric Mann-Whitney test). If significance was observed, these non-parametric analyses were followed by Dunn's multiple comparison post hoc tests. For non-parametric data, correlation analyses were made using Spearman's correlation. Comparing cumulative distributions was made using Kolmogorov-Smirnov test. Apart from t. tests, the asterisks in the figures represent the *P*-values of post hoc tests corresponding to the following values $^{*}p < 0.05$; $^{**}p < 0.01$; $^{***}p < 0.001$ based on mean ± S.E.M.

Results

I. Behavioral results

In order to investigate the neuronal correlates of freezing and avoidance defensive behaviors and figure out whether those two antagonistic behaviors are mediated by the same or different neuronal circuits, we developed a novel behavioral paradigm. This paradigm enabled us to study both freezing and avoidance conditioned behaviors to a single conditioned stimulus in two different contextual configurations. In a two compartment shuttle-box, when the separating door was slided-down (door-opened) mice had a route to escape a started shock or to avoid its delivery during the CS^+. When the door was slided-up, no route of avoiding/escaping the CS^+ being available, the mice usually expressed freezing to CS^+ presentation **(Figure 12)**.

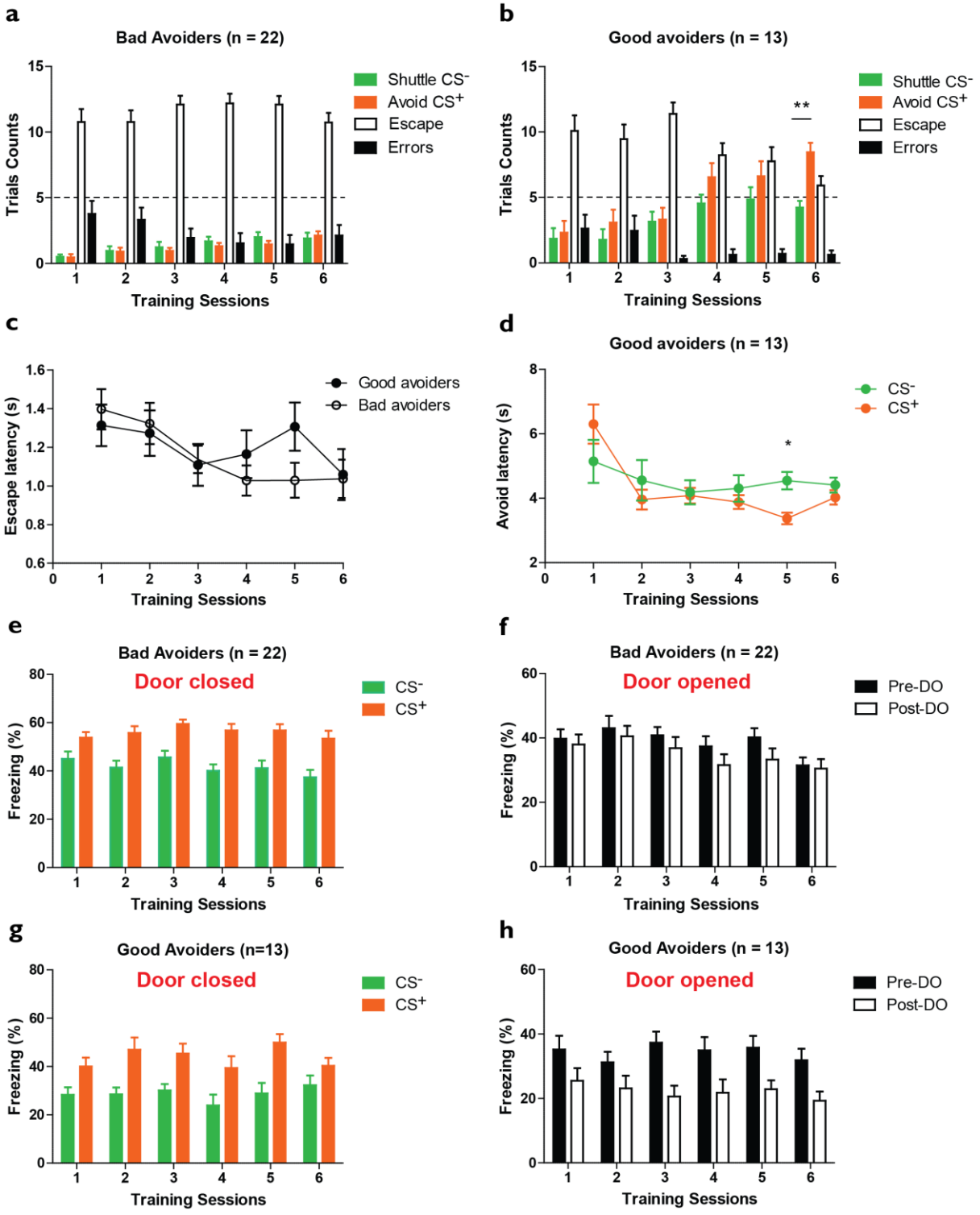

Figure 14. Behavioral characterization of Good and Bad avoiders

a. Trial counts (shuttle CS^-, avoid CS^+, escape, errors) across 6 training sessions in **Bad avoiders** (n = 22) (two-way repeated measures ANOVA; group: $F_{(3,420)} = 104.5$, $p < 0.0001$, training session: $F_{(5,420)} = 0.50$, $p = 0.77$, group x training session: $F_{(15,420)} = 3.98$, $p < 0.0001$). **b.** Trial counts (shuttle CS^-, avoid CS^+, escape, errors) across 6 training sessions in **Good avoiders** (n =13) (two-way repeated measures ANOVA; group: $F_{(3,240)} = 28.43$, $p < 0.0001$, training session: $F_{(5,240)} = 1.13$, $p = 0.34$, group x training session: $F_{(15,240)} = 8.83$, $p < 0.0001$, and $p < 0.01$). **c.** Escape latency (s) for both **Good** and **Bad avoiders** across 6 training sessions (two-way repeated measures ANOVA; group: $F_{(1,184)} = 0.54$, $p = 0.45$, training session: $F_{(5,184)} = 2.55$, $p = 0.02$, group x training session: $F_{(5,184)} = 0.82$, $p = 0.53$). **d.** Avoid latencies during DO trials for both CS^+ and CS^- trials in **Good** avoiders (n = 13) (two-way repeated measures ANOVA; group: $F_{(1,114)} = 1.56$, $p = 0.21$, training session:

$F_{(5,114)}$ = 7.03, $p < 0.0001$, group x training session: F (5,114) = 2.45, $p = 0.03$, * $p < 0.05$). **e.** Averaged freezing behavior in **Bad avoiders** ($n = 22$) across training sessions for both CS^+ and CS^- at door-closed trials (two-way repeated measures ANOVA; group: $F_{(1,210)} = 30.80$, $p < 0.0001$, training session: $F_{(5,210)} = 1.96$, $p = 0.08$, group x training session: $F_{(5,210)} = 0.76$, $p = 0.57$). **f.** Averaged freezing behavior in **Bad avoiders** across training before and after door opening (8.8s pre-DO and post-DO) (two-way repeated measures ANOVA; group: $F_{(1,210)} = 2.05$, $p = 0.15$, training session: $F_{(5,210)} = 3.68$, $p = 0.003$, group x training session: $F_{(5,210)} = 0.34$, $p = 0.88$). **g.** Averaged freezing behavior in **Good avoiders** ($n = 13$) across training sessions for both CS^+ and CS^- at door-closed trials (two-way repeated measures ANOVA; group: $F_{(1,120)} = 17.82$, $p = 0.0003$, training session: $F_{(5,120)} = 1.53$, $p = 0.18$, group x training session: $F_{(5,120)} = 1.04$, $p = 0.39$). **h.** Averaged freezing behavior in **Good avoiders** across training before and after door opening (8.8 s pre-DO and post-DO) (two-way repeated measures ANOVA; group: $F_{(1,120)} = 23.67$, $p < 0.0001$, training session: $F_{(5,120)} = 0.47$, $p = 0.79$, group x training session: $F_{(5,120)} = 0.37$, $p = 0.86$).

Using this behavioral paradigm two behavioral profiles were categorized. The first category corresponds to **Bad avoiders** showing a deficit in avoidance learning **(Figure 14 a)**. The second group of mice consists of **Good avoiders** who learned **(i)** to avoid CS^+ across the 6 training sessions and to **(ii)** discriminate between CS^+ and CS^- in terms of avoidance **(Figure 14 b)**. Indeed, **Good avoiders** after 6 training sessions avoid significantly more to the aversive CS^+ compared to the neutral CS^- **(Figure 14 b)**. Apart the increased number of avoidance being a direct indicator of learning with training, the latency of the learned responses is also a second indicator of learning. With training, **Bad avoiders** did not present any significant change in the number of escape trials. Nevertheless, their escape latency decreased across training. It was also the case for **Good avoiders** for which both the number and the latency of escape responses decreased with training **(Figure 14 b, c)**. Importantly, escape latency in both **Bad** and **Good avoiders** was not significantly different suggesting that both classes of mice present similar escape kinetics **(Figure 14 c)**. Another index of learning in **Good avoiders** is that they learn to avoid the CS^+ quicker with training compared to the CS^- **(Figure 14 d)**.

The second behavioral trait we observed in **Bad avoiders** is that they adopted a general strategy of freezing behavior during CS^+ in both DC **(Figure 14 e)** and DO conditions **(Figure 14 f)**. In DC condition, **Bad avoiders** freeze significantly more to CS^+ as compared to CS^- across training, which indicate that they discriminate between both stimuli **(Figure 14 e)**. In DO condition, freezing before the door was opened (pre-DO) and after door opening (post-DO) was not significantly different in **Bad avoiders (Figure 14 f)**. These data suggested that **Bad avoiders** discriminate both CS^- and CS^+ in terms of freezing and present a bias in their behavioral expression toward freezing expression to an aversive CS^+.

As for **Good avoiders**, they also discriminate CS^+ from CS^- in terms of freezing in the DC configuration **(Figure 14 g)**. In contrast, in the DO condition, **Good avoiders** switch their defensive strategy from passive to active at the door opening. Indeed,

Good avoiders decrease their freezing levels post-DO as compared to pre-DO **(Figure 14 h)**.

We should note that **Good avoiders** freeze less than **Bad avoiders**. This behavioral trait being probably linked to the biased behavior of **Bad avoiders** toward freezing.

Also, one should notice that the acquisition, expression and discrimination learning in terms of freezing occurred very quickly, at the end of the first training session for both **Bad** and **Good avoiders**. As for avoidance acquisition and discrimination, it took at least up to 6 sessions for the animals to acquire both the avoidance response performance and discrimination between CS^+ and CS^-.

In summary, we developed a novel behavioral paradigm allowing a mouse to acquire and perform discriminative passive (freezing) and active (avoidance) behavior to a single conditioned stimulus depending on contextual contingencies. The kinetics of acquisition of both behaviors were dissimilar; discriminative freezing being acquired very rapidly as compared to a progressive acquisition of discriminative avoidance. In terms of our behavioral paradigm, two categories of mice were identified:

- Bad avoiders: acquired discriminative freezing very rapidly but did not acquire discriminative avoidance.

-Good avoiders: acquired discriminative freezing early during training and discriminative avoidance progressively with training.

In **Good avoiders**, we observed that a subgroup of mice generalized between the CS^- and the CS^+ in terms of avoidance as illustrated by a lack of difference in the number of avoidance performed to the CS^- and CS^+ **(Figure 15 a-c)**. Considering the total of mice submitted to our paradigm (*n* = 40), **Bad** and **Good avoiders** represent 55% (*n* = 22) and 45% (*n* = 18), respectively. Among **Good avoiders**, 5 mice generalized (12% of the entire population) whereas 13 discriminated (33% of the entire population) between CS^- and CS^+ in terms of avoidance behavior **(Figure 15 d)**. Nevertheless, generalizers acquired and expressed discriminative freezing behavior since they (i) freeze more to the CS^+ compared to the CS^- **(Figure 15 e)** and (ii) decreased their freezing levels at post-DO as compared to pre-DO **(Figure 15 f)**. In the subsequent analyses, we will use the terminology **Good avoiders** to refer to discriminators and the terminology generalizers otherwise.

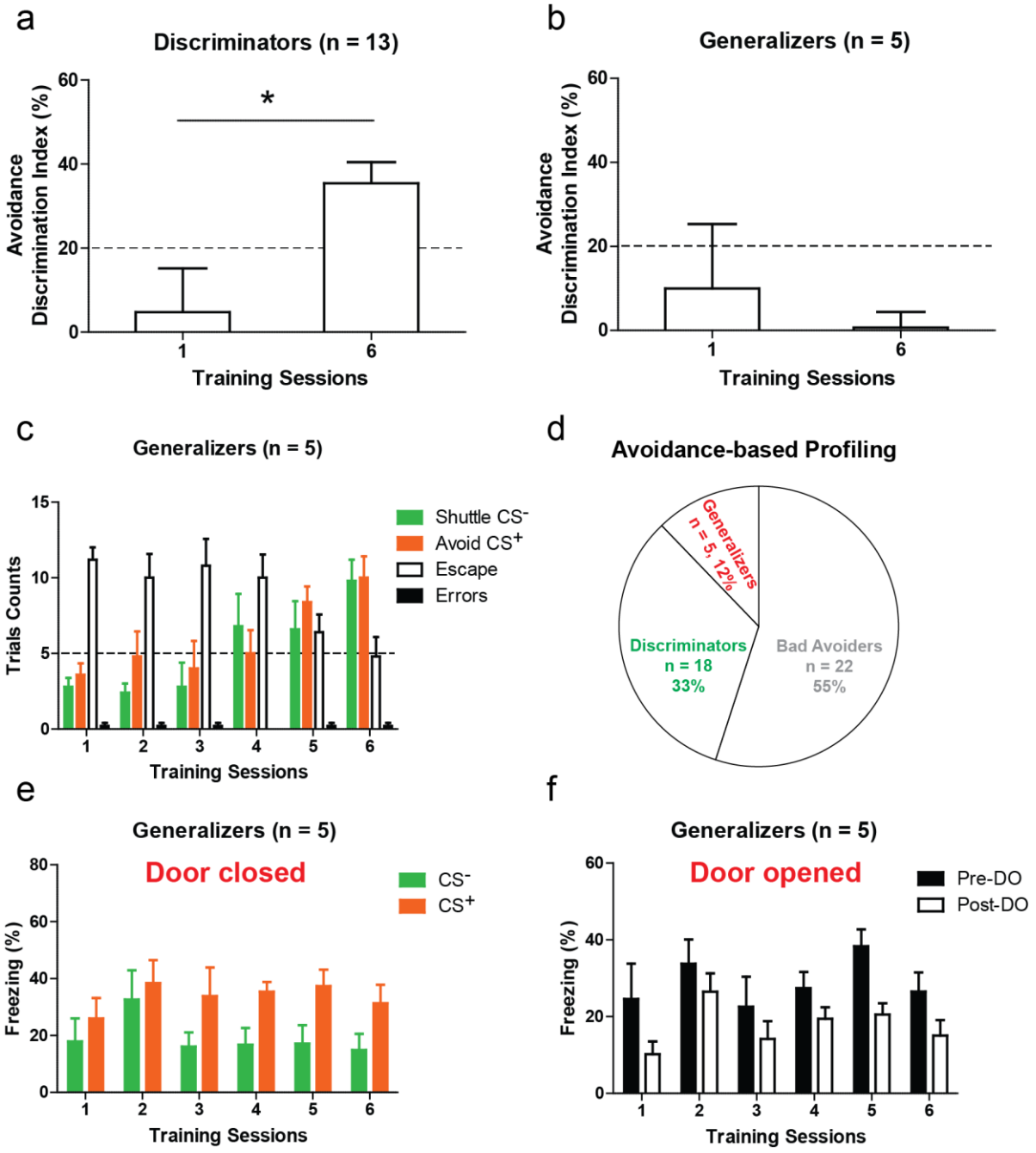

<u>Figure 15.</u> A subset of Good avoiders generalized between CS$^-$ and CS$^+$ during avoidance

a. Avoidance discrimination index calculated as following ((Avoidance counts CS$^+$) - (avoidance counts CS$^-$)) / ((Avoidance counts CS$^+$) + (Avoidance counts CS$^-$ +1)) for **Good avoiders** discriminators (paired t. test: t = 2.81, p = 0.015) and generalizers in panel **b.** (paired t.test: t = 0.57, p = 0.59) at first and sixth training sessions. The dashed line at 20% represents the cut-off that we consider to classify mice as generalizers versus discriminators. **c.** Trial counts (shuttle CS$^-$, avoid CS$^+$, escape, errors) across 6 training sessions in generalizers (n = 5) (two-way repeated measures ANOVA; group: $F_{(3, 80)}$ = 17.90, p < 0.0001, training session: $F_{(5, 80)}$ = 2.30, p = 0.052, group x training session: $F_{(15, 80)}$ = 6.96, p < 0.0001). **d.** Pie-chart representative of avoidance-based profiles for the 40 mice tested. **Bad avoiders** represent 55 % (n = 22), **Good avoiders** discriminators 33 % (n = 13) and generalizers 12 % (n = 5). **e.** Averaged freezing behavior in generalizers (n = 5) across training sessions for both CS$^+$ and CS$^-$ at DC trials. (Two-way repeated measures ANOVA; group: $F_{(1, 40)}$ = 5.36, p = 0.04, training session: $F_{(5, 40)}$ = 1.24, p = 0.30, group x training session: $F_{(5, 40)}$ = 0.47, p = 0.78). **f.** Averaged freezing behavior in generalizers across training before and after door opening (8.8 s pre-DO and post-DO) (two-way repeated measures ANOVA; group: $F_{(1, 40)}$ = 6.05, p = 0.03, training session: $F_{(5, 40)}$ = 2.80, p = 0.02, group x training session: $F_{(5, 40)}$ = 0.40, p = 0.83).

To further evaluate whether **Good** and **Bad avoiders** could be distinguished at the behavioral level before avoidance training, we evaluated freezing and shuttling behavior without (Day 1) and during (Day 2) CS presentations during the habituation period. In both **Bad** and **Good avoiders**, during the habituation to the shuttle-box on Day 1, freezing was low and mice shuttled equally **(Figure 16 a)**. **Bad** and **Good** avoiders spent as much time in one compartment of the shuttle-box (Zone 1: Z1) as in the other (Zone 2: Z2) **(Figure 16 b)**, which suggests that both groups of mice did not show any compartment-preference in the shuttle-box. On the second day of habituation, mice were habituated to the tones used during training. Both **Bad** and **Good avoiders** showed slightly but significantly more freezing to the CS^- compared to the CS^+, which could be linked to the intrinsic properties of the stimulus although freezing values were lower than 20% **(Figure 16 c)**. In addition, **Good avoiders** shuttled significantly more to both tones during habituation **(Figure 16 d)**. These results are interesting because they suggest that **Good** and **Bad avoiders** can be differentiated before avoidance training, solely based on CS-induced shuttle behavior. This could be linked to differences in the perception of the CS for instance or impulsive behavior that would promote shuttling behavior during CS presentations.

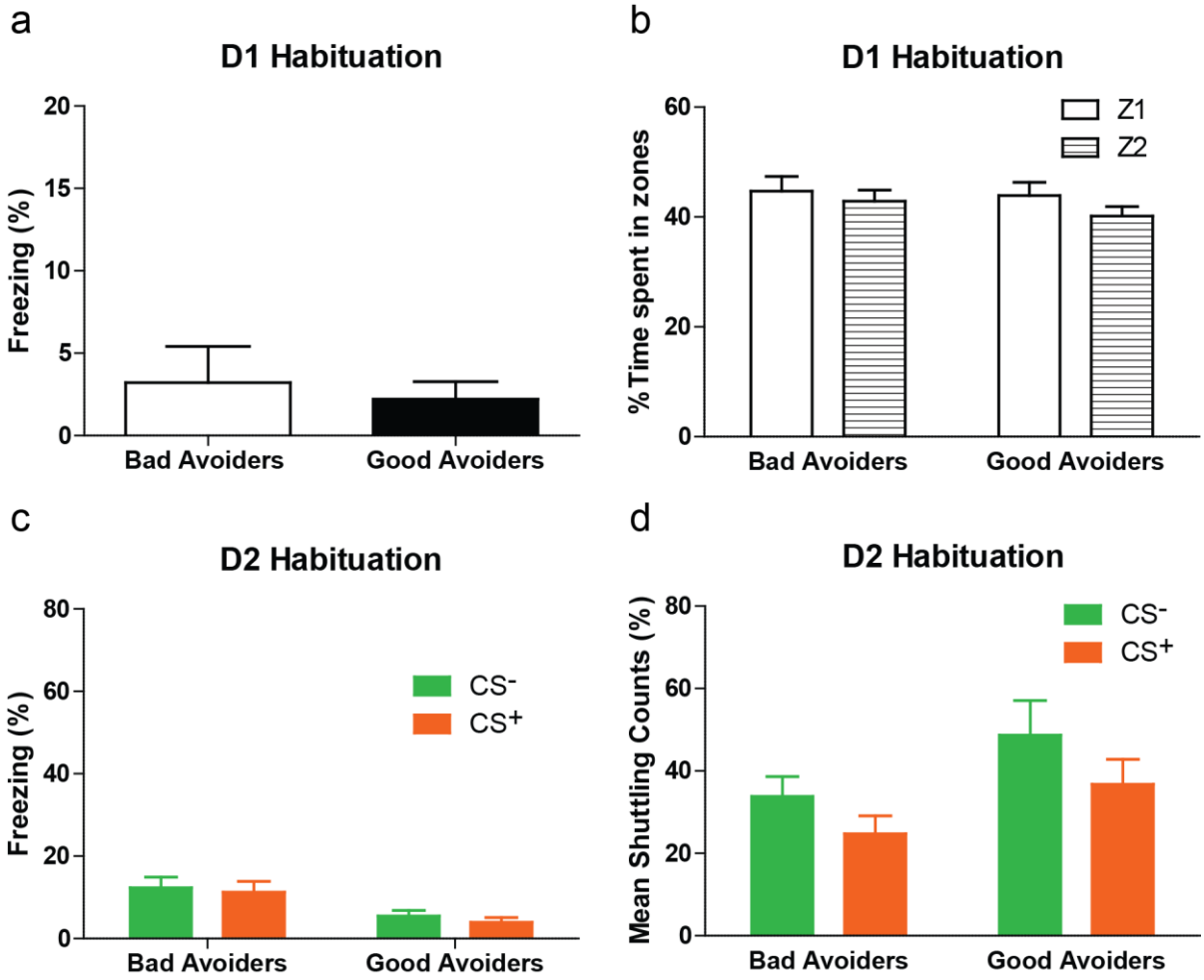

Figure 16. Bad and Good avoiders display different tone-evoked and shuttling responses during habituation.

a. Averaged freezing behavior in **Bad** and **Good avoiders** during shuttle-box habituation (unpaired t.test: $t = 0.33$, $p = 0.74$). **b.** Percentage of time spent in the two compartments of the shuttle-box (Z1 and Z2) during habituation Day 1 (two-way repeated measures ANOVA; zones: $F_{(1, 33)} = 2.36$, $p = 0.13$, avoiders profile: $F_{(1, 33)} = 0.71$, $p = 0.4$, group x training session: $F_{(1, 33)} = 0.08$, $p = 0.77$). **c.** Averaged freezing behavior in **Bad** and **Good avoiders** during door and tone habituation Day 2 (two-way repeated measures ANOVA; CS type: $F_{(1, 33)} = 4.59$, $p = 0.03$, avoiders profile: $F_{(1, 33)} = 1.42$, $p = 0.24$, group x training session: $F_{(1, 33)} = 0.04$, $p = 0.83$). **d.** Mean shuttling counts in **Bad** and **Good avoiders** during door and tone habituation Day 2 (two-way repeated measures ANOVA; CS type: $F_{(1, 33)} = 3.39$, $p = 0.07$, avoiders profile: $F_{(1, 33)} = 7.79$, $p = 0.008$, group x training session: $F_{(1, 33)} = 0.14$, $p = 0.7$).

In our paradigm **(Figure 12)** mice are exposed to unpredictable and uncontrollable stress conditions (in the DC condition), which could lead to the development of a learned helplessness profile, a depression-like symptom in rodents (Chourbaji, et al., 2005). This behavioral profile is characterized by deficits in avoiding the shock when a route of avoidance is accessible (DO condition) that might explain the development of the Bad learner phenotype. To determine whether **Bad avoiders** developed this learned helplessness profile, they were submitted following our behavioral protocol to a depression model in rodents: the forced swim test (FST) **(Figure 17 a)**. The FST is one of the most commonly used behavioral assays to study depressive-like behaviors

in rodents (Yankelevitch-Yahav, et al., 2015). It is based on the assumption that after placing mice in a container filled with water, mice will first try to escape within the first few minutes but then will display a characteristic immobility behavior in which the animal only moves to maintain its head above the water. This physical immobility is considered as an indicator of ‘’behavioral despair’’ and mice presenting depressive-like profile exhibit an increased immobility in the FST (Castagné, et al., 2011). Mice submitted to the FST protocol presented a vigorous swimming activity during the first two minutes (data not shown) and immobility was observed after the third minute of exposure. Our behavioral analyses focused on the last 4 minutes of the FST during which maximal immobility was observed in the mice. **Bad avoiders** when compared to **Good avoiders** did not differ in the amount of time spent immobile during the last 4 minutes of the FST **(Figure 17 c)**. In addition, no significant correlation was observed between the number of CS^+ trials avoided at the end of training (session 6, day 8) and the time spent immobile during the 4 last min of the FST test **(Figure 17 d)**. Interestingly, we were able to characterize two additional behavioral profiles during the FST. First, generalizers (filled red dot in **Figure 17 b**) spent the 4 minutes swimming in the container, almost never being immobile. Second, a mouse which got almost all the shocks during the avoidance training, spent almost the totality of the 4 minutes immobile and had to be rescued before to flow (empty red dot in **Figure 17 b**). Those two profiles represent a very low amount of mice that were excluded from our analyses as they might present a hyper-active profile for the first case and a learned helplessness profile for the second.

This control experiment suggests that Bad avoiders do not present a learned helplessness, depressive-like profile that could explain the lack of avoidance learning.

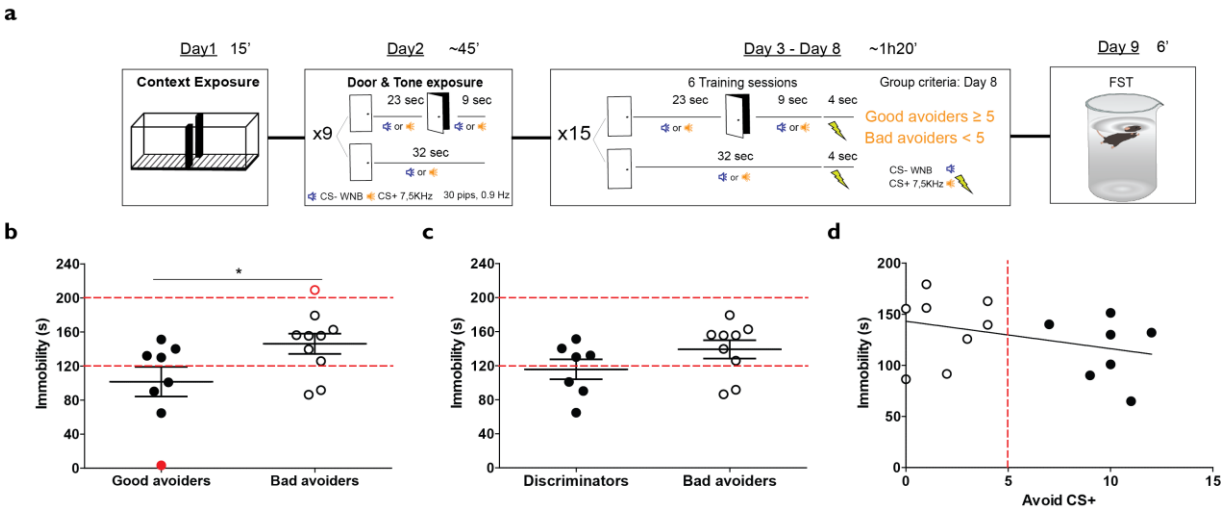

Figure 17. Bad and Good avoiders do not differ in the forced swim test

a. Mice undergoing the avoidance behavioral protocol for 8 days (see **Figure 13**) were classified into **Good** and **Bad avoiders** and were exposed one day later to the forced swim test (FST) during 6 minutes**. b.** Time spent immobile during the 4 last minutes of the FST for **Good and Bad avoiders**. Filled red circle represent a generalizer and empty red circle represent a mouse with a learned helplessness profile which spent all the 4 minutes immobile that was about to drown at the end of the session (unpaired t. test: t = 2.19, p = 0.04). **c.** Time spent immobile during the 4 last minutes of the FST for **Good** and **Bad avoiders** excluding the learned helplessness profile mouse (unpaired t. test: t = 1.47, p = 0.16). **d.** Correlation between the number of avoidance to the CS^+ and the time spent immobile during the 4 last minutes of the FST (Spearman correlation r = -0.34, p = 0.18). Filled circles concern the **Good avoiders** and empty circles concern the **Bad avoiders**. The horizontal dashed lines represent the lower and upper limits of immobility time range of a control group of mice exposed to the same FST protocol (Kara, et al., 2014; Kara, et al., 2016). The vertical dashed red line represents the threshold separating **Bad** and **Good avoiders**.

To evaluate the influence of the CS used as a CS^+ on the phenotype observed, we counterbalanced the CS type in a cohort of animals. In this group the white noise CS was used as a CS^+ and the 7.5 KHz CS was used as a CS^- **(Figure 18 a)**. Our data revealed that in the counterbalanced group, we generated more **Good avoiders** although they were more likely to generalize avoidance behavior to the CS^- **(Figure 18 b)**. Therefore using this experimental design, we would generate less **Good avoiders** showing discrimination. For these reasons we rather used white noise as the CS^- and the 7.5 KHz as a CS^+ throughout the manuscript.

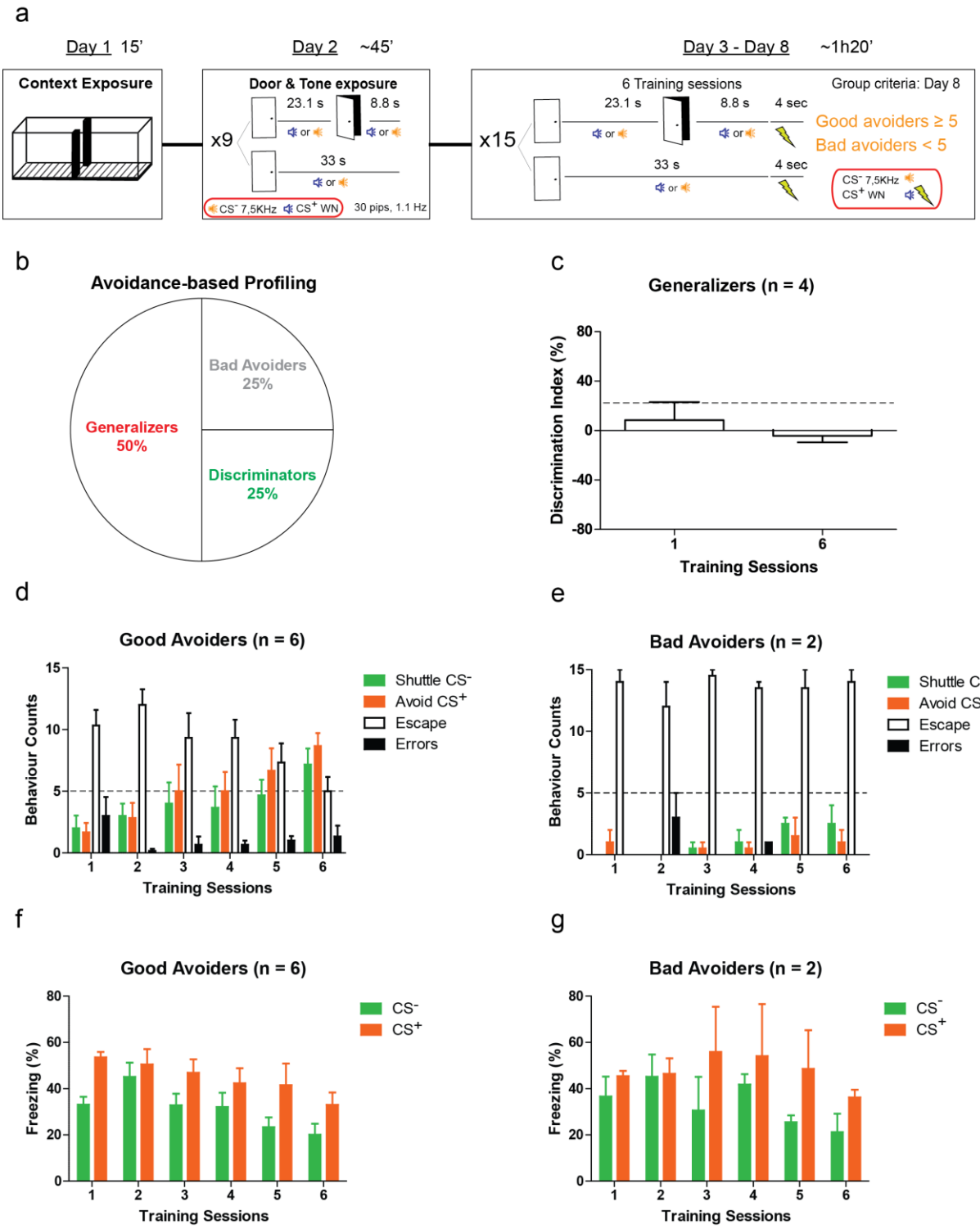

Figure 18. Avoidance behavior when CS$^-$ and CS$^+$ were counterbalanced

a. Behavioral protocol. On Day 1, mice were habituated during 15 min to the shuttle-box. On Day 2, animals were habituated to the presentation of two sounds that were played on two contextual conditions: (i) door-closed (DC) during which the sound was played for 33 s, and (ii) door opened condition during which 23.1 sec following the sound's onset the door is slided-down (DO) and slided-up again 8.8 sec after. 9 trials of each type of trials was played for both sounds and the session lasted about 45 min. From Day 3 to day 8, animals underwent 6 training sessions lasting each about 1h20 and during which the same type of trials than on Day 2 were played except that the number of trials was increased to 15 and CS$^+$ trials were followed by a 4 s shock in the condition DC. At Day 8 animals were categorized into **Good** or **Bad avoiders** based on their behavioral avoidance scores. **b.** Pie-chart representative of avoidance-based profiles of 8 mice. **Bad avoiders** represent 25 % (*n* = 2), **Good avoiders** discriminators 25 % (*n* = 2) and **Good avoiders** generalizers 12 % (*n* = 4). **c.** Avoidance discrimination index % calculated as following ((Avoidance counts CS$^+$) - (avoidance counts CS$^-$)) / ((Avoidance counts CS$^+$) + (avoidance counts CS$^-$+1)) or **Good**

avoiders generalizers at first and sixth training sessions (paired t. test: $t = 0.93$, $p = 0.41$). The dashed line at 20 % represents the cut-off that we consider to classify mice as generalizers versus discriminators. **d.** Trial counts (shuttle CS^-, avoid CS^+, escape, errors) across 6 training sessions in **Good avoiders** generalizers and discriminators (n = 6) (two-way repeated measures ANOVA; group: $F_{(3,100)} = 12.57$, $p < 0.0001$, training session: $F_{(5,100)} = 0.69$, $p = 0.63$, group x training session: $F_{(15,100)} = 4.65$, $p < 0.0001$). **e.** Trial counts (shuttle CS^-, avoid CS^+, escape, errors) across 6 training sessions in **Bad avoiders** (n = 2) (two-way repeated measures ANOVA; group: $F_{(3, 20)} = 159.4$, $p < 0.0001$, training session: $F_{(5, 20)} = 0.44$, $p = 0.81$, group x training session: $F_{(15, 20)} = 1.53$, $p = 0.18$). **f.** Averaged freezing behavior in **Good avoiders** ($n = 6$) across training sessions for both CS^+ and CS^- at DC trials (two-way repeated measures ANOVA; group: $F_{(1, 50)} = 4.83$, $p = 0.052$, training session: $F_{(5, 50)} = 7.07$, $p < 0.0001$, group x training session: $F_{(5, 50)} = 0.89$, $p = 0.49$). **g.** Averaged freezing behavior in **Bad avoiders** ($n = 2$) across training sessions for both CS^+ and CS^- at DC trials (two-way repeated measures ANOVA; group: $F_{(1, 10)} = 1$, $p = 0.42$, training session: $F_{(5, 10)} = 2.04$, $p = 0.15$, group x training session: $F_{(5, 10)} = 0.85$, $p = 0.54$).

We have established a novel behavioral paradigm, which presents several interesting properties. First, it allows investigating both passive and active defensive strategies in the very same animal depending on the type of trial presented. Second, freezing and avoidance responses are generated by the presentation of the same CS^+, which controls for sensory-driven neuronal activations. Third, the disparity in the behavioral profiles observed (Good versus Bad learners) is an interesting phenomenon as it allows investigating the underlying neuronal mechanisms and to perform loss and gain of function optogenetic experiments.

II. C-fos Immunoreactivity

As described in the introduction the neuronal underpinnings of avoidance behavior are controversial given the diversity of the paradigms used (Bravo-Rivera, et al., 2014; Tovote, et al., 2016; LeDoux, 2017; Diehl, et al., 2018). However several lines of evidence point to the prefrontal cortex and the periaqueductal gray as two major brain structures recruited during avoidance and freezing behaviors (Bravo-Rivera, et al., 2014; Tovote, et al., 2016; LeDoux, 2017; Diehl, et al., 2018). Nevertheless, the implication of exact subregion(s) in those two structures strongly depends on the paradigm used. Indeed, in the classical shuttle-box two-way active avoidance paradigm, some data suggested that the IL is crucial in encoding avoidance behavior (LeDoux, 2017). In contrast, using the platform-based avoidance paradigm, other groups suggested that it was rather the dmPFC that was crucial for performing and maintaining avoidance behavior (Bravo-Rivera, et al., 2014; Diehl, et al., 2018). To evaluate whether the mPFC and PAG were structures recruited during our behavioral paradigm, we evaluated the expression of c-fos protein as a marker of neuronal activity. We also evaluated the expression of the c-fos protein following training in the amygdala, a structure known to be crucial for both avoidance and freezing behaviors (LeDoux, 2017). Following six days of training, animals were divided into three groups. The first control group received, at a 7^{th} behavioral session, only 15 CS^- trials. The second and the third groups, which were respectively classified at session 6 as **Bad** and **Good avoiders** underwent a 7^{th} behavioral session during which they received 15 trials of CS^+ presentations without footshocks. A forth group of naïve mice was also used as a control. 90 minutes after training, mice were sacrificed and c-fos expression in the mPFC, amygdala and the PAG subregions were quantified. Our results indicated that c-fos expression was significantly up-regulated in the dmPFC including the ACC and the PL and in the caudal dlPAG but not the basolateral amygdala **(Table 1, Figure 19, and Figure 20)**. Several limitations of the c-fos approach should nevertheless be pinpointed. First, the absence of significance for c-fos expression in **Good avoiders** as compared to **Bad avoiders** and controls in the BLA **(Figure 19)** could be explained by the learning phase at which c-fos expression was quantified. Indeed, amygdala activation probably occurs at early training sessions as previously documented (Poremba and Gabriel, 1999; Manassero, et al., 2018). In addition, c-fos is only expressed in certain types of

neuronal cells and does not mark inhibitory GABAergic cells activation (Kovács, 1998).

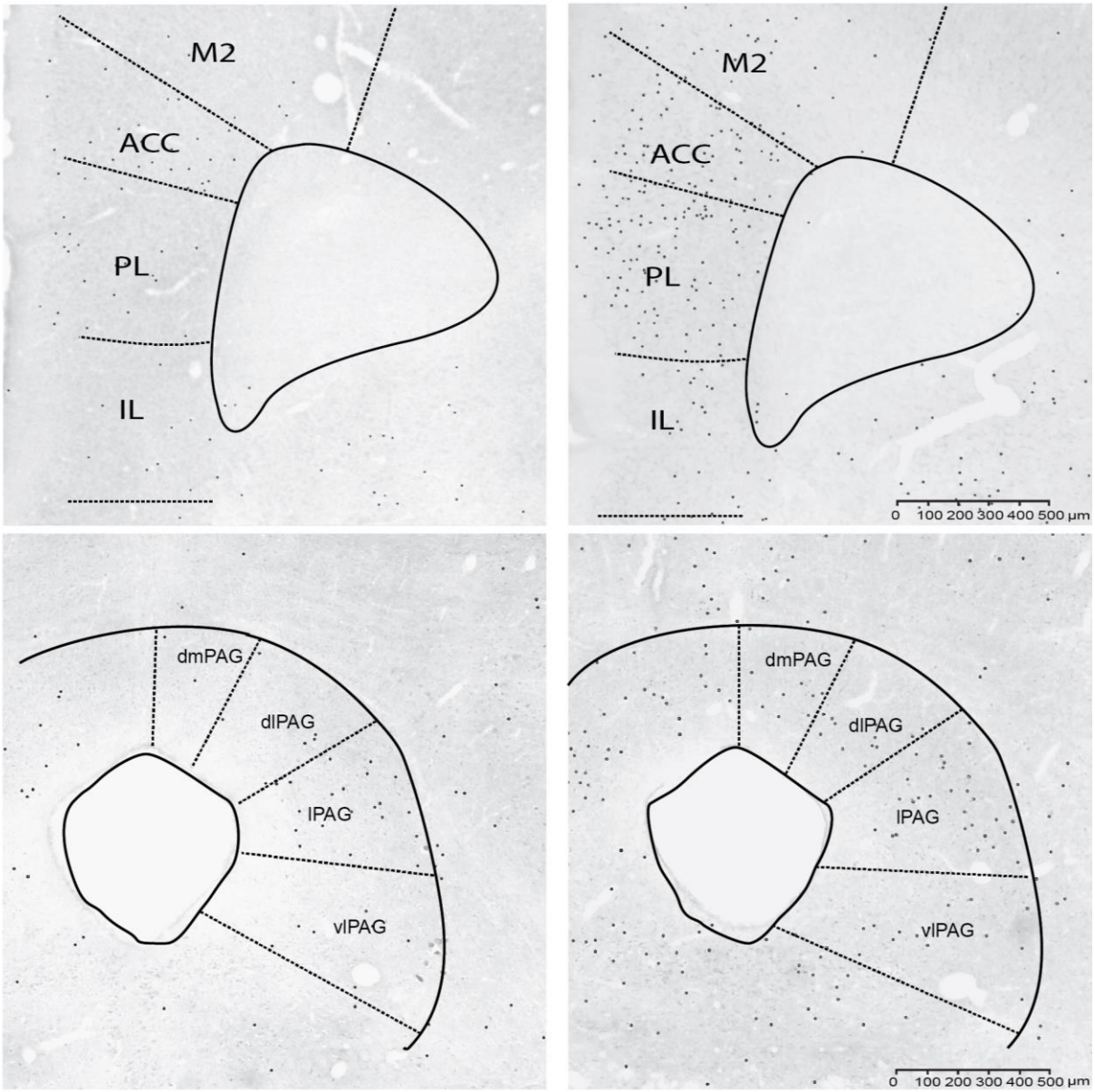

<u>Figure 19.</u> C-fos immunostaining in Bad and Good avoiders
Representative examples of c-fos staining in the prefrontal cortex (top panels) and the PAG (bottom panels) of a **Good avoider** (left column) compared to a **Bad avoider** (right column).

Structures	Atlas level	Groups				F(3,18) ; p
		Home Cage (n=6)	CS- (n=6)	Bad Avoiders (n=5)	Good Avoiders (n=5)	
dmPFC	1,94	539,95 ± 49,41	576,7 ± 56,04	353,03± 53,41	913,28 ± 127,11 °,*,**	8,98 ; 0,0007
vmPFC		294,35 ± 14,69	372,59 ± 6,51	116,56 ± 9,46	439,34 ± 28,27	2,37 ; 0,1043
BLA ant	-1,2	269,85 ± 38,57	278,48 ± 58,14	345,23 ± 64,74	391,21 ± 97,05	2,41 ; 0,1005
BLA post	-1,82	122,71 ± 43,5	142,07 ± 41,9	153,73 ± 42,62	208,06 ± 36,04	2,83 ; 0,0675
BA post		144,54 ± 47,55	157,64 ± 43,76	194,68 ± 38,15	225,99 ± 85,77	2,69 ; 0,0771
LA post		94,64 ± 25,43	124,77 ± 22,1	85,93 ± 47,29	181,56 ± 60,51	2,48 ; 0,0938
PAGdmr	-4,48	171,29 ± 33,11	153,23 ± 39,19	244,17 ± 38,55	285,49 ± 35,47	2,47 ; 0,0948
PAGdlr		102,43 ± 21,38	76,95 ± 13,94	93,71 ± 22,33	110,78 ± 12,56	0,65 ; 0,5934
PAGlr		314,34 ± 57,58	231,19 ± 27,28	286,33 ± 60,07	290,73 ± 42,93	0,58 ; 0,6384
PAGvlr		245,8 ± 67,75	196,19 ± 78,52	196,75 ± 50,51	234,01 ± 173,35	0,39 ; 0,7649
PAGdmc	-4,84	56,81 ± 7,1	64,43 ± 15,88	129,59 ± 33,08	138,6 ± 40,64	2,8 ; 0,0698
PAGdlc		48,34 ± 17,74	25,45 ± 15,34	49,16 ± 21,59	101,88 ± 31,14 °	3,92 ; 0,0258
PAGlc		253,34 ± 54,01	244,58 ± 41,23	220,87 ± 48,18	338,34 ± 46,63	1,05 ; 0,396
PAGvlc		149,12 ± 37,16	127,39 ± 21,5	123,61 ± 22,64	203,71 ± 35,81	1,38 ; 0,2808

Bonferroni/Dunn Post-Hoc test: Comparisons of all groups to Good Avoiders group are not significant unless the corresponding p-value is less than 0,0083.

° Different from Home Cage (HC)
* Different from CS-
** Different from Bad Avoiders

Table 1. C-fos immunostaining in Bad and Good Avoiders

C-fos immunoreactivity cell counts/mm² in the prefrontal cortex, amygdala and PAG of **Bad** and **Good avoiders** following 6 avoidance training sessions. dmPFC includes ACC and PL, vmPFC includes IL. Ant: anterior, post: posterior, r: rostral and c: caudal.

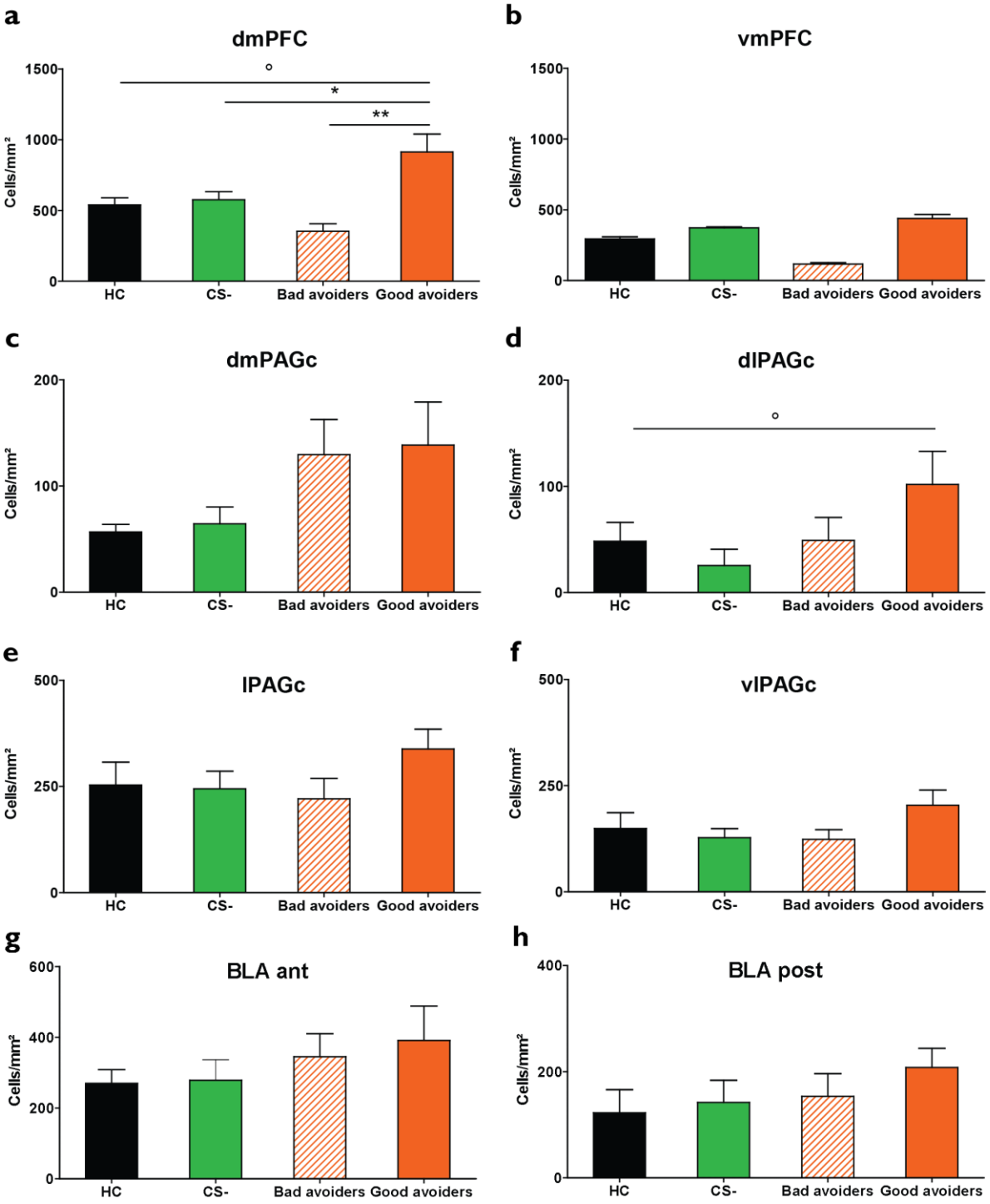

<u>Figure 20.</u> C-fos is expressed in the dmPFC and dlPAG of Good avoiders

Quantification of c-fos expression in home cage controls (HC), mice exposed to CS^-, **Bad** and **Good avoiders** exposed to CS^+ in the dmPFC (a), vmPFC (b), caudal dmPAG (dmPAGc) (c), caudal dlPAG (dlPAGc) (d), caudal lPAG (lPAGc) (e), caudal vlPAG (vlPAGc) (f), BLA ant (g) and BLA post (h).

The present c-fos study, established on our behavioral paradigm provided important information about subregional activations at the level of two structures the mPFC and the PAG suggesting that it is rather the dmPFC (ACC and PL) and the dlPAG which are activated during avoidance learning in our behavioral paradigm.

III. Electrophysiological recordings

Based on the previous c-fos results we concluded that using our behavioral paradigm the dmPFC rather than the vmPFC is implicated in avoidance learning/expression. To further determine the patterns of activity of dmPFC units linked to avoidance behavior we implanted recording electrodes in the caudal dmPFC including the ACC and PL **(Figure 21 a)** and recorded all along the behavioral sessions.

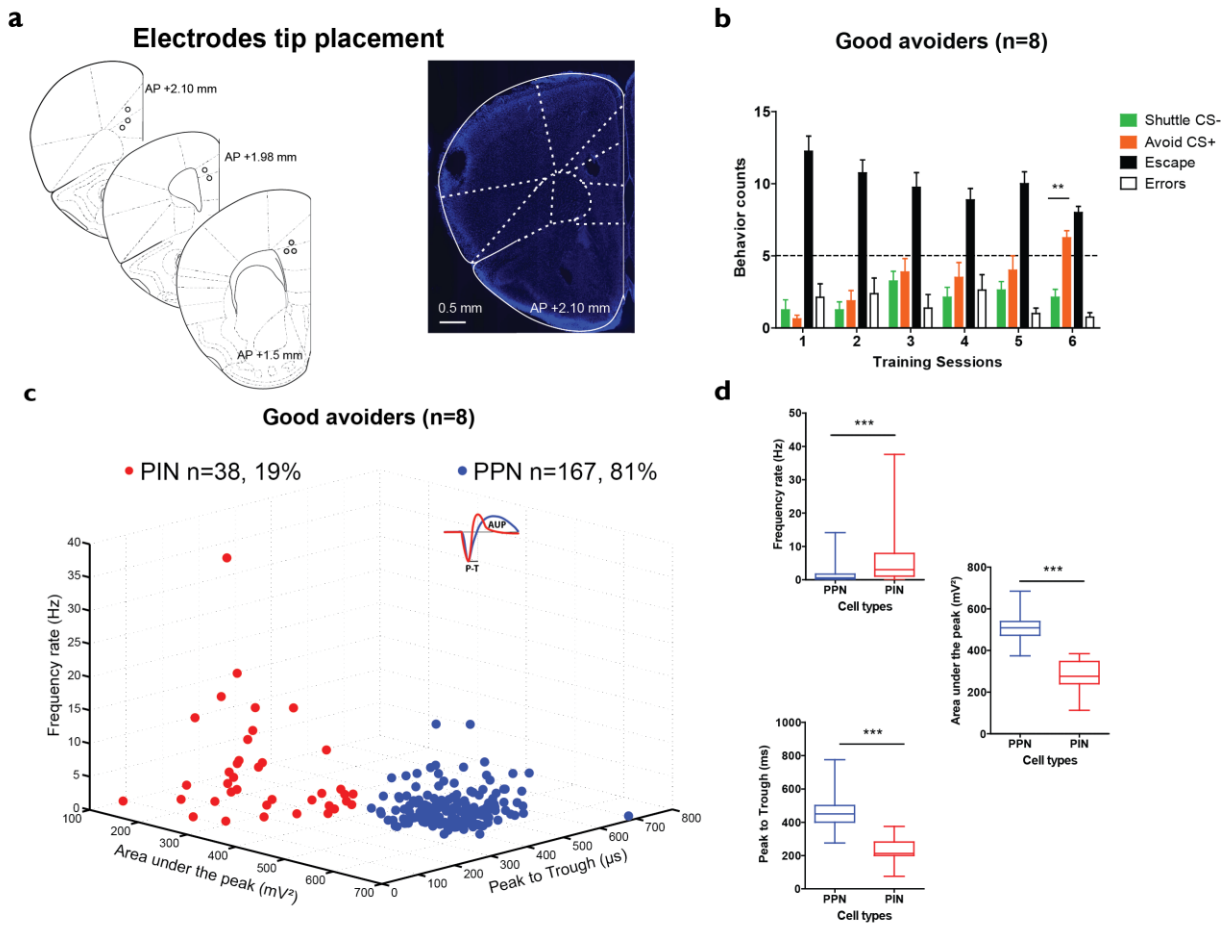

Figure 21. dmPFC recordings during avoidance learning

a. Schematic of the electrodes tip placement in the 8 mice recorded in the dmPFC (left). DAPI stained brain slice representing the electrodes tip placement in the dmPFC (right). **b.** Trial counts (shuttle CS^-, avoid CS^+, escape, errors) across 6 training sessions in **Good avoiders** (n = 8) (two-way repeated measures ANOVA; group: $F_{(3,140)} = 71.70$, $p < 0.0001$, training session: $F_{(5,140)} = 0.30$, $p = 0.90$, group x training session: $F_{(15,140)} = 4.67$, $p < 0.0001$, and $p < 0.01$). **c.** dmPFC single units clustering in **Good avoiders** (n = 8) using an unsupervised, unbiased algorithm based on three extracellular spike features: frequency (Hz), area under the peak (μV^2) and peak to trough (µs). Two classes were identified: putative pyramidal neurons (PPN) in red, putative interneurons (PIN) in blue which proportions are represented in the panel. **d.** PPN and PIN frequency, area under the peak and peak-to-trough comparisons respectively from top to bottom (unpaired t test: $t = 6.64$, $p < 0.0001$; $t = 23.67$, $p < 0.0001$; $t = 16.92$, $p < 0.0001$).

Electrophysiological data were analyzed for the 6th behavioral session, the time point at which we categorized animals into **Good** and **Bad avoiders**. **Good avoiders** presenting at least 10 isolated units were kept for electrophysiological recordings

(*n* = 8 mice) **(Figure 21 b)**. We categorized the recorded neurons into two classes based on three characteristics of their waveforms **(Figure 21 c)**. In accordance with other studies in the dmPFC (Courtin, et al., 2014; Rozeske, et al., 2018), the recorded putative pyramidal neurons (PPN) have in average a lower frequency, bigger area under the peak (an indirect measure of after hyperpolarization) and larger peak-to-trough as compared to putative inhibitory interneurons (PIN) **(Figure 21 d)**. Consistently with other recordings in the dmPFC, we find that 81 % of the neurons recorded were PPNs whereas 19 % belong to the PIN. We only performed our analyses on PPN since we were interested into major dmPFC projection pathways.

Caudal dmPFC putative pyramidal neurons are significantly activated during avoidance behavior

To evaluate the firing pattern of dmPFC PPNs during avoidance learning we computed a principal component analysis (PCA) on the normalized (z-scored) activity of dmPFC PPNs around door opening until the shock delivery during avoidance trials (this corresponds to a time period of 8.8 seconds following door opening). In our analysis, the first principal component (PC1) represented 12.6 % of the variability of the dataset corresponding to the largest variance observed among PCs **(Figure 22 a-b)**. Using Pearson's correlation coefficients, PPNs were classified as positively ($r > 0.2717$), negatively ($r < -0.2717$) and non-correlated ($-0.2717 < r < 0.2717$) with PC1 (Pearson correlation table: two-tailed, degree of freedom = 87, $p = 0.01$, $r = 0.2717$). Our analyses indicate that half of the PPNs were avoidance modulated (*n* = 77/167) among which half were avoidance activated (Avoid +; *n* = 35/167) and the other half avoidance inhibited (Avoid-; *n* = 42/167) **(Figure 22 c)**. Furthermore, we determined among Avoid+ and Avoid- dmPFC PPNs the ones presenting a significant Z-score during freezing behavior (2 consecutive time bins > 1.96, < -1.96 respectively). Interestingly, among avoidance non-responsive neurons (*n* = 90/167), 67 % were freezing non-responsive, 20 % freezing-activated (FZ+) and 13 % freezing-inhibited (FZ-). Similar percentages were observed among Avoid+ neurons (71, 20 and 9 % respectively). In sharp contrast, the vast majority of Avoid- neurons were modulated by freezing with 48 % of Avoid- neurons activated by freezing and 14 % inhibited. These results revealed three main categories of neuronal modulations: neurons

being exclusively modulated during avoidance behavior (24.5 %, *n* = 41 cells); neurons exclusively modulated during freezing responses (18 %, n = 30 cells); and a mixed population of neurons responding to both freezing and avoidance behavior (21.6 %, n = 36 cells). Moreover these results also indicated that the vast majority of Avoid+ neurons did not exhibit freezing-related responses whereas it was the opposite for Avoid- dmPFC neurons.

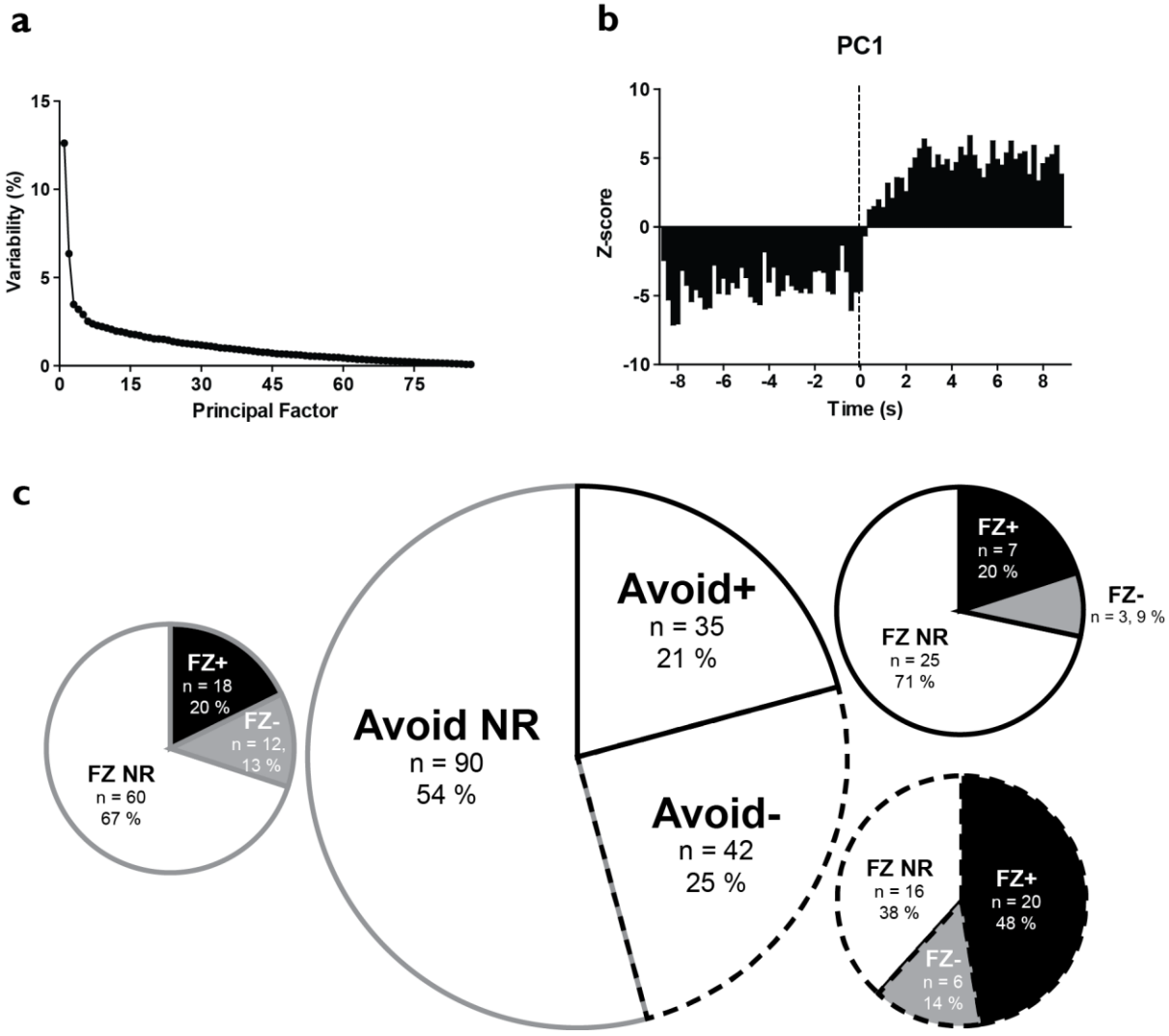

Figure 22. Characterization of avoidance and freezing-modulated dmPFC neurons
a. Variability of the dataset of analyzed PPNs among the different principal components. The first factor PC1 used for our analyses represents 12.6% of the variability. **b.** PC1 scores referenced at the door opening +/- 8.8 seconds (time bins: 200 ms) captured a strong and sustained activation pattern following door opening. **c.** Central pie-chart: proportions of avoidance-activated, -inhibited and non-responsive PPNs (Avoid +, Avoid -, Avoid NR). Side-pie charts: Subcategorization of Avoid +, Avoid – and Avoid NR PPN populations based on their freezing responsiveness into freezing-activated, -inhibited and non-responsive (FZ +, FZ -, FZ NR).

Avoid+ dmPFC PPNs displayed a significant sustained increase in Z-score activity during CS^+ avoided trials as compared to both shock trials (including escape and

error trials) and CS^- shuttle trials **(Figure 23 a-c, left panels and Figure 24 a-b)**. This result strongly suggests that the increased activity of dmPFC PPNs observed during this time period is likely linked to conditioned avoidance behavior and not to the sensory properties of the CS. As for Avoid- dmPFC PPNs, they displayed at door opening a sustained inhibition of activity **(Figure 23 a, center panel and Figure 24 c-d)**. However, Z-scored values were not significant in average. Interestingly, Avoid- dmPFC PPNs seem to be modulated by the sensory properties of the CS as at door opening we observed a sharp and brief inhibition during shock trials **(Figure 23 b center panel)**. As for Avoid NR dmPFC PPNs, they do not display any significant changes in activity at door opening for both avoided and shocked CS^+ and shuttled CS^- trials **(Figure 23 a-c, right panels)**. These results indicated that although we recorded from both Avoid+ and Avoid- dmPFC neurons, in average, only Avoid+ neurons display significant modulation during avoidance. This is probably due to a high variability in the response onset in Avoid- neurons, which results in a flattened and non-significant average z-score.

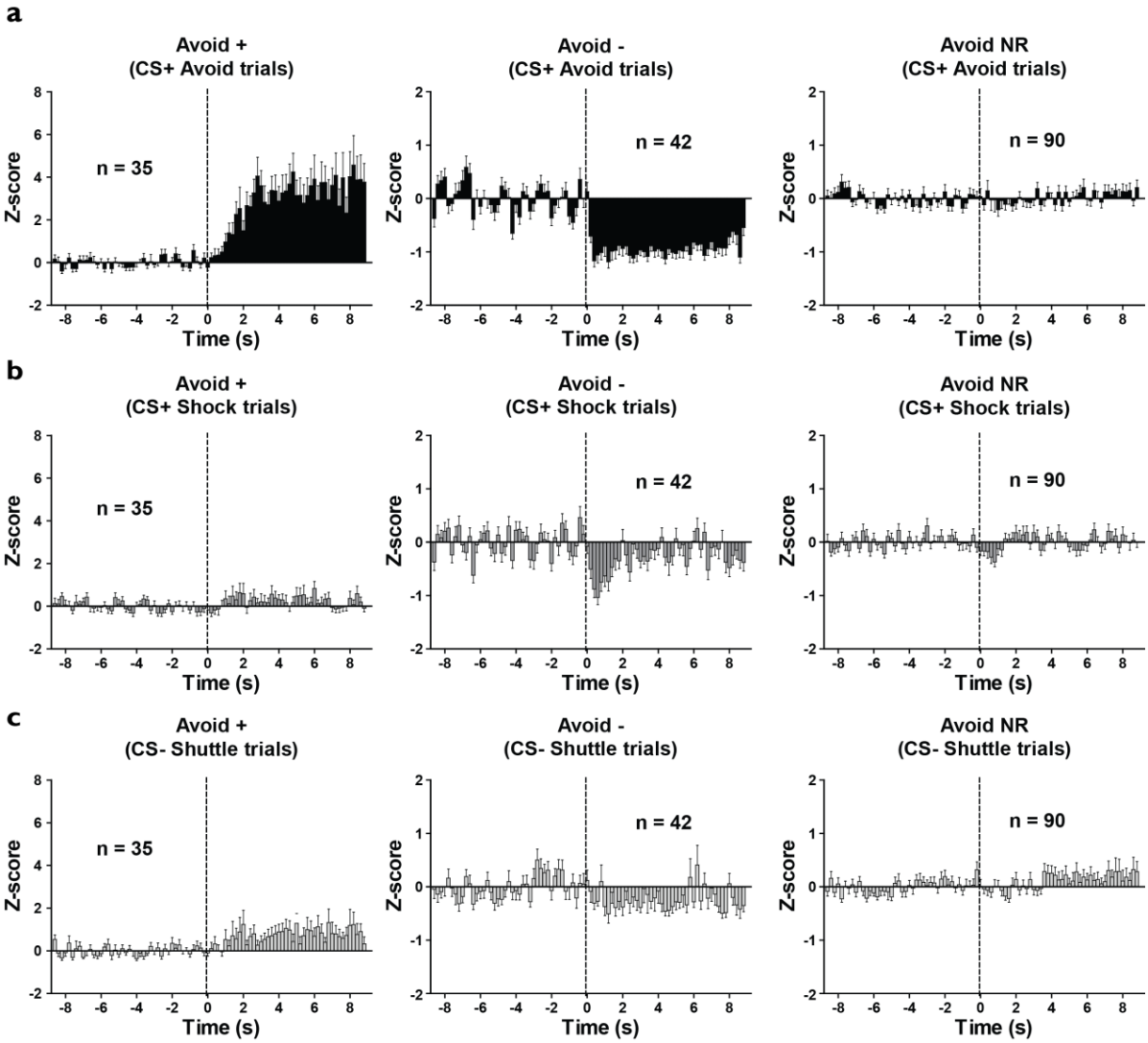

<u>Figure 23.</u> Z-score activity of avoidance-modulated dmPFC neurons

Avoidance-modulated dmPFC putative pyramidal neurons (PPN) patterns. Averaged z-scored peri-stimulus event histograms (PSTH) of neurons activated (Avoid+: all left panels in **a**, **b** and **c**) inhibited (Avoid-: all center panels in **a**, **b** and **c**) and non-modulated (Avoid NR all right panels in **a**, **b** and **c**) during avoid trials (panels **a**) shock trials (including escape and error trials, panels **b**) and CS^- trials (panels **c**). The dashed line at the reference of the PSTH corresponds to the door opening (sliding-down).

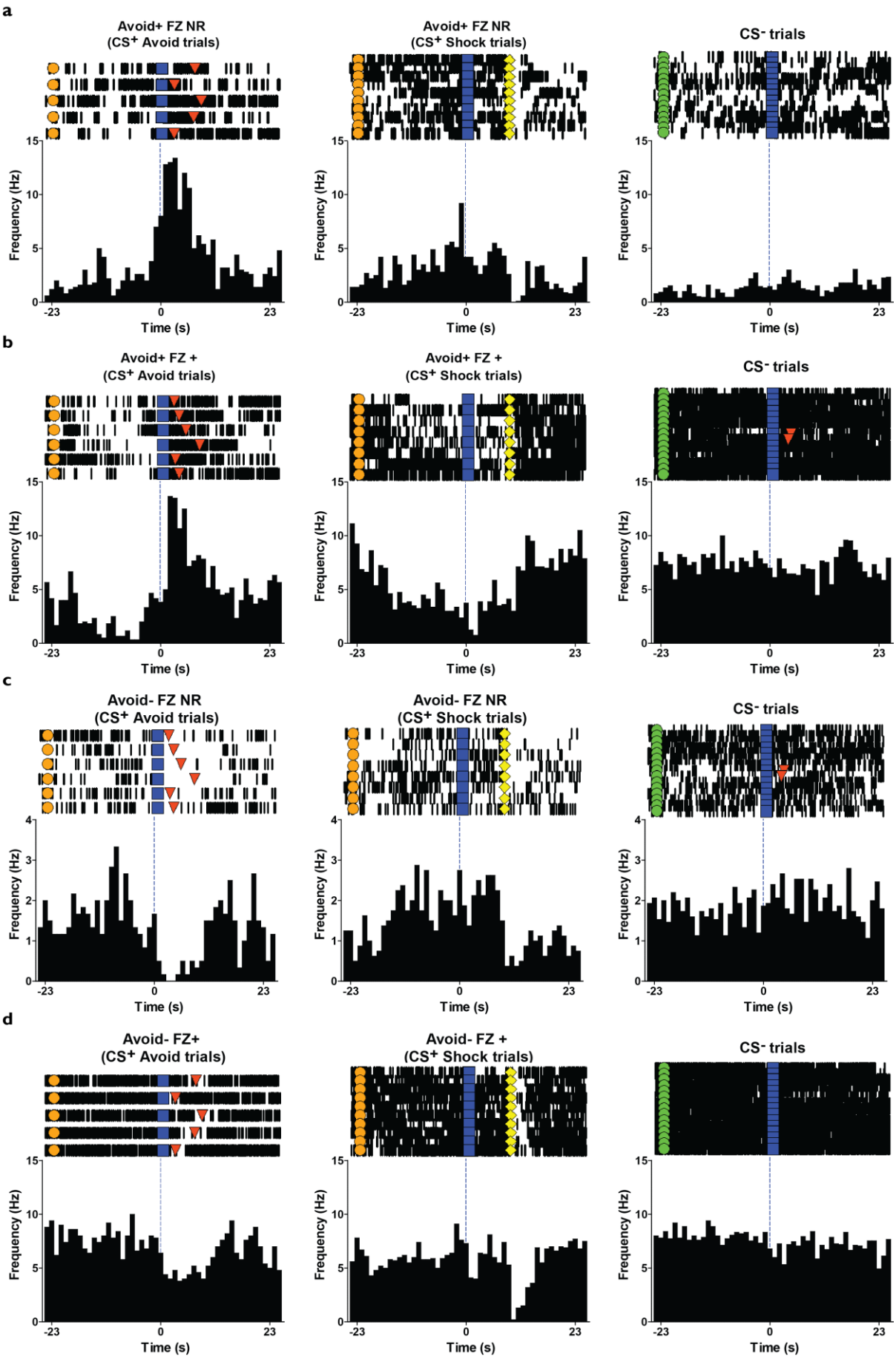
a
Avoid+ FZ NR
(CS+ Avoid trials)
Avoid+ FZ NR
(CS+ Shock trials)
CS- trials
b
Avoid+ FZ +
(CS+ Avoid trials)
Avoid+ FZ +
(CS+ Shock trials)
CS- trials
c
Avoid- FZ NR
(CS+ Avoid trials)
Avoid- FZ NR
(CS+ Shock trials)
CS- trials
d
Avoid- FZ+
(CS+ Avoid trials)
Avoid- FZ +
(CS+ Shock trials)
CS- trials
Frequency (Hz)
Time (s)
-23
0
23

Figure 24. Representative examples of dmPFC neurons avoidance- and freezing- modulated
Peri-event raster plots and mean histograms of the firing rate of representative putative pyramidal cells recorded in the dmPFC in **Good avoiders** at an interval starting around the tone onset (CS^+ onset: orange circles, CS^-: green circles), referenced at the door opening (navy-blue square) and going up-until 25 seconds post-DO. Left columns represent avoid trials, center columns shock (escape and error trials) and right columns correspond to CS^- trials (red triangles representing the moment of avoid CS^+ or shuttle CS^-). Examples of an avoidance activated freezing non-responsive (Avoid+ FZ NR) PPN firing rate in panel **a.**, avoidance activated freezing activated in panel **b.**, avoidance inhibited freezing non-responsive in panel **c.** and avoidance inhibited freezing activated in panel **d.**

Caudal dmPFC putative pyramidal neurons activated during avoidance behavior are in majority freezing non-responsive

We were next interested in identifying the freezing responsiveness of avoidance-modulated dmPFC neurons since avoidance and freezing are two competitive behaviors. As discussed earlier, we determined among avoidance- activated and inhibited dmPFC PPNs the ones presenting a significant Z-score during freezing behavior (2 consecutive time bins > 1.96, < -1.96 respectively). We observed that most avoidance-activated dmPFC PPNs were freezing non-responsive (*n* = 25/35) **(Figures 4.2 c and 4.5 a)**. As for avoidance-inhibited dmPFC PPNs, as much as half of the population was freezing responsive and more specifically activated during freezing behavior (n = 20/42) **(Figures 4.2 c and 4.5 b)**. As for avoidance non-responsive dmPFC PPNs only 33% (n = 30/90) of them were freezing modulated **(Figure 22 c and 4.5 c)**.

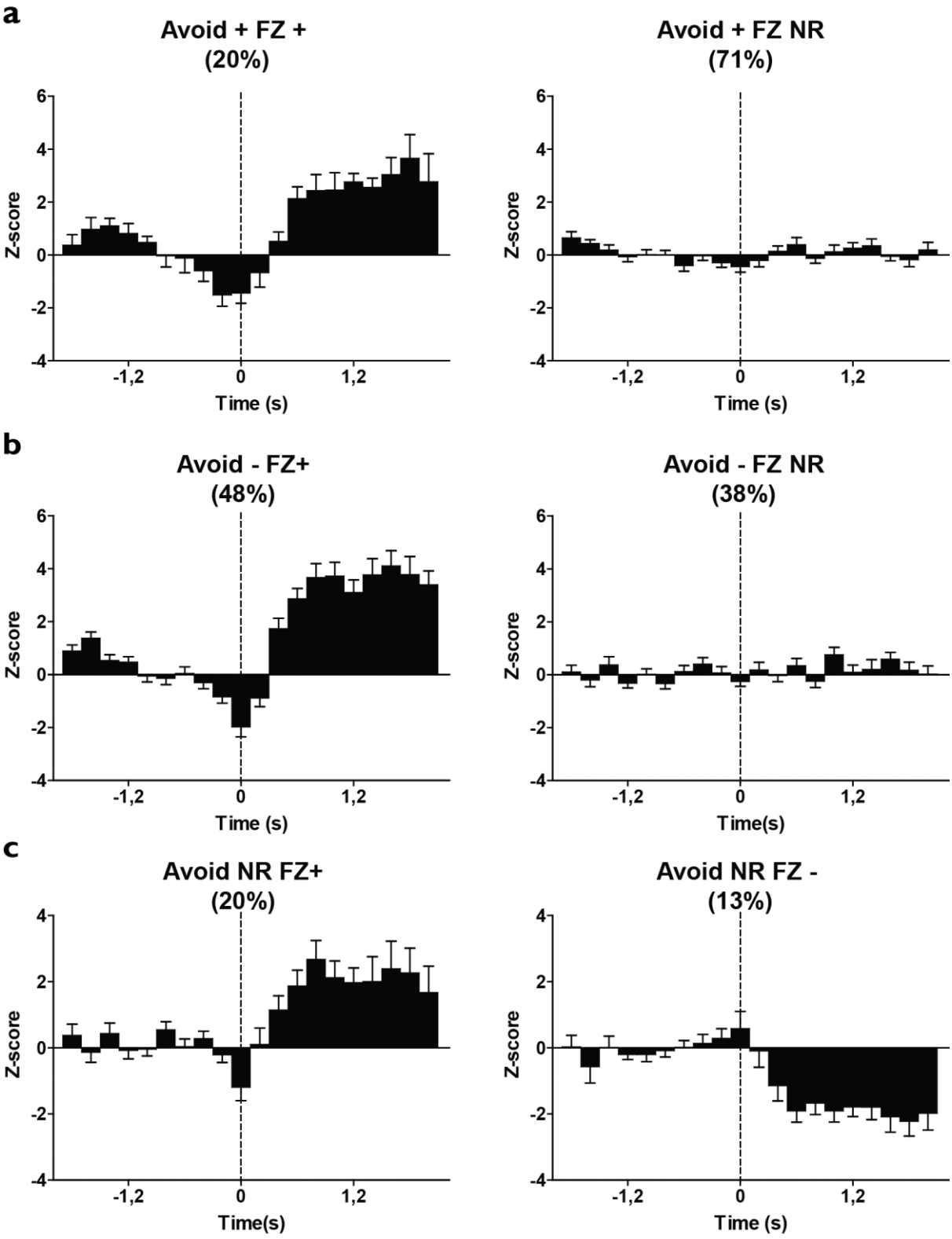

Figure 25. Freezing related neuronal responses in dmPFC PPNs

Subcategorization of avoidance modulated and non-modulated neurons based on their freezing responsiveness. Averaged z-score peri-stimulus time histograms (PSTH) of different PPN populations: avoidance-activated and freezing-activated (Avoid+ FZ+: left panel **a**); avoidance-activated and freezing non-responsive (Avoid+ FZ NR: right panel **a**); avoidance-inhibited freezing-activated (Avoid– FZ+: left panel **b**); avoidance-inhibited freezing non-responsive (Avoid– FZ NR: right panel **b**); avoidance non-responsive freezing-activated (Avoid NR FZ+: left panel **c**); avoidance non-responsive freezing-inhibited (Avoid NR FZ-: right panel **c**).

Avoidance activated PPNs are not modulated by locomotion

Because avoidance is an active motor response, it is possible that the changes in neuronal activity observed in dmPFC PPNs might be related to motor aspects and not linked to conditioned avoidance. To control for this critical aspect, we correlated the firing frequency of each individual dmPFC PPN to the speed of the mouse in trials during which the mouse crosses to the other compartment at the beginning of the session but without any sensory stimulation. We calculated the Pearson's coefficient of correlation for avoidance-modulated dmPFC PPNs **(Figure 26 a)** and for avoidance-activated freezing non-responsive dmPFC PPNs **(Figure 26 b)**. Our results revealed that only a small fraction of the recorded neurons presented a significant correlation between neuronal activity and speed. Indeed for avoidance-activated freezing non-responsive dmPFC PPNs, only 12% (3/25 neurons) displayed a significant positive correlation with speed. These data indicated that the overall increase in activity displayed by Avoid+ dmPFC neurons during CS^{+} trials cannot be explained by a locomotor effect.

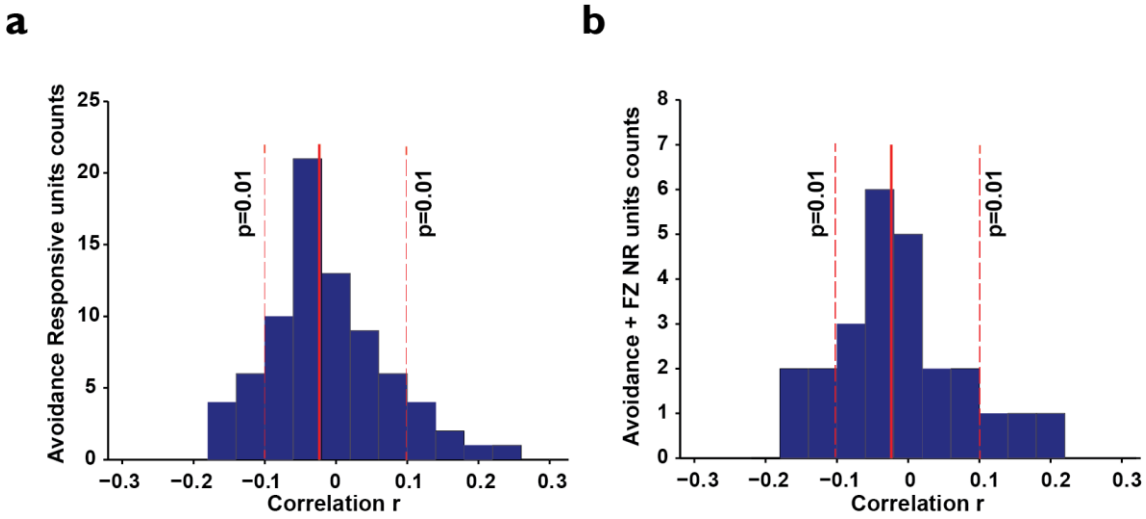

Figure 26. Firing activity of dmPFC neurons activated during avoidance is not linked to motor behavior

Spearman's coefficients of correlation between neuronal firing rates and the mice's speed in function of neuronal counts of avoidance responsive units (Avoid+ and Avoid– populations: panel **a**) and avoidance activated freezing non-responsive units (Avoid+ FZ NR population: panel **b**). The red line represent the median and the dashed red lines represent separates the non-significant *r* (center of the graph) from the significant ones (extremities of the graph).

Altogether, our electrophysiological recordings in the dmPFC of Good avoiders indicated that most avoidance-inhibited dmPFC PPNs are modulated by both freezing and avoidance, while most avoidance-activated dmPFC PPNs are modulated exclusively by avoidance behavior. Moreover, changes in firing activity of avoidance-activated dmPFC neurons cannot be explained by motor behavior during avoidance and likely reflects associative learning.

IV. Antidromic Stimulations

We next thought to investigate the connectivity of dmPFC neurons modulated during avoidance behavior. Based on our c-fos data suggesting that both dmPFC and dlPAG are activated during avoidance learning/expression, and given our electrophysiological data suggesting that different firing profile populations in the dmPFC encode avoidance and/or freezing behaviors, we concentrated our efforts on dmPFC projections onto the dl/lPAG. To identify these projection neurons, we used antidromic stimulations in a subset of implanted mice submitted to our avoidance paradigm. Following completion of the behavioral session, mice were anaesthetized and we stimulated the dl/lPAG with a movable stimulation electrode while simultaneously recording in the dmPFC through chronically implanted electrode bundles **(Figure 27 a-b)**. Using this strategy we were able to characterize the identity of dmPFC neurons during the behavioral session (Avoid+, Avoid- or Avoid NR) and determine whether these neurons project to the dl/lPAG. We used 3 criteria to identify antidromic-responsive neurons **(Figure 27 c)**: stable latency of spike occurrence (< 0.4 ms jitter), collision with evoked or spontaneously occurring spikes, and their capacity to follow high-frequency stimulation (200 Hz). The distribution of spike latencies following stimulation of the dl/lPAG is shown in **Figure 27 c** and revealed that dmPFC neurons projecting to the dlPAG display a latency of response ranging from 8 ms to 17.4 ms **(Figure 27 c)**.

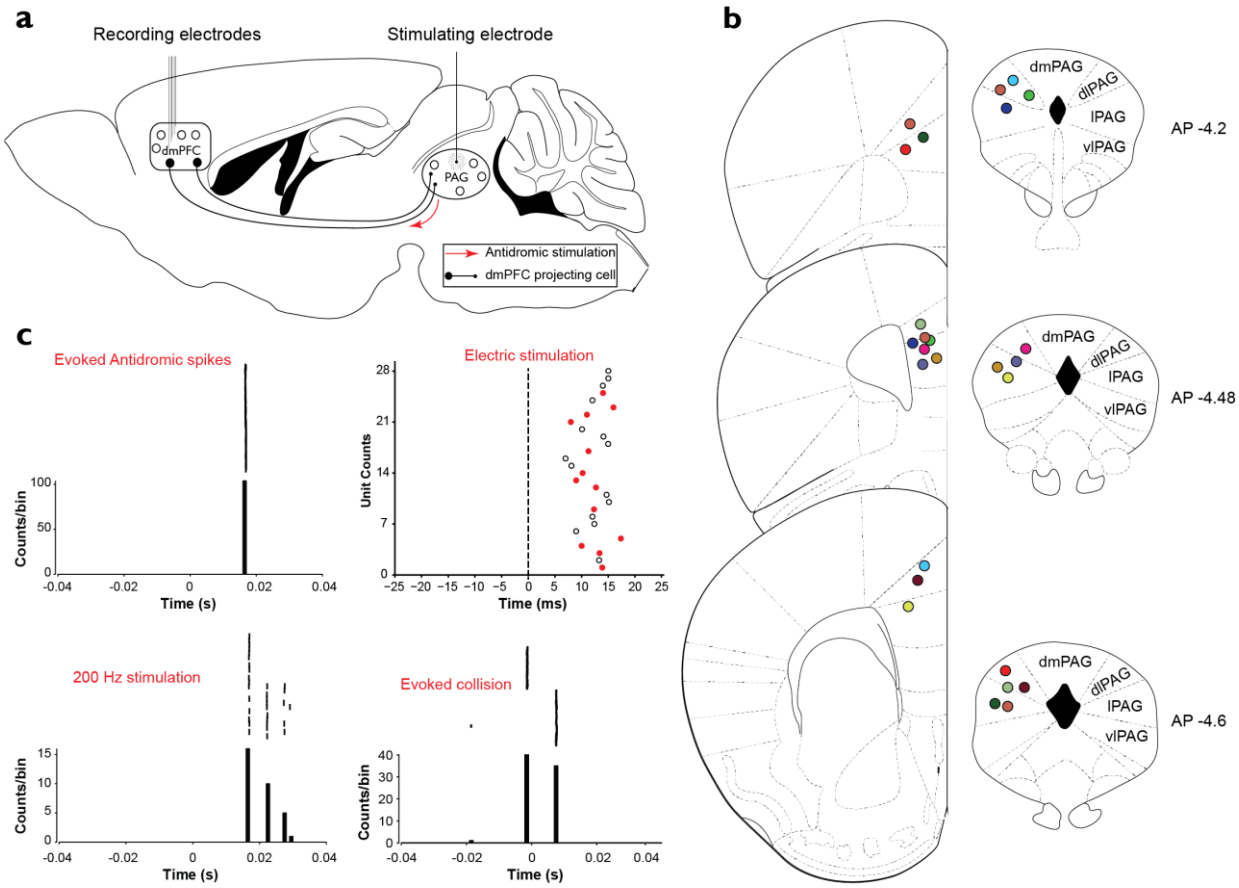

Figure 27. Characterization of dmPFC-dl/lPAG projecting neurons using antidromic stimulations

a. Schematic of the antidromic stimulation strategy used to identify units projecting from the dmPFC to the dl/lPAG. **b.** Representation of the recording electrode tips placement in the dmPFC (left) and the stimulating electrode in the dl/lPAG (right). Each color represents one animal (*n* = 13) **c.** Examples of evoked antidromic spikes and 200 Hz stimulation responsiveness to the electric stimulation of the dl/lPAG (left panels). Top right panel: latency of response of all dmPFC projectors to the dl/lPAG following an antidromic stimulation in the dl/lPAG. Red dots represent the latency of the Avoid responsive units. Bottom right panel: Evoked collision examples.

We identified 28 putative projecting cells from the dmPFC to the dl/lPAG among which half were avoidance responsive (n = 13/28) **(Figure 28 a).** Among the avoidance responsive neurons the vast majority were avoidance-activated (n = 11/13) **(Figure 28 a)**. These dmPFC projecting neurons were activated significantly during CS^{+} avoided trials **(Figure 28 b)** but not during shock trials (escape and error) **(Figure 27 c)**. Most of the avoidance-activated neurons were also freezing non-responsive (n = 9/11) **(Figure 28 a, d)**.

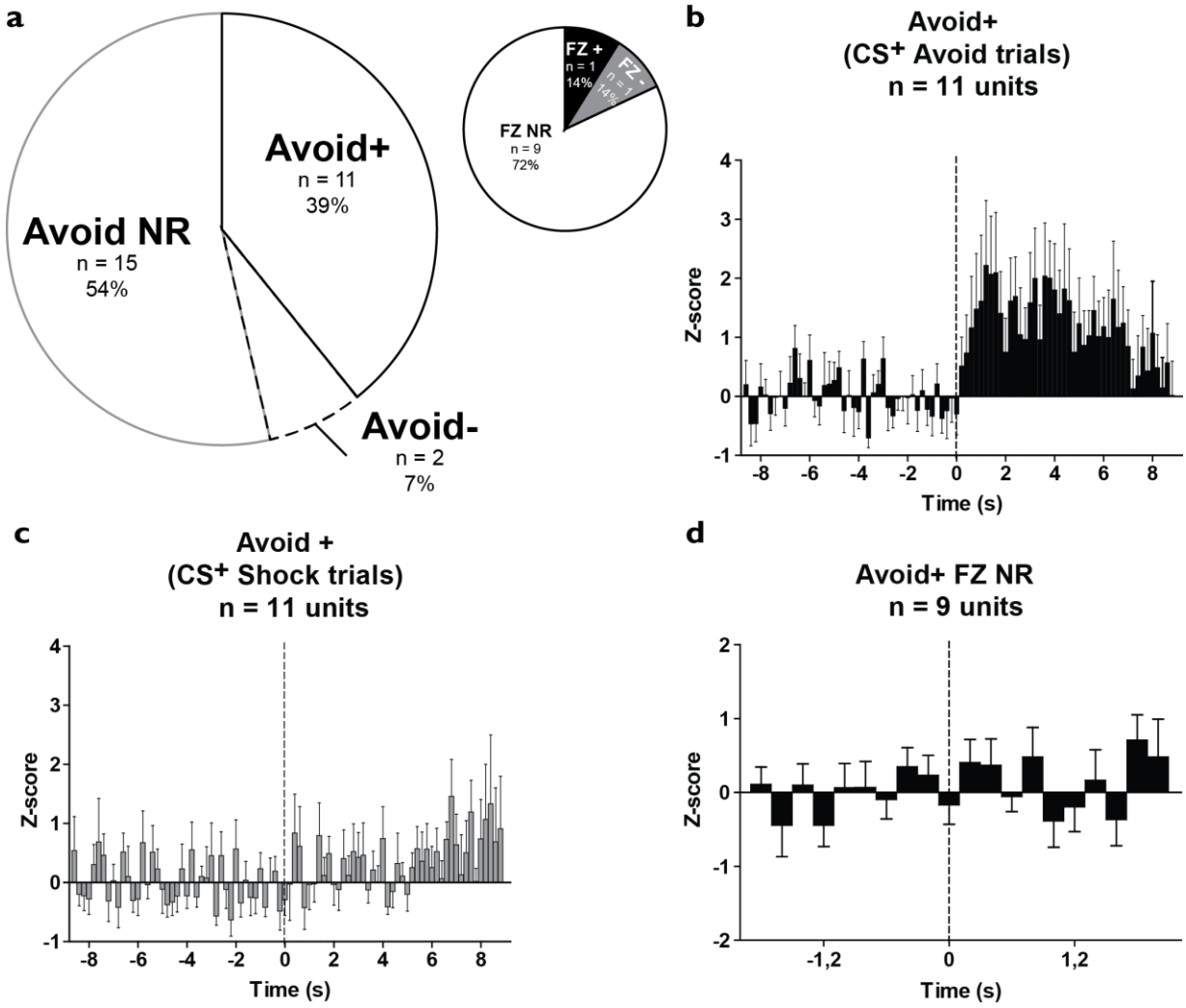

Figure 28. Most avoidance responsive dmPFC-dl/lPAG projecting neurons are avoidance activated freezing non-responsive

a. Pie-chart representative of avoidance and freezing responsiveness of dmPFC units projecting to the dl/lPAG (Avoid +: activated, Avoid -: Inhibited, Avoid NR: non-responsive, FZ +: freezing activated, FZ -: freezing inhibited, FZ NR: freezing non-responsive. **b. c.** Averaged z-score peri-stimulus time histogram (PSTH) referenced at door opening and going up until 8.8 seconds of avoid activated neurons (Avoid +) for both avoid trials (panel **b.**) and shock trials (panel **c.**). **d.** Averaged z-score PSTH of freezing responsiveness of Avoid + FZ NR population of dmPFC units projecting to the dl/lPAG.

The antidromic stimulations data clearly indicate that the subpopulation of dmPFC PPNs neurons exhibiting an increased activity during avoidance learning (avoidance-activated / freezing non responsive cells) project to the dlPAG.

V. Optogenetic manipulation

dmPFC-dl/lPAG optogenetic inhibition in Good avoiders does not affect avoidance expression

To further causally test the hypothesis that dmPFC neurons projecting to the dl/lPAG control avoidance behavior, wild-type mice were injected with a Cre-dependent AAV expressing ArchT in the dmPFC and with a mixture of Cav-Cre, HSV-Cre and AAV-mcherry in the dl/lPAG **(Figure 29 a)**. Following 6 training sessions, **Good avoiders** underwent two sessions of dmPFC-dl/lPAG optogenetic constant inhibition at door opening during CS^- and CS^+ presentations. We did not observe any significant changes neither in avoidance counts during the first (data not shown) or second optogenetic stimulation session **(Figure 29 b, c)**, nor in avoidance latency **(Figure 29 d)**, nor avoidance discrimination **(Figure 29 e)**. During the first (data not shown) or second **(Figure 29 b, c, d)** post-stimulation sessions, there was no change in either of the cited parameters above.

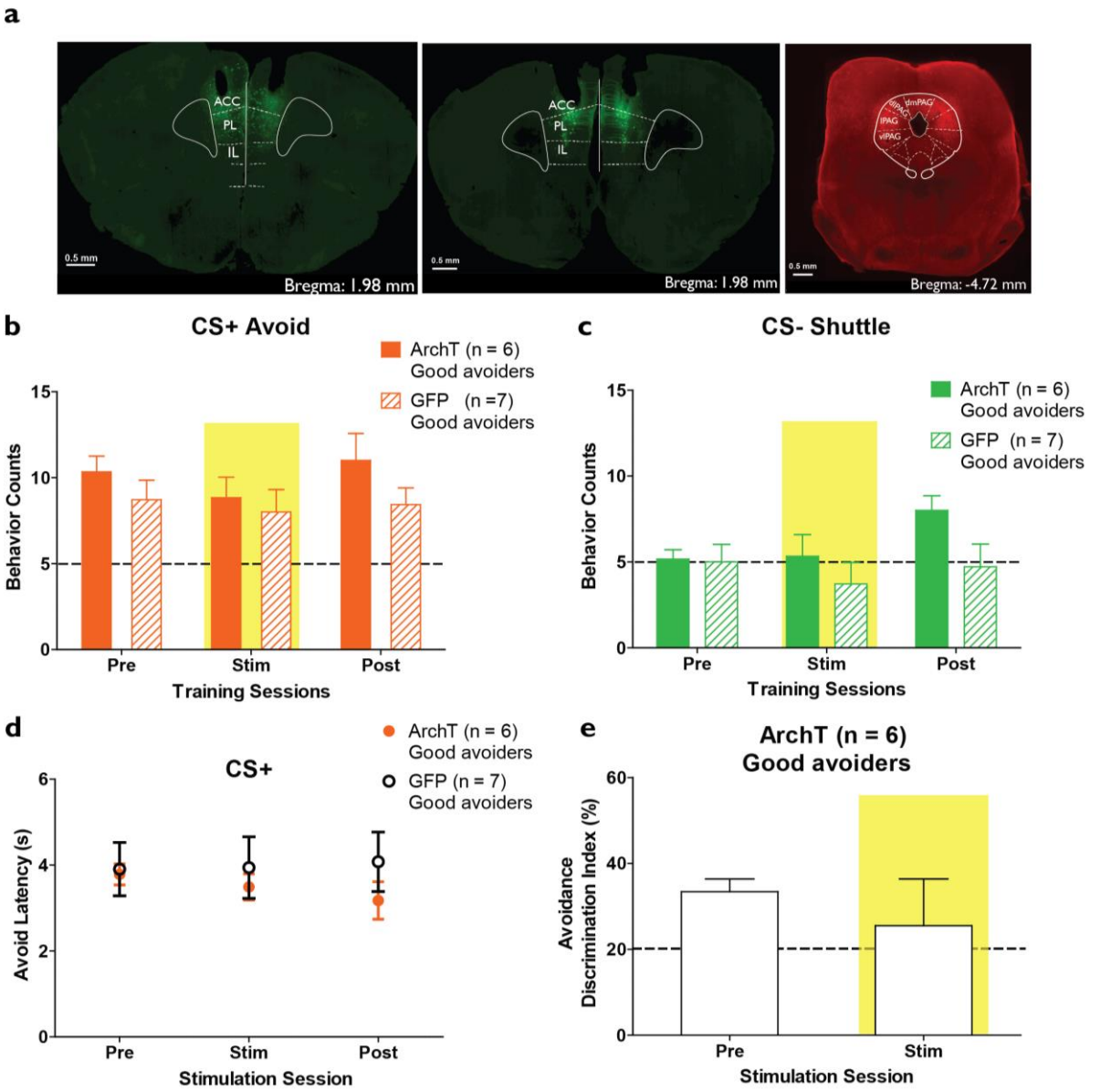

Figure 29. Optogenetic inhibition of the dmPFC-dl/lPAG pathway does not impair avoidance expression

a. CS^+ avoid counts at pre-stimulation, second stimulation and second post-stimulation sessions in two groups of **Good avoiders** infected with ArchT or GFP. (Two-way repeated measures ANOVA; group: $F_{(1, 22)} = 2.50$, $p = 0.14$, training session: $F_{(2, 22)} = 0.74$, $p = 0.48$, group x training session: $F_{(2, 22)} = 0.28$, $p = 0.75$). **b.** CS^- shuttle counts at pre-stimulation, second stimulation and second post-stimulation sessions in two groups of **Good avoiders**: ArchT and GFP groups. (Two-way repeated measures ANOVA; group: $F_{(1, 22)} = 3.01$, $p = 0.11$, training session: $F_{(2, 22)} = 1.56$, $p = 0.23$, group x training session: $F_{(2, 22)} = 1.08$, $p = 0.35$). **c.** Mean avoidance latency to CS^+ trials in two groups of **Good avoiders** expressing ArchT or GFP during the second stimulation session, the pre-stimulation and the post-stimulation sessions (two-way repeated measures ANOVA; group: $F_{(1,33)} = 1.13$, $p = 0.29$, training session: $F_{(2,33)} = 0.07$, $p = 0.92$, group x training session: $F_{(2,33)} = 0.24$, $p = 0.78$). **d.** Avoidance discrimination index in ArchT **Good avoiders** mice during the pre-stimulation session and the second stimulation session (paired t-test: $t = 0.63$, $p = 0.55$).

We next evaluated the effect of the dmPFC-dl/lPAG inhibition in **Good avoiders** on freezing expression levels during door closed CS^- and CS^+ trials **(Figure 30 a, b)**. We did not observe any effect of the optogenetic inhibition on the first (data not shown),

or second **(Figure 30 a, b)** optogenetic stimulation sessions nor during the post-stimulation sessions **(Figure 30 a, b; first post-stimulation session not shown)**. During shock trials, the optogenetic inhibition of the dmPFC-dl/lPAG pathway in **Good avoiders** promoted a significant increase in freezing levels during the post-stimulation period, compared to GFP controls, although there was no effect during the stimulation session **(Figure 30 c)**. This ''post-stimulation effect'' could be explained by the low number of shock trials as compared to avoid trials in the group of **Good avoiders** exposed to the optogenetic inhibition. In addition, freezing levels during the interval of 8.8 seconds preceding and following the door-opening were not significantly different between ArchT and control mice before, during, or after the optogenetic stimulation **(Figure 30 e)**. ***All together these results indicate that the optogenetic inhibition of the dmPFC-dl/lPAG pathway after avoidance learning has been established, do not affect conditioned avoidance or freezing expression.***

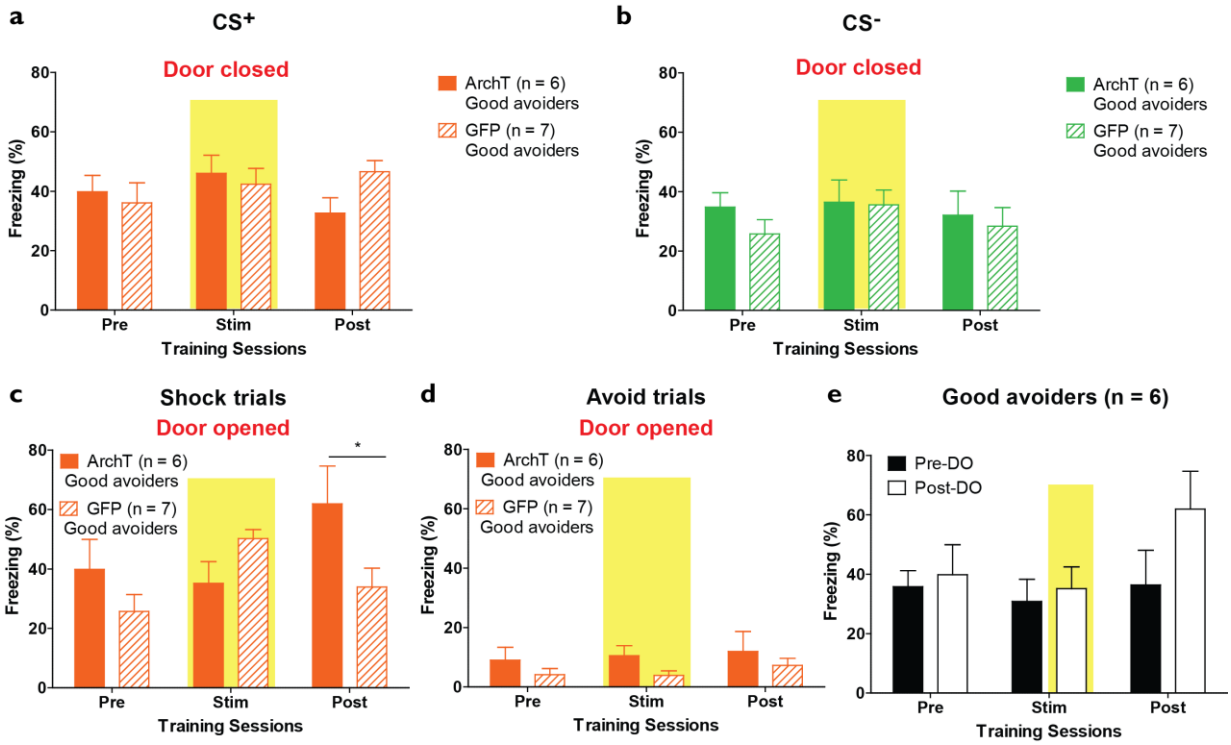

Figure 30. Optogenetic inhibition of the dmPFC-dl/lPAG pathway does not impair freezing expression

CS^+ -evoked freezing (across 15 trials) **(a),** and CS^- -evoked freezing (across 15 trials) **(b)** at pre-stimulation, second stimulation and second post-stimulation sessions in two groups of good avoiders: ArchT and GFP groups (panel **a**: two-way repeated measures ANOVA; group: $F_{(1, 22)} = 0.10$, $p = 0.75$, training session: $F_{(2, 22)} = 1.66$, $p = 0.21$, group x training session: $F_{(2, 22)} = 4.12$, $p = 0.03$, and panel **b**: two-way repeated measures ANOVA; group: $F_{(1, 26)} = 0.47$, $p = 0.50$, training session: $F_{(2, 26)} = 0.91$, $p = 0.41$, group x training session: $F_{(2, 26)} = 0.35$, $p = 0.70$). CS^+ -evoked freezing during (i) the interval between the door opening and the shock delivery (shock trials) **(c)** and (ii) the interval between the door opening and avoidance response (avoid trials) **(d)** at pre-stimulation, second stimulation and second post-stimulation sessions in ArchT and GFP control mice (panel **c,**

two-way repeated measures ANOVA; group: $F_{(1, 32)} = 2.15$, $p = 0.15$, training session: $F_{(2, 32)} = 2.07$, $p = 0.14$, group x training session: $F_{(2, 32)} = 4.24$, $p = 0.02$, and panel **d**: two-way repeated measures ANOVA; group: $F_{(1, 33)} = 3.37$, $p = 0.07$, training session: $F_{(2, 33)} = 0.39$, $p = 0.67$, group x training session: $F_{(2, 33)} = 0.04$, $p = 0.95$). e. CS^+ -evoked freezing during the interval between the DO and the shock delivery (post-DO) and the same interval of time (namely 8.8 seconds) preceding the door opening (pre-DO) at pre-stimulation, second stimulation and second post-stimulation sessions in **Good avoiders** (two-way repeated measures ANOVA; group: $F_{(1, 28)} = 0.001$, $p = 0.96$, training session: $F_{(2, 28)} = 0.05$, $p = 0.94$, group x training session: $F_{(2, 28)} = 0.34$, $p = 0.70$).

dmPFC-dl/lPAG optogenetic inhibition impairs the acquisition of avoidance behavior

Because we did not observe any expression phenotype upon the optogenetic manipulation of the dmPFC-dl/lPAG pathway, we next sought to evaluate whether the manipulation of this pathway could impair the acquisition of avoidance learning. We reasoned that the best strategy to use would be to inhibit the dmPFC-dl/lPAG pathway during the first 6 training sessions in **Good avoiders**. However, using our behavioral paradigm, it is quite clear that Good learners cannot be differentiated from Bad learners before session 6. To turn around this problem we simplified our behavioral protocol in order to generate a majority of Good learners **(Figure 31 a, b)**. To this purpose we designed a paradigm in which only DO trials were presented **(Figure 31 a)**. Using this paradigm we generated 87.5% of Good learners (including discriminators and generalizers) and 12.5% of Bad learners **(Figure 31 b)**. This adapted paradigm did not significantly change the proportions of **Good avoiders discriminators** that slightly increased from 33% in the original paradigm to 37.5% in the adapted paradigm (**Figure 31 b)**. We hypothesized that, using the adapted simplified paradigm, if dmPFC-dl/lPAG pathway was necessary for avoidance learning, inhibiting this pathway during learning would abolish avoidance learning and therefore decrease the percentage of **Good avoiders** after 6 sessions of training. Our results confirmed our hypothesis since the optogenetic inhibition of the dmPFC-dl/lPAG pathway during 6 training sessions completely abolished avoidance learning in all stimulated mice **(Figure 31 c, d)** in comparison to GFP controls. Mice optogenetically inhibited remained **Bad avoiders** even after 6 supplementary training sessions without light stimulation, whereas the GFP control group still increased avoidance counts **(Figure 31 c, d)**. Moreover, the inhibition of the dmPFC-dl/lPAG pathway did not change freezing levels during the stimulation or non-stimulated sessions as compared to GFP controls **(Figure 31 e, f)**.

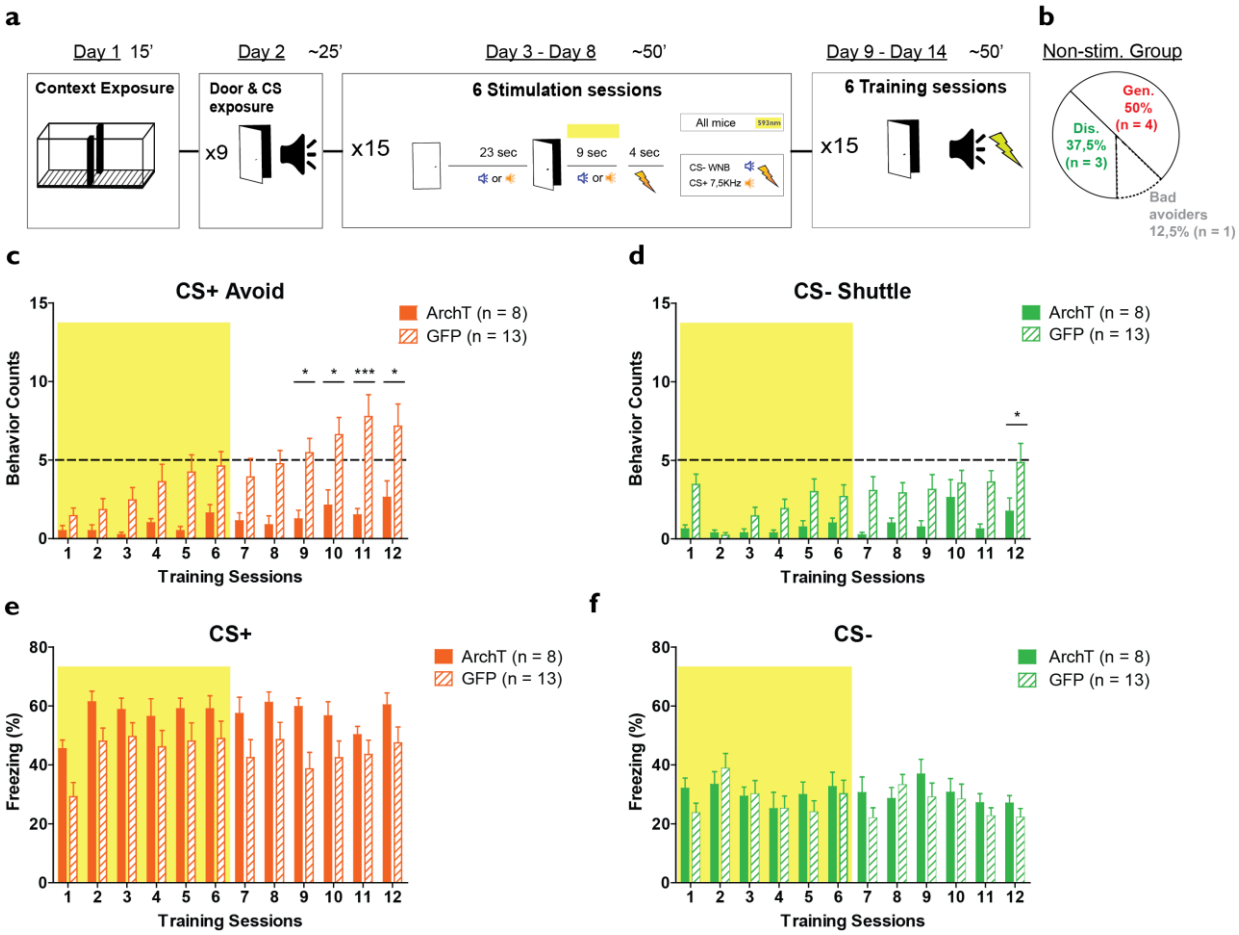

Figure 31. Inhibition of the dmPFC-dl/lPAG pathway abolished avoidance learning

a. Adapted behavioral protocol. On Day 1, mice were habituated during 15 min to the shuttle-box. On Day 2, animals were habituated to the presentation of the CS^- and CS^+ during opened condition (DO) only. After 23.1 seconds following the sound's onset, the door was slided-down (DO) and slided-up again 8.8 seconds after. 9 trials of CS^- and CS^+ were played. From Day 3 to Day 8, animals underwent 6 training during which the same type of trials were played except that the number of trials was increased to 15 CS^+ followed by a 4 s shock if the animal did not escape or avoid, and the yellow laser was turned on continuously for 9 seconds following door opening. From day 9 till 14 animals underwent the same training sessions except that no laser stimulation was delivered. **b.** Avoidance-based profiling after 6 sessions of training with no laser stimulation (non-stimulated group). **c.** CS^+ avoidance counts (two-way repeated measures ANOVA; group: $F_{(1, 209)} = 10.06$, $p = 0.005$, training session: $F_{(11, 209)} = 7.62$, $p < 0.0001$, group x training session: $F_{(11, 209)} = 2.42$, $p = 0.007$). **d.** CS^- shuttles counts (two-way repeated measures ANOVA; group: $F_{(1, 209)} = 7.72$, $p = 0.01$, training session: $F_{(11, 209)} = 3.91$, $p < 0.0001$, group x training session: $F_{(11, 209)} = 1.38$, $p = 0.18$,). **e, f.** Averaged freezing behavior during pre-door opening CS^+ trials (**e:** two-way repeated measures ANOVA; group: $F_{(1, 209)} = 4.19$, $p = 0.05$, training session: $F_{(11, 209)} = 4.27$, $p < 0.0001$, group x training session: $F_{(11, 209)} = 0.61$, $p = 0.81$), and CS^- trials (**f**: two-way repeated measures ANOVA; group: $F_{(1, 209)} = 0.35$, $p = 0.55$, training session: $F_{(11, 209)} = 2.72$, $p = 0.002$, group x training session: $F_{(11, 209)} = 1.22$, $p = 0.27$).

Importantly, the lack of avoidance learning upon optogenetic inhibition of the dmPFC-dl/lPAG pathway cannot be explained by altered locomotion since the stimulation of dmPFC-dl/lPAG pathway did not change several parameters including freezing, the total distance traveled during the stimulation as compared to before and after the stimulation, the number of shuttling events, and the escape latency **(Figure 32)**.

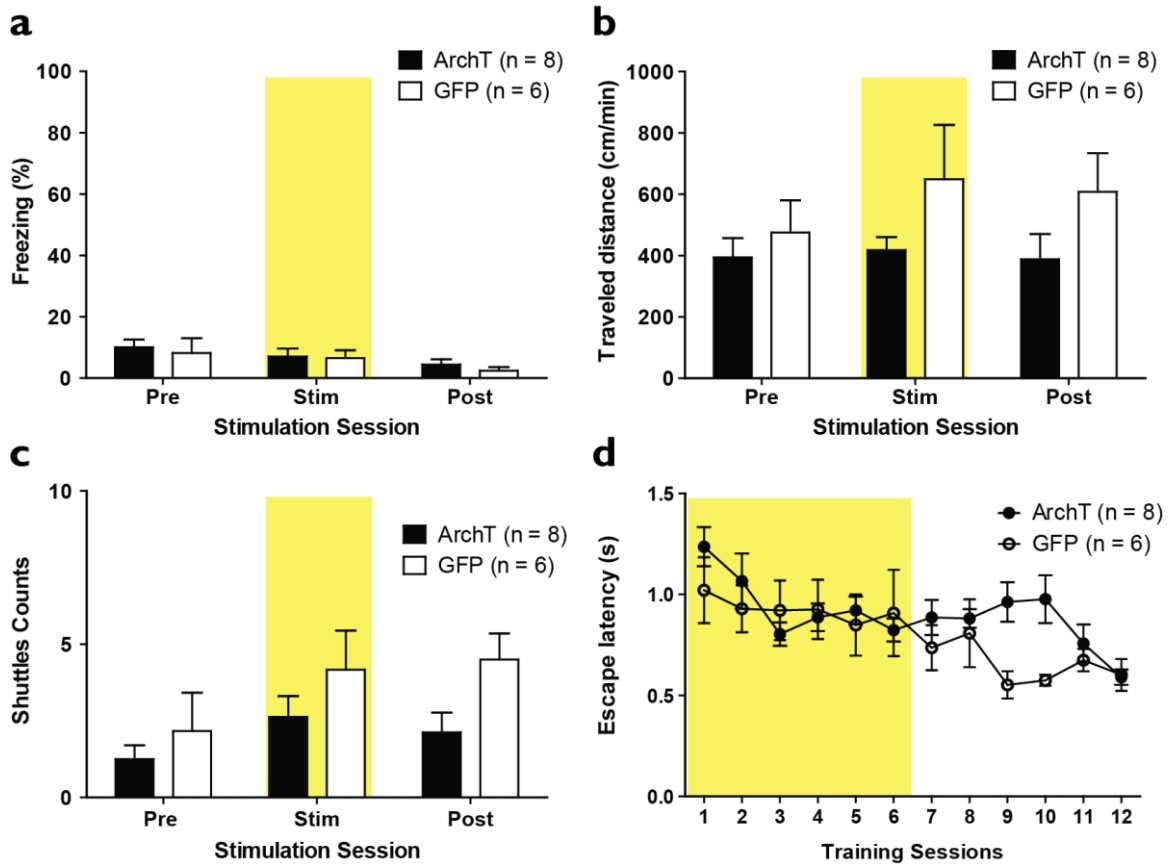

Figure 32. Inhibition of the dmPFC-dl/lPAG pathway did not promote motor alterations

Mice were submitted to a 9 minutes freely moving exploration of a shuttle-box and exposed to 3 minutes of continuous yellow light (10 mw light intensity) that was turned on from minute 4 to 6. **a.** Averaged freezing behavior before (Pre), during (stim) and after (Post) optogenetic inhibition in bad avoiders expressing ArchT and GFP (two-way repeated measures ANOVA; group: $F_{(1, 36)} = 0.44$, $p = 0.51$, training session: $F_{(2, 36)} = 2.23$, $p = 0.12$, group x training session: $F_{(2, 36)} = 0.04$, $p = 0.95$). **b.** Mean traveled distance in the shuttle-box before (Pre), during (stim) and after (Post) optogenetic inhibition in bad avoiders expressing ArchT and GFP (two-way repeated measures ANOVA; group: $F_{(1, 24)} = 2.98$, $p = 0.10$, training session: $F_{(2, 24)} = 0.71$, $p = 0.49$, group x training session: $F_{(2, 24)} = 0.50$, $p = 0.61$). **c.** Shuttles counts before (Pre), during (stim) and after (Post) optogenetic inhibition in bad avoiders expressing ArchT and GFP (two-way repeated measures ANOVA; group: $F_{(1, 24)} = 3.49$, $p = 0.08$, training session: $F_{(2, 24)} = 3.47$, $p = 0.04$, group x training session: $F_{(2, 24)} = 0.51$, $p = 0.60$). **d.** Escape latency throughout the 12 training sessions in bad avoiders expressing ArchT and GFP (two-way repeated measures ANOVA; group: $F_{(1,143)} = 6.08$, $p = 0.01$, training session: $F_{(11,143)} = 3.22$, $p = 0.0006$, group x training session: $F_{(11,143)} = 1.27$, $p = 0.24$).

Altogether, these results strongly suggest that inhibition of the dmPFC-dl/lPAG pathway during the time course of avoidance learning abolished avoidance learning but did not affect conditioned freezing behavior.

dmPFC-dl/lPAG optogenetic activation in Bad avoiders promotes avoidance learning

To further causally test the hypothesis that dmPFC neurons projecting to the dl/lPAG control avoidance learning, we performed gain of function experiments in **Bad avoiders.** One week after the surgery, animals were submitted to our classical behavioral protocol **(Figure 33 a)** and after 6 days of training, mice were classified into **Good** or **Bad avoiders** based on their avoidance scores to CS^+ presentations. **Bad avoiders** were submitted to two sessions of optogenetic activation whereas **Good avoiders** underwent two sessions of optogenetic inhibition **(Figure 33 a)**. This manipulation was followed by two additional training days to identify any long lasting effects **(Figure 33 a)**. 10 Hz optogenetic activation of the dmPFC-dl/lPAG pathway at door opening during CS^+ and CS^- trials in **Bad avoiders** induced a long-lasting increase in avoidance behavior in comparison to GFP controls and Bad learners non stimulated **(Figure 33 b).** Although the stimulation induced a significant post-stimulation increase of avoidance behavior during CS^- trials in ChR2 mice as compared to non-stimulated mice **(Figure 33 c)**, the animals discriminated CS^- and CS^+ presentations.

Furthermore avoidance scores were significantly increased during the second optogenetic stimulation session **(Figure 33 d)** as compared to the first one, and animals displayed discriminative avoidance learning upon the second stimulation session as compared to before the stimulation of the pathway **(Figure 33 e)**. Moreover, throughout the stimulation session the kinetics of avoidance performances did not vary across the session (first and second stimulation sessions) **(Figure 33 f)**. This later result suggests that attentional processes to the CS^+ are similarly engaged throughout the two stimulation sessions. ***Altogether those data point out that the optogenetic stimulation of dmPFC-dl/lPAG projections progressively promotes learning of avoidance behavior, although the dynamics of avoidance responses to CS^+ presentations are not altered within the stimulation sessions.***

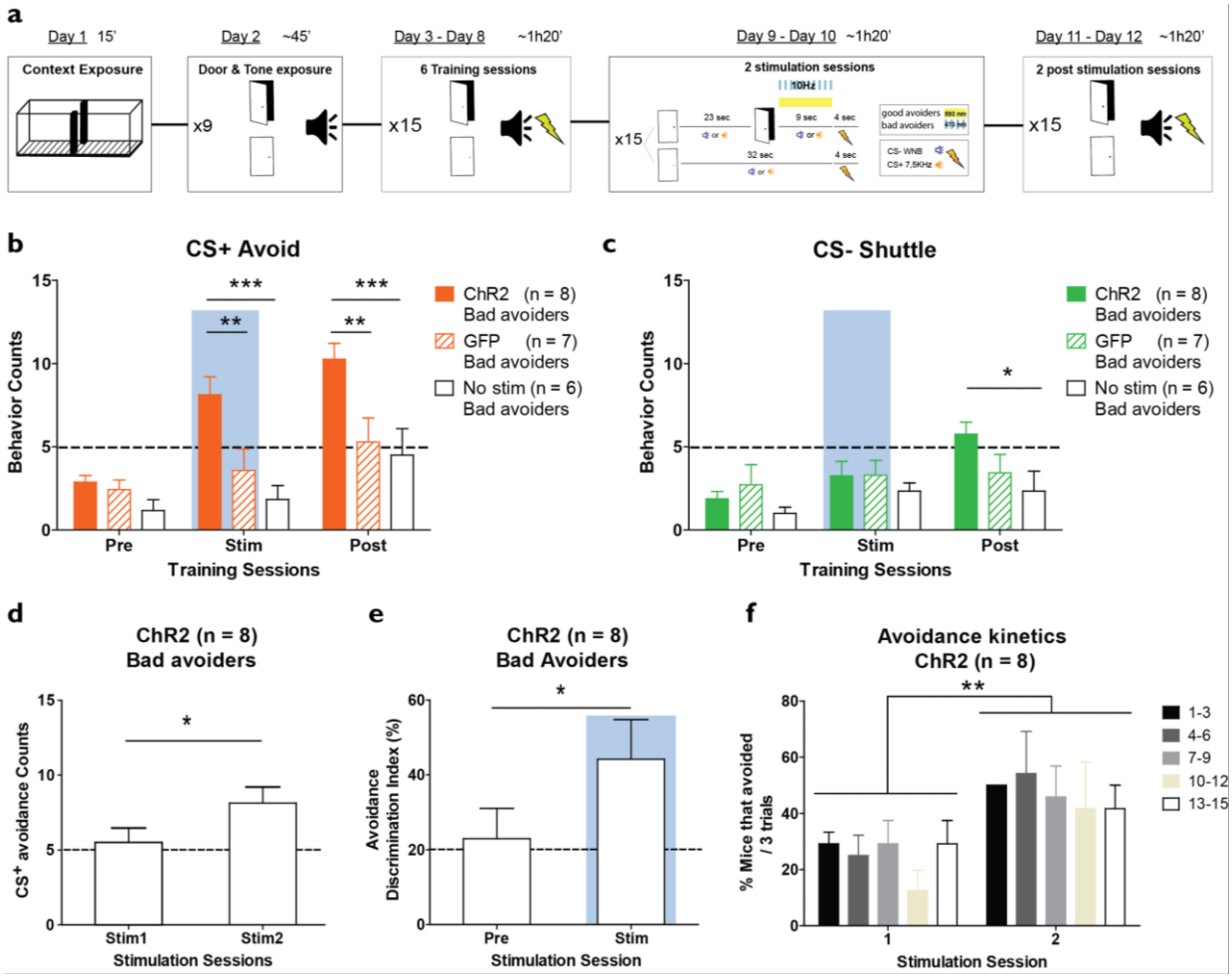

Figure 33. Optogenetic activation of the dmPFC-dl/lPAG pathway promotes avoidance learning

a. Optogenetic protocol. Following habituation and 6 days of training animals underwent 2 optogenetic stimulation sessions based on their avoidance scores; bad avoiders were submitted to 10 Hz (10 ms ON, 90 ms OFF) blue light pulses, whereas good avoiders were illuminated with yellow light continuously. The laser was turned on at both CS^- and CS^+ door opened trials, at the door-opening onset and turned off when the door was slided up at the end of the trial. Animals were in the end submitted to two behavioral post-stimulation sessions. **b.** CS^+ avoid counts at pre-stimulation, second stimulation and second post-stimulation sessions in three groups of bad avoiders: ChR2, GFP and long training no-stimulation groups. (Two-way repeated measures; ANOVA group: $F_{(2, 36)} = 12.60$, $p < 0.0004$ training session: $F_{(2, 36)} = 16.41$, $p < 0.0001$, group x training session: $F_{(4, 36)} = 2.43$, $p = 0.065$, $p < 0.01$, $p < 0.001$). **c.** CS^- shuttle counts at pre-stimulation, second stimulation and second post-stimulation sessions in three groups of bad avoiders: ChR2, GFP and long training no-stimulation groups (two-way repeated measures ANOVA; group: $F_{(2, 36)} = 1.79$, $p = 0.19$, training session: $F_{(2, 36)} = 5.92$, $p = 0.006$, group x training session: $F_{(4, 36)} = 1.80$, $p = 0.14$, $p < 0.05$). **d.** CS^+ avoidance counts in ChR2 bad avoiders mice during the first and the second stimulation sessions (paired t-test: $t = 3.28$, $p = 0.013$). **e.** Avoidance discrimination index in percent in ChR2 bad avoiders group during pre-stimulation session and second stimulation session (paired t-test: $t = 2.77$, $p = 0.02$). **f.** Percentage of ChR2 mice that performed avoidance to CS^+ across the 15 CS^+ door-opened trials of the first and second stimulation sessions in blocks of 3 trials (two-way repeated measures ANOVA; group: $F_{(4,10)} = 0.53$, $p = 0.71$, training session: $F_{(1,10)} = 13$, $p = 0.004$, group x training session: $F_{(4,10)} = 0.30$, $p = 0.86$).

Another potential confound of our results might be that the optogenetic stimulation promotes locomotor behavior instead of driving avoidance learning. To check whether our 10 Hz light stimulation might affect locomotion per se, we performed a locomotion test before the optogenetic sessions **(Figure 34 a)**. The 10 Hz optogenetic stimulation of the dmPFC-dl/lPAG pathway was performed during three

minutes which did not affect neither freezing levels **(Figure 34 b)**, nor the traveled distance **(Figure 34 c)**, nor the shuttles counts **(Figure 34 d)** in comparison to the same period of time before or after the stimulation.

Therefore, 10 Hz optogenetic activation of dmPFC-dl/lPAG pathway promoting avoidance learning can't be explained by an effect on locomotion behavior.

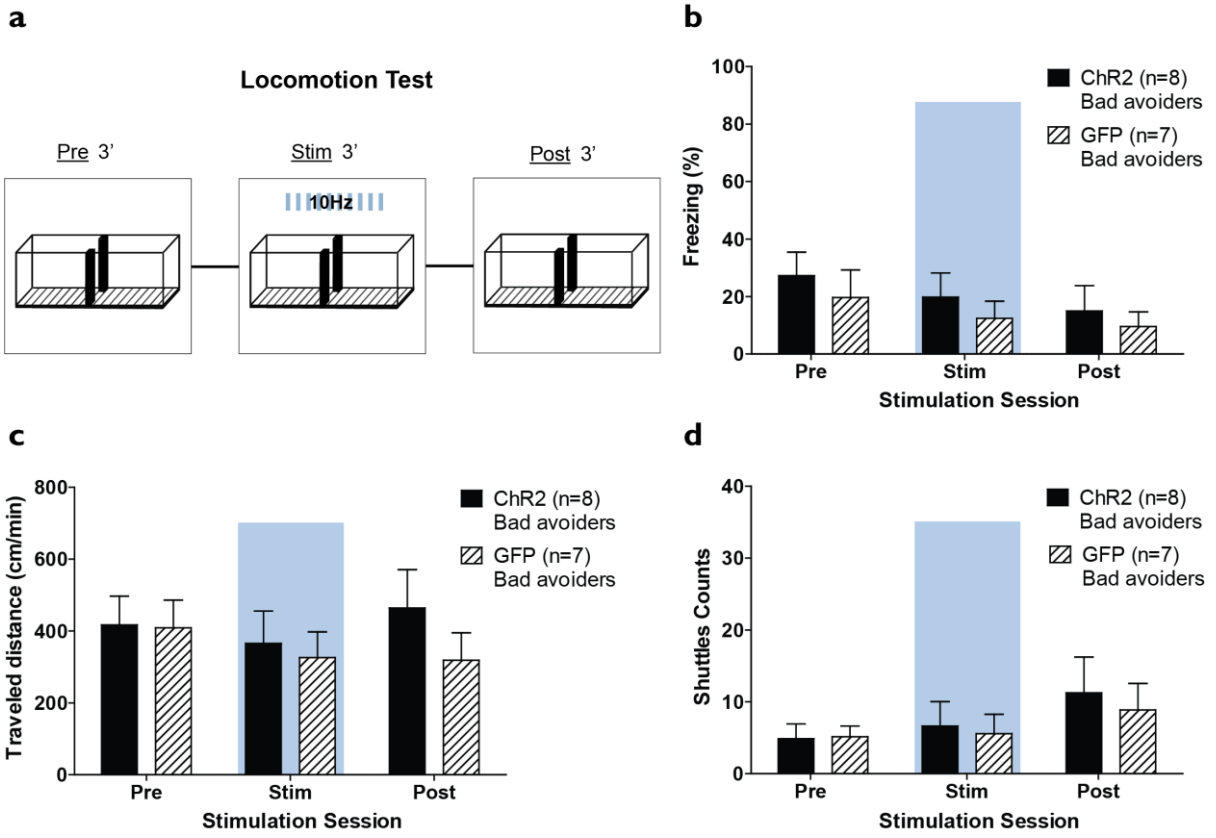

Figure 34. Activation of the dmPFC-dl/lPAG pathway did not promote motor alterations
a. Locomotion test protocol. Mice were submitted to a 9 minutes freely moving exploration of a shuttle-box and exposed to 10 Hz blue light stimulation (10 ms pulse width, 10 mw light intensity) that was turned on from minute 4 to 6. **b.** Mean freezing percent during the 3 minutes of stimulation (Stim), the three minutes preceding (Pre) and succeeding (Post) the stimulation (two-way repeated measures ANOVA; group: $F_{(1,26)} = 0.42$, $p = 0.52$, training session: $F_{(2,26)} = 5.27$, $p = 0.01$ group x training session: $F_{(2,26)} = 0.06$, $p = 0.94$). **c.** Mean traveled distance in the shuttle-box per minute during the stimulation (Stim), the three minutes preceding (Pre) and succeeding (Post) it (two-way repeated measures ANOVA; group: $F_{(1,26)} = 0.33$, $p = 0.57$, training session: $F_{(2,26)} = 1.28$, $p = 0.29$, group x training session: $F_{(2,26)} = 1.42$, $p = 0.25$). **d.** Shuttles counts during the stimulation (Stim), the three minutes preceding (Pre) and succeeding (Post) it (two-way repeated measures ANOVA; group: $F_{(1,26)} = 0.07$, $p = 0.78$, training session: $F_{(2,26)} = 2.68$, $p = 0.08$, group x training session: $F_{(2,26)} = 0.16$, $p = 0.84$).

Finally, the optogenetic 10Hz activation of the dmPFC-dl/lPAG pathway did not change freezing expression neither during door closed trials **(Figure 35 a-b)** nor during DO trials (avoid or shock trials) **(Figure 35 c-d)** nor in post-DO as compared to pre-DO period during the stimulation as compared to pre- and post-stimulation days **(Figure 35 e)**. ***Therefore our results suggest that the optogenetic***

activation of dmPFC neurons projecting to the dl/lPAG promoted avoidance learning but do not affect conditioned freezing behavior

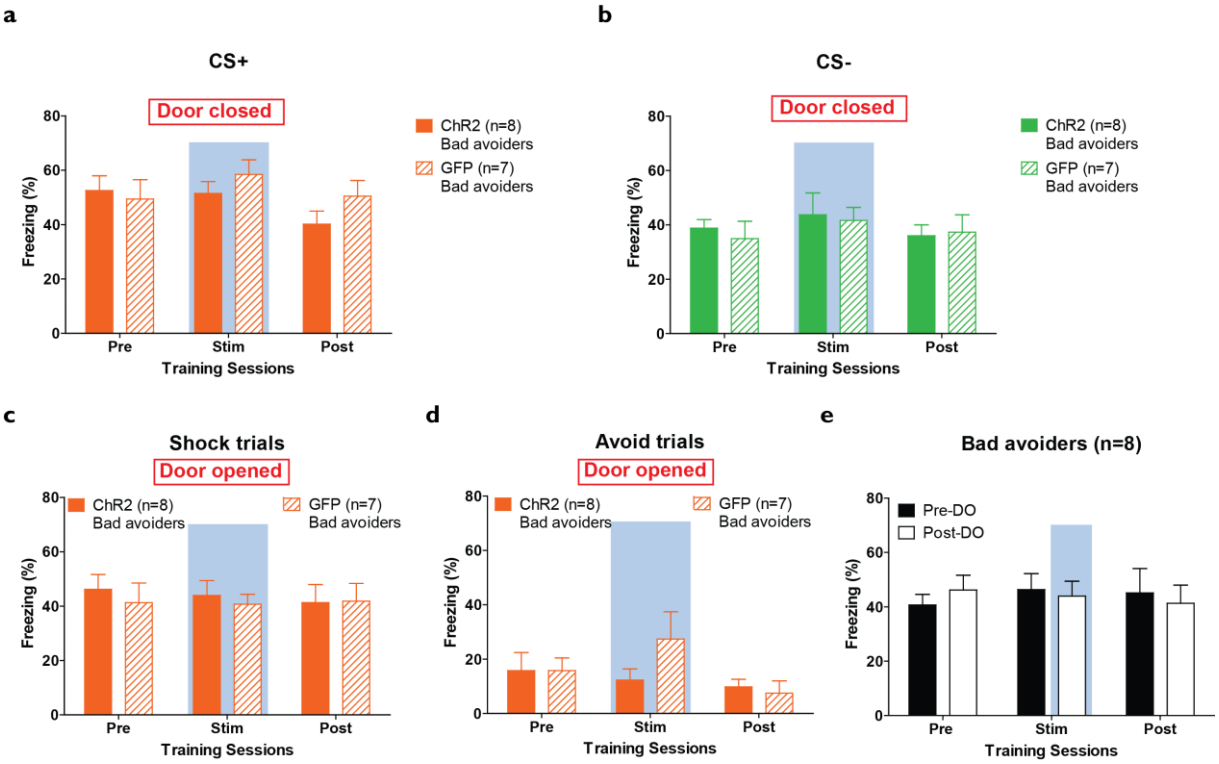

<u>Figure 35.</u> Optogenetic activation of the dmPFC-dl/lPAG pathway does not impair freezing expression

CS^+-evoked freezing behavior (across 15 trials of DO trials) (**a)** and CS^--evoked freezing behavior (across 15 trials) (**b)** before the first stimulation, (Pre) during the second stimulation (Stim) and after (Post) optogenetic stimulation of ChR2 and GFP **Bad avoiders** (**a**: two-way repeated measures ANOVA; group: $F_{(1,26)} = 0.49$, $p = 0.49$, training session: $F_{(2,26)} = 4.06$, $p = 0.02$, group x training session: $F_{(2,26)} = 2.10$, $p = 0.14$ and panel **b**: two-way repeated measures ANOVA; group: $F_{(1,26)} = 0.07$, $p = 0.78$, training session: $F_{(2,26)} = 0.91$, $p = 0.41$, group x training session: $F_{(2,26)} = 0.13$, $p = 0.87$). CS^+ averaged freezing behavior during the interval between the door opening and the shock delivery (shock trials) (**c)** and the interval between the door opening and avoidance response (avoid trials) (**d)** before the first stimulation, (Pre) during the second stimulation (Stim) and after (Post) optogenetic stimulation of ChR2 and GFP **Bad avoiders** (**c**: two-way repeated measures ANOVA; group: $F_{(1,26)} = 0.19$, $p = 0.66$, training session: $F_{(2,26)} = 0.08$, $p = 0.91$, group x training session: $F_{(2,26)} = 0.13$, $p = 0.87$ and panel **d**: two-way repeated measures ANOVA; group: $F_{(1,38)} = 0.77$, $p = 0.38$, training session: $F_{(2,38)} = 1.84$, $p = 0.17$, group x training session: $F_{(2,38)} = 1.28$, $p = 0.28$). **e.** CS^+ averaged freezing behavior during the interval between the door opening and the shock delivery (post-DO) and the same interval of time (8.8 seconds) preceding the door opening (pre-DO) before the first stimulation, (Pre) during the second stimulation (Stim) and after (Post) optogenetic stimulation of ChR2 and GFP **Bad avoiders** (two-way repeated measures ANOVA; group: $F_{(1,28)} = 0.001$, $p = 0.96$, training session: $F_{(2,28)} = 0.05$, $p = 0.94$, group x training session: $F_{(2,28)} = 0.34$, $p = 0.70$).

Place-preference test

Our data indicate that the optogenetic activation of the dmPFC-dl/lPAG pathway promoted avoidance behavior. This increased avoidance behavior is likely to be explained through a negative reinforcement learning (the fact that avoiding will prevent the footshock and stop the CS presentation) but could also be explained through positive reinforcement processes. Indeed, the optogenetic activation might be rewarding and promote avoidance behavior. To test this possibility, mice were exposed to a place-preference test during which they were first placed for a 15 min habituation period to determine the preferred compartment **(Figure 36 a, b)**. The next day mice were optogenetically stimulated in their non-preferred compartment **(Figure 36 a)**. On day 2, mice were exposed to the same stimulation protocol than the one used during the behavioral paradigm (dmPFC-dl/lPAG optogenetic activation at 10Hz, 10 ms pulse width, 10 mw). Light was delivered each time the mouse enters its non-preferred zone. Therefore if the stimulation was rewarding, the time spent in the non-preferred compartment during the stimulation and/or the post stimulation day would increase as compared to the first day without stimulation. This was not the case since, across the three days, mice did neither change their freezing levels significantly **(Figure 36 c)** nor the amount of time spent in the non-preferred zone of the shuttle-box **(Figure 36 d)**. Across the 3 days, mice decreased their number of shuttles **(Figure 36 e)** surely due to a habituation to the apparatus. ***These results indicate that the optogenetic activation of the dmPFC-dl/lPAG pathway is not rewarding, a possibility that cannot explain the optogenetic-induced increase in avoidance behavior.***

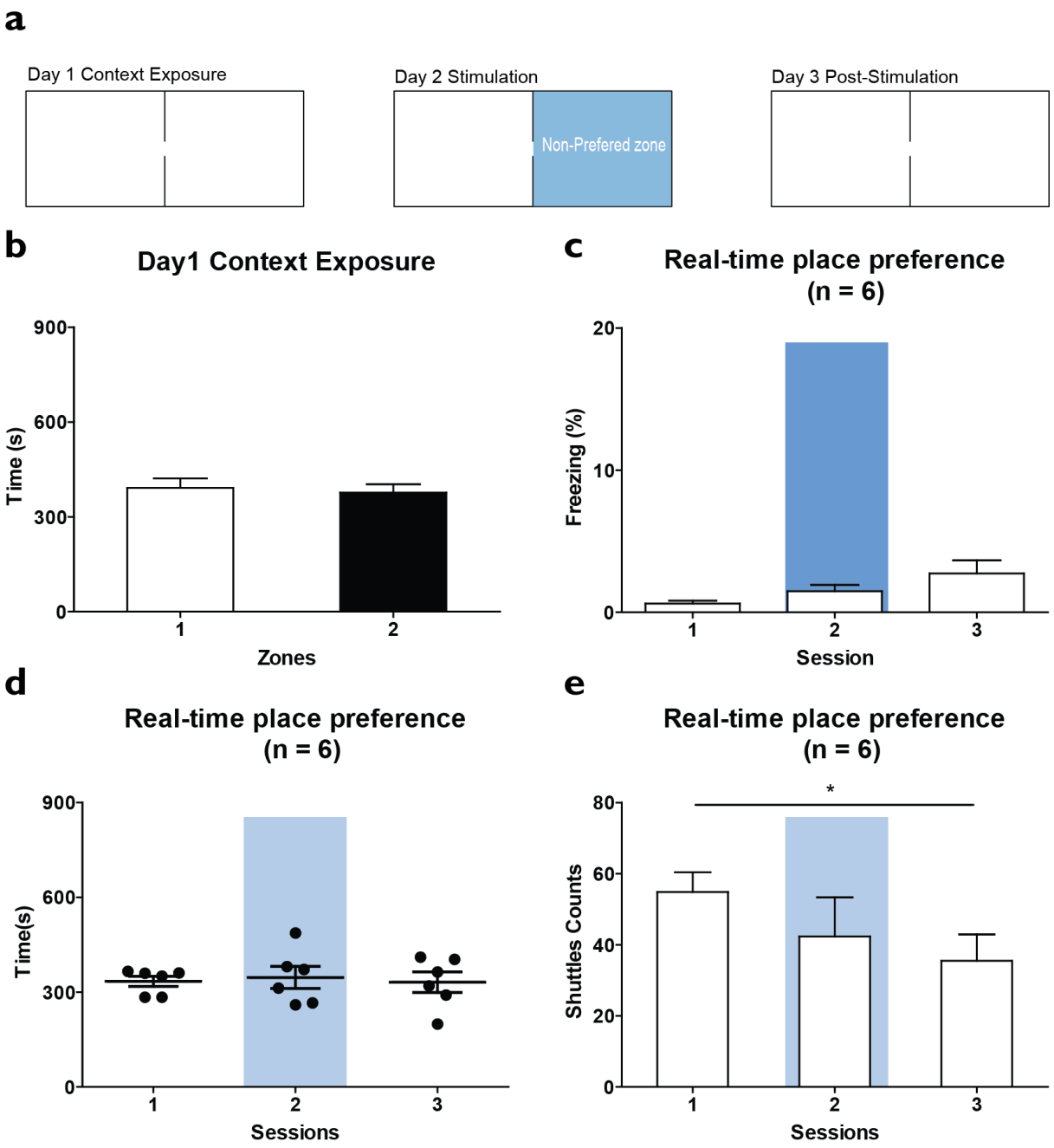

<u>Figure 36.</u> The optogenetic activation of the dmPFC-dl/lPAG pathway is not rewarding

a. Behavioral protocol. On Day 1 mice were exposed to 15 minutes of habituation in a shuttle-box. On Day 2 animals are exposed to the same apparatus in which they were stimulated with a laser blue light (10Hz, 10 mw, 10 ms pulse width) in the non-preferred compartment. On the last day, animals were re-exposed to the shuttle-box without any light stimulation. **b.** Time spent in the 2 identical zones of the shuttle-box on context exposure Day 1 (paired t.test: $t = 0.27$, $p = 0.79$). **c, d.** Averaged freezing behavior (**c**) and spent time (**d**) in the non-preferred zone of the shuttle-box, during the first, second and third testing days (the blue light laser was turned on each time the mouse enters the non-preferred zone) (**c**. One-way repeated measures ANOVA: $F_{(2, 10)} = 3.16$, $p = 0.08$; **d**. One-way repeated measures ANOVA: $F_{(2, 10)} = 0.20$, $p = 0.81$). **e.** Shuttles counts on Day 1-3 (One-way repeated measures ANOVA: $F_{(2, 10)} = 11.72$, $p = 0.01$, Bonferroni post-hoc: $t_{(1, 3)} = 3.51$, $p < 0.05$).

Hot-plate test

Another possibility that could explain the optogenetic-induced increase in avoidance behavior in **Bad avoiders** is an effect of the light stimulation on pain perception. For instance, if the optogenetic stimulation induces pain behavior, it could be associated with avoidance behavior. To investigate this hypothesis, **Bad avoiders** (*n* = 8 mice) were submitted to a commonly used test for evaluating thermal pain sensitivity: the hot-plate test. **Bad avoiders** were placed in a square arena with a floor consisting of a heated plate which temperature increased with time (6°C / min). The plate stopped heating up and started to cool down when one of two behavioral reactions were performed by the mouse, namely jumping or hind paw licking. The reaction time, at which these two behaviors were expressed, was used to quantify the latency of the response, as well as the nociceptive temperature. No significant differences were detected neither in the nociceptive temperature nor in the latency of the behavioral responses whether the optogenetic stimulation was delivered or not **(Figure 37 a, b)**. ***Therefore the optogenetic activation of the dmPFC-dl/lPAG pathway did not change the thermal nociceptive sensitivity in mice and the increased avoidance responses upon optogenetic stimulation cannot be explained by a change in nociception.***

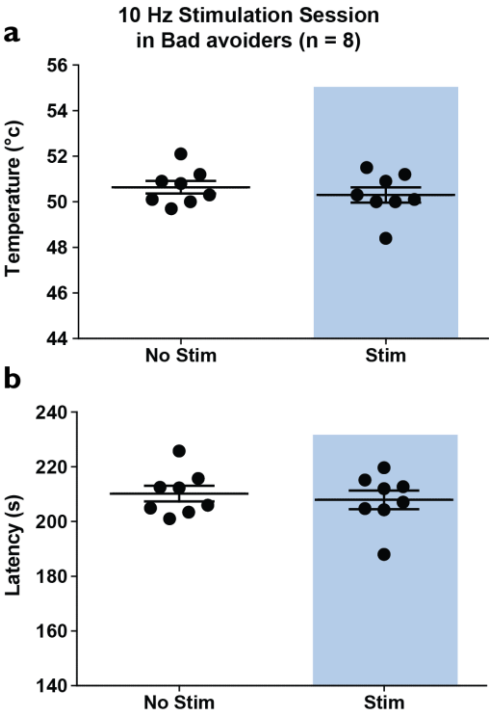

Figure 37. The optogenetic activation of the dmPFC-dl/lPAG pathway is not nociceptive
a. Nociceptive temperature with and without dmPFC-dl/lPAG optogenetic activation (paired t.test: t = 0.85, p = 0.42). **b.** Latency to express hind paw licking or jumping responses during and outside the optogenetic stimulation (paired t.test: t = 0.51, p = 0.62). The blue area represents the optogenetic stimulation session.

Synaptic potentiation of the dmPFC-dlPAG pathway correlates with avoidance behavior

Together the above data suggest that a subpopulation of dmPFC neurons projecting to the dl/lPAG is involved in avoidance learning but not expression. This raises the question as to whether this pathway exhibits synaptic plasticity during avoidance associative learning in **Good avoiders**. To address this question we evaluated (i) whether dmPFC to dlPAG pathway stimulation is associated with changes in synaptic plasticity at prefrontal inputs to dlPAG neurons as measured by NMDA/AMPA ratios and (ii) whether changes in NMDA/AMPA ratios at prefrontal inputs to dl/lPAG neurons in **Bad** and **Good avoiders** correlate with behavioral performance. This part of the thesis has been done in collaboration with Dr. Yann Humeau (IINS, Bordeaux, France) and his Ph.D. student, Ha Rang Kim.

To test the hypothesis that 10 Hz optogenetic activation performed in **Bad avoiders,** promoted avoidance performance by potentiating dmPFC inputs to dl/lPAG neurons, mice were injected in the dmPFC with either a Channelrhodopsin expressed in all projection cells or a retrograde strategy to target specifically dmPFC to dl/lPAG projecting cells **(Figure 38 a)**. First, we demonstrated that optogenetic 10 Hz stimulation at the level of the dmPFC activated local neurons **(Figure 38 a inset)**. Next, cells were patched blindly in the dlPAG and their AMPA and NMDA currents were measured in voltage-clamp mode, at -70 mv and + 50 mv respectively. The rationale being that dl/lPAG neurons receive mainly glutamatergic afferents from the dmPFC. Glutamatergic synaptic transmission is mediated by α-amino-3-hydroxy-5-methyl-4-isoxazolepropionate (AMPA-R) receptors and *N*-methyl-D-aspartate (NMDA-R) receptors. 10 Hz activation of dmPFC afferents on dl/lPAG neurons induces at the pre-synaptic level the release of glutamate, which bounds post-synaptically to AMPA-R thereby producing a post-synaptic depolarization. This depolarization facilitates the activation of voltage-dependent NMDA receptors. AMPA-R open and close quickly (1ms) **(Figure 38 a)**, and are thus responsible for a fast excitatory synaptic transmission. NMDA-R when activated allow the influx of Na^{+} and Ca^{2+} into the cell and the efflux of K^{+}, with a slow inactivation kinetics **(Figure 38 a)**. Once activated NMDA-R, by allowing a $Ca^{2}+$ influx into the cell, activate a cascade of transcription factors which ultimately increase the conductance of many receptors and allow the docking and the expression of new AMPA-R at the cell

surface which thereby potentiates post-synaptic EPSCs (Rao and Finkbeiner, 2007). For instance, our data indicated that in-vitro 10 Hz high-frequency stimulation (HFS: 5 trains of 10 Hz, 10 ms pulse-width, 8 seconds each) of dmPFC-afferents synapsing onto dlPAG cells produce an increase in AMPA-R-mediated EPSCs **(Figure 38 b1, b2)**. We then quantified NMDA/AMPA ratio in 27 cells patched in the dlPAG from naïve mice after performing the HFS protocol *in vitro* **(Figure 38 b1).** We observed that NMDA/AMPA ratio significantly increased several minutes (2 to 5 minutes) after the stimulation **(Figure 38 b3)**. ***This strongly suggests that our optogenetic stimulation protocol used in vivo is able to induce synaptic plasticity at dmPFC inputs to dlPAG cells.***

Next, we compared NMDA/AMPA ratios in dlPAG cells from 5 different groups of mice **(Figure 38 c)**: naïve mice, mice optogenetically stimulated and mice submitted to 6 sessions of our behavioral paradigm and classified into **Bad avoiders** (Bad), **Good avoiders** that discriminate or that generalize. Our analyses revealed that NMDA/AMPA ratios were significantly lower in **Good avoiders** discriminators as compared to **Bad avoiders** suggesting that plasticity occurred in the dmPFC-dlPAG pathway during avoidance learning. However, despite a tendency for lower NMDA/AMPA ratios in stimulated versus naïve animals, this was not significant. Also, no significant differences were detected between **Good avoiders** that discriminate and the ones generalizing which also show reduced NMDA/AMPA ratios **(Figure 38 c)**.

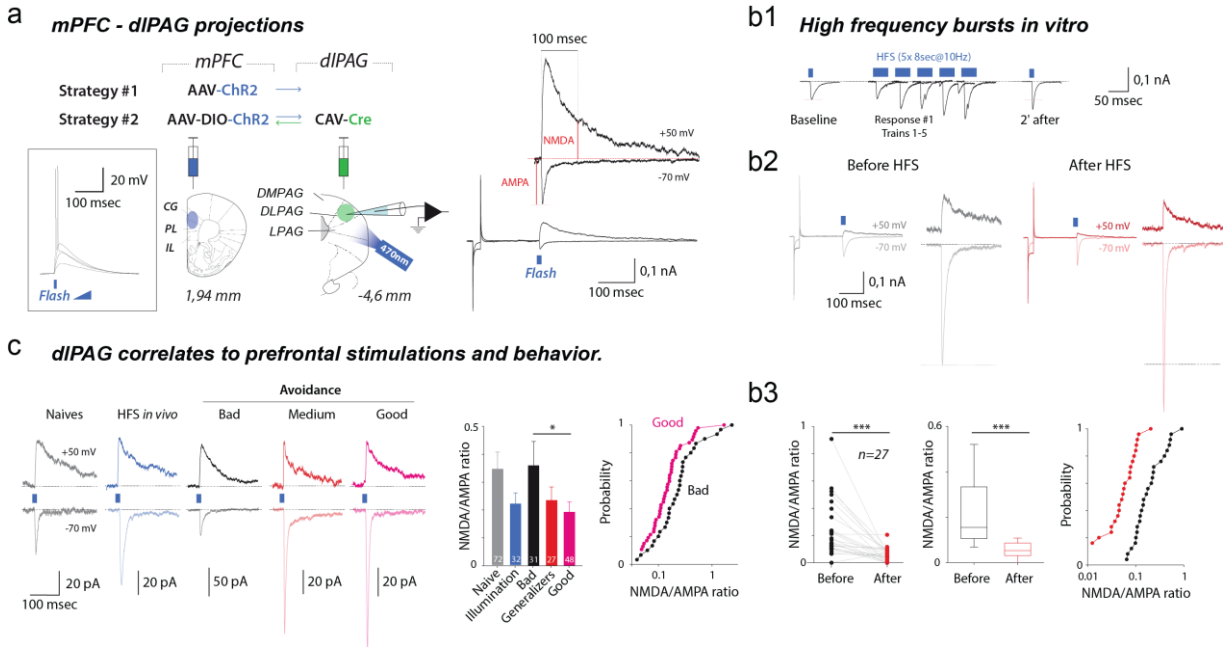

Figure 38. Plasticity at dmPFC to dl/lPAG synapses during behavioral avoidance

a. Two strategies were used to characterize functionally the dmPFC-dlPAG projections. In strategy 1, wild-type C57BL6/J mice were injected with AAV-ChR2 in the dmPFC (ACC, PL). In strategy 2, a retrograde mixture consisted of Cav-Cre, HSV-Cre was injected in the dlPAG. The retrograde virus travels back to dlPAG afferents among which the dmPFC in which we injected an AAV-DIO-ChR2. In both strategies mice are sacrificed 4 to 5 weeks after injections and voltage-clamp recordings were performed at -70 mV and +50 mV to record respectively AMPAR- and NMDAR-mediated conductance, in presence of a $GABA_AR$ antagonist. Left: The inset illustrates the activation of dmPFC neurons upon light pulses of increasing amplitudes. Right: schematic of how AMPA and NMDA currents were quantified. **b1.** Example of AMPA currents measured before (baseline) and 2 minutes after the high frequency stimulation (HFS) protocol delivered *in vitro* (5 pulses, 10 Hz, 10 ms pulse width, 8s). **b2.** Example of AMPA and NMDA traces before and after dmPFC-dlPAG *in vitro* HFS stimulation. **b3.** Left: NMDA/AMPA ratio before and after the *in vitro* HFS protocol (Paired t.test (n = 27 pairs): t = 4.46, p = 0.0001). Center: NMDA/AMPA ratio average (p = 0.0001). Right: NMDA/AMPA cumulative distributions before and after the *in-vitro* HFS stimulation protocol (Kolmogorov-Smirnov two-tailed test: D = 0.654, p = 0.0001, alpha = 0.05). **c.** Left: examples of AMPA and NMDA voltage-clamp, current traces in slice preparations from mice undergoing different protocols: naïve, HFS *in vivo* (30 stimulations, 470 nm, 10 Hz, 10 ms pulse width, 8 seconds), **bad**, generalizers, **good** (discriminators) **avoiders** undergoing 6 sessions of behavioral training with no light stimulation. Center panel: NMDA/AMPA ratio average in the five different groups (Non-parametric Mann-Whitney test of comparison of Naïve group to all the other groups: Naïve vs. Illunination: p = 0.32; Naïve vs. Bad: p = 0.40; Naïve vs. Generalizers: p = 0.51; Naïve vs. Good: p = 0.059. Non-parametric Mann-Whitney test of comparison of Bad group to all the other groups: Bad vs. Naïve: p = 0.57; Bad vs. Illuminated: p = 0.20; Bad vs. Generalizers: p = 0.23; Bad vs. Good: p = 0.02, *). Right panel: NMDA/AMPA ratio cumulative probability distribution of good and bad avoiders (Kolmogorov-Smirnov two-tailed test: D = 0.029, p = 1, alpha = 0.05).

All together these data demonstrated that the phenotypic switch of Bad avoiders into Good avoiders upon the optogenetic stimulation of the dmPFC-dl/lPAG pathway is associated with the development of synaptic potentiation at dmPFC inputs onto dl/lPAG cells.

Cell-type specific connectivity of dmPFC neurons projecting to the dl/lPAG

Finally an important question to address is related to the cell-type specific connectivity of dmPFC afferents in the dl/lPAG. To address this question, we used *in vitro* recordings coupled with immunostaining approaches to determine the electrophysiological and morphological characteristics of dlPAG neurons receiving dmPFC projections. For this purpose, we used VGLUT2-Cre, GAD-Cre and SST-Cre mice injected with ChR2 in the dmPFC and a Cre-dependent AAV expressing GFP in the dl/lPAG **(Figure 39 a)**. Cells were patched in the dlPAG region. Each dlPAG patched cell was first recorded in voltage-clamp mode to detect whether an excitatory post-synaptic current (EPSC) was evoked by the blue light (470 nm) **(Figure 39 b)**.

In a second step, the same patched cell was recorded in current-clamp with different injected currents ranging from 50 to 350 pA to determine its' electrophysiological spiking characteristics (the spiking pattern and the spiking kinetics) **(Figure 39 b)**. In current-clamp mode, the spiking pattern and kinetics were discriminative criterions between SST^+ and $VGLUT2^+$/ GAD^+ neurons. Indeed, SST^+ dlPAG cells spike significantly more and faster with high depolarizing steps (350 pA) compared to both $VGLUT2^+$ and GAD^+ dl/lPAG cells **(Figure 39 c)**.

In voltage-clamp mode, we also compared a morphological criterion between the three cell types, namely the cell's capacitance which is directly proportional to the cell's surface. This analysis revealed that SST^+ dlPAG cells are significantly bigger than $VGLUT2^+$ cells and almost significantly bigger than GAD^+ neurons **(Figure 39 c)**. However, the differences in cell's capacitance should be interpreted with caution because the cell capacitance is proportional to the cell's body' as well as the neurites' surface of the patched cell. If the patched cell display ablated neurites due to the slicing process, this will alter the capacitance measure.

Finally, we characterized dmPFC afferents to each of the three cell types $VGLUT2^+$, GAD^+ and SST^+ in the dlPAG. First, we quantified these connections by analyzing the number of cells responsive to 10 Hz optogenetic stimulation of dmPFC inputs. Among the $VGLUT2^+$ recorded cells, only (5/16, 31%) received connections from the dmPFC whereas most of the GAD^+ cells (18/23, 78%) received dmPFC synaptic contacts **(Figure 39 d)**. Also most of the SST^+ cells (12/16, 75%) received dmPFC synaptic connections **(Figure 39 d)**. From this analysis, we can conclude that a large

proportion of GAD^+ and SST^+ dl/lPAG cells received dmPFC inputs. Interestingly, among dlPAG cells receiving dmPFC afferents, $VGLUT2^+$ cells receive a significantly stronger magnitude of light-evoked current as compared to GAD^+ and SST^+ cells **(Figure 39 d)**. Importantly, GAD^+ dlPAG cells light-evoked currents' amplitude was positively correlated with the cell's size (proportional to tau) **(Figure 39 d)**. Knowing that SST^+ dl/lPAG cells are bigger than GAD^+ cells **(Figure 39 c)** we can hypothesize that GAD^+ cells receiving large EPSCs upon activation of dmPFC inputs are in fact SST^+ cells **(Figure 39 d)**. To further confirm these observations we used a second strategy based on the anatomical quantification of dmPFC inputs labeled with synaptophysin, a pre-synaptic protein. AAV virus expressing a synaptophysin (red) was injected in the dmPFC of $VGLUT2^+$, GAD^+ and SST^+, which were tagged in the dlPAG with a green fluorophore (Cre-dependent AAV expressing GFP) **(Figure 39 e)**. Our data indicate that GAD^+ dl/lPAG cells receive more synaptic dmPFC contacts compared to $VGLUT2^+$ cells. Moreover only a small proportion of SST^+ cells receive dmPFC inputs **(Figure 39 e)**. These data do not confirm the previous *in vitro* and this could be due to our quantification method, which is based on the detection of synaptophysin puncta at the levels of the cell body and primary dendrites but not onto distal dendrites. To have a more accurate measure of synaptic inputs it would be important in the future to analyze distal dendrites where synapses are in general known to be massively present.

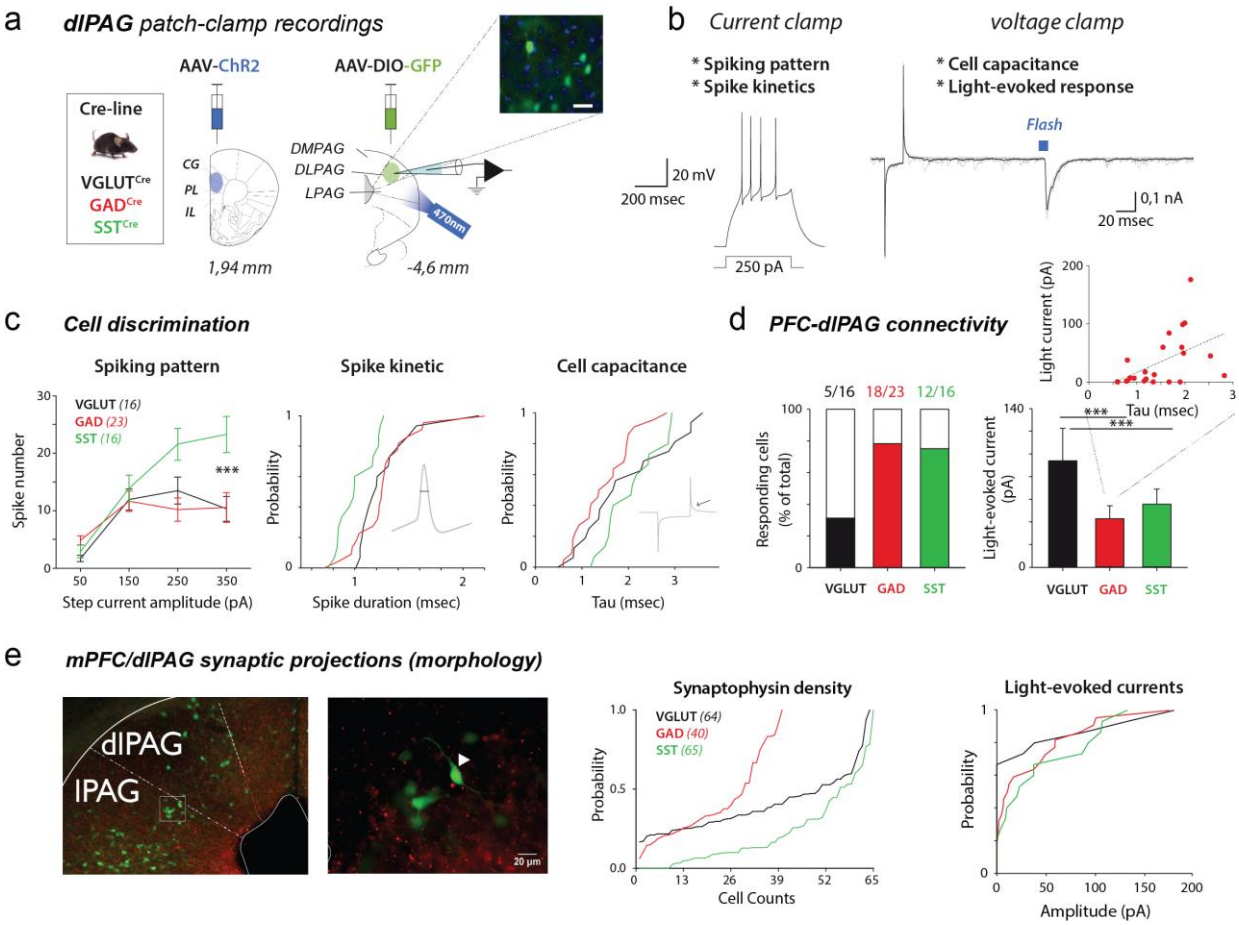

Figure 39. Cell-type specific connectivity of dmPFC inputs onto dl/lPAG

a. Scheme of the viral injections and the patch-clamp recordings. VGLUT2-Cre, GAD-Cre or SST-Cre transgenic mice were injected with an AAV-ChR2 virus under the control of a synaptophysin promoter in the dmPFC (ACC, PL) and with an AAV-DIO-GFP in the dlPAG. Four to five weeks after the surgery, animals are sacrificed and green cells in the dl/lPAG were patched using a whole-cell patch-clamp approach. Inset represents green patched cells in the dl/lPAG. **b.** Electrophysiological techniques used to measure intrinsic properties and synaptic activities in dl/lPAG cell populations. Using current clamp technique, we record the variations of the membrane potential by injecting 400 msec long current steps of various amplitudes (-50, 50, 150, 250 and 350 pA). Spiking pattern and spikes' kinetics were determined. Using voltage clamp we measure light-evoked (470 nm) synaptic currents from dmPFC axons while maintaining the membrane potential at -70 mV. Using this recording mode, short hyperpolarization steps (seal tests) also allowed determining the cell's capacitance (proportional to the patched-cell surface area) and resistance. **c.** VGLUT2, GAD and SST cells exhibit discriminative parameters. Spiking pattern refers to the mean spike number emitted by each cell type during different 400 msec long current step amplitudes. (One way ANOVA: $p < 0.0001$, Bonferroni post-hoc test: VGLUT2 vs. SST and GAD vs. SST $p < 0.0001$, VGLUT2 vs. GAD p = ns). Spiking kinetics refers to spike duration (width at half amplitude) as illustrated in the inset for each cell type (Kolmogorov-Smirnov two-tailed test (alpha = 0.05): VGLUT2 vs. GAD: D = 0.26, p = 0.47; SST vs. VGLUT2: D = 0.68, p = 0, SST vs. GAD: D = 0.76, p = 0.0001). Cell capacitance (represented in the inset) refers to the distribution of the seal test's tau (an index of the surface area) for each cell type (Kolmogorov-Smirnov two-tailed test (alpha = 0.05): VGLUT2 vs. GAD: D = 0.20, p = 0.74; SST vs. VGLUT2: D = 0.46, p = 0.039, SST vs. GAD: D = 0.39, p = 0.075). **d.** Left panel: Proportions of $VGLUT2^+$, GAD^+ and SST^+ cells in which light-evoked currents were observed. Right panel: light-evoked currents amplitude were quantified only in light-responsive cells of the three cell types (Kruskal-Whallis test: $p < 0.0001$; Dunn's multiple-comparison post-hoc test: GAD vs VGLUT2 and VGLUT2 vs. SST $p < 0.0001$, GAD vs. SST p = ns). Inset represents the amplitude of light-evoked currents in GAD cells. (Spearman's correlation coefficient $r = 0.59$, $p = 0.002$). **e.** Left: Confocal microscopy on slices of PAG (x10 and x40 magnification) showing the labelled (green) in Cre-dependent manner cells in the dl/lPAG (VGLUT2, GAD or SST) and red dots representing synaptophysin positive synaptic contacts Center panel: Cumulative probability of synaptophysin density onto VGLUT2, GAD and SST positive cells in the dl/lPAG (Kolmogorov-Smirnov two-tailed test (alpha = 0.05): VGLUT2 vs. GAD: D = 0.16, p = 0.47; SST vs. VGLUT2: D = 0.58, p = 0.0001; SST vs. GAD: D = 0.50, p = 0.0001). Right panel: cumulative probability of light evoked currents in VGLUT2, GAD and SST-Cre mice.

Our data suggest that dmPFC projections onto the dlPAG connect a subset of VGLUT2^{+} cells and SST^{+} among GAD^{+} cells. Among GAD^{+} cells, even though SST^{+} dlPAG cells do not receive massive synaptic contacts, these contacts are efficient enough since their activation evokes large EPSCs.

In summary, the optogenetic activation of dmPFC-dl/lPAG promoting avoidance behavior in initially Bad avoiders can't be explained by neither an increased locomotion per se, nor an appetite effect of the light stimulation nor a change in pain sensitivity. The optogenetic activation of dmPFC-dl/lPAG pathway rather produces a synaptic potentiation of the pathway promoting avoidance learning in Bad avoiders.

Discussion and Perspectives

We developed a novel behavioral paradigm during which a single CS was associated with two conditioned behavioral outcomes (freezing versus avoidance) as a function of contextual contingencies. Conditioned freezing behavior was evident in all the mice tested in our paradigm. All mice froze significantly more to the CS^+ compared to the CS^- and discriminated between the two CSs although freezing levels evoked by the CS^- were relatively high in all mice. This could be potentially explained by the fact that mice cannot predict whether the door will open or stay close in our paradigm. This potentially increases attentional processes and promote immobility. A second potential explanation of the relatively high freezing levels to CS^- is linked to the random trial presentation. Even though random presentation of different trial types makes the learning more complex, it also potentially enhances attentional processes and prevents the development of habitual avoidance learning (Dickinson, 1985; Wood and Neal, 2007). Our goal being to study goal-directed avoidance learning and not habitual avoidance we opted for presenting the trials in an intermingled manner.

Interestingly, the second behavioral outcome (avoidance) was not learned by all mice. Indeed, we categorized mice based on (i) avoidance scores and (ii) discrimination between CS^- and CS^+ trials into **Bad avoiders** (mice that did not learn to avoid), **Good avoiders** (mice that learned discriminative avoidance) and generalizers (**Good avoiders** that learned to shuttle/avoid to the other compartment each time the door got opened regardless of the CS). In terms of freezing, **Bad avoiders**, **Good avoiders** and generalizers also differ at two levels even though all three groups discriminate between CS^- and CS^+. During DC condition, **Bad avoiders** present the highest freezing levels to CS^+ (mean~55-60%) followed by discriminators (mean~45-50%) and generalizers which exhibited very low freezing levels to CS^+ presentations (mean~35-40%). Therefore, it seems that the DC condition allows to categorize animals in terms of freezing levels. During DO trials, at door opening **Bad avoiders** continue to freeze at high levels post-DO whereas **Good avoiders** and generalizers present a drop in their freezing levels since they switch to an active defensive strategy.

This heterogeneity in acquiring active defensive strategies have been already reported in active avoidance studies (Galatzer-Levy, et al., 2014) and is of a relative importance from a clinical point of view because it transduces the heterogeneity of

response of humans facing traumatic events. Regarding the proportions of the different behavioral profiles, both the original paradigm and the simplified adapted paradigm (only DO condition) resulted in ~35% of **Good avoiders** discriminators which acquired discriminative avoidance behavior. For connected animals (optic fibers, electrodes cables), around 45 to 55% of the population were classified as **Bad avoiders** and the rest as Generalizers. In all the experiments, generalizers were not further considered.

The high amount of **Bad avoiders** we obtain in our paradigm could be explained by their higher anxiety levels as compared to **Good avoiders**. However, all animals we used in this project are obtained by inbreeding method which implicates that all animals are genetically equivalent. In addition, during our pre-training habituation session **Bad** and **Good avoiders** did not show any significant difference in their basal contextual freezing levels. Nevertheless, one could think that animals throughout their life time could have been submitted to differential epigenetic modifications leading to changes in their genomes. Indeed some of those mice during the course of their life were maybe submitted to some sort of environmental stress or modifications which changed the methylation of some of their genes and therefore impacted on the transcribed proteins. This could be the case of **Bad avoiders** in which the increase or the decrease in the methylation of some genes increased the production of the corticosterone (the main hormone of stress). An elevated-plus maze test performed before training allowing to assess the time spent in the opened arms of the maze, will determine whether **Bad avoiders** present a predisposition to be more anxious than **Good avoiders**.

However, given all the available data in our hands, we think that the most plausible explanation of the high percentage of **Bad avoiders** obtained in our task is the complexity of the task. Indeed animals have to acquire two types of learning: to avoid the threatful tone (discriminative avoidance) and also to freeze to the same threatful tone (discriminative freezing). Indeed when we simplify the task, the percentage of **Bad avoiders** decreases therefore we suppose that **Bad avoiders** are generated because of the complexity of the task.

The difference in the kinetics of acquisition of freezing and avoidance behavior is obvious. Animals acquire discriminative freezing starting from the first training session while discriminative avoidance behavior is acquired at later sessions (sessions 5-6). One plausible explanation is the presence of a neuronal break

stopping the animals from acquiring avoidance behavior. One structure that could be playing the role of the break by its sustained activation throughout learning is the rostral dmPFC. Indeed, it has been shown that platform mediated avoidance (Diehl, et al, 2018) is disrupted by activating the rostral dmPFC. Therefore in our paradigm one possibility which would explain the late acquisition of avoidance behavior in **Good avoiders** is the sustained activation of the rostral dmPFC at early training sessions blocking avoidance behavior driven by the activation of the caudal dmPFC to the dl/lPAG. To address this possibility, c-fos protein expression could be checked in **Bad avoiders** after 6 training sessions and compared to c-fos expression in **Good avoiders** in the rostral dmPFC. Indeed, if the rostral dmPFC is blocking avoidance acquisition, the expression of c-fos protein in **Bad avoiders** should be significantly up-regulated as compared to **Good avoiders** at late training sessions (session 6).

The immediate-early gene c-fos study we performed revealed a clear significant up-regulation of c-fos in **Good avoiders** as compared to **Bad avoiders** and controls in the caudal dmPFC (ACC, PL). Our results are in concordance with several studies in rodents using a platform-mediated avoidance paradigm (Bravo-Rivera, et al., 2015) or lever-press avoidance paradigm (Beck, et al., 2014) demonstrating that PL drives avoidance behavior acquisition/expression. Our results are also consistent with clinical results indicating that in healthy humans avoidance is linked to an increased reactivity of the anterior ACC and the dmPFC (Schlund, et al., 2015). Based on our c-fos results, we also identified a structure considered to regulate the defensive output behavioral responses, namely the PAG and more specifically the dlPAG.

Another important observation from our single-unit recordings is the fact that dmPFC neurons involved in conditioned freezing and avoidance behaviors represent functionally segregated populations of neurons. Indeed only a small fraction of dmPFC neurons encode both freezing and avoidance behavior whereas most of the neurons either encode avoidance or freezing. Although we didn't identify dmPFC ouputs directly controlling freezing behavior in our paradigm, it is very likely based on the literature that it involves a projection from the dmPFC to the amygdala (Courtin, et al., 2014; Jhang, et al., 2018).

One caveat of the responsiveness of avoidance inhibited freezing activated neurons recorded in the dmPFC is that their avoidance inhibition detected as a decreased z-score can be only a return to their baseline activity. Indeed avoidance inhibited freezing activated putative cells are activated during freezing which occurs before

door opening. Therefore the drop in avoidance responsiveness we observe at door opening can be conferred to a return of those recorded putative neurons to their baseline activity. Hence the proportions of avoidance inhibited freezing activated putative pyramidal neurons recorded in the dmPFC is for sure over estimated. Indeed those neurons represent a population activated during freezing behavior exclusively.

As for the sustained increase in the activity of the neurons recorded in the dmPFC classified as avoidance activated, it could be linked to the shock expectancy. To test this possibility, principal component analysis could be ran on populations of putative pyramidal neurons recorded throughout learning when avoidance behavior started to be acquired (training sessions 3, 4 and 5) to check whether the proportions of the activated dmPFC neurons is changed. Indeed, if shock expectancy is linked to an increased activation of the dmPFC at door opening we would expect the avoidance activated population to be more numerous at early training sessions as compared to late training sessions, the stage at which learning starts to be stabilized. One argument that excludes this hypothesis is the fact that shock expectancy would be encoded the same way at door opening regardless the behavior of the animal (avoid trials or shock trials). Nevertheless it is not the case since avoidance activated neurons are continuously activated during avoid trials but not shock trials which suggests that this increased activity is more linked to the behavior (avoidance) than to shock expectancy.

We next demonstrated for the first time that dmPFC projections to the dl/lPAG are functionally necessary and sufficient for driving avoidance learning. Indeed, using antidromic stimulations and single-unit recordings, we determined that neurons projecting from the dmPFC to the dl/lPAG were activated during avoidance. We then optogenetically activated the dmPFC-dl/lPAG pathway in **Bad avoiders**, a process that engendered a progressive increase in avoidance performances. We demonstrated that this increase was not linked to an increase in locomotion, nor to pain perception, nor to an appetitive effect of the stimulation. We rather demonstrated that conditioned avoidance was associated with synaptic plasticity at dmPFC inputs onto dl/lPAG neurons in **Good avoiders** as compared to **Bad avoiders**. We showed that plasticity at this particular pathway was associated with changes in NMDA-R/AMPA-R ratio at the postsynaptic level. In our protocol, a possible *in vivo* demonstration of the implication of AMPA-R and NMDA-R in synaptic plasticity would be to quantify the expression of transcription factors in **Good avoiders** as compared

to **Bad avoiders** known to be regulated during associative learning. Another possibility to demonstrate that changes in synaptic plasticity at dmPFC-dlPAG synapses correlate with avoidance learning would be the infusion of APV (2R)-amino-5-phosphonovaleric acid) an NMDA antagonist to abolish plasticity mechanisms during learning. In this case, the daily infusion of APV along avoidance acquisition should abolish avoidance learning and lead to only **Bad avoiders**.

We also demonstrated that the manipulation of the dmPFC-dl/lPAG pathway is associated in our paradigm with specific changes in avoidance learning without any effect on freezing behavior. Those results go along with other findings showing that manipulating the dmPFC changes platform-mediated avoidance but not freezing behavior (Bravo-Rivera, et al., 2014; Diehl, et al, 2018). This corroborates our findings that distinct pools of dmPFC neurons encode freezing and avoidance behaviors, and suggest that a different dmPFC pathway could be involved in driving freezing expression such as the dmPFC-BLA pathway (Courtin, et al., 2014). However, one should keep in mind that freezing quantified in avoidance learning paradigms after chronic training may be encoded differently than freezing elicited by acute conditioning paradigms. Therefore it would be worth to test whether freezing in our behavioral paradigm is driven by dmPFC-BLA pathway (Courtin, et al., 2014) and whether dmPFC neurons projecting to the BLA are synchronized at 4 Hz oscillations during freezing as recently shown in our laboratory (Karalis et al., 2016; Dejean et al., 2016).

In addition, the combination of our *in vivo* electrophysiological, antidromic and optogenetic data strongly suggest that avoidance behavior is driven by an activation of the dmPFC which opposes the results of a recent paper (Diehl, et al., 2018) suggesting that avoidance is rather associated with an inhibition of dmPFC activity. We think that those discrepancies are linked to the differences in the rostro-caudal axis of manipulation/recordings at the dmPFC level. Indeed our recordings in the dmPFC and optogenetic manipulations are made in the caudal dmPFC (A.P. < +2.1) whereas in the platform-mediated paradigm (Diehl, et al., 2018) the results concern the rostral dmPFC (A.P. > 2.1). The opposing roles in avoidance learning played by the rostral dmPFC and caudal dmPFC highlight an important question being to determine which structure is critically involved in the selection of the behavioral response during avoidance. Does the selection of avoidance behavior depend on the rostral vs caudal dmPFC connectivity or is the selection made at downstream

structures like the dl/lPAG? Additional experiments will be required to specifically address this question.

Our electrophysiological patch-clamp *in vitro* recordings point out that cdmPFC project to both VGLUT2$^+$ and GAD$^+$ dlPAG neurons. We still need to determine whether one or both connections are important in driving avoidance behavior. To do so, we need to specifically manipulate VGLUT2$^+$ cells in the dl/lPAG receiving dmPFC inputs by using a rabies-based optogenetic manipulation of this pathway. A recent self-inactivating ΔG-rabies (SiR) has been developed allowing the switch OFF of ΔG-rabies following the primary infection, thereby preventing cytotoxicity but in the same time providing permanent access to the mapped neural elements via a CRE/FLP-mediated recombination triggered soon after the infection (Ciabatti , et al., 2017). Using this approach in VGLUT2$^+$ and GAD$^+$ dl/lPAG cells, we will be able to determine whether, as for flight behavior (Tovote, et al., 2016), learned avoidance is promoted by dlPAG glutamatergic activation and more specifically dmPFC to dlPAG glutamatergic activation. If, so this activation could be mediated directly by dmPFC glutamatergic projections targeting VGLUT2$^+$ dlPAG cells, or indirectly by a disinhibition of VGLUT2$^+$ dl/lPAG neurons **(Figure 40)**.

Finally, in our c-fos study we also had an increased activation at the level of the nucleus accumbens (not shown) in **Good avoiders** as compared to **Bad avoiders** and controls. In addition on one hand, in the platform-mediated avoidance (Bravo Rivera, et al., 2014) it has been demonstrated that muscimol inactivation of both PL and Nac impaired avoidance behavior. One the other hand, it was already reported that the activation of PV GABAergic projections from the mPFC (including both the PL and the IL) to the nucleus accumbens shell elicited acute aversion in a real-time place aversion task. Therefore, in our active avoidance task it would be worth to test whther the recorded avoidance inhibited neurons in the dmPFC project to the nucleus accumbens shell and whether the optogenetic activation of this inhibitory population would elicit avoidance acquisition/expression.

Another structure is known to be important in avoidance expression namely the central amygdala. In Fadok, et al. paper (Fadok, et al., 2017) CRF+ cells were shown to be activated during flight behavior. It has been also shown in this same paper that this population of cells projects directly to all columns of the PAG. One hypothesis worth testing is that the activation of CRF+ CeL neurons projecting to dlPAG would induce avoidance behavior since we found that in **Bad avoiders** at

the level of the CeA c-fos levels are increased in **Bad avoiders** as compared to **Good avoiders** in the door closed condition (data not shown). Therefore, one possibility is that the activation of CRF+ neurons in the CeL projecting to the dlPAG would promote avoidance learning in Bad avoiders.

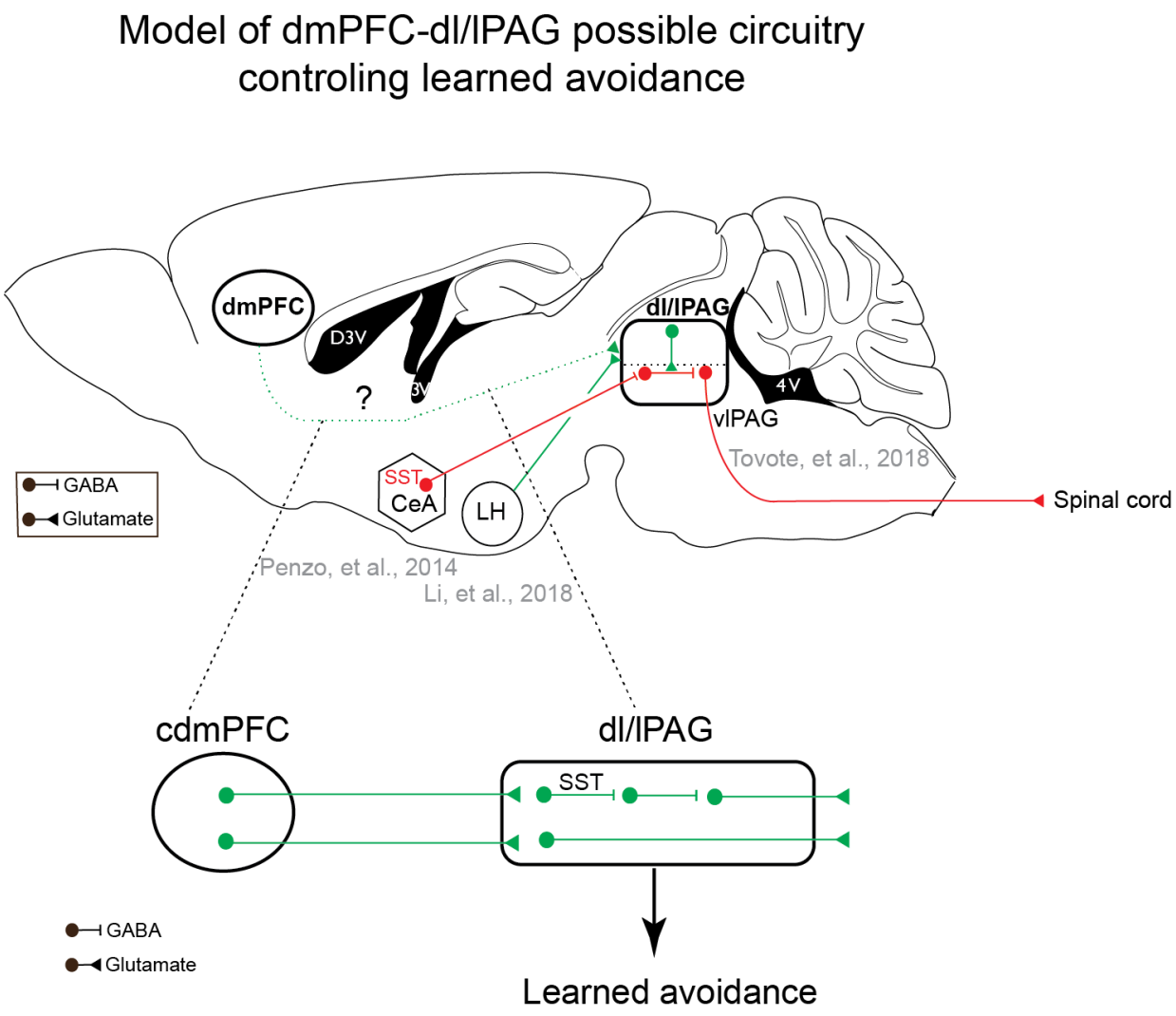

Figure 40.

Proposed model underlying cdmPFC-dl/lPAG control of learned avoidance behavior. The activation of dl/lPAG VGLUT2$^+$ neurons promote avoidance behavior through direct dmPFC VGLUT2$^+$ projections or through indirect disinhibition of VGLUT2$^+$ dl/lPAG neurons by the activation of excitatory dmPFC projections activating SST$^+$ dlPAG interneurons which inhibit another type of IN and thereby disinhibit VGLUT2$^+$ dl/lPAG neurons.

Altogether, the results collected within the time frame of this thesis demonstrate a key role of the dmPFC-dl/lPAG pathway in the acquisition of avoidance behavior. More generally these data along with other data recently published in the laboratory (Rozeske, et al., 2018) strongly suggest that in parallel to amygdala-brainstem projections, direct prefrontal inputs to the brainstem can efficiently regulate fear-related behaviors.

Bibliography

Adolphs, R., Tranel, D., Damasio, H., Damasio, A. «Impaired recognition of emotion in facial expressions following bilateral damage to the human amygdala.» *Nature 372, 669–672* , 1994.

Akirav, I., Raizel, H., Maroun, M. «Enhancement of conditioned fear extinction by infusion of the GABA(A) agonist muscimol into the rat prefrontal cortex and amygdala.» *The European journal of neuroscience 23: 758-764*, 2006.

Albutaihi, I.A., DeJongste, M.J., Ter Horst, G.J. «An integrated study of heartpain and behavior in freely moving rats (using fos as a marker for neuronalactivation).» *Neurosignals 13, 207–226*, 2004.

Alheid, G.F., De Olmos, J., Beltramino, C.A. *Amygdala and extended amygdala. In: The Rat Nervous System.* Orlando: Paxinos G., FL: Academic, p. 495–578, 1995.

Allen, M.T., Myers, C.E., Servatius, R.J. «Avoidance prone individuals self reporting behavioral inhibition exhibit facilitated acquisition and altered extinction of conditioned eyeblinks with partial reinforcement schedules.» *Frontiers in Behavioral Neuroscience* , 2014.

Amano, T., Duvarci, S., Popa, D., Pare, D. «The fear circuit revisited: contributions of the basal amygdala nuclei to conditioned fear.» *The Journal of neuroscience : the official journal of the Society for Neuroscience 31:15481-15489*, 2011.

Ambroggi, F., Ishikawa, A., Fields, H.L., Nicola, S.M. «Basolateral amygdala neurons facilitate reward-seeking behavior by exciting nucleus accumbens neurons.» *Neuron 59: 648–661*, 2008.

Ambrogi Lorenzini, C., Baldi, E., Bucherelli, C., Sacchetti, B., Tassoni, G. «Neural topography and chronology of memory consolidation: A review of functional inactivation findings.» *Neurobiology of Learning and Memory 71(1),1-18*, 1999.

Amorapanth, P., LeDoux, J.E., Nader, K. «Different lateral amygdala outputs mediate reactions and actions elicited by a fear-arousing stimulus.» *Nat Neurosci 3: 74-79*, 2000.

An, B., Hong, I., Choi, S. «Long-term neural correlates of reversible fear learning in the lateral amygdala.» *The Journal of neuroscience : the official journal of the Society for Neuroscience 32:16845-16856*, 2012.

Anderson, C.J. «The psychology of doing nothing: forms of decision avoidance result from reason and emotion.» *Psychological Bulletin* , 2003: 139-167.

Anglada-Figueroa, D., Quirk, G.J. «Lesions of the basal amygdala block expression of conditioned fear but not extinction .» *The Journal of neuroscience : the official journal of the Society for Neuroscience 25:9680-9685*, 2005.

Annau Z., Kamin L.J. «The conditioned emotional response as a function of the intensity of the US .» *J Comp Physiol Psychol 54: 428- 432*, 1961.

Ascoli, G.A., Alonso-Nanclares, L., Anderson, S.A., Barrionuevo, G., Benavides-Piccione, R., Burkhalter, A., Buzsáki, G., Cauli, B., Defelipe, J., Fairén, A., Feldmeyer, D., Fishell, G., Fregnac, Y., Freund, T.F., Gardner, D., Gardner, E.P.,et al. «Petilla terminology: nomenclature of features of GABAergic interneurons of the cerebral cortex.» *Nat. Rev. Neurosci. 9:557–568*, 2008.

Ascoli, G.A., Alonso-Nanclares, L., Anderson, S.A., Barrionuevo, G., Benavides-Piccione, R., Burkhalter, A., Buzsaki, G., Cauli, B., Defelipe, J., Fairen, A., Feldmeyer, D., Fishell, G., Fregnac, Y., Freund, T.F., Gardner, D., TO COMPLETE MANUALLY. «Petilla terminology: nomenclature of features of GABAergic interneurons of the cerebral cortex.» *Nature reviews Neuroscience 9:557-568*, 2008.

Assaf, M., Rabany, L., Zertuche, L., Bragdon, L., Tolin, D., Goethe, J., Diefenbach, G. «Neural functional architecture and modulation during decision making under uncertainty in individuals with generalized anxiety disorder.» *Brain Behav.* , 2018.

Audi, E.A., de Aguiar, J.C., Graeff F.G. «Mediation by serotonin of the antiaversive effect of zimelidine and propranolol injected into the dorsal midbrain central grey.» *Psychopharmacology 2: 26-32*, 1988.

Avcu P., Jiao X., Myers C.E., Beck K.D., Pang K.C.H., Servatius R.J. «Avoidance as expectancy in rats: sex and strain differences in acquisition .» *Front. Behav. Neurosci.*, 2014.

Babbini M., Marvin Davis W. «Active avoidance in hamsters.» *Psychonomic science*, 1967: 149-150.

Bae, E.J., Chen, B.H., Shin, B.N., Cho, J.H., Kim, I.H., Park, J.H., Lee, J.C., Tae, H.J., Choi, S.Y., Kim, J.D., Lee, Y.L., Won, M.H., Ahn, J.H. «Comparison of immunoreactivities of calbindin-Dé_k, calretinin and parvalbumin in the striatum between young, adult and aged mice, rats and gerbils.» *Neurochem. Res.*, 2015.

Bailey, D.J., Kim, J.J., Sun, W., Thompson, R.F., Helmstetter, F.J. « Acquisition of fear conditioning in rats requires the synthesis of mRNA in the amygdala.» *Behav. Neurosci. 113:276–282*, 1999.

Balleine, B.W., O'Doherty, J.P. «BalleinHuman and rodent homologies in action control: corticostriatal determinants of goal-directed and habitual action.» *Balleine, B. W., and O'Doherty, J. P. (2010). Human and rodent homologies in actioNeuropsychopharmacology 35, 48–69*, 2010.

Bandler (a), R., Carrive, P. «Integrated defence reaction elicited by excitatory amino acid microinjection in the midbrain periaqueductal grey region of the unrestrained cat.» *Brain Res. 439, 95-106*, 1988.

Bandler (b), R., Depaulis, A. «Elicitation of intraspecific defence reactions in the rat from midbrain periaqueductal grey by microinjection of kainic acid, without neurotoxic effects.» *Neurosci. Lett. 88, 291-296*, 1988.

Bandler, R., Depauli, A. *Midbrain periaqueductal gray control of defensive behavior in the cat and the rat. In: The Midbrain Periaqueductal Gray Matter: Functional, Anatomical and Neurochemical Organization, pp. 175-198.* New York: Eds A. Depaulis and R. Bandler. Plenum Press, 1991.

Bandler, R., Depaulis, A. *Midbrain periaqueductal gray control of defensive behavior in the cat and rat.* New York: The midbrain periaqueductal gray matter: functional, anatomical and neurochemical organization, Plenum Press, pp. 175-198, 1991.

Bandler, R., Keay, K.A. «Columnar organization in the midbrain periaqueductal gray and the integration of emotional expression .» *Progress in brain research 107: 285-300*, 1996.

Bandler, R., Prineas, S., McCulloch, T. «Further localization of midbrai:a neurones mediating the defence reaction in the cat by microinjections of excitatory amino acids.» *Neurosci. Lett. 56, 311-316*, 1985.

Bandler, R., Shipley, M.T. «Columnar organization in the midbrain periaqueductal gray: modules for emotional expression? .» *Trends in Neurosciences, 17: 379-389*, 1994.

Barak, S. et al. «Disruption of alcohol-related memories by mTORC1 inhibition prevents relapse.» *Nature Neurosci. 16*, 2013: 1111–1117.

Barbaresi, P., Manfrini, E. «Glutamate decarboxylase-immunoreactive neurons and terminals in the periaqueductal gray of the rat.» *Neuroscience 27*, 1988: 183-191.

Bastos, A.F., Vieira, A.S., Oliveira, J.M., Pereira, M.G., Figueira, I., Erthal, F.S., Volchan, E. «Stop or move: Defensive strategies in humans .» *Behavioural Brain Research* , 2016: 252-262.

Baum, M. «Extinction of avoidance behavior: Comparaison of various flooding procedures in rats.» *Bulletin of the psychonomic society*, 1973: 22-24.

Beart, P.M., Summers, R.J., Stephenson, J.A., Cook, C.J., Christie, M.J. «Excitatory amino acid projections to the periaqueductal gray in the rat: a retrograde transport study utilizing D[3H]aspartate and [3H]GABA.» *Neuroscience 34(1): 163-76*, 1990.

Beck, C.H., Fibiger, H.C. «Conditioned fear-induced changes in behavior and in the expression of the immediate early gene c-fos: with and without diazepam pretreatment.» *The Journal of neuroscience : the official journal of the Society for Neuroscience 15:709-720*, 1995.

Beck, K.D., Jiao, X., Smith, I.M., Myers, C.E., Pang, K.C.H., Servatius, R.J. «ITI-signals and prelimbic cortex facilitate avoidance acquisition and reduce avoidance latencies, respectively, in male WKY rats.» *Frontiers in Behavioral Neuroscience* , 2014.

Behbehani, M.M. «Functional characteristics of the midbrain periaqueductal gray .» *Progress in Neurobiology Vol. 46* , 1995: 575-605.

Behbehani, M.M., Jiang, M.R., Chandler, S.D., Ennis,M. «The effect of GABA and its antagonists on midbrain periaqueductal gray neurons in the rat .» *Pain 40, 195-204*, 1990.

Beitz, A.J., Shepard, R.D. «The midbrain periaqueductal gray in the rat. II. A Golgi analysis .» *The Journal of comparactive neurology 237: 460-475*, 1985.

Beitz, A.J., Williams, F.G. *Localization of putative amino acid transmitters in the PAG and their relationship to the PAG-Raphe Magnus pathway.* New York: Edited by A. Depaulis and R. Bandler, Plenum Press , 1991.

Bekhterev, V. *La Psychologie Objective.* Paris: Alcan, 1913.

Benarroch, E.E. «Periaqueductal gray : An interface for behavioral control.» *Neurology 78-210*, 2012.

Bissière, S., Plachta, N., Hoyer, D., McAllister, K. H., Olpe, H.-R., Grace, A. A., et al. «The rostral anterior cingulate cortex modulates the efficiency of amygdala-dependent fear learning.» *Biol. Psychiatry 63, 821–831*, 2008.

Bittencourt, A.S., Carobrez, A.P., Zamprogno, L.P.,Tufik, S., Schenberg, L.C. «Organization of single components of defensive behaviors within distinct columns of periaqueductal gray matter of the rat: role of N-METHYL-d-aspartic acid glutamate receptors.» *Neuroscience* , 2004: 71-89.

Blair, H.T., Schafe, G.E., Bauer, E.P., Rodrigues, S.M., LeDoux, J.E. «Synaptic plasticity in the lateral amygdala: a cellular hypothesis of fear conditioning.» *Learning and Memory 8:229–242* , 2001.

Blanchard, D.C. «Translating dynamic defense patterns from rodents to people .» *Neuroscience and biobehavioral review* , 2017: 22-28.

Blanchard, D.C. «Translating dynamic defense patterns from rodents to people .» *Neuroscience and behavioral reviews* , 2017: 22-28.

Blanchard, D.C., Blanchard, R.J. «Innate and conditioned reactions to threat in rats with amygdaloid lesions.» *J. Comp. Physiol. Psychol. 81, 281–290*, 1972.

Blanchard, D.C., Griebel, G., Blanchard, R.J. «Conditioning and residual emotionality effects of predator stimuli: Some reflections on stress and emotions.» *Prog Neuropsychopharmacol Biol Psychiatry 27:1177-1185*, 2003.

Blanchard, D.C., Griebel, G., Blanchard, R.J. «The mouse defense test battery: pharmacological and behavioral assays for anxiety and panic.» *European Journal of Pharmacology* , 2003: 97-116.

Blanchard, D.C., Griebel, G., Pobbe, R., Blanchard, R.J. «Risk assessment as an evolved threat detection and analysis process .» *Neuroscience and behavioral reviews* , 2010.

Blanchard, R.J., Yudko, E.B., Rodgers, R.J., Blanchard, D.C. «Defense system psychopharmacology: an ethological approach to the pharmacology of fear and anxiety.» *Behav. Brain Res. 58:155-65* , 1993.

Blanco, E., Castilla-Ortega, E., Miranda, R., Begega, A., Aguirre, J.A., Arias, J.L., et al. «Effects of medial prefrontal cortex lesions on anxiety-like behaviour in restrained and non-restrainted rats.» *Behavioural Brain Research 201(2):338–42*, 2009.

Blancoa, E., Castilla-Ortegaa, E., Mirandab, R., Begegac, A., Aguirred, J.A. «Effects of medial prefrontal cortex lesions on anxiety-like behaviour in restrained and non-restrained rats.» *Behavioural Brain Research 201* , 2009: 338–342.

Bloom F.E., Bjorkland A., Hokfelt T. *The human basal forebrain. Part II. .* Amsterdam: Elsevier; Handbook of Chemical Neuroanatomy 57–226, 1999.

Boeke, E.A., Moscarello, J.M., LeDoux, J.E., Phelps, E.A., Hartley, C.A. «Active avoidance: neural mechanisms and attenuation of pavlovian conditioned responding.» *J. Neurosci. 37(18): 4808-4818*, 2017.

Bolam, J.P., Hanley, J.J., Booth, P.A., Bevan, M.D. «Synaptic organisation of the basal ganglia.» *J. Anat. 196(Pt 4), 527–542*, 2000.

Bolles, R.C. «Avoidance and escape learning: simultaneous acquisition of different responses.» *J. Comp. Physiol. Psychol. 68(3): 355-8*, 1969.

Bolles, R.C. «Species-specific defense reactions and avoidance learning.» *Psychol Rev 77: 32-48*, 1970.

Bonini, J.S., Cammarota, M., Kerr, D.S., Bevilaqua, L.R.M., Izquierdo, I. «Inhibition of PKC in basolateral amygdala and posterior parietal cortex impairs consolidation of inhibitory avoidance memory.» *Pharmacology, Biochemistry and Behavior 80: 63–67*, 2005.

Borellia, K.G., Ferreira-Nettoa, C. «Fos-like immunoreactivity in the brain associated with freezing or escape induced by inhibition of either glutamic acid decarboxylase or GABAA receptors in the dorsal periaqueductal gray .» *Brain Research 1051*, 2005: 100-111.

Bovin, M.J., Jager-Hyman, S., Gold, S.D., Marx, S.D., Sloan, D.M. «Tonic immobility mediates the influence of periotraumatic fear and perceived inescapability on posttraumatic stress symptoms severity among sexual assault survivors.» *J.Trauma Stress* , 2008: 402-409.

Brandão, M.L., de Aguiar, J.C., Graeff, F.G. «GABA mediation of the anti-aversive action of minor tranquilizers.» *Pharmacol. Biochem. Behav. 16(3): 397-402*, 1982.

Bravo-Rivera C., Roman-Ortiz C., Montesinon-Cartagena M., Quirk G.J. «Persistent active avoidance correlates with activity in prelimbic cortex and ventral striatum.» *Front Behav Neurosci*, 2015.

Bravo-Rivera*, C., Diehl*, M.M.,Roman-Ortiz*, C., Rodriguez-Romaguera*,J., Rosas-Vidal*, L.E.,Bravo-Rivera*, H., Quiñones-Laracuente*,K., Do-Monte*, F.H. «Long-range GABAergic neurons in the prefrontal cortex modulate behavior.» *J. Neurophysiol. 114: 1357–1359*, 2015.

Bravo-Rivera, C., Roman-Ortiz, C., Brignoni-Perez, E., Sotres-Bayon, F., Quirk, G.J. «Neural structures mediating expression and extinction of plateform-mediated avoidance.» *J. Neurosci. 34, 9736-9742*, 2014.

Brener, J., Goesling, W.J. «Avoidance conditioning of activity and immobility in rats.» *J. Comp. Physiol. Psychol. 70(2): 276-80*, 1970.

Brennan, J.F., Powell, E.A., Vicedomini, J.P. «Differential effects of dorsomedial prefrotal lesions on active and passive avoidance in young and adult rats .» *Acta. Neurobiol. Exp. 37: 151-177*, 1977.

Brennan, J.F., Wisniewska, C. «The efficacy of response prevention on avoidance behavior in young and adult rats with prefrontal and cortical injuries.» *Behavioural Brain Research, 4*, 1982: 117-131.

Brodmann, K. «Vergleichende Lokalisationslehre der Groβhirnrinde in ihren Prinzipien dargestellt auf Grund des Zellenbaues .» *Barth*, 1909.

Brog, J.S., Salyapongse, A., Deutch, A.Y., Zahm, D.S. «The patterns of afferent innervation of the core and shell in the “accumbens” part of the rat ventral striatum: immunohistochemical detection of retrogradely transported fluoro-gold.» *J. Comp. Neurol. 338, 255–278*, 1993.

Buffalari, D.M., See, R.E. «Amygdala mechanisms of Pavlovian psychostimulant conditioning and relapse.» *Curr. Top. Behav. Neurosci. 3, 73–99* , 2010.

Burgos-Robles, A., Kimchi, E.Y., Izadmehr, E.M., Porzenheim, M.J., Ramos-Guasp, W.A., Nieh, E.H., Felix-Ortiz, A.C., Namburi, P., Leppla, C.A., Presbrey, K.N., Anandalingam, K.K., Pagan-Rivera, P.A., Anahtar, M., Beyeler, A., Tye, K.M. «Amygdala inputs to prefrontal cortex guide behavior amid conflicting cues of reward and punishment.» *Nature Neuroscience* , 2017.

Burgos-Robles, A., Vidal-Gonzalez, I., Quirk, G.J. «Sustained conditioned responses in prelimbic prefrontal neurons are correlated with fear expression and extinction failure.» *J Neurosci, 29*, 2009: 8474-8482.

Burgos-Robles, A., Vidal-Gonzalez, I., Santini, E., Quirk, G.J. «Consolidation of fear extinction requires NMDA receptor-dependent bursting in the ventromedial prefrontal cortex.» *Neuron, 53* , 2007: 871-880.

Burns, S.M., Wyss, J.M. «The involvement of the anterior cingulate cortex in blood pressure control.» *Brain Res 340:71–77*, 1985.

Burton, M. «Fear behavior and passive avoidance deficits in mice with amygdala lesions.» *Physiology and behavior*, 1973: 717-720.

Buzsáki, G., Draguhn, A. «Neuronal oscillations in cortical networks.» *Science 304, 1926–1929* , 2004.

Cameron, A.A., Khan, I.A., Westlund, K.N., Cliffer, K.D., Willis, W.D. «The efferent projections of the periaqueductal gray in the rat: A phaseolus vulgaris-LeucoAgglutinin study. I. Ascending projections.» *The journal of comparative neurology 351:568-584*, 1995.

Cameron, A.A., Khan, I.A., Westlund, K.N., Willis, W.D. «The efferent projections of the periaqueductal gray in the rat: A phaseolus vulgaris-leucoagglutinin study. II. Descending projections.» *The journal of comparative neurology 351: 585-601*, 1995.

Cammarota, M., Bevilaqua, L.R., Rossato, J.I., Ramirez, M., Medina, J.H., Izquierdo, I. «Relationship between short- and long-term memory and short and long-term extinction.» *Neurobiol. Learn. Mem. 84:25–32*, 2005.

Campeau, S., Davis, M. «Involvement of subcortical and cortical afferents to the lateral nucleus of the amygdala in fear conditioning measured with fear-potentiated startle in rats trained concurrently with auditory and visual conditioned stimuli.» *The Journal of neuroscience : the official journal of the Society for Neuroscience 15:2312-2327*, 1995.

Canteras, N.S., Got, M. «Fos-like immunoreactivity in the periaqueductal gray of rats exposed to a natural predator.» *NeuroReport 10:413–418*, 1999.

Canteras, N.S., Simerly, R.B., Swanson, L.W. «Organization of projections from the ventromedial nucleus the hypothalamus: a Phaseolus vulgaris-leucoagglutinin study in the rat.» *The Journal of comparative neurology 348: 41-79*, 1994.

Canteras, N.S., Swanson, L.W. «Projections of the ventral subiculum to the amygdala, septum, and hypothalamus: a PHAL anterograde tract-tracing study in the rat.» *J. Comp. Neurol. 324: 180–194* , 1992.

Cao, C., Wang, L., Wang, R., Quing, Y., Zhang, J. «TPH2 genotype is associated with PTSD's avoidance symptoms in Chinese female earthquake survivors .» *Psychiatric Genetics* , 2014: 257-261.

Carlén, M. «What constitutes the prefrontal cortex .» *Science 358, 478–482* , 2017.

Carrive, P. «The periaqueductal gray and defensive behavior: functional representation and neuronal organization.» *Behav. Brain Res. 58, 27–47*, 1993.

Carrive, P. «The periaqueductal gray and defensive behavior: functional representation and neuronal organization.» *Behav. Brain Res. 58, 27–47*, 1993.

Carrive, P., Bandler, R. «Viscerotopic organization of neurons subserving hypotensive reactions within the midbrain periaqueductal grey: a correlative functional and anatomical study.» *Brain research 541: 206-215*, 1991.

Carrive, P., Morgan, M.M. *In book: The Human Nervous System. Chapter: Periaqueductal Gray.* 2012.

Cassell, M.D., Wright, D.J. «Topography of projections from the medial prefrontal cortex to the amygdala in the rat.» *Brain Res. Bull. 17(3): 321-33*, 1986.

Castagné, V., Moser, P., Roux, S., Porsolt, R.D. «Rodent models of depression: forced swim and tail suspension behavioral despair tests in rats and mice.» *Curr. Protoc. Neurosci.* , 2011.

Castilho, V.M., Brandao, M.L. «Conditioned antinociception and freezing using electrical stimulation of the dorsal periaqueductal gray or inferior colliculus as unconditioned stimulus are differentially regulated by 5-HT2A receptors in rats.» *Psychopharmacology 155: 154–62*, 2001.

Castilho, V.M., Macedo, C.E., Brandao, M.L. «Role of benzodiazepine and serotonergic mechanisms in conditioned freezing and antinociception using electrical stimulation of the dorsal periaqueductal gray as unconditioned stimulus in rats. .» *Psychopharmacology 165: 77–85*, 2002.

Cenquizca, L.A., Swanson, L.W. «Spatial organization of direct hippocampal field CA1 axonal projections to the rest of the cerebral cortex.» *Brain research reviews 56:1-26*, 2007.

Chandler, S.C., Liu, H., Murphy, A.Z., Shipley, M.T., Behbehani, M.M. «Columnar organization in PAG: Physiological evidence for inter-columnar interactions.» *Soc. Neurosci. Abstr. 19, 1408*, 1993.

Chang, C.H., Maren, S. «Medial prefrontal cortex activation facilitates re-extinction of fear in rats.» *Learn Mem 18: 221-225*, 2011.

Chang, C.H., Maren, S. «Strain difference in the effect of infralimbic cortex lesions on fear extinction in rats.» *Behav. Neurosci. 124(3): 391-7*, 2010.

Chaudhri, N., Woods, C.A., Sahuque, L.L., Gill, T.M., Janak, P.H. «Unilateral inactivation of the basolateral amygdala attenuates context-induced renewal of Pavlovian-conditioned alcohol-seeking.» *Eur. J. Neurosci. 38, 2751–2761*, 2013.

Chiou, L.C., Chou, H.H. «Characterization of synaptic transmission in the ventrolateral periaqueductal gray of rat brain slices.» *Neuroscience 100(4): 829-34*, 2000.

Choi, J.S., Cain, C.K., LeDoux, J.E. «The role of amygdala nuclei in the expression of auditory signaled two-way active avoidance in rats.» *Learn. Mem. 17, 139–147*, 2010.

Choi, J.S., Kim., J.J. «Amygdala regulates risk of predation in rats foraging in a dynamic fear environment .» *PNAS*, 2010.

Chourbaji, S., Zacher, C., Sanchis-Segura, C., Dormann, C., Vollmayr, B., Gass, P. «Learned helplessness: Validity and reliability of depressive-like states in mice.» *Brain Research Protocols*, 2005: Volume 16, Issues 1–3, Pages 70-78.

Ciabatti, E., González-Rueda, A., Mariotti, L., Morgese, F., Tripodi, M. «Life-long genetic and functional access to neural circuits using self-inactivating rabies virus.» *Cell*, 2017.

Ciocchi, S., Herry, C., Grenier, F., Wolff, S.B.E., Letzkus, J.J., Vlachos, I., Ehrlich, I., Sprenfel, R., Deisseroth, K., Stadler, M.B., Muller, C., Luthi, A. «Encoding of conditioned fear in central amygdala inhibitory circuits.» *Nature 468, 277–284*, 2010.

Clarke, R.J. «Flight behaviour elicited by electrical stimulation of the hypothalamus and midbrain in rats: escape and avoidance properties.» *Master of Science thesis, University of british Columbia, Vancouver, Canada*, 1972.

Coimbra, N.C., Paschoalin-Maurin, T., Bassi, G.S., Kanashiro, A., Biagioni, A.F., Felippotti, T.T., Elias-Filho, D.E., Mendes-Gomes, J., Cysne-Coimbra, J.P., Almada, R.C., Loba, B. «Critical neuropsychobiological analysis of panic attackand anticipatory anxiety-like behaviors in rodents confronted with snakes in polygonal arenas and complex labyrinths: a comparison to the elevated plus- and T-maze behavioral tests.» *Revista Brasileira de Psiquiatria 39:72–83* , 2017.

Collins, K.A., Mendelsohn, A., Cain, C.K., Schiller, D. «Taking action in the face of threat: neural synchronization predicts adaptive coping.» *J. Neurosci. 34(44): 14733-8*, 2014.

Commons, K.G., Aicher, S.A., Kow, L.M., Pfaff, D.W. «Presynaptic and postsynaptic relations of μ-opioid receptors to γ-aminobutyric acid-immunoreactive and medullary projecting periaqueductal gray neurons.» *The Journal of Comparative Neurology, vol. 419, no. 4*, 2000: 532–542.

Comoli, E., Ribeiro-Barbosa, E.R., Canteras, N.S. «Predatory hunting and exposure to a live predator induce opposite patterns of Fos immunoreactivity in the PAG.» *Behavioural brain research 138:17-28*, 2003.

Conde, F., Maire-Lepoivre, E., Audinat, E., Crepel, F. «Afferent connections of the medial frontal cortex of the rat: II. Cortical and subcortical afferents.» *J Comp Neurol, 352* , 1995: 567-593.

Conti, F., Barbaresi, P., Fabri, M. «Cytochrome oxidase histochemistry reveals regional subdivisions in the rat periaqueductal gray matter.» *Neuroscience, 24*, 1988: 629-633.

Cooper, W.E. «When and how does starting distance affect flight initiation distance .» *Canadian journal of zoology 83(8)*, 2005.

Corbit, L.H., Muir, J.L., Balleine, B.W. «The role of the nucleus accumbens in instrumental conditioning: evidence of a functional dissociation between accumbens core and shell.» *J. Neurosci. 21: 3251–3260*, 2001.

Corcoran, K.A., Quirk, G.J. «Activity in prelimbic cortex is necessary for the expression of learned, but not innate, fears.» *J. Neurosci., 27* , 2007: 840-844.

Courtin, J., Chaudun, F., Rozeske, R.R., Karalis, N., Gonzalez-Campo, C., Wurtz, H., Abdi, A., Baufreton, J., Bienvenu, T.C., Herry, C. «Prefrontal parvalbumin interneurons shape neuronal activity to drive fear expression.» *Nature*, 2014: 92-96.

Cousens, G., Otto, T. «Both pre- and posttraining excitotoxic lesions of the basolateral amygdala abolish the expression of olfactory and contextual fear conditioning.» *Behavioral neuroscience 112:1092-1103*, 1998.

Dalley, J.W., Cardinal, R.N., Robbins, T.W. «Prefrontal executive and cognitive functions in rodents: neural and neurochemical substrates.» *Neurosci Biobehav Rev 28:771–784*, 2004.

Darwin, C. *On the origin of species by means of natural selection, or the preservation of favourade races in the struggle for life.* 1859.

—. *The expression of the emotions in man and animals .* London, 1872.

Davila, J.C., Olmos, L., Legaz, I., Medina, L., Guirado, S., Real, M.A. «Dynamic patterns of colocalization of calbindin, parvalbumin and GABA in subpopulations of mouse basolateral amygdalar cells during development.» *J. Chem. Neuroanat. 35, 67-76*, 2008.

Davis, M., Rainnie, D., Cassell, M. «Neurotransmission in the rat amygdala related to fear and anxiety.» *Trends in neurosciences 17: 208-214*, 1994.

Davis, M., Whalen, P.J. «The amygdala: vigilance and emotion.» *Molecular Psychiatry 6, 13–34*, 2001.

De Luca, M.C.Z., Brandao, M.L., Motta, V.A., Landeira-Fernandez, J. «Antinociception induced by stimulation of ventrolateral periaqueductal gray at the freezing threshold is regulated by opioid and 5-HT2A receptors as assessed by the tail-flick and formalin tests.» *Pharmacol. Biochem. Behav. 75:459–66*, 2003.

De Oca, B.M., DeCola, J.P., Maren, S., Fanselow, M.S. «Distinct regions of the periaqueductal gray are involved in the acquisition and expression of defensive responses.» *The Journal of Neuroscience, 18(9): 3426–3432*, 1998.

De Paula Soares, V., Zangrossi Jr.H. «Stimulation of 5-HT1A or 5-HT2A receptors in the ventrolateral periaqueductal causes anxiolytic-, but not panicolytic-like effect in rats.» *Behavioural Brain Research 197*, 2009: 178–185.

Deakin, J.F.W. *Roles of serotonergic systems in escape, avoidance and other behaviours. In Cooper S J (ed.), Theory in Psychopharmacology. Vol. 2. .* New York, pp. 149-193: Academic Press, 1983.

DeFelipe, J., Farinas, I. «The pyramidal neuron of the cerebral cortex: morphological and chemical characteristics of the synaptic inputs.» *Progress in neurobiology 39:563-607*, 1992.

Deisseroth, K. «Optogenetics: 10 years of microbial opsins in neuroscience.» *Nature neuroscience 18:1213-1225*, 2015 .

Dejean, C., Courtin, J., Karalis, N., Chaudun, F., Wurtz, H., Bienvenu, T.C., Herry, C. «Prefrontal neuronal assemblies temporally control fear behaviour.» *Nature* , 2016.

Delgado, M.R., Jou, R.L., Ledoux, J.E., Phelps, E.A. «Avoiding negative outcomes: tracking the mechanisms of avoidance learning in humans during fear conditioning.» *Front. Behav. Neurosci.*, 2009.

Delgado, M.R., Li, J., Schiller, D., Phelps, E.A. «The role of the striatum in aversive learning and aversive prediction errors.» *Philos. Trans. R. Soc. Lond. B Biol. Sci. 363, 3787-3800*, 2008.

Depaulis, A., Helfer, V., Deransart, C., Marescaux, C. «Anxiogenic-like consequences in animal models of complex partial seizures.» *Neurosci. Biobehav. Rev. 21, 767–774*, 1997.

Di Scala, G., Mana, M.J., Jacobs, W.J., Phillips, A.G. «Evidence of pavlovian conditioned fear following electrical stimulation of the periaqueductal grey in the rat.» *Physiology & Behavior, Vol. 40*, 1987: 55-63.

Dickinson, A. «Actions and habits: the development of behavioural autonomy.» *Phil. Trans. R. Soc. B: Biological Sciences* , 1985: 67-78.

Dickinson, A. «Contemporary animal learning theory.» *Cambridge: Cambridge university press*, 1980.

Diehl, M.M., Bravo-Rivera, C., Rodriguez-Romaguera, J., Pagan-Rivera, P.A., Burgos-Robles, A., Roman-Ortiz, C., Quirk, G.J. «Active avoidance requires inhibitory signaling in the rodent prelimbic prefrontal cortex.» *Elife*, 2018.

Dielenberg, R.A., Hunt, G.E., McGregor I.S. «"When a rat smells a cat": The distribution of fos immunoreactivity in rat brain following exposure to a predatory odor.» *Neuroscience 104: 1085-1097*, 2001.

Dixon, A.K. «Ethological strategies for defence in animals and humans: Their role in some psychiatric disorders.» *British Journal of Medical Psychology 71, 417-445*, 1998.

Dombrowskia, P.A., Maiab, T.V., Boschena, S.L., Bortolanzaa, M., Wendlera, E., Schwarting, R.K.W., Brandãoe, M.L., Winnf, P., Blahag, C.D., Da Cunhaa, C. «Evidence that conditioned avoidance responses are reinforced by positive prediction errors signaled by tonic striatal dopamine.» *Behavioural Brain Research 241* , 2013: 112– 119.

Domjan, M. *Learning theory and behaviour. in Learning and Memory: A Comprehensive Reference.* 2008.

Dong, S., Allen, J.A., Farrell, M., Roth, B.L. «A chemical-genetic approach for precise spatio-temporal control of cellular signaling.» *Mol. BioSyst. 6(8): 1376-1380*, 2010.

Dumont, E.C., Martina, M., Samson, R.D., Drolet, G., Paré, D. «Physiological properties of central amygdala neurons: species differences.» *Eur. J. Neurosci. 15, 544-552*, 2002.

Eckersdorf, B. «Effect of electrical stimulation of the posterior cingulate cortex on acquisition of active avoidance response in cats.» *Department of Animal Physiology, Institute of Physiology and Cytology*, 1905.

Ehrlich, I., Humeau, Y., Grenier, F., Ciocchi, S., Herry, C., Lüthi, A. «Amygdala inhibitory circuits and the control of fear memory.» *Neuron 62, 757–771* , 2009.

Ekman, P., Friesen, W. *Facial Action Coding System: A Technique for the Measurement of Facial Movement.* Palo Alto: Consulting Psychologists Press, 1978.

Ekman, P., Sorenson, E. R., & Friesen, W. V. «Pancultural elements in facial displays of emotion.» *Science, 164(3875), 86-88.*, 1969.

Ellard, C.G., Eller, M.C. «Spatial cognition in the gerbil: computing optimal escape routes from visual threats.» *Anim. Cogn. 12, 333-345*, 2009.

Fadok, J.P., Krabbe, S., Markovic, M., Courtin, J., Xu, C., Massi, L., Botta, P., Bylund, K., Müller, C., Kovacevic, A., Tovote, P., Lüthi, A. «A competitive inhibitory circuit for selection of active and passive fear responses.» *Nature Vol.542*, 2017.

Fadok, J.P., Markovic, M., Tovote, P., Luthi, A. «New perspectives on central amygdala function.» *Current Opinion in Neurobiology 49:141–147*, 2018.

Fanselow, M.S. *The midbrain periaqueductal gray as a coordinator of action in response to fear and anxiety.* New York: Edited by A. Depaulis and R. Bandler, Plenum Press , 1991.

Fanselow, M.S., Kim, J.J. «Acquisition of contextual Pavlovian fear conditioning is blocked by application of an NMDA receptor antagonist D,L-2-amino-5-phosphonovaleric acid to the basolateral amygdala.» *Behav. Neurosci. 108: 210–212*, 1994.

Felix-Ortiz, A.C., Beyeler, A., Seo, C., Leppla, C.A., Wildes, C.P., Tye, K.M. «BLA to vHPC inputs modulate anxiety-related behaviors.» *Neuron 79, 658–664*, 2013.

Felix-Ortiz, A.C., Burgos-Robles, A., Bhagat, N.D., Leppla, C.A., Tye, K.M. «Bidirectional modulation of anxiety-related and social behaviors by amygdala projections to the medial prefrontal cortex.» *Neuroscience 321: 197-209*, 2016.

Fendt, M. «Injections of the NMDA receptor antagonist aminophosphonopentanoic acid into the lateral nucleus of the amygdala block the expression of fear-potentiated startle and freezing.» *J. Neurosci. 21: 4111–4115*, 2001.

Ferreira-Netto, C., Borelli, K.G., Brandao, M.L. «Neural segregation of Fos-protein distribution in the brain following freezing and escape behaviors induced by injections of either glutamate or NMDA into the dorsal periaqueductal gray of rats.» *Brain Research 1031* , 2005: 151–163.

Ferrier, D. «The Functions of the Brain .» *Putamen, ed.2*, 1886.

Ferrya, B., Parrota, S., Marienc, M., Lazarus, C., Casseld, J.C., McGaughea, J.L. «Noradrenergic influences in the basolateralamygdala on inhibitory avoidance memoryare mediated by an action on alpha 2-adrenoceptors.» *Psychoneuroendocrinology 51, 68-79*, 2015.

Fields, H.L., Basbaum, A.I. *Central nervous system mechanisms of pain modulation.* Edinburgh: Churchill Livingstone: In: Wall PD, Melzack R, editors. Textbook of pain. 4th ed. p. 309–27, 2000.

Fillinger, C., Yalcin, I., Barrot, M., Veinante, P. «Efferents of anterior cingulate areas 24a and 24b and midcingulate areas 24a' and 24b' in the mouse.» *Brain Structure and Function 223:1747–1778* , 2018.

Fleming, S.M., Huijgen, J., Dolan, R.J. «Prefrontal contributions to metacognition in perceptual decision making.» *J. Neurosci. 32, 6117–6125*, 2012.

Floyd, N.S., Price, J.L., Ferry, A.T., Keay, K.A., Bandler, R. «Orbitomedial prefrontal cortical projections to distinct longitudinal columns of the periaqueductal gray in the rat.» *J. Comp. Neurol.*, 2000.

Fonberg, E. «Control of emotional behavior through the hypothalamus and amygdaloid complex.» *Ciba Found. Symp. 8, 131–150*, 1972.

Fox, A.S., Oler, J.A., Tromp do, P.M., Fudge, J.L., Kalin, N.H. «Extending the amygdala in theories of threat processing.» *Trends Neurosci.* , 2015.

Fox, A.S., Shackman, A.J. «The central extended amygdala in fear and anxiety: Closing the gap between mechanistic and neuroimaging research.» *Neurosci. Lett.* , 2017.

Fozzard, H. A., Lipkind, G. M. «The tetrodotoxin binding site is within the outer vestibule of the sodium channel.» *Mar. Drugs 8, 219–234*, 2010.

Fragale, J.E.C., Khariv, V., Gregor, D.M., Smith, I.M., Jiao, X., Elkabes, S. «Dysfunction in amygdala–prefrontal plasticity and extinction-resistant avoidance: A model for anxiety disorder vulnerability.» *Experimental Neurology 275* , 2016: 59–68.

Franklin, T.B., Silva, B.A., Perova, Z., Marrone, L., Masferrer, M.E., Zhan, Y., Kaplan, A., Greetham, L., Verrechia, V., Halman, A., Pagella, S., Vyssotski, A.L., Illarionova, A., Grinevich, V., Branco, T., Gross, C.T. «Prefrontal cortical contral of a brainstem social behavior circuit.» *Nature Neuroscience*, 2017.

Freedman, D.G. «Smiling in blind infants and the issue of innate vs. acquired. .» *Journal of Child Psychology and Psychiatry, 5(1), 171-184*, 1964.

Friedman, D.P., Aggleton, J.P., Saunders, R.C. «Comparison of hippocampal, amygdala, and perirhinal projections to the nucleus accumbens: Combined anterograde and retrograde tracing study in the Macaque brain.» *J. Comp. Neurol. 450: 345–65*, 2002.

Fritts, M.E., Asbury, E.T., Horton, J.E., Isaac, W.L. «Medial prefrontal lesion deficits involving or sparing the prelimbic area in the rat.» *Physiology and behavior*, 1998: 373-380.

Frysztak, R. J., Neafsey, E. J. « The effect of medial frontal cortex lesions on respiration, “freezing,” and ultrasonic vocalizations during conditioned emotional responses in rats.» *Cereb. Cortex 1, 418–425*, 1991.

Fudge, J.L., Haber, S.N. «Defining the caudal ventral striatum in primates: cellular and histochemical features.» *J. Neurosci.*, 2002.

Fudge, J.L., Kunishio, K., Walsh, C., Richard, D., Haber, S.N. «Amygdaloid projections to ventromedial striatal subterritories in the primate.» *Neuroscience 110: 257–75*, 2002.

Gabbott, P.L., Warner, T.A., Jays, P.R., Salway, P., Busby, S.J. «Prefrontal cortex in the rat: projections to subcortical autonomic, motor, and limbic centers.» *J. Comp. Neurol. 492, 145–177* , 2005.

Gabriel, M., Kubota, Y., Sparenborg, S., Straube, K., Vogt, B.A. «Effects of cingulate cortical lesions on avoidance learning and training-induced unit activity in rabbits.» *Exp. Brain Res. 86: 585 600*, 1991.

Galatzer-Levy, I.R., Moscarello, J., Blessing, E.M., Klein, J., Cain, C.K., LeDoux, J.E. «Heterogeneity in signaled active avoidance learning: substantive and methological relevance of diversity in instrumental defensive responses to threat cues.» *Front. Syst. Neurosci.*, 2014.

Galindo, L. E., Garín-Aguilar, M. E., Medina, A. C., Serafín, N., Quirarte, G. L., Prado-Alcalá, R. A. «Acquisition and retention of enhanced active avoidance are unaffected by interference with serotonergic activity.» *Behav. Brain Res. 195, 153–158*, 2008.

Garcia, R.,Chang, C.H., Maren, S. «Electrolytic lesions of the medial prefrontal cortex do not interfere with long-term memory of extinction of conditioned fear.» *Learn Mem. 13(1): 14–17*, 2006.

García-Cabezas, M.Á., Barbas, H. «Anterior Cingulate Pathways May Affect Emotions Through Orbitofrontal Cortex .» *Cerebral Cortex, Volume 27, Issue 10*, 2017: 4891-4910.

Garcia-Junco-Clemente, P., Ikrar, T., Tring, E., Xu, X., Ringach, D.L.,Trachtenberg, J.T. « An inhibitory pull-push circuit in frontal cortex.» *Nat. Neurosci.* , 2017: 389-392.

Garcia-Lopez, M., Abellan, A., Legaz, I., Rubenstein, J.L., Puelles, L., Medina, L. «Histogenetic compartments of the mouse centromedial and extended amygdala based on gene expression patterns during development.» *J. Comp. Neurol, 506*, 2008: 46-74.

Gauriau, C., Bernard, J.F. «Pain pathways and parabrachial circuits in the rat .» *Exp. Physiol. 87: 251–258*, 2002.

Gean, P.W., Chang, F.C., Huang, C.C., Lin, J.H., Way, L.J. «Long-term enhancement of EPSP and NMDA receptor-mediated synaptic transmission in the amygdala.» *Brain Res. Bull. 31: 7–11*, 1993.

Gebhardt, N., Bar, K.J., Boettger, M.K., Grecksch, G., Keilhoff, G., Reichart, R., Becker, A. «Vagus nerve stimulation ameliorated deficits in one-way active avoidance learning and stimulated hippocampal neurogenesis in bulbectomized rats.» *Brain Stimul 6(1): 78-83*, 2013.

Gentry, R.N., Lee, B., Roesch, M.R. «Phasic dopamine release in the rat nucleus accumbens predicts approach and avoidance performance.» *Nat. Commun. 7, 13154*, 2016.

Gentry, R.N., Roesch, M.R. «Neural activity in ventral medial prefrontal cortex is modulated more before approach than avoidance during reinforced and extinction trial blocks .» *The Journal of Neuroscience 38(19):4584–4597*, 2018.

Geoffrion, S., Goncalves, J., Marchand, A., Boyer, R., Marchand, A., Corbière, M., Guay, S. «Post-traumatic reactions and their predictors among workers who experienced serious violent acts: are there sex differences?» *Ann Work Expo Health*, 2018.

Gewirtz, J.C., Falls, W.A., Davis, M. «Normal conditioned inhibition and extinction of freezing and fear-potentiated startle following electrolytic lesions of medical prefrontal cortex in rats.» *Behav. Neurosci. 111: 712-726*, 1997.

Gillan, C.M., Robbins T.W. «Goal-directed learning and obsessive-compulsive disorder.» *Phil. Trans. R. Soc. B 369:20130475*, 2014.

Gillan, C.M., Zamir, S.M., Urcelay, G.P., Sule, A., Voon, V., Apergis-Schoute, A.M., Fineberg, N.A., Sahakian, B.J., Robbins, T.W. «Enhanced avoidance habits in obsessive-compulsive disorder .» *Biol. Psychiatry*, 2014.

Gladwin, T.E., Hashemi, M.M., Van Ast, V., Roelofs, K. «Ready and waiting: freezing as active action preparation under threat .» *Neuroscience Letters* , 2016.

Goddard, G.V. «Functions of the amygdala.» *Psychol. Bull. 62, 89–109*, 1964.

Gold, P.E., Macri, J., Mcgaugh, J.L. «Retrograde amnesia produced by subseizure amygdala stimulation.» *Behav. Biol., 9: 671-680*, 1973.

Goosens, K.A., Maren, S. «Contextual and auditory fear conditioning are mediated by the lateral, basal, and central amygdaloid nuclei in rats.» *Learn. Mem. 8, 148-155*, 2001.

Goosens, K.A., Maren, S. «Contextual and auditory fear conditioning are mediated by the lateral, basal, and central amygdaloid nuclei in rats.» *Learn Mem. 8(3): 148-155*, 2001.

Grabiel M., Kubota Y., Sparenborg S., Straube K., Vogt B.A. «Effects of cingutale cortical lesions on avoidance learning and training-induced unit activity in rabbits.» *Experimental Brain Research*, 1991: 583-600.

Graeff, F.G. «Neuroanatomy and neurotransmitter regulation of defensive behaviors and related emotions in mammals.» *Braz. J. Med. Biol. Res. 27, 811–829*, 1994.

Graeff, F.G.,Brandão, M.L., Audi, E.A., Schütz, M.T.B. «Modulation of the brain aversive system by GABAergic and serotonergic mechanisms.» *Behavioural Brain Research*, 1986: 65-72.

Gray, T.S., Magnuson, D.J. «Neuropeptide neuronal efferents from the bed nucleus of the stria terminalis and central amygdaloid nucleus to the dorsal vagal complex in the rat.» *J. Comp. Neurol. 262, 365–374*, 1987.

Gray, T.S., Magnuson, D.J. «Peptide immunoreactive neurons in the amygdala and the bed nucleus of the stria terminalis project to the midbrain central gray in the rat.» *Peptides 13(3): 451-60*, 1992.

Graybiel, A.M. «The basal ganglia.» *Trends Neurosci. 18(2): 60–2*, 1995.

Greenberg, M.E., Ziff, E.B. «Stimulation of 3T3 cells induces transcription of the c-fos proto-oncogene.» *Nature, 311*, 1984: 433-438.

Griffiths, J.L., Lovick, T.A. «Co-localization of 5-HT2A-receptor- and GABA-immunoreactivity in neurones in the periaqueductal grey matter of the rat.» *Neuroscience Letters 326* , 2002: 151–154.

Groenewegen, H.J. «Organization of the afferent connections of the mediodorsal thalamic nucleus in the rat, related to the mediodorsal-prefrontal topography.» *Neuroscience 24:379-431*, 1988.

Grossman, S.P., Grossman, L., Walsh, L. «Functional organization of the rat amygdala with respect to avoidance behavior.» *J. Comp. Physiol. Psychol. 88: 829-850*, 1975.

Gruber, A.J., McDonald, R.J. «Context, emotion, and the strategic pursuit of goals: interactions among multiple brain systems controlling motivated behavior.» *Front. Behav. Neurosci.*, 2012.

Gruber-Dujardin, E.,. *Role of the periaqueductal gray in expressing vocalization.* Amsterdam: In: Brudzynski, S.M. (Ed.), The Handbook of Mammalian Vocalization: an Integrative Neuroscience Approach. Elsevier, pp.313–327, 2010.

Gründemann, J., Lüthi, A. «Ensemble coding in amygdala circuits for associative learning.» *Curr. Opin. Neurobiol.*, 2015.

Guandalini, P. «The corticocortical projections of the physiologically defined eye field in the rat medial frontal cortex.» *Brain Res. Bull. 47:377–385*, 1998.

Guldin, W.O., Pritzel, H.J., Markowitsch, H.J. «Prefrontal cortex of the mouse defined as cortical projection area of the thalamic mediodorsal nucleus.» *Brain Behav. Evol. 19, 93–107*, 1981.

Haber S.N., Lynd E., Klein C., Groenewegen H.J. «Topographic organization of the ventral striatal efferent projections in the rhesus monkey: An anterograde tracing study.» *J. Comp. Neurol. 293: 282–98*, 1990.

Haber, S.N. «Corticostriatal circuitry .» *Dialogues Clin. Neurosci.*, 2016.

—. *Neurobiology of Sensation and Reward. Chapter 11: Neuroanatomy of Reward: A View from the Ventral Striatum Gottfried J.A.* Boca Raton (FL): CRC Press-Taylor & Francis, 2011.

Haber, S.N., Fudge, J.L., McFarland, N.R. «Striatonigrostriatal pathways in primates form an ascending spiral from the shell to the dorsolateral striatum.» *J. Neurosci. 20, 2369–2382*, 2000.

Halabisky, B., Shen, F., Huguenard, J.R., Prince, D.A. «Electrophysiological classification of somatostatin-positive interneurons in mouse sensorimotor cortex.» *J. Neurophysiol. 96:834–845*, 2006.

Halabisky, B., Shen, F., Huguenard, J.R., Prince, D.A. «Electrophysiological classification of somatostatin-positive interneurons in mouse sensorimotor cortex.» *J. Neurophysiol. 96:834–845*, 2006.

Hall, E. «The amygdala of the cat: a Golgi study.» *Z. Zellforsch Mikrosk Anat. 134: 439-458*, 1972.

Halladay, L.R., Blair, H.T. «Distinct ensembles of medial prefrontal cortex neurons are activated by threatening stimuli that elicit excitation vs. inhibition of movement.» *J. Neurophysiol.* , 2015.

Hamilton, B.L. «Cytoarchitectural subdivisions of the periaqueductal gray matter in the cat .» *The Journal of comparative neurology 149: 1-27*, 1973.

Hamilton, B.L. «Cytoarchitectural subdivisions of the periaqueductal gray matter in the cat.» *J.Comp.Neurol. 152*, 1980: 45-58.

Han, S., Soleiman, M., Soden, M., Zweifel, L., Palmiter, R.D. «Elucidating an affective pain circuit that creates a threat memory.» *Cell 162: 363-374*, 2015.

Han, W., Tellez, L.A., Rangel, Jr.,M.J., Motta, S.C., Zhang, X., Perez, I.O., Canteras, N.S., Shammah-Lagnado, S.J., van den Pol, A.N., de Araujo, I.E. «Integrated control of predatory hunting by the central nucleus of the amygdala.» *Cell 168, 311–324*, 2017.

Han, W., Tellez, L.A., Rangel, M.J. Jr., Motta, S.C., Zhang, X., Perez, I.O., Canteras, N.S., Shammah-Lagnado, S.J., van den Pol, A.N., de Araujo, I.E. «Integrated control of predatory hunting by the central nucleus of the amygdala .» *Cell*, 2017.

Handwerker, M.J., Gold, P.E., Mcgaugh, J.L. «Impairment of active avoidance learning with post-training amygdala stimulation.» *Brain Research, 75: 324-327*, 1974.

Harris, J.A. «Descending antinociceptive mechanisms in the brainstem: their role in the animal's defensive system .» *J. Physiol. Paris 90:15–25*, 1996.

Harris, K.D., Shepherd, G.M. «The neocortical circuit: themes and variations.» *Nature neuroscience 18:170-181*, 2015.

Hart, G., Harris, J.A., Westbrook, R.F. « Systemic or intra-amygdala injection of a benzodiazepine (midazolam) impairs extinction but spares re-extinction of conditioned fear responses.» *Learn Mem. 16:53-61*, 2009.

Hartley, C.A., Gorun, A., Reddan, M.C., Ramirez, F., Phelps, E.A. «Stressor controlability modulates fear extinction in humans .» *Neurobiology of learning and memory* , 2014: 149-156.

Haubensak, W. et al. «Genetic dissection of an amygdala microcircuit that gates conditioned fear.» *Nature 468, 270–276* , 2010.

Haubensak, W., Kunwar, P.S., Cai, H., Ciocchi, S., Wall, N.R., Ponnusamy, R., Biag, J., Dong, H., Deisseroth, K., Callawau, E.M., Fanselow, M.S., Luthi, A., Anderson, D.J. «Genetic dissection of an amygdala microcircuit that gates conditioned fear.» *Nature 468, 270–278*, 2010.

Hayashi, T., Umemori, H., Mishina, M., Yamamoto, T. «The AMPA receptor interacts with and signals through the protein tyrosine kinase Lyn.» *Nature* , 1999.

Hebb, D.O. *The organization of behavior.* New York: John Wiley and Sons, 1949.

Hefner, K., Whittle, N., Juhasz, J., Norcross, M., Karlsson, R.M., Saksida, L.M., Bussey, T.J., Singewald, N. Holmes, A. «mpaired fear extinction learning and cortico-amygdala circuit abnormalities in a common genetic mouse strain.» *J. Neurosci., 28* , 2008: 8074-8085.

Heidbreder, C.A., Groenewegen, H.J. «The medial prefrontal cortex in the rat: evidence for a dorso-ventral distinction based upon functional and anatomical characteristics.» *Neurosci Biobehav Rev 27:555–579* , 2003.

Heidbreder, C.A., Groenewegen, H.J. «The medial prefrontal cortex in the rat: evidence for a dorsoventral distinction based upon functional and anatomical characteristics. .» *Neuroscience and biobehavioral reviews 27:555-579*, 2003.

Heinisch, S., Palma, J., Kirby, L.G. «Interactions between chemokine and mu-opioid receptors: anatomical findings and electrophysiological studies in the rat periaqueductal grey.» *Brain Behav. Immun. 25(2): 360-372*, 2011.

Heinricher, M.M., Tavares, I., Leith, J.L., Lumb, B.M. «Descending control of nociception: Specificity, recruitment and plasticity. .» *Brain research reviews 60: 214-225*, 2009.
Helmstetter, F.J., Bellgowan, P.S. «Effects of muscimol applied to the basolateral amygdala on acquisition and expression of contextual fear conditioning in rats.» *Behav. Neurosci. 108: 1005–1009*, 1994.
Herbert, H., Saper, C.B. « Organization of medullary adrenergic and noradrenergic projections to the periaqueductal gray matter in the rat.» *J. Comp. Neurol. 315: 34–52*, 1992.
Herrnstein, R.J. «Method and theory in the study of avoidance .» *Psychological Reviews 76, 49-69*, 1969.
Herry, C., Ciocchi, S., Senn, V., Demmou, L., Muller, C., Luthi, A. «Switching on and off fear by distinct neuronal circuits.» *Nature 454: 600-606*, 2008.
Herry, C., Mons, N. «Resistance to extinction is associated with impaired immediate early gene induction in medial prefrontal cortex and amygdala.» *The European journal of neuroscience 20: 781-790*, 2004.
Herry, C., Trifilieff, P., Micheau, J., Lüthi, A., Mons, N. «Extinction of auditory fear conditioning requires MAPK/ERK activation in the basolateral amygdala.» *Eur. J. Neurosci. 24(1): 261-9*, 2006.
Hikind, N., Maroun, M. «Microinfusion of the D1 receptor antagonist, SCH23390 into the IL but not the BLA impairs consolidation of extinction of auditory fear conditioning.» *Neurobiol Learn Mem, 90*, 2008: 217-222.
Hitchcock, J., Davis, M. «Lesions of the amygdala, but not of the cerebellum or red nucleus, block conditioned fear as measured with the potentiated startle paradigm.» *Behav. Neurosci. 100, 11–22* , 1986.
Hjorztsjö, C.H. *Man's face and mimic language.* 1969.
Holahan, M.R., White, N.M. «Conditioned memory modulation, freezing, and avoidance as measures of amygdala-mediated conditioned fear.» *Neurobiology of Learning and Memory 77, 250–275* , 2002.
Holstege, G., Bandler, R., Saper, C.B. «The emotional motor system.» *Prog. Brain Res. 107: 3–6*, 1996.
Hoover, W.B., Vertes, R.P. « Anatomical analysis of afferent projections to the medial prefrontal cortex in the rat.» *Brain structure & function 212:149-179*, 2007.
Houbaert, X., Zhang, C.L., Gambino, F., Lepleux, M., Deshors, M., Normand, E., Levet, F., Ramos, M., Billuart, P., Chelly, J., Jerzog, E., Humeau, Y. «Target-specific vulnerability of excitatory synapses leads to deficits in associative memory in a model of intellectual disorder.» *J. Neurosci.*, 2013.
Hu, H., Jonas, P. « A supercritical density of Na(+) channels ensures fast signaling in GABAergic interneuron axons.» *Nat. Neurosci. 17:686–693*, 2014.
Huanga, A.C.W., Shyub, B.C., Hsiaoc, S., Chenb, T.C., Hea, A.B.H. «Neural substrates of fear conditioning, extinction, and spontaneous recovery in passive avoidance learning: A c-fos study in rats.» *Behavioural Brain Research 237* , 2013: 23-31.
Huber, D., Veinante, P., Stoop, R. « Vasopressin and oxytocin excite distinct neuronal populations in the central amygdala.» *Science 308: 245-248*, 2005.
Huff, M.L., Emmons, E.B., Narayanan, N.S., LaLumiere, R.T. «Basolateral amygdala projections to ventral hippocampus modulate the consolidation of footshock, but not contextual, learning in rats.» *Learn. Mem. 23: 51-60*, 2016.
Humeau, Y., Herry, C., Kemp, N., Shaban, H., Fourcaudot, E., Bissière, S., Luthi, A. «Dendritic spine heterogeneity determines afferent-specific Hebbian plasticity in the amygdala.» *Neuron*, 2005.
Ivanov, A., Pellegrino, C., Rama, S., Dumalska, I., Salyha, Y., Ben-Ari, Y., Medina, I. «Opposing role of synaptic and extrasynaptic NMDA receptors in regulation of the extracellular signal-regulated kinases (ERK) activity in cultured rat hippocampal neurons.» *J. Physiol., 572* , 2006.
Izquierdo, I., Quillfeldtl, J.A., Zanatta, M.S., Quevedol, J., Schaeffer, E., Schmitz, P.K., Medina, J.H. «Sequential role of hippocampus and amygdala, entorhinal cortex and

parietal cortex in formation and retrieval of memory for inhibitory avoidance in rats.» *European Journal of Neuroscience, Vol. 9*, 1997: 786-793.

J.B., Watson. «Psychology as the behaviorist views it.» *Psychological Review, 20,158-177*, 1913.

Janak, P.H., Tye, K.M. «From circuits to behaviour.» *Nature Vol. 517*, 2015.

Jasnow, A.M., Ressler, K.J., Hammack, S.E., Chhatwal, J.P., Rainnie, D.G. «Distinct subtypes of cholecystokinin (CCK)-containing interneurons of the basolateral amygdala identified using a CCK promoter-specific lentivirus.» *J. Neurophysiol. 101, 1494-1506*, 2009.

Jenck, E., Broekkamp, C.L.E., Van Delft, A.M.L. «Opposite control mediated by central 5HT1A and non-5HT1A (5HT or 5HT1C) receptors on periaqueductal gray aversion.» *Eur. J. Pharmacol. 1:61 219-221*, 1989.

Jensen, J., McIntosh, A.R., Crawley, A.P., Mikulis, D.J., Remington, G., Kapur, S. «Direct activation of the ventral striatum in anticipation of aversive stimuli.» *Neuron 40, 1251-1257*, 2003.

Jhang, J., Lee, H., Kang, M.S., Lee, H.S., Park, H., Han, J.H. «Anterior cingulate cortex and its input to the basolateral amygdala control innate fear response.» *Nat. Commun.*, 2018.

Jiao, X., Beck, K.D., Myers, C.E., Servatius, R.J., Pang, K.C.H. «Altered activity of the medial prefrontal cortex and amygdala during acquisition and extinction of active avoidance task .» *frontiers in Behavioral Neuroscience* , 2015.

Jiao, X., Pang, K.C., Beck, K. D., Minor, T.R., Servatius R.J. «Avoidance perseveration during extinction training in Wistar-Kyoto rats: an interaction of innate vulnerability and stressor intensity.» *Behav. Brain Res. 221, 98-107*, 2011.

Jinks, A. L., McGregor, I. S. «Modulation of anxiety-related behaviours ollowing lesions of the prelimbic or infralimbic cortex in the rat.» *Brain Res. 772, 181–190*, 1997.

Jinks, A.L., McGregor, I.S. «Modulation of anxiety-related behaviours following lesions of the prelimbic or infralimbic cortex in the rat.» *Brain Research 772* , 1997: 181–190.

Johansen, J.P., Hamanaka, H., Monfils, M.H., Behnia, R., Deisseroth, K., Blair, H.T., et al. « Optical activation of lateral amygdala pyramidal cells instructs associative fear learning.» *Proc. Natl. Acad. Sci. 107(28): 12692–12697*, 2010.

Johansen, J.P., Tarpley, J.W., Ledoux, J.E., Blair, H.T. «Neural substrates for expectation-modulated fear learning in the amygdala and periaqueductal gray.» *Nature Neuroscience, 13(8)*, 2010: 979–986.

Jolkkonen, E., Pitkanen, A. «Intrinsic connections of the rat amygdaloid complex: projections originating in the central nucleus.» *J. Comp. Neurol. 395: 53–72*, 1998.

Jones, J.L., Day, J.J., Wheeler, R.A., Carelli, R.M. «The basolateral amygdala differentially regulates conditioned neural responses within the nucleus accumbens core and shell.» *Neuroscience 169(3): 1186-98*, 2010.

Jurgens, U., Pratt, R. «Role of the periaqueductal grey in vocal expression of emotion.» *Brain research 167: 367-378*, 1979.

Kalaf, J., Coutinho, E.S.F., Vilete, L.M.P., Luz, M.P., Berger, W., Mendlowicz, M., Volchan, E., Andreoli, S.B., Quintana, M.I., Mari, J.J., Figueira, I. «Sexual trauma is more strongly associated with tonic immobility than other types of trauma- A population based study.» *Journal of Affective Disorders* , 2017: 71-76.

Kara, N., Karpel, O., Toker, L., Agam, G., Belmaker, R.H., Einat, H. «Chronic oral carbamazepine treatment elicits mood stabilizing effects in mice.» *Acta Neuropsychiatrica, 26* , 2014: pp. 29-34.

Kara, N.Z., Agam, G., Anderson, G.W., Zitron, N., Einat, H. «Lack of effect of chronic ketamine administration on depression-like behavior or frontal cortex autophagy in female and male ICR mice.» *Behav. Brain Res., 26* , 2016: pp. 30712-30714.

Karalis, N., Dejean, C., Chaudun, F., Khoder, S., Rozeske, R.R., Wurtz, H., Bagur, S., Benchenane, K., Sirota, A., Courtin, J., Herry, C. «4-Hz oscillations synchronize prefrontal-amygdala circuits during fear behavior.» *Nat. Neurosci.* , 2016.

Keay, K.A., Bandler, R. «Parallel circuits mediating distinct emotional coping reactions to different types of stress.» *Neurosci Biobehav. Rev. 25: 669–678*, 2001.

Kemppainen, S., Pitkanen, A. «Distribution of parvalbumin, calretinin, and calbindin-D(28k) immunoreactivity in the rat amygdaloid complex and colocalization with gamma-aminobutyric acid.» *J. Comp. Neurol. 426, 441-467*, 2000.

Killcross, S., Robbins, T.W., Everitt, B.J. «Different types of fear-conditioned behaviour mediated by separate nuclei within amygdala.» *Nature 388: 377–380*, 1997.

Kim, E.J., Horovitz, O., Pellman, B.A., Tan, L., M., Li, Q., Richter-Levin, G., Kim, J.J. «Dorsal periaqueductal gray-amygdala pathway conveys both innate and learned fear responses .» *Proceedings of the National Academy of Sciences, USA, 110, 14795-14800*, 2013.

Kim, E.J., Kim, N., Kim, H.T., Choi, J.S. «The prelimbic cortex is critical for context-dependent fear expression.» *Front. Behav. Neurosci. 21;7:73*, 2013.

Kim, W.B., Cho, J.H. «Synaptic Targeting of Double-Projecting Ventral CA1 Hippocampal Neurons to the Medial Prefrontal Cortex and Basal Amygdala.» *J. Neurosci. 37(19): 4868-4882*, 2017.

Kimmel, H.D., Kimmel, E.B., Silver, A.I. «The effect of UCS intensity in classical and avoidance GSR conditioning .» *Conditional reflex: a Pavlovian journal of research and therapy* , 1969.

Kincheski, C.G., Mota-Ortiz, S.R., Pavesi, E., Canteras, N.S., Carobrez, A.P. «The Dorsolateral periaqueductal gray and its role in mediating fear learning to life threatening events.» *PLOS ONE vol. 7*, 2012.

Kirkerud, N.H., Schlegel, U., Galizia, C.G. «Aversive learning of colored lights in walking honeybees .» *Frontiers in behavioral neuroscience* , 2017.

Kiser, R.S.Jr., Lebovitz, R.M. «Monoaminergic mechanisms in aversive brain stimulation.» *Physiol. Behav. 15: 47-53*, 1975.

Klausberger, T., Magill, P.J., Márton, L.F., Roberts, J.D., Cobden, P.M., Buzsáki, G., Somogyi, P. «Brain-state- and cell-type-specific firing of hippocampal interneurons in vivo.» *Nature 421, 844–848* , 2003.

Klausberger, T., Márton, L. F., Baude, A., Roberts, J., Magill, J. S., Somogyi, P. «Spike timing of dendrite-targeting bistratified cells during hippocampal network oscillations in vivo.» *Nature Neurosci. 7, 41–47* , 2004.

Klein, M.O., Cruz Ade, M., Machado, F.C., Picolo, G., Canteras, N.S., Felicio, L.F. «Periaqueductal gray μ and κ opioid receptors determine behavioral selection from maternal to predatory behavior in lactating rats.» *Behav. Brain Res. 274:62-72*, 2014.

Kluver, H., Bucy, P.C. «Psychic blindness and other symptoms following bilateral temporal lobectomy in rhesus monkeys.» *Am. J. Physiol. 119, 352–353*, 1937.

Knapska, E., Maren, S. «Reciprocal patterns of c-Fos expression in the medial prefrontal cortex and amygdala after extinction and renewal of conditioned fear.» *Learn. Mem.* , 2009: 486-493.

Kolb, B. «International Encyclopedia of the Social & Behavioral Sciences.» 811-816. Elsevier, ed. 2, 2015.

Koo, J.W., Han, J.S., Kim, J.J. «Selective neurotoxic lesions of basolateral and central nuclei of the amygdala produce differential effects on fear conditioning.» *J. Neurosci. 24, 7654-7662*, 2004.

Kovács, K.J. «Invited review c-Fos as a transcription factor: a stressful (re)view from a functional map.» *Neurochemistry International*, 1998: Volume 33, Issue 4, Pages 287-297.

Krabbe, S., Gründemann, J., Lüthi, A. «Amygdala inhibitory circuits regulate associative fear conditioning.» *Biol. Psychiatry*, 2018.

Krout, K.E., Loewy, A.D. «Periaqueductal gray matter projections to midline and intralaminar thalamic nuclei of the rat.» *The Journal of comparative neurology 424: 111-141*, 2000.

Kyosseva, S.V. «Mitogen-activated protein kinase signaling.» *International Review of Neurobiology 59*, 2004: 201–220.

Lang, P., Davis, M., & Ohman, A. «Fear and anxiety: animal models and human cognitive psychophysiology.» *Journal of Affective Disorders, 61, 137-159*, 2000.

Lanuza, E., Nader, K., Ledoux, J.E. «Unconditioned stimulus pathways to the amygdala: effects of posterior thalamic and cortical lesions on fear conditioning.» *Neuroscience 125, 305–315*, 2004.

Laurent, V., Westbrook, R.F. «Inactivation of the infralimbic but not the prelimbic cortex impairs consolidation and retrieval of fear extinction.» *Learn Mem, 16* , 2009: 520-529.

Lázaro-Muñoz, G., LeDoux, J.E., Cain, C.K. «Sidman instrumental avoidance initially depends on lateral and basal amygdala and is constrained by central amygdala mediated pavlovian processes.» *Biol. Psychiatry 67(12): 1120–1127*, 2010.

Lázaro-Muñoz, G., LeDoux, J.E., Cain, C.K. «Sidman instrumental avoidance initially depends on lateral and basal amygdala and is constrained by central amygdala-mediated Pavlovian processes.» *Biol. Psychiatry 15;67(12):1120-7*, 2010.

Leaton, R.B. «Potentiated startle: it's relation to freezing and shock intensity in rats .» *J. Exper. Psychol.: An. Behav. Proc., 2, 248-259*, 1985.

Lebow, M.A., Chen, A. «Overshadowed by the amygdala: the bed nucleus of the stria terminalis emerges as key to psychiatric disorders.» *Mol. Psychiatry*, 2016.

Lebron, K., Milad, M.R., Quirk, G.J. «Delayed recall of fear extinction in rats with lesions of ventral medial prefrontal cortex. .» *Learn. Mem. 11: 544-548*, 2004.

LeDoux J.E., Moscarello J., Sears R., Campese V. «The birth, death and resurrection of avoidance: a reconceptualization of a troubled paradigm.» *Molecular Psychiatry 22, 24-36*, 2017.

LeDoux, J. «The amygdala .» *Current Biology Vol. 17(20): R869-74*, 2007.

LeDoux, J.E. «Emotion circuits in the brain .» *Annual review of neurosceince 23:155-158*, 2000.

LeDoux, J.E., Cicchetti, P., Xagoraris, A., Romanski, L.M. «The lateral amygdaloid nucleus: sensory interface of the amygdala in fear conditioning.» *J. Neurosci. 10, 1062–1069*, 1990.

LeDoux, J.E., Farb, C., Ruggiero, D.A. «Topographic organization of neurons in the acoustic thalamus that project to the amygdala.» *J. Neurosci. 10: 1043–1054*, 1990.

LeDoux, J.E., Farb, C., Ruggiero, D.A. «Topographic organization of neurons in the acoustic thalamus that project to the amygdala.» *Journal of Neuroscience Vol. 10, Issue 4*, 1990: 1043-1054.

LeDoux, J.E., Gorman, J.M. «A call to action: overcoming anxiety through active coping.» *Am. J. Psychiatry 158, 1953–1955*, 2001.

LeDoux, J.E., Iwata, J., Cicchetti, P., Reis, D.J. «Different projections of the central amygdaloid nucleus mediate autonomic and behavioral correlates of conditioned fear.» *J. Neurosci. 8: 2517–2529*, 1988.

Lee, A.T., Vogt, D., Rubenstein, J.L., Sohal, V.S. «A class of GABAergic neurons in the prefrontal cortex sends long-range projections to the nucleus accumbens and elicits acute avoidance behavior.» *Journal of Neuroscience 34 (35)* , 2014: 11519-11525.

Lee, H.J., Choi, J.S., Brown, T.H., Kim, J.J. «Amygdalar N-methyl-D-aspartate receptors are critical for the expression of multiple conditioned fear responses.» *J. Neurosci. 21: 4116-4124*, 2001.

Lee, H.J., Kim, J.J. «Amygdalar NMDA receptors are critical for new fear learning in previously fear-conditioned rats.» *J. Neurosci. 18: 8444-8454*, 1998.

Lee, Y.K., Choi, J.S. «Inactivation of the medial prefrontal cortex interferes with the expression but not the acquisition of differential fear conditioning in rats.» *Experimental neurobiology 21: 23-29*, 2012.

Letinic, K., Zoncu, R., Rakic, P. «Origin of GABAergic neurons in the human neocortex.» *Nature 417:645-649*, 2002.

Levita, L., Hoskin, R., Champi, S. «Avoidance of harm and anxiety: a role for the nucleus accumbens.» *Neuroimage, 62* , 2012: 189-198.

Li, G., Shao, C., Chen, Q., Wang, Q., Yang, K. «Accumulated GABA activates presynaptic GABAB receptors and inhibits both excitatory and inhibitory synaptic transmission in rat midbrain periaqueductal gray.» *Neuroreport. 12; 28(6)*, 2017: 313-318.

Li, H., Penzo, M.A., Taniguchi, H., Kopec, C.D., Huang, Z.J., Li, B. «Experience-dependent modification of a central amygdala fear circuit.» *Nature Neurosci. 16, 332–339*, 2013.

Li, Y., Zeng, J., Zhang, J., Yue, C., Zhong, W., Liu, Z., Feng, Q., Luo, M. «Hypothalamic circuits for predation and evasion.» *Neuron*, 2018: 911-924.

Lichtenberg, N.T., Kashtelyan, V., Burton, A.C., Bissonelte, G.B., Roesch, M.R. «Nucleus accumbens core lesions enhance two-way active avoidance .» *Neuroscience 31;258:340-6*, 2014.

Lichtenberg, N.T., Kashtelyan, V., Burton, A.C., Bissonette, G.B., Roesch, M.R. «Nucleus accumbens core lesions enhance two-way active avoidance.» *Neuroscience 258*, 2014: 340–346.

Likhtik, E., Popa, D., Apergis-Schoute, J., Fidacaro, G.A., Pare, D. «Amygdala intercalated neurons are required for expression of fear extinction.» *Nature, 454* , 2008: 642-645.

Lima, A.A., Fiszman, A., Marques-Portella, C., Mendlowicz, M.V., Coutinho, E.S.F., Maia, D.C.B., Berger, W., Rocha-Rego, V., Volchan, E., Mari, J.J., Figueira, I. «The impact of tonic immobility reaction on the prognosis of posttraumatic stress disorder.» *Journal of Psychiatric Research*, 2010: 224–228.

Lin, C., Disterhoft, J., Weiss, C. «Whisker-signaled eyeblink classical conditioning in head-fixed mice.» *J. Vis. Exp.*, 2016.

Lin, C.H., Yeh, S.H., Lu, H.Y., Gean, P.W. «The similarities and diversities of signal pathways leading to consolidation of conditioning and consolidation of extinction of fear memory.» *The Journal of neuroscience : the official journal of the Society for Neuroscience 23:8310-8317*, 2003.

Linnman, C., Moulton, E.A., Barmettler, G., Becerra, L., Borsook, D. «Neuroimaging of the periaqueductal gray: State of the field.» *NeuroImage 60* , 2012: 505–522.

Linnman, C., Rougemont-Bucking, A., Beucke, J.C., Zeffiro, T.A., Milad, M.R. «Unconditioned responses and functional fear networks in human classical conditioning.» *Behav. Brain Res. 221, 237–245*, 2011.

Lipski, J. «Antidromic activation of neurones as an analytic tool in the study of the central nervous system.» *J. Neurosci. Methods, 4 , pp. 1-32*, 1981.

Lovick, T.A. «The periaqueductal gray-rostral medulla connection in the defence reaction: efferent pathways and descending control mechanisms.» *Behavioural brain research 58: 19-25*, 1993.

Lovick, T.A., Parry, D.M., Stezhka, V.V., Lumb, B.M. «Serotonergic transmission in the periaqueductal gray matter in relation to aversive behaviour: morphological evidence for direct modulatory effects on identified output neurons.» *Neuroscience 95, 763–772*, 2000.

Low, A., Weymar, M., Hamm, A.O. «When threat is near, get out of here: dynamics of defensive behavior during freezing and active avoidance .» *Association for psychological science* , 2015: 1706-1716.

Loyd, D.R., Murphy, A.Z. «The Role of the Periaqueductal Gray in theModulation of Pain inMales and Females: Are the Anatomy and Physiology Really that Different?» *Hindawi Publishing Corporation, Neural Plasticity* , 2009.

Lu, J., Jhou, T.C., Saper, C.B. «Identification of wake-active dopaminergic neurons in the ventral periaqueductal gray matter.» *J. Neurosci. 26: 193–202*, 2006.

Lu, K.T., Walker, D.L., Davis, M. «Mitogen-activated protein kinase cascade in the basolateral nucleus of amygdala is involved in extinction of fear-potentiated startle.» *The Journal of neuroscience : the official journal of the Society for Neuroscience 21:RC162*, 2001.

Lumb, B.M. «Hypothalamic and midbrain circuitry that distinguishes between escapable and inescapable pain.» *News Physiol. Sci. 19: 22–26*, 2004.

Lynch, J.W. «Molecular structure and function of the glycine receptor chloride channel.» *Physiological Reviews 84(4): 1051–1095*, 2004.

Ma, Y., Hu, H., Berrebi, A.S., Mathers, P.H., Agmon, A. «Distinct subtypes of somatostatin-containing neocortical interneurons revealed in transgenic mice.» *J. Neurosci. 26:5069–5082*, 2006.

Maaswinkel, H., Gispen, W.H., Spruijt, B.M. «Effects of an electrolytic lesion of the prelimbic area on anxiety-related and cognitive tasks in the rat.» *Behavioural Brain Research 79*, 1996: 51-59.

Maatsch, J.L. «Learning and fixation after a single shock trial.» *J. Comp. Physiol. Psychol. 52: 408-10*, 1959.

Magoun, H.W., Atlas, D., Ingersoll, E.H., Ransom, S.W. «Associated facial, vocal and respiratory components of emotional expression: An experimental study.» *J. Neurol. Psychopath. 17, 241-255*, 1937.

Malin, E. L., McGaugh, J. L. «Differential involvement of the hippocampus, anterior cingulate cortex, and basolateral amygdala in memory for context and footshock.» *Proc. Natl. Acad. Sci. U.S.A. 103, 1959–1963*, 2006.

Manassero, E., Renna, A., Milano, L., Sacchetti, B. «Lateral and basal amygdala account for opposite behavioral responses during the long-term expression of fearful memories.» *Sci. Rep. 8: 518*, 2018.

Mantyh, P.W. « The midbrain periaqueductal gray in the rat, cat, and monkey: a Nissl, Weil, and Golgi analysis.» *The Journal of comparative neurology 204: 349-363*, 1982.

Mantyh, P.W. «Connections of midbrain periaqueductal gray in the monkey: II: descending efferent projections.» *J. Neurophysiol. 49: 582–594* , 1983.

Marchand, J.E., Hagino, N. «Afferents to the periaqueductal gray in the rat. A horseradish peroxidase study.» *Neuroscience, Vol.9*, 1983: 95-106.

Maren, S., Aharonov, G., Stote, D.L., Fanselow, M.S. «N-methyl-D-aspartate receptors in the basolateral amygdala are required for both acquisition and expression of conditional fear in rats.» *Behav. Neurosci. 10: 1365-1374*, 1996.

Markowitsch, H.J., Pritzel, M. «The prefrontal cortex: Projection area of the thalamic mediodorsal nucleus?» *Physiol. Psychol. 7, 1–6* , 1979.

Markram, H., Toledo-Rodriguez, M., Wang, Y., Gupta, A., Silberberg, G., Wu, C. «Interneurons of the neocortical inhibitory system.» *Nature reviews Neuroscience 5:793-807*, 2004.

Martina, M., Royer, S., Pare, D. «Physiological properties of central medial and central lateral amygdala neurons.» *J. Neurophysiol., 82* , 1999: 1843-1854.

Martinez, R.C.R., Gupta, N., Lázaro-Muñoz, G., Sears, R.M., Kim, S., Moscarello, J.M., LeDoux, J.E., Cain, C.K. «Active vs. reactive threat responding is associated with differential c-Fos expression in specific regions of amygdala and prefrontal cortex.» *Learn Mem.* , 2013: 446-452.

Martins, M.A., Carobrez, A.P., Tonussi, C.R. «Activation of dorsal periaqueductal gray by glycine produces long lasting hyponociception in rats without overt defensive behaviors.» *Life Sciences (83)*, 2008: 118-121.

Marx, B.P., Forsyth, J.P., Gallup, G.G., Lexington, J.M. «Tonic immobility as an evolved predator defense: implications for sexual assault survivors .» *Clin. psychol.: Sci. Pract. 15(1), 74-90*, 2008.

Mascagni, F., McDonald, A.J. « Immunohistochemical characterization of cholecystokinin containing neurons in the rat basolateral amygdala.» *Brain Res. 976, 171-184*, 2003.

Mascagni, F., McDonald, A.J. «Immunohistochemical characterization of cholecystokinin containing neurons in the rat basolateral amygdala .» *Brain Res. 976, 171-184*, 2003.

McCormick, D.A., Connors, B.W., Lighthall, J.W., Prince, D.A. «Comparative electrophysiology of pyramidal and sparsely spiny stellate neurons of the neocortex.» *J. Neurophysiol. 54:782–806*, 1985.

McDonald, A.J. «Cortical pathways to the mammalian amygdala.» *Prog; Neurobiol. 55(3): 257-332*, 1998.

McDonald, A.J. «Cytoarchitecture of the central amygdaloid nucleus of the rat.» *J. Comp. Neurol. 208, 401–418*, 1982b.

Mcdonald, A.J. «Neurons of the lateral and basolateral amygdaloid nuclei: a Golgi study in the rat.» *J. Comp. Neurol. 212: 293–312*, 1982.
Mcdonald, A.J. «Organization of amygdaloid projections to the prefrontal cortex and associated striatum in the rat.» *Neuroscience*, 1991: 1-14.
McDonald, A.J. «Organization of amygdaloid projections to the prefrontal cortex and associated striatum in the rat.» *Neuroscience 44:1-14*, 1991.
McDonald, A.J. «Topographical organization of amygdaloid projections to the caudatoputamen, nucleus accumbens, and related striatal-like areas of the rat brain.» *Neuroscience 44(1): 15-33*, 1991.
McDonald, A.J., Mascagni, F. «Immunohistochemical characterization of somatostatin containing interneurons in the rat basolateral amygdala.» *Brain Res. 943, 237-244*, 2002.
McDonald, A.J., Mascagni, F. «Localization of the CB1 type cannabinoid receptor in the rat basolateral amygdala: high concentrations in a subpopulation of cholecystokinin-containing interneurons.» *Neuroscience 107, 641-652*, 2001.
Mcdonald, A.J., Mascagni, F., Guo, L. «Projections of the medial and lateral prefrontal cortices to the amygdala: A Phaseolus Vulgaris Leucoagglutinin study in the rat .» *Neuroscience Vol. 71, No. I, pp. 5-75*, 1996.
McDonald, A.J., Mascagni, F., Guo, L. «Projections of the medial and lateral prefrontal cortices to the amygdala: a Phaseolus vulgaris leucoagglutinin study in the rat.» *Neuroscience*, 1996: 55-75.
McDonald, A.J., Mascagni, F., Zaric, V. «Subpopulations of SOM-immunoreactive non-pyramidal neurons in the amygdala and adjacent external capsule project to the basal forebrain: evidence for the existence of GABAergic projection neurons in the cortical nuclei and basolateral nuclear complex.» *Frontiers in neural circuits 6:46*, 2012.
McGarry, L.M., Packer, A.M., Fino, E., Nikolenko, V., Sippy, T., Yuste, R. «Quantitative classification of somatostatin-positive neocortical interneurons identifies three interneuron subtypes.» *Front. Neural Circuits 4:12*, 2010.
McGaugh, J.L. «The amygdala modulates the consolidationof memories of emotionally arousing experiences.» *Annu. Rev. Neurosci. 27, 1-28*, 2004.
McGeorge, A.J., Faull, R.L. «The organization of the projection from the cerebral cortex to the striatum in the rat.» *Neuroscience 29, 503–537*, 1989.
Medina, L., Legaz, I., Gonzalez, G., De Castro, F., Rubenstein, J.L., Puelles, L. «Expression of Dbx1, Neurogenin 2, Semaphorin 5A, Cadherin 8, and Emx1 distinguish ventral and lateral pallial histogenetic divisions in the developing mouse claustroamygdaloid complex.» *J. Comp. Neurol., 474*, 2004: 504-523.
Mehdipour, S., Alaei, H.A., Pilehvariyan A.A. «The effect of medial prefrontal cortex electrical stimulation on passive avoidance memory in healthy and addict rats.» *Advanced Biomedical Research* , 2015.
Mello e Souza, T., Roesler, R.,Madruga, M., de-Paris, F., Quevedo, J., Rodrigues, C., et al. «Differential effects of post-training muscimol and AP5 infusions into different regions of the cingulate cortex on retention for inhibitory avoidance in rats .» *Neurobiol. Learn. Mem. 72, 118–127*, 1999.
Melzer*, S., Michael*,M., Caputi*,A., Eliava, A., Fuchs, E.C., Whittington, M.A., Monyer, H. «Long-Range–Projecting GABAergic Neurons Modulate Inhibition in Hippocampus and Entorhinal Cortex.» *Science* , 2012.
Miller, N.E. «Studies of fear as an acquirable drive: I. Fear as motivation and fear reduction as reinforcement in the learning of new responses .» *J. Exp. Psychol. 38:89–101*, 1948.
Millhouse, O.E., Deolmos, J. «Neuronal configurations in lateral and basolateral amygdala.» *Neuroscience 10: 1269–1300*, 1983.
Min, B.I., Kim, C.J., Rhee, J.S., Akaike, N. «Modulation of glycine-induced chloride current in acutely dissociated rat periaqueductal gray neurons by μ-opioid agonist, DAGO.» *Brain Research 734 (1-2): 72–78*, 1996.

Mitchell, I.J., Dean, P., Redgrave, P. «The projection from superior colliculus to cuneiform area in the rat. II. Defence-like responses to stimulation with glutamate in cuneiform nucleus and surrounding structures.» *Experimental brain research 72: 626-639*, 1988.

Mitsuto, N.A., Onoda, K., Clifford Foo, J., Haji,T., Akaishi, R., Yamaquchi, S., Sakai, K., Morita, K. «Neural mechanisms for adaptive learned avoidance of mental effort.» *J. Neurosci.*, 2018.

Mobbs, D., Kim, J.J. «Neuroethological studies of fear, anxiety, and risky decision-making in rodents and humans.» *Curr. Opin. Behav. Sci. 5:8–15*, 2015.

Moga, M.M., Weis, R.P., Moore, R.Y. «Efferent projections of the paraventricular thalamic nucleus in the rat.» *Journal of Comparative Neurology Vol. 359, Issue 2*, 1995: 221-238.

Mogenson, G.J., Jones, D.L., Yim, C.Y. «From motivation to action: functional interface between the limbic system and the motor system.» *Prog. Neurobiol. 14*, 1980: 69–97.

Morawska, M.M., Fendt, M. «The effects of muscimol and AMN082 injections into the medial prefrontal cortex on the expression and extinction of conditioned fear in mice.» *The Journal of experimental biology 215: 1394-1398*, 2012.

Morgan, M.A., LeDoux, J.E. «Differential contribution of dorsal and ventral medial prefrontal cortex to the acquisition and extinction of conditioned fear in rats.» *Behavioral neuroscience 109:681-688*, 1995.

Morgan, M.A., Romanski, L.M., LeDoux, J.E. «Extinction of emotional learning: Contribution of medial prefrontal cortex.» *Neurosci. Lett. 163: 109–113*, 1993.

Morgan, M.M., Reid, R.A., Stormann, T.M., Lautermilch, N.J. «Opioid selective antinociception following microinjection into the periaqueductal gray of the rat.» *J. Pain 15(11):1102-1109* , 2014.

Morrow, B.A., Elsworth, J.D., Rasmusson, A.M., Roth, R.H. «The role of mesoprefrontal dopamine neurons in the acquisition and expression of conditioned fear in the rat.» *Neuroscience 92: 553-564*, 1999.

Moscarello, J.M., LeDoux, J.E. «Active avoidance learning requires prefrontal suppression of amygdala-mediated defensive reactions.» *The Journal of Neuroscience 33(9):3815–3823* , 2013.

Moscarello, J.M., Maren, S. «Flexibility in the face of fear: hippocampal-prefrontal regulation of fear and avoidance.» *Current Opinion in Behavioral Sciences*, 2018: 44-49.

Mota-Ortiz, S.R., Sukikara, M.H., Felicio, L.F., Canteras, N.S. «Afferent connections to the rostrolateral part of the periaqueductal gray: a critical region influencing the motivation drive to hunt and forage.» *Neural Plast.* , 2009.

Mota-Ortizab, S.R., Sukikaraac, M.H., Bittencourt, J.C., Baldod, M.V., Eliasbe, C.F., Felicioc, L.F., Canteras, N.S. «The periaqueductal gray as a critical site to mediate reward seeking during predatory hunting.» *Behavioural Brain Research Vol. 226*, 2012: 32-40.

Mottaa, S.C., Carobrezb, A.P., Canteras, N.S. «The periaqueductal gray and primal emotional processing critical to influence complex defensive responses, fear learning and reward seeking.» *Neuroscience and behavioral reviews 76* , 2017: 39–47.

Mowrer, O.H. «On the dual nature of learning-a reinterpretation of conditioning and problem solving.» *Harvard Educational Review, 17, 102-148*, 1947.

Mowrer, O.H., Lamoreaux, R.R. «Fear as an intervening variable in avoidance conditioning.» *J. Comp. Psychol. 39: 29–50*, 1946.

Mugnaini, E., Oertel, W.H. *An atlas of the distribution of GABAergic neurons and terminals in the rat CNS as revealed by GAD immunohistochemistry. In: Handbook of chemical neuroanatomy. Vol.4: GABA and neuropeptides in the CNS, Part 1.* Amsterdam : Elsevier, 1985.

Muller, J., Corodimas, K.P., Fridel, Z., LeDoux, J.E. «Functional inactivation of the lateral and basal nuclei of the amygdala by muscimol infusion prevents fear conditioning to an explicit CS and to contextual stimuli.» *Behav. Neurosci. 111: 683-691*, 1997.

Muller, J.F., Mascagni, F., McDonald, A.J. «Coupled networks of parvalbumin immunoreactive interneurons in the rat basolateral amygdala.» *J. Neurosci. 25, 7366-7376*, 2005.
Muller, J.F., Mascagni, F., McDonald, A.J. «Postsynaptic targets of somatostatin containing interneurons in the rat basolateral amygdala.» *J. Comp. Neurol. 500, 513-529*, 2007.
Muller, J.F., Mascagni, F., McDonald, A.J. «Pyramidal cells of the rat basolateral amygdala: synaptology and innervation by parvalbumin-immunoreactive interneurons.» *J. Comp. Neurol. 494, 635-650*, 2006.
Muller, J.F., Mascagni, F., McDonald, A.J. «Synaptic connections of distinct interneuronal subpopulations in the rat basolateral amygdalar nucleus.» *J. Comp. Neurol. 456, 217-236*, 2003.
Myers, K.M., Davis, M. «Behavioral and neural analysis of extinction.» *Neuron 36: 567-584*, 2002.
Nader, K., Majidishad, P., Amorapanth, P., LeDoux, J.E. «Damage to the lateral and central, but not other, amygdaloid nuclei prevents the acquisition of auditory fear conditioning.» *Learn Mem 8: 156–163*, 2001.
Nashold, Jr.B.S., Wilson, W.P., Slaughter, D.G. «Sensations evoked by stimulation in the midbrain of man.» *J. Neurosurg. 30, 14–24*, 1969.
Nestler, E.J. « Molecular basis of long-term plasticity underlying addiction.» *Nature Reviews Neuroscience 2*, 2001: 119–128.
Nitschke, J.B., Sarinopoulos, I., Mackiewicz, K.L., Schaefer, H.S., Davidson, R.J. «Functional neuroanatomy of aversion and its anticipation.» *Neuroimage, 29* , 2006: 106-116.
Nobuyuki, K., Reiko, K., Sanae, S. «Avoidance learning in the crayfish (Procambarus clarkii) depends on the predatory imminence of the unconditioned stimulus: a behavior systems approach to learning in invertebrates.» *Behavioural Brain Research*, 2004: 229-237.
Nowak, L.G., Azouz, R., Sanchez-Vives, M.V., Gray, C.M., McCormick, D.A. «Electrophysiological classes of cat primary visual cortical neurons in vivo as revealed by quantitative analyses.» *J Neurophysiol 89:1541–1566*, 2003.
O'Donnell, A., Odrowaz, Z., Sharrocks, A.D. «Immediate-early gene activation by the MAPK pathways: what do and don't we know?» *Biochem. Soc. Trans., 40* , 2012: 58-66.
Oka, T., Tsumori, T., Yokota, S., Yasui, Y. «Neuroanatomical and neurochemical organization of projections from the central amygdaloid nucleus to the nucleus retroambiguus via the periaqueductal gray in the rat.» *Neuroscience Research*, 2008: 286-298.
Oleson, E.B., Gentry, R.N., Chioma, V.C., Cheer, J.F. «Subsecond dopamine release in the nucleus accumbens predicts conditioned punishment and its successful avoidance.» *J. Neurosci. 32, 14804-14808*, 2012.
Onstott, D., Mayer, B., Beitz, A.J. «Nitric oxide synthase immunoreactive neurons anatomically define a longitudinal dorsolateral column within the midbrain periaqueductal gray of the rat: analysis using laser confocal microscopy.» *Brain Res. 610: 317–324* , 1993.
Orsinia, C.A., Maren, S. «Neural and cellular mechanisms of fear and extinction memory formation.» *Neuroscience and Biobehavioral Reviews 36*, 2012: 1773–1802.
Osada, K., Kurihara, K., Izumi, H., Kashiwayanaqi, M. «Pyrazine analogues are active components of wolf urine that induce avoidance and freezing behaviours in mice.» *PLoS One 8(4):e61753*, 2013.
Ostlund, S.B., Balleine, B.W. «Lesions of medial prefrontal cortex disrupt the acquisition but not the expression of goal-directed learning.» *J. Neurosci. 25: 7763–7770*, 2005.
Palazzo, E., Luongo, L., Novellis, V., Rossi, F., Maione, S. «The role of cannabinoid receptors in the descending modulation of pain.» *Pharmaceuticals 16; 3(8): 2661-2673*, 2010.
Pare, D., Gaudreau, H. «Projection cells and interneurons of the lateral and basolateral amygdala: distinct firing patterns and differential relation to theta and delta rhythms in conscious cats.» *J. Neurosci. 16, 3334-3350*, 1996.

Paré, D., Smith, Y., Paré, J.F. « Intra-amygdaloid projections of the basolateral and basomedial nuclei in the cat: Phaseolus vulgaris leucoagglutinin anterograde tracing at the light and electron microscopic level.» *Neuroscience 69: 567–583*, 1995.

Parry, D.M., Macmillan, F.M., Koutsikou, S., McMullan, S., Lumb, B.M. «Separation of A-versus C-nociceptive inputs into spinal-brainstem circuits.» *Neuroscience 152: 1076–1085*, 2008.

Paschoalin-Maurin, T., dos Anjos-Garcia, T., Falconi-Sobrinho L.L., de Freitas, R.L., Cysne Coimbra, J.P., Laure, C.J., Cysne Coimbra, N. «The rodent-versus-wild snake paradigm as a model for studying anxiety- and panic-like behaviors: face, construct and predictive validities.» *Neuroscience 369*, 2018.

Paschoalin-Maurin, T., dos Anjos-Garcia, T., Falconi-Sobrinho, L.L., de Freitas, R.L., Coimbra, J.P.C., Laure, C.J., Coimbra, N.C. «The rodent-versus-wild snake paradigm as a model for studying anxiety- and panic-like behaviors: face, construct and predictive validities.» *Neuroscience 369* , 2018: 336–349.

Pavlov, I.P. *Conditioned Reflexes.* London: Courier Dover Publications, 1927.

Paxinos, G., Franklin, K. *The Mouse Brain in Stereotaxic Coordinates.* Elsevier/Academic Press, ed. 3, 2008.

Paxinos, G., Mai, J.K.,. *The Human Nervous System, 2nd ed.* Amsterdam ; Boston: Elsevier Academic Press, 2004.

Paxinos, G., Watson, C. *The rat brain in stereotaxic coordiantes.* New York: Academic Press , 1986.

Penny, G.R., Conley, M., Diamond, I.T., Schemechel, D.E. «The distribution of glutamic acid decarboxylase immunoreactivity in the diencephalon of the opossum and rabbit .» *J. Comp. Neurol., 228*, 1984: 38-57.

Penzo, M.A., Robert, V., Li, B. « Fear conditioning potentiates synaptic transmission onto long-range projection neurons in the lateral subdivision of central amygdala.» *J. Neurosci. 34, 2432-2437* , 2014.

Penzo, M.A., Robert, V., Li, B. «Fear conditioning potentiates synaptic transmission onto long-range projection neurons in the lateral subdivision of central amygdala.» *The Journal of neuroscience : the official journal of the Society for Neuroscience 34: 2432-2437*, 2014.

Penzo, M.A., Robert, V., Li, B. «Fear conditioning potentiates synaptic transmission onto long-range projection neurons in the lateral subdivision of central amygdala.» *J. Neurosci.*, 2014.

Penzo, M.A., Robert, V., Tucciarone, J., De Bundel, D., Wang, M., Van Aelst, L., Darvas, M., Parada, L.F., Palmiter, R.D., He, M., Huang, Z.J., Li, B. «The paraventricular thalamus controls a central amygdala fear circuit.» *Nature 519(7544): 455-9*, 2015.

Perrotti, L.I., Dennisa, T.S., Jiao, X., Servatius, R.J., Pang, K.C.H., Beck, K.D. «Activation of extracellular signal-regulated kinase (ERK) and delta-FosB in emotion-associated neural circuitry after asymptotic levels of active avoidance behavior are atteined .» *Brain Research Bulletin 98* , 2013: 102– 110.

Petrides, M., Tomaiuolo, F., Yeterian, E.H., Pandya, D.N. «The prefrontal cortex: Comparative architectonic organization in the human and the macaque monkey brains.» *Cortex 48, 46–57*, 2012.

Petrovic, P., Dietrich, T., Fransson, P., Andersson, J., Carlsson, K., Ingvar, M. «Placebo in emotional processing-induced expectations of anxiety relief activate a generalized modulatory network.» *Neuron 46, 957–969*, 2005.

Petrovich, G.D., Canteras, N.S., Swanson, L.W. «Combinatorial amygdalar inputs to hippocampal domains and hypothalamic behavior systems.» *Brain Res. Brain Res. Rev. 38(1-2): 247-89*, 2001.

Pi, H.J., Hangya, B., Kvitsiani, D., Sanders, J.I., Huang, Z.J., Kepecs, A. «Cortical interneurons that specialize in disinhibitory control.» *Nature* , 2013: 521-524.

Piantadosi, P.T., Yeates, D.C.M., Floresco, S.B. «Cooperative and dissociable involvement of the nucleus accumbens core and shell in the promotion and inhibition of actions during active and inhibitory avoidance.» *Neuropharmacology vol.138*, 2018: 57-71.

Pitkanen, A. *Connectivity of the rat amygdaloid complex. In: The Amygdala: A Functional Analysis.* Oxford, U.K.: edited by Aggleton JP. Oxford Univ. Press, p. 31–115, 2000.

Pitkanen, A., Amaral, D.G. «The distribution of GABAergic cells, fibers, and terminals in the monkey amygdaloid complex: an immunohistochemical and in situ hybridization study.» *J. Neurosci. 14: 2200–2224*, 1994.

Pitkanen, A., Savander, V., Ledoux, J.E. «Organization of intraamygdaloid circuitries in the rat: an emerging framework for understanding functions of the amygdala .» *Trends Neurosci. 20: 517–523*, 1997.

Pitkanen, A., Stefanacci, L., Farb, C.R., Go, G.G., Ledoux, J.E., Amaral, D.G. «Intrinsic connections of the rat amygdaloid complex: projections originating in the lateral nucleus.» *J. Comp. Neurol. 356: 288-310*, 1995.

Popova, N.K. «The role of brain serotonin in the expression of genetically determined.» *Genetika 40: 770–8*, 2004.

Poremba, A., Gabriel, M. «Amygdala Neurons Mediate Acquisition But Not Maintenance of instrumental avoidance behavior in rabbits.» *The Journal of Neuroscience 19(21): 9635–9641*, 1999.

Poremba, A., Grabiel, M. «Amygdala neurons mediate acquisition but not maintenance of instrumental avoidance behavior in rabbits.» *Journal of neuroscience 19 (21) 9635-9641*, 1999.

Pot, A.L. «Catatonia .» *Encephale 41(3): 274-9*, 2015.

Preuss, T.M. «Do rats have prefrontal cortex? The Rose-Woolsey-Akert program reconsidered.» *J. Cogn. Neurosci. 7, 1–24*, 1995.

Qi, S., Hassabis, D., Sun, J., Guo, F., Daw, N., Mobbs, D. «How cognitive and reactive fear circuits optimize escape decisions in humans.» *PNAS 115 (12) 3186-3191*, 2018.

Quirk, G.J., Mueller, X. «Neural mechanisms of extinction learning and retrieval.» *Neuropsychopharmacology, 33*, 2008: 56-72.

Quirk, G.J., Repa, J.C., LeDoux, J.E. «Fear conditioning enhances short-latency auditory responses of lateral amygdala neurons: Parallel recordings in the freely behaving rat.» *Neuron 15: 1029–1039*, 1995.

Quirk, G.J., Russo, G.K., Barron, J.L., Lebron, K. «The role of ventromedial prefrontal cortex in the recovery of extinguished fear.» *J. Neurosci. 20: 6225–6231* , 2000.

Ragozzino, M.E., Adams, S., Kesner, R.P. «Differential involvement of the dorsal anterior cingulate and prelimbic-infralimbic areas of the rodent prefrontal cortex in spatial working memory.» *Behav. Neurosci. 112:293–303*, 1998.

Rainnie, D.G., Mania, I., Mascagni, F., McDonald, A.J. «Physiological and morphological characterization of parvalbumin-containing interneurons of the rat basolateral amygdala.» *J. Comp. Neurol. 498, 142-161*, 2006.

Rajasethupathy, P., Sankaran, S., Marshel, J.H., Kim, C.K., Ferenczi, E., Lee, S.Y., Berndt, A., Ramakrishnan, C., Jaffe, A., Lo, M., Liston, C., Deisseroth, K. «Projections from neocortex mediate top-down control of memory retrieval.» *Nature* , 2015.

Rajasethupathy, P., Sankaran, S., Marshel, J.H., Kim, C.K., Ferenczi, E., Lee, S.Y., Berndt, A., Ramakrishnan, C., Jaffe, A.,Lo, M., Liston, C., Deisseroth, K. «Projections from neocortex mediate top-down control of memory retrieval.» *Nature 526:653-659*, 2015.

Ramirez F., Moscarello J.M., LeDoux J.E., Sears R.M. «Active avoidance requires a serial basal amygdala to nucleus accumbens shell circuit.» *J neurosci 35(8): 3470-7*, 2015.

Rao, V.R., Finkbeiner, S. «NMDA and AMPA receptors: old channels, new tricks.» *Cell*, 2007: 284-291.

Rattel, J.A., Miedl, S.F., Blechert, J., Wilhelm, F.H. «Higher threat avoidance costs reduce avoidance behaviour which in turn promotes fear extinction in humans .» *Behaviour Research and Therapy* , 2017: 37-46.

Ray, J.P., Price, J.L. «The organization of the thalamocortical connections of the mediodorsal thalamic nucleus in the rat, related to the ventral forebrain-prefrontal cortex topography.» *The journal of comparative neurology 323:167-197*, 1992.

Redgrave, P., Dean, P., Mitchell, I.J., Odekunle, A., Clark, A. «The projection from superior colliculus to cuneiform area in the rat. I. Anatomical studies.» *Experimental brain research 72: 611-625*, 1988.

Redgrave, P., Rodriguez, M., Smith, Y., Rodriguez-Oroz, M., Lehericy, S., Bergman, H., et al. «Goal-directed and habitual control in the basal ganglia: implications for Parkinson's disease.» *Nat. Rev. Neurosci. 11, 760–772*, 2010.

Reep, R.L., Cheatwood, J.L., Corwin, J.V. «The associative striatum: organization of cortical projections to the dorsocentral striatum in rats.» *J. Comp. Neurol. 467, 271–292*, 2003.

Reep, R.L., Corwin, J.V. «Topographic organization of the striatal and thalamic connections of rat medial agranular cortex.» *Brain Res. 841:43–52.*, 1999.

Reichling, D.B., Basbaum, A.I. «Contribution of brainstem GABAergic circuitry to descending antinociceptive controls: I. GABA-immunoreactive projection neurons in the periaqueductal gray and nucleus raphe magnus.» *J. comp. Neurol. 302* , 1990a: 370-377.

Reichling, D.B., Basbaum, A.I. «Contribution of brainstem GABAergic circuitry to descending antinociceptive controls: II. Electron microscopic immunocytochemical evidence of GABAergic control over the projection from the periaqueductal gray and nucleus raphe magnus in the rat .» *J. comp. Neurol. 302*, 1990b: 378-393.

Reichling, D.T., Kwiat, G.C., Basbaum, A.I. «Anatomy, physiology and pharmacology of the periaqueductal gray contribution to antinociceptive controls.» *Prog. Brain Res. 77*, 1988: 31-46.

Reimer, A.E., de Oliveira, A.R., Brandão, M.L. «Glutamatergic mechanisms of the dorsal periaqueductal gray matter modulate the expression of conditioned freezing and fear-potentiated startle.» *Neuroscience*, 2012: 72-81.

Reimer, A.E., Oliveira, A.R, Brandão, M.L. «Selective involvement of GABAergic mechanisms of the dorsal periaqueductal gray and inferior colliculus on the memory of the contextual fear as assessed by the fear potentiated startle test.» *Brain Res. Bull., 76* , 2008: 545-550.

Reis, F.M., Almada, R.C., Fogaça, M.V., Brandão, M.L.. «Rapid activation of glucocorticoid receptors in the prefrontal cortex mediates the expression of contextual conditioned fear in rats.» *Cereb. Cortex*, 2016.

Repa, J.C., Muller, J., Apergis, J., Desrochers, T.M., Zhou, Y., LeDoux, J.E. «Two different lateral amygdala cell populations contribute to the initiation and storage of memory.» *Nat. Neurosci. 4: 724–731*, 2001.

Reppucci, C.J., Petrovich, G.D. «Organization of connections between the amygdala, medial prefrontal cortex, and lateral hypothalamus: a single and double retrograde tracing study in rats.» *Brain Struct. Funct. 221(6): 2937–2962*, 2016.

Resstel, L.B., Joca, S.R., Guimaraes, F.G., Correa, F.M. «Involvement of medial prefrontal cortex neurons in behavioral and cardiovascular responses to contextual fear conditioning.» *Neuroscience 143: 377-385*, 2006.

Reynolds, D.V. «Surgery in the rat during electrical analgesia induced by focal brain stimulation.» *Science 164: 444–5*, 1969.

Riekkinen, P., Kuitunen, J., Riekkinen, M. «Effects of scopolamine infusions into the anterior and posterior cingulate on passive avoidance and water maze navigation.» *Brain Res. 685, 46–54*, 1995.

Rizvi, T.A., Ennis, M., Behbehani, M.M., Shipley, M.T. «Connections between the central nucleus of the amygdala and the midbrain periaqueductal gray: topography and reciprocity .» *The Journal of comparative neurology 303: 121-131*, 1991.

Robbins, T.W., Cador, M., Taylor, J.R., Everitt, B.J. «Limbic–striatal interactions in reward-related processes.» *Neurosci. Biobehav. Rev. 13, 155–162*, 1989.

Roberts, G.W., Woodhams, P.L., Polak, J.M., Crow, T.J. «Distribution of neuropeptides in the limbic system of the rat: the amygdaloid complex.» *Neuroscience 7: 99-131*, 1982.

Rodrigues, S.M., Schafe, G.E., LeDoux, J.E. «Intraamygdala blockade of the NR2B subunit of the NMDA receptor disrupts the acquisition but not the expression of fear conditioning.» *J. Neurosci. 21: 6889–6896*, 2001.

Rodriguez-Romaguera, J., Greenberg, B.D., Rasmussen, S.A., Quirk, G.J. «An avoidance-based rodent model of exposure with response prevention therapy for obsessive-compulsive disorder.» *Biological psychiatry* , 2016.

Rogan, M., Staubli, U., LeDoux, J. «Fear conditioning induces associative long-term potentiation in the amygdala .» *Nature 390: 604–607*, 1997.

Romanski, L.M., LeDoux, J.E., Clugnet, M.C., Bordi, F. « Somatosensory and auditory convergence in the lateral nucleus of the amygdala.» *Behav. Neurosci. 107: 444-450*, 1993.

Rose, J.E., Woolsey, C.N. «The orbitofrontal cortex and its connections with the mediodorsal nucleus in rabbit, sheep and cat.» *Res. Publ. Assoc. Res. Nerv. Ment. Dis. 27, 210–232*, 1948.

Routtenberg, A., Cantallops, I., Zaffuto, S., Serrano, P., Namgung, U. «Enhanced learning after genetic overexpression of a brain growth protein.» *Proc. Natl. Acad. Sci. 97: 7657-62*, 2000.

Rozeske, R.R., Herry, C. «Neuronal coding mechanisms mediating fear behavior.» *Current Opinion in Neurobiology, Volume 52* , 2018: 60-64.

Rozeske, R.R., Jercog, D., Karalis, N., Chaudun, F., Khoder, S., Girard, D., Winke, N., Herry, C. «Prefrontal-periaqueductal gray-projecting neurons mediate context fear discrimination.» *Neuron 97(4): 898-910*, 2018.

Rudy, B., Fishell, G., Lee, S., Hjerling-Leffler, J. «Three groups of interneurons account for nearly 100% of neocortical GABAergic neurons.» *Dev. Neurobiol. 71:45–61*, 2011.

S. Nakanishi, Y. NakajmaMasu, M., Ueda, Y., Nakahara, K.,Watanabe, D.,Yamaguchi, S., Kawabata, S., Okada, M. «Glutamate receptors: brain function and signal transduction.» *Brain Research Reviews, 26* , 1998: 230-235.

Sacchetti, B., Baldi, E., Lorenzini, C.A., Bucherelli, C. «Differential contribution of some cortical sites to the formation of memory traces supporting fear conditioning .» *Experimental brain research 146: 223-232*, 2002.

Sagliano, L., Cappuccio, A., Trojano, L., Conson, M. «Approaching threats elicit a freeze-like response in humans.» *Neuroscience letters* , 2014: 35-40.

Sah, P., Faber, E.S., Lopez De Armentia, M., Power, J. «The amygdaloid complex: anatomy and physiology.» *Physiol. Rev. 83, 803-834*, 2003.

Samson, R.D., Paré, D. «Activity-dependent synaptic plasticity in the central nucleus of the amygdala.» *J. Neurosci. 25, 1847–1855*, 2005.

Sandner, G., Di Scala, G., Rocha, B., Angst, M.J. «C-fos immunoreactivity in the brain following unilateral electrical stimulation of the dorsal periaqueductal gray in freely moving rats.» *Brain Research, 573*, 1992: 276-283.

Savander, V., Go, C.G., Ledoux, J.E., Pitkanen, A. «Intrinsic connections of the rat amygdaloid complex: projections originating in the basal nucleus.» *J. Comp. Neurol. 361: 345-368*, 1995.

Savander, V., Miettinen, R., Ledoux, J.E., Pitkanen, A. «Lateral nucleus of the rat amygdala is reciprocally connected with basal and accessory basal nuclei: a light and electron microscopic study.» *Neuroscience 77: 767–781*, 1997.

Schafe, G.E., LeDoux, J.E. «Memory consolidation of auditory pavlovian fear conditioning requires protein synthesis and protein kinase A in the amygdala.» *J. Neurosci. 20: RC96(1–5)*, 2000.

Schafe, G.E., Nader, K., Blair, H.T., LeDoux, J.E. «Memory consolidation of Pavlovian fear conditioning: a cellular and molecular perspective.» *Trends Neurosci. 24: 540-546*, 2001.

Schenberg, L.C., Costa, M.B., Borges, P.C.L., Castro, M.F.S. «Logistic analysis of the defense reaction induced by electrical stimulation of the rat mesencephalic tectum.» *Neurosci. Biobehav. Rev., 14* , 1990: 473-479.

Schiess, M.C., Callahan, P.M., Zheng, H. «Characterization of the electrophysiological and morphological properties of rat central amygdala neurons in vitro.» *J. Neurosci. Res., 58* , 1999: 663-673.

Schlund, M.W., Brewer, A.T., Richman, D.M., Magee, S.K., Dymond, S. «Not so bad: avoidance and aversive discounting modulate threat appraisal in anterior cingulate and medial prefrontal cortex.» *Frontiers in behavioral neuroscience*, 2015.

Schutz, M.T.B., de Aguiar, J.C., Graeff, F.G. «Antiaversive role of serotonin on the dorsal periaqueductal gray matter.» *Psychopharmacology 85: 340-345*, 1985.

Schwaber, J.S., Kapp, B.S., Higgins, G.A., Rapp, P.R. «Amygdaloid basal forebrain direct connections with the nucleus of the solitary tract and the dorsal motor nucleus.» *J. Neurosci. 2: 1424–1438*, 1982.

Schwartz, N., Miller, C., Fields, H.L. «Cortico-accumbens regulation of approach-avoidance behavior Is modified by experience and chronic pain.» *Cell Reports* , 2017.

Seger, C.A., Spiering, B.J. «A critical review of habit learning and the basal ganglia.» *Front. Syst. Neurosci. 5:66*, 2011.

Senn, V., Wolff, S.B., Herry, C., Grenier, F., Ehrlich, I., Grundemann, J., Fadok, J.P., Muller, C., Letzkus, J.J., Luthi, A. «Long-range connectivity defines behavioral specificity of amygdala neurons.» *Neuron 81:428-437*, 2014.

Servatius, R.J., Jiao, X., Beck, K.D., Pang, K.C., Minor, T.R. «Rapid avoidance acquisition in Wistar-Kyoto rats.» *Behav. Brain Res. 192:191–7*, 2008.

Servatius, R.J., Pang, K.C.H., Quirk, G.J., Myers, C.E. «Avoidance: From basic science to psychopathology.» *Frontiers in Behavioral neuroscience* , 2016.

Sesack, S.R., Deutch, A.Y., Roth, R.H., Bunney, B.S. «Topographical organization of the efferent projections of the medial prefrontal cortex in the rat: an anterograde tract-tracing study with Phaseolus vulgaris leucoagglutinin.» *J. Comp. Neurol. 290, 213–242*, 1989.

Seymour, B., Dolan, R. «Emotion, decision making, and the amygdala.» *Neuron 58(5): 662-71*, 2008.

Sheynin, J., Shind, C., Radell, M., Ebanks-Williams, Y, Gilbertson, M.W., Beck, K.D., Myers, C.E. «Greater avoidance behavior in individuals with posttraumatic stress disorder symptoms.» *STRESS*, 2017: 285-293.

Shi, C.J., Cassell, M.D. «Cortical, thalamic, and amygdaloid projections of rat temporal cortex.» *J. Comp. Neurol. 382: 153–175*, 1997.

Shinonaga, Y., Takada, M., Mizuno, N. «Topographic organization of collateral projections from the basolateral amygdaloid nucleus to both the prefrontal cortex and nucleus accumbens in the rat.» *Neuroscience 58:389-397*, 1994.

Shinonaga, Y., Takada, M., Mizuno, N. «Topographic organization of collateral projections from the basolateral amygdaloid nucleus to both the prefrontal cortex and nucleus accumbens in the rat.» *Neuroscience 58:389-397*, 1994.

Sidman, M. «Avoidance conditioning with brief shock and no exteroceptive warning signal .» *Science 118(3058): 157-8*, 1953.

Siegel, A., Pott, C.B. «Neural substrates of aggression and flight in the cat.» *Progress in Neurobiology Vol. 31*, 1988: 261-283.

Sierra-Mercado, D., Padilla-Coreano, N., Quirk, G.J. «Dissociable roles of prelimbic and infralimbic cortices, ventral hippocampus, and basolateral amygdala in the expression and extinction of conditioned fear.» *Neuropsychopharmacology : official publication of the American College of Neuropsychopharmacology 36: 529-538*, 2011.

Sierra-Mercado, D.Jr., Corcoran, K.A., Lebron-Milad, K., Quirk, G.J. «Inactivation of the ventromedial prefrontal cortex reduces expression of conditioned fear and impairs subsequent recall of extinction.» *The European journal of neuroscience 24: 1751-1758*, 2006.

Skinner, B.F. *The behavior of organisms: An experimental analysis.* New York: Appleton-Century, 1938.

Smith, G.S.S., Savery, D., Marden, C., Lopez Costa ,J.J., Averill, S., Priestley, J.V., Rattray, M. «Distribution of messenger RNAs encoding enkephalin, substance P,

somatostatin, galanin, vasoactive intestinal polypeptide, neuropeptide Y, and calcitonin-gene related peptide in the midbrain periaqueductal gray in the rat .» *The Journal of Comparative Neurology 350: 23-40* , 1994.

Smith, M.A., Banerjee, S., Gold, P.W., Glowa, J. «Induction of c-fos mRNA in rat brain by conditioned and unconditioned stressors .» *Brain research 578: 135-141*, 1992.

Sobieraj, J.C., Kim, A., Fannon, M.J., Mandyam, C.D. «Chronic wheel running-induced reduction of extinction and reinstatement of methamphetamine seeking in methamphetamine dependent rats is associated with reduced number of periaqueductal gray dopamine neurons.» *Brain Struct. Funct. 221, 261–276*, 2016.

Solomon, R.L., Turner, L.H. «Discriminative classical conditioning in dogs paralyzed by curare can later control discriminative avoidance responses in the normal state.» *Psychol Rev. 69: 202-19*, 1962.

Sotres-Bayon, F. , Bush, D., LeDoux, J. «Emotional perseveration: an update onprefrontal–amygdala interactions in fear extinction .» *Learn. Mem. 11*, 2004: 525–535.

Sotres-Bayon, F., Bush, D.E., LeDoux, J.E. «Acquisition of fear extinction requires activation of NR2B containing NMDA receptors in the lateral amygdala.» *Neuropsychopharmacology: official publication of the American College of Neuropsychopharmacology 32:1929-1940*, 2007.

Sotres-Bayon, F., Quirk, G.J. «Prefrontal control of fear: more than just extinction.» *Curr. Opin. Neurobiol. 20(2):231-5*, 2010.

Spampanato, J., Polepalli, J., Sah, P. «Interneurons in the basolateral amygdala.» *Neuropharmacology 60*, 2011: 765-773.

Sparta, D.R., Smithuis, J., Stamatakis, A.M., Jennings, J.H., Kantak, P.A., Ung, R.L., Stuber, G.D. «Inhibition of projections from the basolateral amygdala to the entorhinal cortex disrupts the acquisition of contextual fear.» *Front. Behav. Neurosci.*, 2014.

Sparta, D.R., Smithuis, J., Stamatakis, A.M., Jennings, J.H., Kantak, P.A., Ung, R.L., Stuber, G.D. «Inhibition of projections from the basolateral amygdala to the entorhinal cortex disrupts the acquisition of contextual fear.» *Frontiers in Behavioural Neuroscience*, 2014.

Spruston, N. «Pyramidal neurons: dendritic structure and synaptic integration.» *Nature reviews Neuroscience 9:206-221*, 2008.

Stamatakis, A.M., Sparta, D.R., Jennings, J.H., McElligott, Z.A., Decot, H., Stuber, G.D. «Amygdala and bed nucleus of the stria terminalis circuitry: Implications for addiction-related behaviors.» *Neuropharmacology*, 2014.

Starr, M.D., Mineka, S. «Determinants of fear over the course of avoidance learning.» *Learn Motiv 8: 331-350*, 1977.

Steenland, H.W., Zhuo, M. «Neck electromyography is an effective measure of fear behavior.» *J. Neurosci. Methods*, 2009 .

Stefanik, M.T., Kalivas, P.W. «Optogenetic dissection of basolateral amygdala projections during cue-induced reinstatement of cocaine seeking.» *Front. Behav. Neurosci.*, 2013.

Stevens, C.F. «CREB and memory consolidation.» *Neuron 13: 769–770*, 1994.

Stevenson, C.W. «Role of amygdala-prefrontal cortex circuitry in regulating the expression of contextual fear memory.» *Neurobiology of learning and memory 96: 315-323*, 2011.

Stuber, G.D., Sparta, D.R., Stamatakis, A.M., van Leeuwen, W.A., Hardjoprajitno, J.E., Cho, S., Tye, K.M., Kempadoo, K.A., Zhang, F., Deisseroth, K., Bonci, A. «Excitatory transmission from the amygdala to nucleus accumbens facilitates reward seeking.» *Nature, 475 (7356)* , 2011: 377-380.

Sudré, E.C.M., Barros, M.R., Sudré, G.N., Schenberg, L.C. «Thresholds of electrically induced defence reaction of the rat: short- and long-term adaptation mechanisms.» *Behav. Brain Res., 58* , 1993: 141-154.

Sun, W., Li, X., An, L. «Distinct roles of prelimbic and infralimbic proBDNF in extinction of conditioned fear .» *Neuropharmacology 131* , 2018: 11-19.

Svoboda, J., Lobellová, V., Popelíková, A., Ahuja, N., Kelemen, E., Stuchlík,A. «Transient inactivation of the anterior cingulate cortex in rats disrupts avoidance of a dynamic object.» *Neurobiology of Learning and Memory 139* , 2017: 144–148.

Takashina, K., Saito, H., Nishiyama, N. «Preferential impairment of avoidance performances in amygdala lesioned mice.» *Jpn. J. Pharmacol. 67, 107-115* , 1995.

Tang, J., Ko, S., Ding, H.K., Qiu, C.S., Calejesan, A.A., Zhuo, M. «Pavlovian fear memory induced by activation in the anterior cingulate cortex.» *Molecular pain 1:6*, 2005.

Taniguchi, H., Huang, Z. J., Callaway, E. M. «Contrast dependence and differential contributions from somatostatin- and parvalbumin-expressing neurons to spatial integration in mouse V1.» *J. Neurosci. 33, 11145–11154* , 2013.

Tapias-Espinosa, C., Kádárc, E., Segura-Torresa, P. «Spaced sessions of avoidance extinction reduce spontaneous recovery and promote infralimbic cortex activation.» *Behavioural Brain Research 336*, 2018: 59–66.

Telonis, A.M. «Phobos: A novel software for recording rodents' behavior during the thigmotaxis and the elevated plus-maze test.» *Neurosci. Lett.*, 2015.

Temizer, I., Donovan, J.C., Baier, H., Semmelhack, J.L. «A visual pathway for looming-evoked escape in larval zebrafish.» *Current Biology*, 2015: 1823-1834.

Thompson, B.M., Baratta, M.V., Biedenkapp, J.C., Rudy, J.W., Watkins, L.R., Maier, S.F. «Activation of the infralimbic cortex in a fear context enhances extinction learning.» *Learn Mem. 17: 591-599*, 2010.

Thomson, A.M., Lamy, C. «Functional maps of neocortical local circuitry .» *Frontiers in neuroscience* , 2007.

Thorn, C.A., Atallah, H., Howo, M., Graybiel, A.M. «Differential dynamics of activity changes in dorsolateral and dorsomedial striatal loops during learning.» *Neuron 66, 781-795*, 2010.

Tian, S., Huang, F., Gao, J., Li, P., Ouyang, X., Zhou, S., Deng, H., Yan, Y. «Ventrolateral prefrontal cortex is required for fear extinction in a modified delay conditioning paradigm in rats.» *Neuroscience 189: 258-268*, 2011.

Tomaz, C., Brandão, M., Bagri, A., Carrive, P., Schmitt, P. «Flight behavior induced by microinjection of GABA antagonists into periventricular structures in detelencephalated rats.» *Pharmacol. Biochem. Behav. 30(2): 337-42*, 1988.

Torres-García, M.E., Medina, A.C., Quirarte, G.L., Prado-Alcalá, R.A. «Differential effects of inactivation of discrete regions of medial prefrontal cortex on memory consolidation on moderate and intense inhibitory avoidance training.» *frontiers in Pharmacology* , 2017.

Tovote, P., Esposito, M.S., Botta, P., Chaudun, F., Fadok, J.P., Markovic, M., Wolff, S.B., Ramakrishnan, C., Fenno, L., Deisseroth, K., Herry, C., Arber, S., Lüthi, A. «Midbrain circuits for defensive behaviour.» *Nature*, 2016.

Tovote, P., Fadok, J.P., Lüthi, A. «Neuronal circuits for fear and anxiety.» *Nat. Rev. Neurosci. 16(6): 317-31*, 2015.

Treanor, M., Barry, T.J. «Treatment of avoidance behavior as an adjunct to exposure therapy: Insights from modern learning theory.» *Behaviour research and therapy*, 2017: 30-36.

Tritsch, N.X., Ding, J.B., Sabatini, B.L. «Dopaminergic neurons inhibit striatal output through non-canonical release of GABA.» *Nature 490 (7419): 262–6*, 2012.

Tsutsui-Kimura, I., Bouchekioua, Y., Mimura, M., Tanaka, K.F. «A new paradigm for evaluating avoidance/escape motivation .» *Int J Neuropsychopharmacol 1;20(7):593-601*, 2017.

Tukker, J.J., Fuentealba, P., Hartwich, K., Somogyi, P., Klausberger, T. «Cell type-specific tuning of hippocampal interneuron firing during gamma oscillations in vivo.» *J. Neurosci. 27, 8184–8189*, 2007.

Tulogdi, A., Sörös, P., Tóth, M., Nagy, R., Biró, L., Aliczki, M., Klausz, B., Mikics, E., Haller, J. «Temporal changes in c-Fos activation patterns induced by conditioned fear.» *Brain Research Bulletin 88* , 2012: 359–370.

Turner, B.H., Herkenham, M. «Thalamoamygdaloid projections in the rat: a test of the amygdala's role in sensory processing.» *J. Comp. Neurol. 313, 295–325*, 1991.
Tye, K.M. et al. «Amygdala circuitry mediating reversible and bidirectional control of anxiety .» *Nature 471, 358–362*, 2011.
Ueda, K., Okamoto, Y., Okada, G., Yamashita, H., Hori, T. , Yamawaki, S. «Brain activity during expectancy of emotional stimuli: an fMRI study.» *Neuroreport, 14 (1)*, 2003: 51-55.
Uylings, H.B., Van Eden, C.G. «Qualitative and quantitative comparison of the prefrontal cortex in rat and in primates, including humans.» *Progress in brain research 85:31-62*, 1990.
Uylings, H.B.M., Groenewegen, H.J., Kolb, B. «Do rats have a prefrontal cortex?» *Behav. Brain Res. 146, 3–17* , 2003.
Van Eden, C.G., Uylings, H.B. «Cytoarchitectonic development of the prefrontal cortex in the rat. The.» *The Journal of comparative neurology 241:253-267*, 1985.
Varela, C., Kumar, S., Yang, J.Y., Wilson, M.A. «Anatomical substrates for direct interactions between hippocampus, medial prefrontal cortex, and the thalamic nucleus reuniens.» *Brain structure and function 219:911-929*, 2014.
Varga, C., Golshani, P., Soltesz, I. «Frequency-invariant temporal ordering of interneuronal discharges during hippocampal oscillations in awake mice.» *Proc. Natl. Acad. Sci. USA 109, E2726–E2734* , 2012.
Varga, C., Golshani, P., Soltesz, I. «Frequency-invariant temporal ordering of interneuronal discharges during hippocampal oscillations in awake mice.» *Proc. Natl. Acad. Sci. USA 109, E2726–E2734*, 2012.
Vargas, L.C., Marques, T.A., Schenberg, L.C. «Micturition and defensive behaviors are controlled by distinct neural networks within the dorsal periaqueductal gray and deep gray layer of the superior colliculus of the rat.» *Neurosci Lett 280:45–48* , 2000.
Vargas, L.C., Marques, T.A., Schenberg, L.C. «Micturition and defensive behaviors are controlled by distinct neural networks within the dorsal periaqueductal gray and deep gray layer of the superior colliculus of the rat.» *Neurosci. Lett., 280* , 2000: 45-48.
Veinante, P., Stoeckel, M.E., Freund-Mercier, M.J. «GABA- and peptide-immunoreactivities co-localize in the rat central extended amygdala.» *Neuroreport 8: 2985-2989*, 1997.
Verberne, A.J.M., Lewis, S.J., Worland, P.J., Beart, P.M., Jarrott, B., Christie, M.J., Louis, W.J. «Medial prefrontal cortical lesions modulate baroreflex sensitivity in the rat.» *Brain Res. 426:243–249*, 1987.
Vertes, R.P. «Interactions among the medial prefrontal cortex, hippocampus and midline thalamus in emotional and cognitive processing in the rat.» *Neuroscience 142:1-20*, 2006.
Vertes, R.P., Hoover, W.B., Szigeti-Buck, K., Leranth, C. «Nucleus reuniens of the midline thalamus: link between the medial prefrontal cortex and the hippocampus.» *Brain research bulletin 71:601-609*, 2007.
Vervliet, B., Indekeu, E. «Low-cost avoidance behaviors are resistant to fear extinction in humans.» *Frontiers in Behavioral Neuroscience*, 2015.
Vianna, D.M., Brandao, M.L. «Anatomical connections of the periaqueductal gray: specific neural substrates for different kinds of fear.» *Brazilian journal of medical and biological research 36: 557-566*, 2003.
Vianna, D.M., Landeira-Fernandez, J., Brandão, M.L. «Dorsolateral and ventral regions of the periaqueductal gray matter are involved in distinct types of fear.» *Neurosci. Biobehav. Rev. 25*, 2001: 711–719.
Vidal-Gonzalez, I., Vidal-Gonzalez, B., Rauch, S. L., Quirk, G. J. «Microstimulation reveals opposing influences of prelimbic and infralimbic cortex on the expression of conditioned fear.» *Learn. Mem. 13, 728–733*, 2006.
Vidal-Gonzalez, I., Vidal-Gonzalez, B., Rauch, S.L., Quirk, G.J. «Microstimulation reveals opposing influences of prelimbic and infralimbic cortex on the expression of conditioned fear.» *Learn Mem. 13(6): 728-33*, 2006 .

Viviani, D., Charlet, A., ven den Burg, E., Robinet, C., Hurni, N., Abatis, M., Magara, F., Stoop, R. «Oxytocin selectively gates fear responses through distinct outputs from the central amygdala.» *Science 333: 104–107*, 2011.

Viviani, D., Stoop, R. «Opposite effects of oxytocin and vasopressin on the emotional expression of the fear response.» *Prog. Brain Res. 170: 207–218*, 2008.

Vogt, B.A., Vogt, L., Farber, N.B., Bush, G. «Architecture and neurocytology of monkey cingulate gyrus.» *J. Comp. Neurol. 485:218–239*, 2005.

Voorn, P., Vanderschuren, L.J.M.J., Groenewegen, H.J., Robbins, T.W., Pennartz, C.M.A. «Putting a spin on the dorsal-ventral divide of the striatum.» *Trends Neurosci 27:468–474*, 2004.

Waller, B.M., Cray, Jr., James, J., Burrows, A.M. «Selection for universal facial emotion.» *Emotion, 8(3), 435-439*, 2008.

Wang, L., Chen, I.Z., Lin, D. «Collateral pathways from the ventromedial hypothalamus mediate defensive behaviors.» *Neuron*, 2015: 1344-1358.

Wang, M.Y., Lu, F.M., Hu, Z., Zhang, J., Yuan, Z. «Optical mapping of prefrontal brain connectivity and activation during emotion anticipation.» *Behavioural Brain Research* , 2018.

Wang, Y., Gupta, A., Toledo-Rodriguez, M., Wu, C.Z., Markram, H. « Anatomical, physiological, molecular and circuit properties of nest basket cells in the developing somatosensory cortex.» *Cereb Cortex 12:395–410*, 2002.

Wang, Y., Toledo-Rodriguez, M., Gupta, A., Wu, C., Silberberg, G., Luo, J., Markram, H. «Anatomical, physiological and molecular properties of Martinotti cells in the somatosensory cortex of the juvenile rat.» *J. Physiol. 561:65–9*, 2004.

Wassum, K.M., Izquierdo, A. «The basolateral amygdala in reward learning and addiction.» *Neurosci. Biobehav. Rev. 57:271-83*, 2015.

Watson, J.B. «Pychology as the Behaviorist views it.» *Psychological Review, 20, 158-177*, 1913.

Weiskrantz, L. «Behavioral changes associated with ablation of the amygdaloid complex in monkeys.» *J. Comp. Physiol. Psychol. 49, 381–391*, 1956.

Weisskopf, M.G., LeDoux, J.E. «Distinct populations of NMDA receptors at subcortical and cortical inputs to principal cells of the lateral amygdala.» *J. Neurophysiol. 81: 930–934*, 1999.

Wellman, C.L., Izquierdo, A., Garrett, J.E., Martin, K.P., Carroll, J., Millstein, R., Lesch, K.P., Murphy, D.L., Holmes, A. «Impaired stress-coping and fear extinction and abnormal corticolimbic morphology in serotonin transporter knock-out mice.» *J. Neurosci., 27* , 2007: 684-691.

Wendlera, E., Gaspara, J.C.C., Ferreira, T.L., Barbieroa, J.K., Andreatinia, R., Vitala, M.A.B.F., Blahac, C.D., Winnd, P., Da Cunha, C. «The roles of the nucleus accumbens core, dorsomedial striatum, and dorsolateral striatum in learning: Performance and extinction of Pavlovian fear-conditioned responses and instrumental avoidance responses.» *Neurobiology of Learning and Memory Vol.109*, 2014.

Wendt, J., Low, A., Weymar, M., Lotze, M., Hamm., A.O. «Active avoidance and attetive freezing in the face of approaching threat .» *NeuroImage*, 2017: 196-204.

West, A.E., Griffith, E.C., Greenberg, M.E. «Regulation of transcription factors by neuronal activity.» *Nature Neuroscience* , 2002.

Wilensky, A.E., Schafe, G.E., Kristensen, M.P., LeDoux, J.E. «Rethinking the fear circuit: the central nucleus of the amygdala is required for the acquisition, consolidation, and expression of Pavlovian fear conditioning.» *J. Neurosci. 26, 12387-12396*, 2006.

Wilensky, A.E., Schafe, G.E., LeDoux, J.E. «Functional inactivation of the amygdala before but not after auditory fear conditioning prevents memory formation.» *J. Neurosci. 19: RC48*, 1999.

Wilensky, A.E., Schafe, G.E., LeDoux, J.E. «The amygdala modulates memory consolidation of fear-motivated inhibitory avoidance learning but not classical fear conditioning.» *The Journal of Neuroscience, 20(18): 7059-7066*, 2000.

Wilson W.J., Ferrara N.C., Blaker A.L., Giddings C.E. «Escape and avoidance learning in the earthworm Eisenia hortensis.» *PeerJ*, 2014.

Wilson-Poe, A.R., Pocius, E., Herschbach, M., Morgan, M.M. «The periaqueductal gray contributes to bidirectional enhancement of antinociception between morphine and cannabinoids.» *Pharmacol. Biochem. Behav.103(3): 444-449*, 2013.

Wolff, S.B., Grundemann, J., Tovote, P., Krabbe, S., Jacobson, G.A., Muller, C., et al. «Amygdala interneuron subtypes control fear learning through disinhibition.» *Nature 509(7501): 453-458*, 2014.

Wood, W., Neal, D.T. «A new look at habits and the habit-goal interface.» *Psychol. Rev. 114, 843-863*, 2007.

Woodruff, A.R., Sah, P. « Inhibition and synchronization of basal amygdala principal neuron spiking by parvalbumin-positive interneurons.» *J. Neurophysiol. 98, 2956-2961*, 2007.

Woodruff, A.R., Sah, P. «Inhibition and synchronization of basal amygdala principal neuron spiking by parvalbumin-positive interneurons.» *J. Neurophysiol. 98, 2956-2961*, 2007.

Wynne L.C., Solomon R.L. «Traumatic avoidance learning: acquisition and extinction in dogs deprived of normal peripheral autonomic function.» *Genet Psychol Monogr 52(2): 241-84*, 1955.

Xia, W., Dymond, S., Lloyd, K., Vervliet, B. «Partial reinforcement of avoidance and resistance to extinction in humans .» *Behaviour Research and Therapy 96* , 2017: 79-89.

Xu, H., Jeong, H. Y., Tremblay, R., Rudy, B. «Neocortical somatostatin-expressing GABAergic interneurons disinhibit the thalamorecipient layer 4.» *Neuron 77, 155–167*, 2013.

Xu, X., Roby, K.D., Callaway, E.M. « Immunochemical characterization of inhibitory mouse cortical neurons: three chemically distinct classes of inhibitory cells.» *J. Comp. Neurol. 518:389–404*, 2010.

Xu, X., Roby, K.D., Callaway, E.M. «Mouse cortical inhibitory neuron type that coexpresses somatostatin and calretinin.» *J. Comp. Neurol. 499:144–160*, 2006.

Xu, X., Scott-Scheiern, T., Kempker, L., Simons, K. «Active avoidance conditioning in zebrafish (Dania rerio).» *Neurobiol Learn Mem.*, 2007.

Yaguez, L., Coen, S., Gregory, L.J., Amaro Jr., E., Altman, C., Brammer, M.J., Bullmore, E.T.,Williams, S.C., Aziz, Q. « Brain response to visceral aversive conditioning: a functional magnetic resonance imaging study.» *Gastroenterology 128, 1819–1829*, 2005.

Yaksh, T.L., Rudy, T.A. «Narcotic analgetics: CNS sites and mechanisms of action as revealed by intracerebral injection techniques.» *Pain, vol. 4, no. 4* , 1978: 299–359.

Yang, F.C., Liang, K. C. «Interactions of the dorsal hippocampus, medial prefrontal cortex and nucleus accumbens in formation of fear memory: difference in inhibitory avoidance learning and contextual fear conditioning.» *Neurobiology of Learning and Memory 112* , 2014: 186–194.

Yang, Y., Wang, J.Z. «From structure to behavior in basolateral amygdala-hippocampus circuits.» *Front. neural circuits*, 2017.

Yankelevitch-Yahav, R., Franko, M., Huly, A., Doron, R. «The forced swim test as a model of depressive-like behavior.» *J. Vis. Exp. 2;(97)*, 2015.

Yasuno, K., Takahashi, E., Igarashi, I., Iguchi, T., Tsuchiya, Y., Kai, K., Mori, K. «Gene expression analysis of Arc mRNA as a neuronal cell activity marker in the hippocampus and amygdala in two-way active avoidance test in rats .» *Journal of pharmacological and toxicological methods* , 2017: 140-146.

Yilmaz, M., Meister, M. «Rapid innate defensive responses of mice to looming visual stimuli .» *Curr Biol 21;23(20): 2011-5*, 2013.

Yin, J.B., Wu, H.H., Dong, Y.L., Zhang, T., Wang, J., Zhang, Y., Wei, Y.Y., Lu, Y.C., Wu, S.X., Wang, W., Li, Y.Q. «Neurochemical properties of BDNF-containing neurons projecting to rostral ventromedial medulla in the ventrolateral periaqueductal gray.» *Front. Neural Circuits*, 2014.

Yizhar, O., Klavir, O. «Reciprocal amygdala-prefrontal interactions in learning.» *Curr. Opin. Neurobiol.* , 2018.

Yu, H., Wang, Y., Pattwell, S., Jing, D., Liu, T., Zhang, Y., Bath, K.G., Lee, F.S. , Chen, Z.Y. «Variant BDNF Val66Met polymorphism affects extinction of conditioned aversive memory.» *J.Neurosci., 29* , 2009: 4056-4064.

Yu, K., Ahrens, S., Zhang, X., Schiff, H.C., Ramakrishnan, C., Fenno, L.E., Deisseroth, K., Zhou, P., Paninski, L., Li, B. «The central amygdala controls learning in the lateral amygdala.» *Nat. Neurosci. 20:1680-1685*, 2017.

Yu, K., da Silva, P.G., Albeanu, D.F., Li, B. «Central amygdala somatostatin neurons gate passive and active defensive behaviors.» *The Journal of Neuroscience, 36(24): 6488–6496*, 2016.

Zaborszky, L., Cullinan, W.E. «Projections from the nucleus accumbens to cholinergic neurons of the ventral pallidum: A correlated light and electron microscopic double-immunolabeling study in rat.» *Brain Res. 570: 92–101*, 1992.

Zalcman, S.S., Siegel, A. «The neurobiology of aggression and rage: role of cytokines .» *Brain Behav. Immun. 20, 507–514*, 2006.

Zangrossi, H.Jr., Graeff, F.G. «Serotonin in anxiety and panic: contributions of the elevated T-maze.» *Neurosci. Biobehav. Rev.*, 2014.

Zanoto De Luca-Vinhas, M.C., Macedo, C.E., Brandao, M.L. «Pharmacological assessment of the freezing, antinociception, and exploratory behavior organized in the ventrolateral periaqueductal gray.» *Pain 121* , 2006: 94–104.

Zanoto De Luca-Vinhas, M.C., Macedo, C.E.,Brandao, M.L. «Pharmacological assessment of the freezing, antinociception, and exploratory behavior organized in the ventrolateral periaqueductal gray.» *Pain 121*, 2006: 94–104.

Zeng, X.S., Geng, W.S., Jia, J.J., Chen, L., Zhang, P.P. «Cellular and Molecular Basis of Neurodegeneration in Parkinson Disease.» *Front. Aging Neurosci.* , 2018.

Zhang, Y., Fukushima, H., Kida, S. «Induction and requirement of gene expression in the anterior cingulate cortex and medial prefrontal cortex for the consolidation of inhibitory avoidance memory .» *Molecular Brain* , 2011.

Zimmerman, J.M., Maren, S. « The central nucleus of the amygdala is essential for acquiring and expressing conditioned fear after overtraining.» *Learn. Mem. 14, 634–644*, 2007.

Zohar, J., Juven-Wetzier, A., Myers, V., Fostick, L. «Post-traumatic stress disorder: facts and fiction.» *Curr Opin Psychiatry 21(1):74-7*, 2008.

You will find in the following attached:

- Rozeske, et al., 2018 paper in which I contributed by performing optogenetic experiments and in-vivo extracellular single-unit recordings in the dmPFC.

- Karalis, et al., 2016 paper in which I performed electromyography (EMG) recordings in the neck's muscles of mice.

Article

Neuron

Prefrontal-Periaqueductal Gray-Projecting Neurons Mediate Context Fear Discrimination

Highlights

- dmPFC units are activated during transitions between fear and non-fear contexts
- l/vlPAG-projecting dmPFC units are activated during context fear discrimination
- Activation of l/vlPAG-projecting dmPFC units is necessary for fear discrimination
- Activation of l/vlPAG-projecting dmPFC units is sufficient for fear discrimination

Authors

Robert R. Rozeske, Daniel Jercog, Nikolaos Karalis, ..., Delphine Girard, Nânci Winke, Cyril Herry

Correspondence

cyril.herry@inserm.fr

In Brief

Using single-unit recording and optogenetic manipulations in a fear-conditioning paradigm, Rozeske et al. demonstrate that activation of a subpopulation of cells in the prefrontal cortex projecting to the periaqueductal gray is necessary and sufficient for context fear discrimination.

Rozeske et al., 2018, Neuron *97*, 898–910
February 21, 2018
https://doi.org/10.1016/j.neuron.2017.12.044

CellPress

CellPress

Neuron
Article

Prefrontal-Periaqueductal Gray-Projecting Neurons Mediate Context Fear Discrimination

Robert R. Rozeske,[1,2,4] Daniel Jercog,[1,2] Nikolaos Karalis,[1,2,3] Fabrice Chaudun,[1,2] Suzana Khoder,[1,2] Delphine Girard,[1,2] Nânci Winke,[1,2] and Cyril Herry[1,2,5,*]

[1]INSERM, Neurocentre Magendie, U1215, 146 Rue Léo-Saignat, 33077 Bordeaux, France
[2]Université de Bordeaux, Neurocentre Magendie, U1215, 146 Rue Léo-Saignat, 33077 Bordeaux, France
[3]Faculty of Medicine, Ludwig-Maximilians-Universität München, 82152 Planegg-Martinsried, Germany
[4]Present address: Department of Psychiatry, Douglas Mental Health University Institute, McGill University, 6875 Blvd. LaSalle, Montréal, QC H4H 1R3, Canada
[5]Lead Contact
*Correspondence: cyril.herry@inserm.fr
https://doi.org/10.1016/j.neuron.2017.12.044

SUMMARY

Survival critically depends on selecting appropriate defensive or exploratory behaviors and is strongly influenced by the surrounding environment. Contextual discrimination is a fundamental process that is thought to depend on the prefrontal cortex to integrate sensory information from the environment and regulate adaptive responses to threat during uncertainty. However, the precise prefrontal circuits necessary for discriminating a previously threatening context from a neutral context remain unknown. Using a combination of single-unit recordings and optogenetic manipulations, we identified a neuronal subpopulation in the dorsal medial prefrontal cortex (dmPFC) that projects to the lateral and ventrolateral periaqueductal gray (l/vlPAG) and is selectively activated during contextual fear discrimination. Moreover, optogenetic activation and inhibition of this neuronal population promoted contextual fear discrimination and generalization, respectively. Our results identify a subpopulation of dmPFC-l/vlPAG-projecting neurons that control switching between different emotional states during contextual discrimination.

INTRODUCTION

The expression of adaptive behavior is critical for the survival of an organism, and it is heavily governed by the surrounding environment (Nadel, 1991). Depending on the perceived threat of an environment, organisms can express a broad spectrum of behaviors, ranging from exploration and foraging to defensive behaviors, including fear and avoidance (LeDoux, 2000; Maren, 2001). Although defensive behaviors are often adaptive, in humans, pathologic expression of these defensive behaviors is a hallmark of anxiety disorders (Bonne et al., 2004; McCullough et al., 2016; Rosen and Schulkin, 1998). To develop novel treatments for clinical populations, an understanding of the fundamental circuits and mechanisms governing transitions between exploratory and defensive behaviors during periods of contextual uncertainty is necessary.

It is well documented that the encoding and retrieval of contextual memories rely on pattern completion and separation processes within the hippocampal formation (Kim et al., 1993; Knierim and Neunuebel, 2016; Maren et al., 2013; Rudy and O'Reilly, 2001); however, the mechanisms underpinning behavioral selection among different environments remain unknown. Interestingly, anatomical and physiological data indicate that the dorsal medial prefrontal cortex (dmPFC) receives neuronal projections from the hippocampus (Cenquizca and Swanson, 2007; Hoover and Vertes, 2007; Jay and Witter, 1991). Moreover, the dmPFC is recruited during periods of uncertainty (Antoniadis and McDonald, 2006; Burgess et al., 2001; Hyman et al., 2012; Ma et al., 2016; Mobbs et al., 2007; Sharpe and Killcross, 2015; Xu and Südhof, 2013; Yoshida and Ishii, 2006), and it is critical for the regulation of emotional memory (Bukalo et al., 2015; Courtin et al., 2014; Dejean et al., 2016; Likhtik et al., 2014; Livneh and Paz, 2012; Milad and Quirk, 2002; Motzkin et al., 2015; Rozeske et al., 2015; Sotres-Bayon and Quirk, 2010). In particular, the dmPFC projects to both the basolateral amygdala (BLA) and the lateral and ventrolateral periaqueductal gray (l/vlPAG) (Floyd et al., 2000; Mcdonald et al., 1996; Vertes, 2004; Vianna and Brandão, 2003), two critical structures for the acquisition and expression of fear behavior (De Oca et al., 1998; Kim et al., 1993; Nader et al., 2001; Tovote et al., 2016; Vianna et al., 2001). Thus, the dmPFC is well positioned to integrate contextual information (Cenquizca and Swanson, 2007; Hoover and Vertes, 2007; Jay and Witter, 1991) and select appropriate emotional behavior (Del Arco et al., 2017; Karlsson et al., 2012; Yoshida and Ishii, 2006) during periods of ambiguity.

In rodents, environmental control of adaptive behavior can be investigated using contextual fear conditioning, in which an aversive stimulus is associated with a particular context. Following conditioning, rodents exhibit high levels of freezing behavior due to the perceived threat of that context (Blanchard and Blanchard, 1969), a response that is absent when exposed to a context sufficiently different from the conditioned one, a

A

Day 1	Day 2	Days 3 & 4	Day 7
Baseline	Fear conditioning	Tests 1 & 2	Test 3
Context D	Context A	Contexts A or ABCA'	Contexts A or CAC'A'
5 min	9 min	12 min	12 min

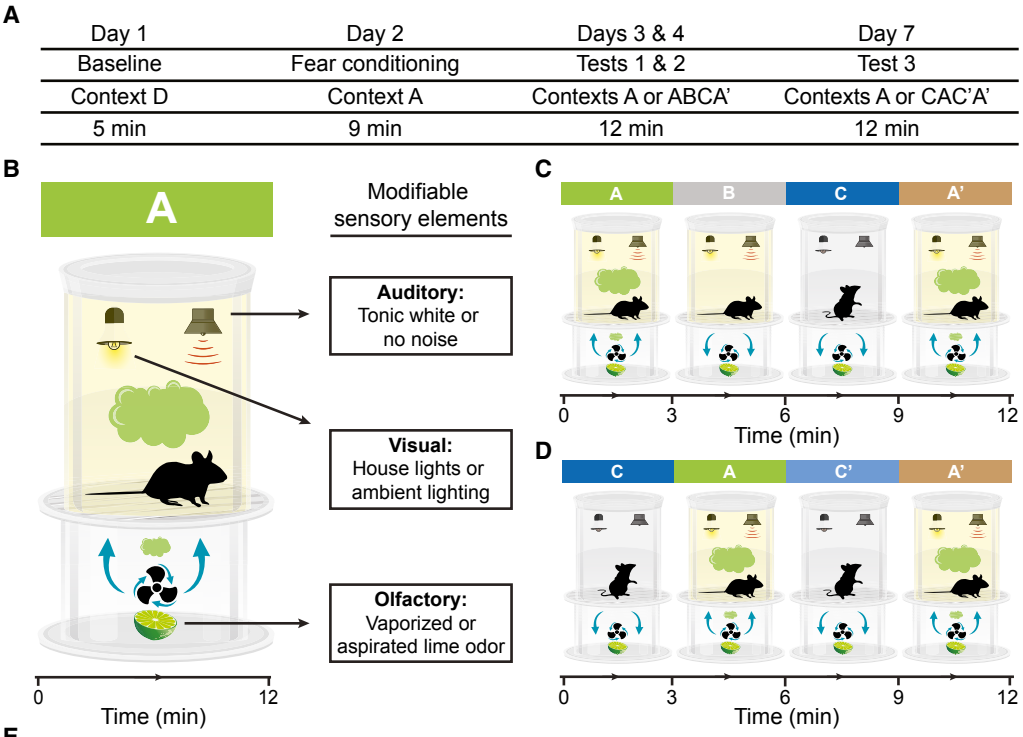

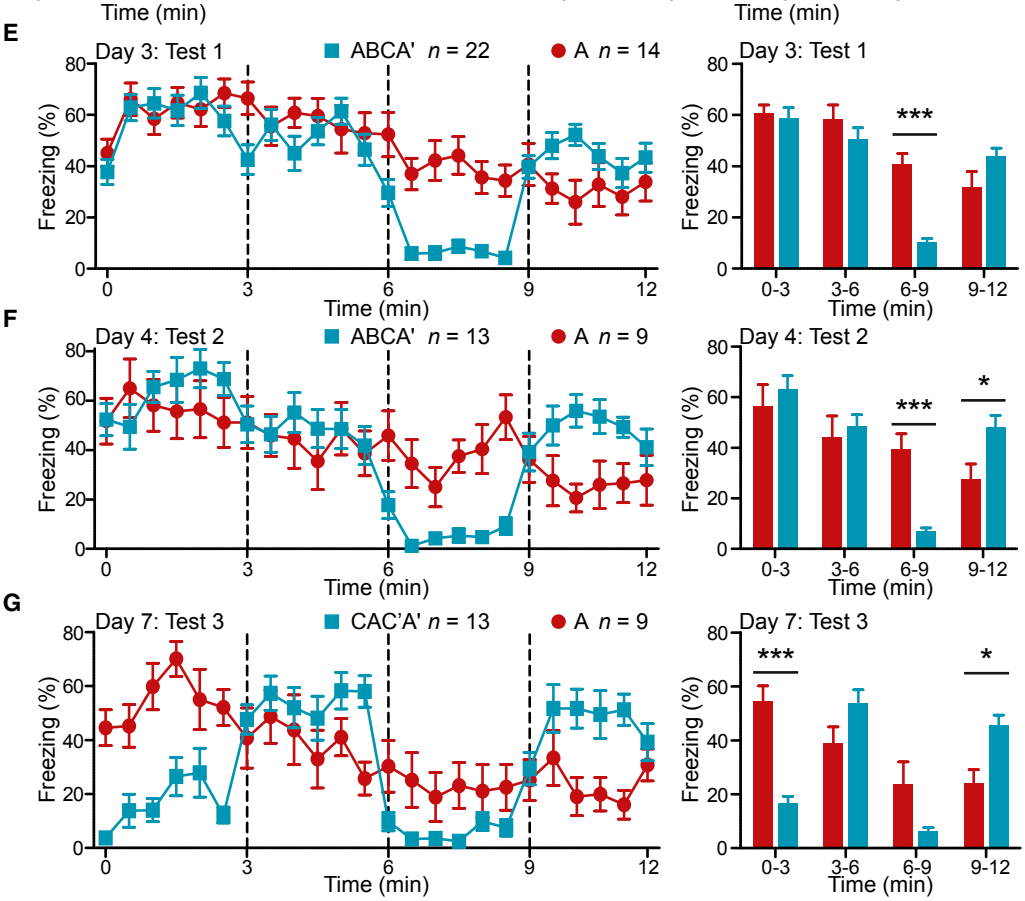

(legend on next page)

process termed contextual fear discrimination (Frankland et al., 1998). It has been previously shown that pharmacological prefrontal lesion or blockade of prefrontal synaptic transmission prevented contextual fear discrimination (Antoniadis and McDonald, 2006; Xu and Südhof, 2013). However, to date, the precise prefrontal circuits involved in discriminating a previously threatening context from a neutral context are virtually unknown.

Here we developed a novel contextual fear discrimination paradigm in which the rodent remains undisturbed during a series of context presentations. During context fear expression and discrimination, we used single-unit recordings to monitor changes in activity within the dmPFC. This approach was combined with optogenetic and antidromic electrical identification of dmPFC neurons projecting to the BLA or l/vlPAG to determine the precise neuronal circuits that control the selection of appropriate behavioral responses during contextual fear discrimination. Finally, optogenetic manipulations were used to investigate the role of specific dmPFC circuits during context fear discrimination. We found that dmPFC single-unit activity was modulated during switching between threatening and non-threatening contexts. Moreover, we identified a subpopulation of dmPFC neurons projecting to the l/vlPAG that controlled freezing behavior during context fear discrimination.

RESULTS

Behavioral Expression of Context Fear Discrimination

To evaluate the contribution of dmPFC neurons in contextual fear discrimination, we developed an innovative contextual fear-conditioning paradigm in which the conditioning context is sequentially transformed into distinct contexts during testing. In this paradigm, following fear conditioning, we tested mice for contextual fear in the same physical chamber while contextual features were rapidly modified to create generalized and discriminated contexts (Figures 1A–1D). In a first set of experiments, mice were exposed to a suite of four sequentially transformed contexts, termed configuration ABCA' (Figure 1C). This consisted of successive 3 min exposures to first the original conditioning context A, then to context B, followed by context C, and back to the original conditioning context, A'. Sensory elements were manipulated to create different contexts as follows: (1) context A contained lime odor, tonic white noise, and house lights; (2) context B was identical to A, except no lime odor was delivered; (3) context C was identical to B, except lighting was altered to ambient levels and tonic white noise was turned off; and (4) context A' was identical to A.

In these conditions, mice exhibited high contextual fear in contexts A, B, and A' while showing virtually no contextual fear in context C (group ABCA'; Figure 1E). This gradient of fear behavior was not observed in mice exposed to context A for 12 min (group A; Figure 1E), nor was it attributable to pre-conditioning levels of immobility or differences in the acquisition of context fear (Figures S1A–S1C). To assess whether fear discrimination during context C was due to novelty, order, or timing effects of context presentations, a subset of mice was re-exposed 24 hr later to configuration ABCA' and 72 hr later to configuration CAC'A' (Figure 1D). Consistent with our previous observation, mice exhibited contextual fear discrimination in context C during exposure to configurations ABCA' and CAC'A', compared to control mice (Figures 1F and 1G). Importantly, contextual fear discrimination in context C could not be attributed to a low associability of this context with foot shock conditioning (Figures S1D and S1E). Furthermore, pre-exposure to configuration ABCA' before conditioning was not associated with changes in basal contextual fear levels (Figures S1F–S1I), revealing the specificity of the behavioral changes observed upon post-conditioning ABCA' exposure.

dmPFC Unit Population Activity Encodes Context Transitions

To identify dmPFC activity changes related to contextual fear discrimination, we performed single-unit recordings in the anterior cingulate and prelimbic cortices of the dmPFC in freely behaving mice submitted to our behavioral paradigm (Figures 2A and S2A–S2F). We evaluated whether the switch between high- and low-fear states during contextual fear discrimination was represented in the firing activity of dmPFC neurons (Figure 2B). To identify if the firing of dmPFC neurons contained context-related information, we performed population analyses

Figure 1. Modifying Sensory Elements Controls Contextual Fear Expression

(A) Experimental protocol.

(B) Schematic depiction of the paradigm developed to study contextual fear discrimination. Auditory, visual, and olfactory sensory elements were manipulated to produce contexts that more, or less, resembled the conditioned context. The conditioned context A contained tonic white noise, house lights, and vaporized lime odor. Control mice were tested for 12 min in context A.

(C) Configuration ABCA' consisted of 3 min sequential exposures to four contexts while the mouse remained in the same testing chamber. Context B was identical to context A except the lime odor was aspirated from the testing chamber. Context C was the most distinct from context A, specifically the audible white noise was removed, the house lights were dimmed, and the lime odor was aspirated. Context A' was identical to context A.

(D) Configuration CAC'A' was used to assess timing effects of context C presentation. Context C' was identical to C and all other contexts were as described previously.

(E and F) Left: dynamics of freezing behavior 24 hr (E) and 48 hr (F) after conditioning for mice tested in configuration ABCA' and control mice tested in configuration A (bin size = 30 s; day 3: ABCA' group, n = 22; A group, n = 14; day 4: ABCA' group, n = 13; A group, n = 9). Right: corresponding average freezing values during context exposure 24 hr (E) and 48 hr (F) after conditioning reveal robust freezing behavior in contexts A, B, and A' and a significant reduction in freezing behavior in mice exposed to context C compared to controls (day 3: two-way repeated-measures ANOVA [RM ANOVA], $F_{(3, 102)} = 13.09$, $p < 0.0001$; day 4: two-way RM ANOVA, $F_{(3, 60)} = 11.96$, $p < 0.0001$, Bonferroni multiple comparison post hoc tests). Testing in configuration ABCA' on day 4 was to assess novelty effects of context C.

(G) Left: dynamics of freezing behavior 5 days after conditioning for mice tested in configuration CAC'A' and control mice tested in configuration A (bin size = 30 s; day 7: CAC'A' group, n = 13; A group, n = 9). Right: corresponding average freezing values during context exposure are shown. Context C produced fear discrimination independently of timing, and presentation of context A' produced a robust renewal of freezing (two-way RM ANOVA, $F_{(3, 60)} = 29.58$, $p < 0.0001$, Bonferroni multiple comparison post hoc tests). Data are expressed as mean ± SEM (*$p < 0.05$ and ***$p < 0.001$).

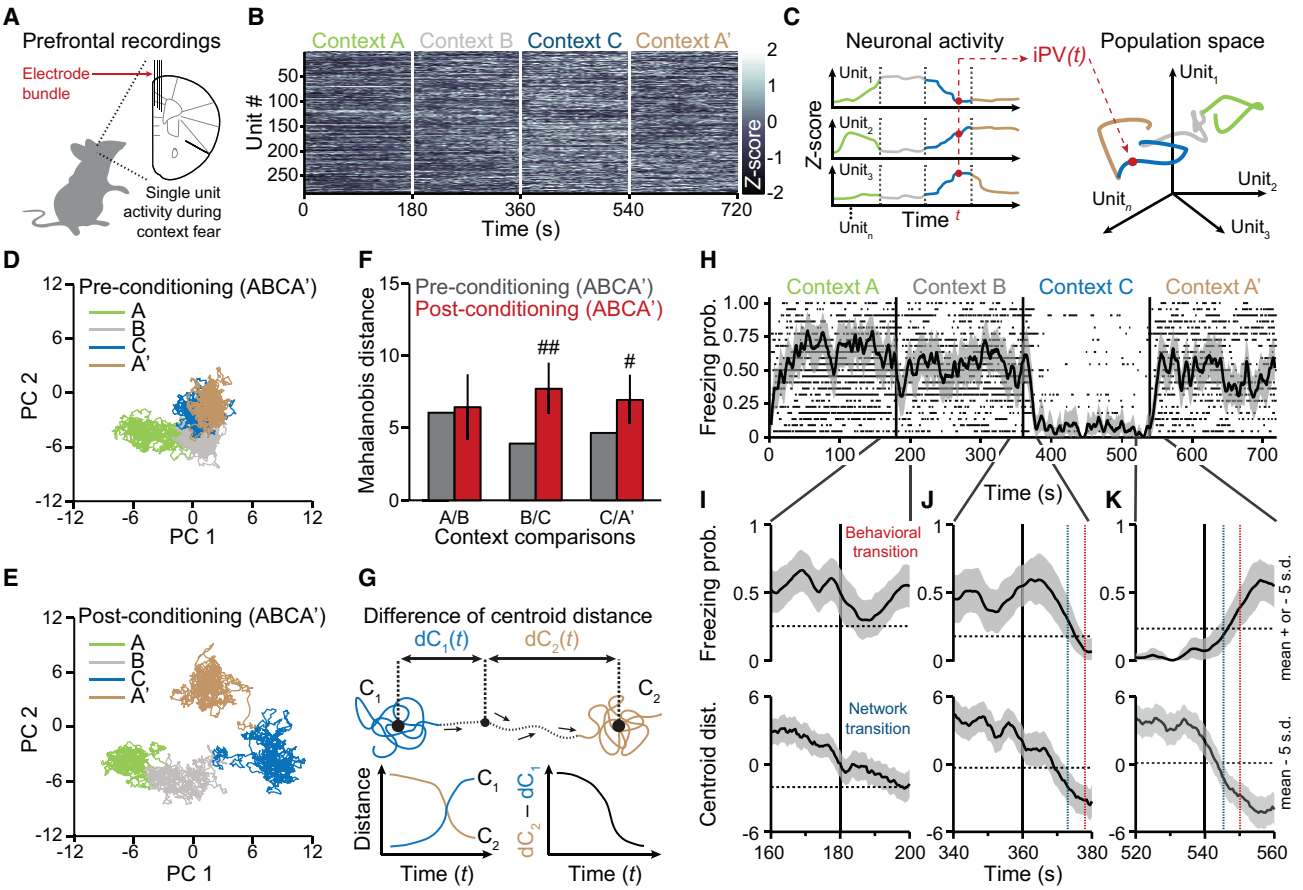

Figure 2. Involvement of the dmPFC during Contextual Fear Discrimination and Context Transitions

(A) A schematic representing single-unit recordings in the dmPFC during context fear behavior.

(B) A heatmap of neuronal activity during exposure to configuration ABCA' (n = 285 units; bin size = 5 s).

(C) A schematic of the method used for population analysis. Left: the heterogeneous activity of *n* recorded units during behavior is normalized by *Z* score, and the instantaneous population vector (iPV; STAR Methods) is calculated for units 1 through *n* from time 0 to *t*. Right: each unit represents one dimension in an *n*-dimensional population space with the color-coded iPV.

(D) Principal component analysis (PCA)-based two-dimensional (2D) projection of the iPV for dmPFC units recorded during exposure to configuration ABCA' before conditioning (n = 60 units).

(E) PCA-based 2D projection of the iPV for dmPFC units recorded during contexts ABCA' after conditioning (n = 285 units).

(F) Quantification of Mahalanobis distances in the full dimensional space among A/B, B/C, and C/A' contexts for the pre- and post-conditioning groups using the resampling procedure (STAR Methods). Exposure to contexts ABCA' following conditioning differentially engaged the dmPFC population as compared to pre-conditioning exposure.

(G) Schematic of the method used to analyze context transitions. Top: the Euclidean distance (d) between the iPV at a given time (*t*) and the centroids of two neuronal population clusters, contexts C_1 and C_2, is calculated. Bottom left: distances between iPV and C_1 or C_2 centroids are then plotted as a function of time. Bottom right: the difference of the iPV distance between C_1 and C_2 centroids is finally plotted as a function of time.

(H) Raster plot of individual freezing epochs for all mice during post-conditioning ABCA'. Superimposed is the probability of freezing (n = 22 mice).

(I) Top: transition between contexts A and B was not associated with a significant change in the probability of freezing. Bottom: transition between contexts A and B was not associated with a significant change in dmPFC network activity. Dotted black horizontal lines in top and bottom panels indicate significance thresholds (mean ± 5 SD).

(J) Transition between contexts B and C was associated with a significant reduction in freezing probability (top) and a significant alteration in dmPFC population activity (bottom). Dotted red vertical line indicates time of significant change in freezing probability, and dotted blue vertical line indicates time of significant change in dmPFC population activity.

(K) Transition between contexts C and A' was associated with a significant increase in freezing probability (top) and a significant change in dmPFC population activity (bottom). Data are expressed as mean ± 95% confidence interval, so an absence of overlap indicates significance ($^{\#}p < 0.05$ and $^{\#\#}p < 0.01$ based on the confidence interval).

to evaluate the ensemble activity of dmPFC neurons during ABCA' exposure before and after fear conditioning (Figures 2C–2E). This analysis revealed that during pre-conditioning exposure to ABCA', the dmPFC neuronal population was largely undifferentiated, as revealed by minor changes in the Mahalanobis distance between clusters representing individual contexts

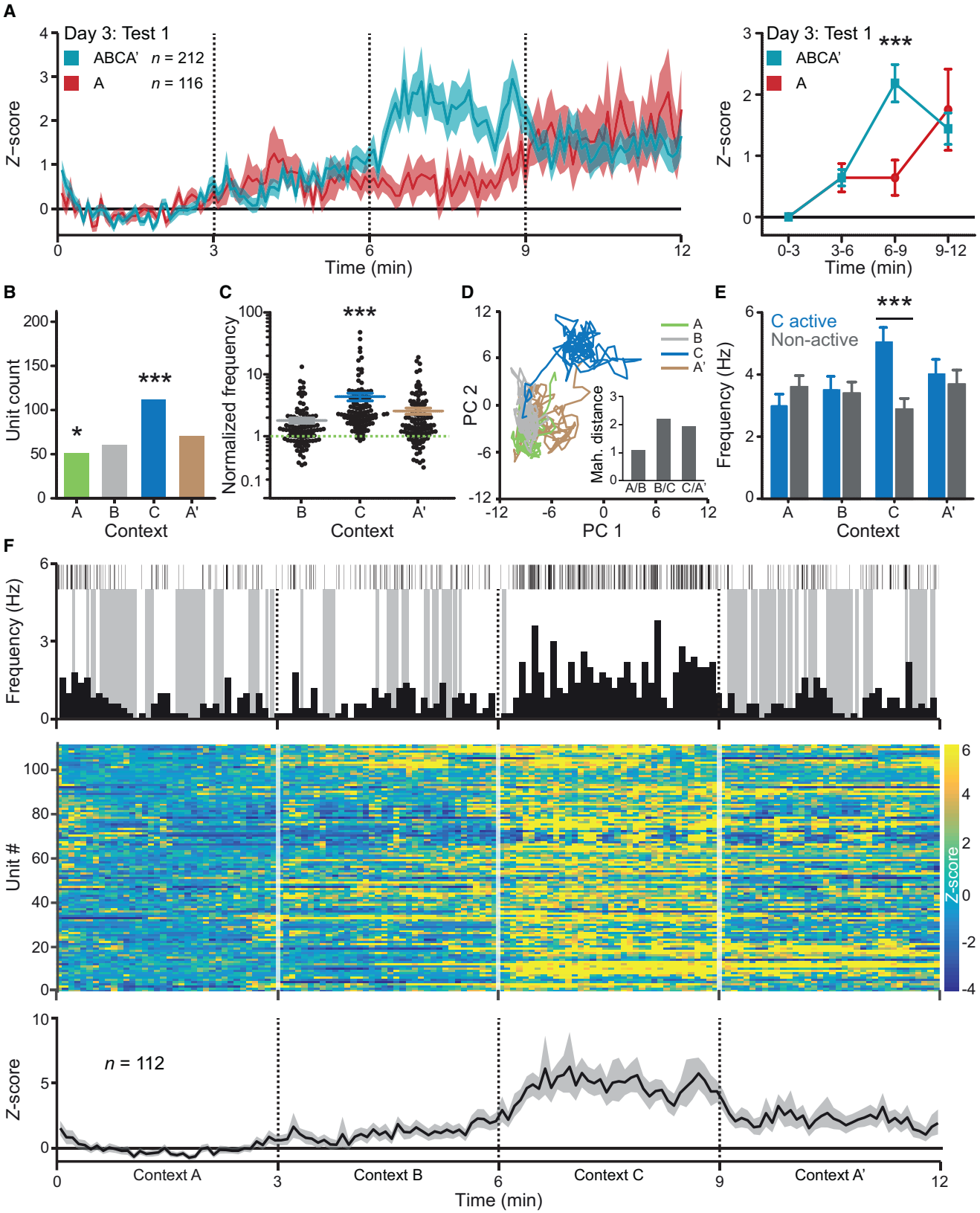

(legend on next page)

(Figures 2D and 2F). In contrast, following conditioning, we observed an expansion of Mahalanobis distances between context clusters associated with switching between high- and low-fear states (from B to C and C to A'), a phenomenon not observed for contextual transitions between the two high-fear contexts A and B (Figures 2E and 2F). Strikingly, we observed that the overall activity profile of dmPFC neurons during context A' at the end of the session was significantly different compared to context A. This instability is in line with previous reports of gradual shifts in the contextual representation across dmPFC populations (Hyman et al., 2012). However, during the pertinent time point when mice transitioned from context B to C, we observed significant changes in the Mahalanobis distance when comparing ABCA' to conditioned control mice exposed to context A for 12 min (Figures S3A and S3B), demonstrating that transition from high- to low-fear contexts dominantly alters the dmPFC neuronal representation compared to the passage of time or unstable dmPFC representations evoked by context reinstatement. Moreover, we controlled that the neuronal representation of context was not biased by a particular animal (Figure S3F).

Next, to evaluate the temporal relationship of dmPFC neuronal changes at the population level and the animal's behavioral state during periods of contextual transitions, we identified time points when significant changes in freezing behavior and dmPFC network activity were present (Figures 2G and 2H). Our results indicated that the transition between high-fear contexts A and B was not associated with significant alterations in freezing behavior or network activity around the transition period (Figures 2H and 2I). In contrast, context transitions associated with switching between high- and low-fear states were characterized by substantial changes in dmPFC network activity, followed by a significant change in freezing behavior (Figures 2H, 2J, and 2K). Importantly, these context transition-induced alterations in dmPFC network states were absent in non-conditioned mice exposed to configuration ABCA' or post-conditioning control mice only exposed to context A (Figures S3G–S3N). Together these data strongly suggest that transitions between high and low contextual fear states, regardless of directionality, are represented in dmPFC population activity.

Context Transitions Activate Principal Neurons in the dmPFC

This previous observation raises the question as to whether a dmPFC neuronal subpopulation is selectively activated during contextual fear discrimination in context C. Single-unit firing rate analyses revealed that dmPFC putative excitatory principal neurons (PNs, n = 212) exhibited a strong increase in firing activity in the discriminative context C (Figure 3A), a phenomenon not observed in mice only exposed to context A (PNs, n = 116) or for dmPFC putative interneurons (Figure S2G). Moreover, this increase in firing activity in context C was not due to sensory alterations of the contexts (Figure S2H). Importantly, neuronal activity in mice exposed to contexts A, B, and A' was not different from control animals, suggesting selective dmPFC PN modulation during contextual fear discrimination (Figure 3A).

We subsequently investigated if subpopulations of dmPFC PNs were activated during contextual discrimination using a bootstrap-resampling approach (Figures S4A and S4B; STAR Methods). This analysis revealed that ~50% (n = 112/212) of significantly activated dmPFC PNs exhibited an increase in firing activity during contextual discrimination in context C when freezing behavior was minimal (Figures 3B, 3C, and 3F). We obtained an analogous result using a more conservative analysis that identified dmPFC PNs exclusively activated in a single context (Figures S4C and S4D). Additionally, we observed that only a minority of PNs had reduced activity during context C (Figure S4E). Importantly, to determine whether the increased firing rate of dmPFC PNs activated in context C was due to locomotion, we correlated locomotor activity with firing rate of dmPFC neurons significantly activated during context C (PNs, n = 112) and the units that were significantly activated in context C and kept from the baseline recording session (PNs, n = 26). Our results indicated that the vast majority of dmPFC PNs active in context C, or active in context C and recorded during baseline session, were not significantly correlated with the locomotion of the animal (n = 103/112, 91.96% and n = 20/26, 76.92%, respectively; Figures S4F and S4G).

Finally, we performed population analysis of dmPFC PNs significantly active in context C that was restricted to non-freezing periods throughout ABCA' exposure. This analysis

Figure 3. A Subpopulation of dmPFC PNs Is Significantly Activated during Contextual Fear Discrimination

(A) Left: firing rate dynamics of dmPFC PNs (bin size = 5 s) during contexts ABCA' (n = 212 units) and control group context A for 12 min (n = 116 units), normalized to 0–3 min. Right: corresponding average dmPFC PN firing rate 24 hr after conditioning reveals a significant increase in firing activity in context C compared to the control group (Wilcoxon rank-sum tests, $p < 0.001$, Bonferroni multiple comparison post hoc test).

(B) Bootstrap-resampling method used to identify neurons significantly active in a context. Among the neurons selected, a larger fraction than expected by chance was highly active in context C (two-tailed binomial test, $p < 0.0001$, Bonferroni multiple comparison post hoc test), whereas a smaller fraction than expected by chance was highly active in context A (two-tailed binomial test, $p < 0.05$, Bonferroni multiple comparison post hoc test).

(C) The firing rates of PNs selected by the bootstrap method as significantly active in context C were elevated in C compared to contexts B and A' (Friedman's rank test, $p < 0.0001$, Dunn's multiple comparison post hoc test).

(D) PNs selected by the bootstrap method as significantly active in context C (n = 112) with activity restricted to non-freezing periods in the 2D PCA space. Inset: analysis in the full dimensional space revealed a 2-fold increase in Mahalanobis distances for context C in comparison to contexts A/B.

(E) Firing rate of PNs restricted to non-freezing periods during ABCA'. PNs selected by the bootstrap method as active during context C (C active) displayed a selective and significantly higher firing rate in context C as compared to contexts A, B, and A' (Friedman's rank test, $p < 0.0001$, Dunn's multiple comparison post hoc test). Firing rate for C active PNs was also significantly elevated compared to units not selected by the bootstrap method as active in context C (non-active) for all contexts (Wilcoxon rank-sum tests, $p < 0.0001$, Bonferroni multiple comparison post hoc test).

(F) Top: representative firing rate of a PN selected by the bootstrap method as highly active in context C (bin size = 5 s). Gray bars represent freezing epochs and at the top is a raster plot of firing rate. Middle: heatmap of the normalized firing activity (Z score) of all PNs selected by the bootstrap method as highly active in context C is shown (bin size = 5 s). Bottom: mean firing activity of all PNs that were selected by the bootstrap method as significantly active during context C is shown (bin size = 5 s). Data are expressed as mean ± SEM (*$p < 0.05$ and ***$p < 0.001$).

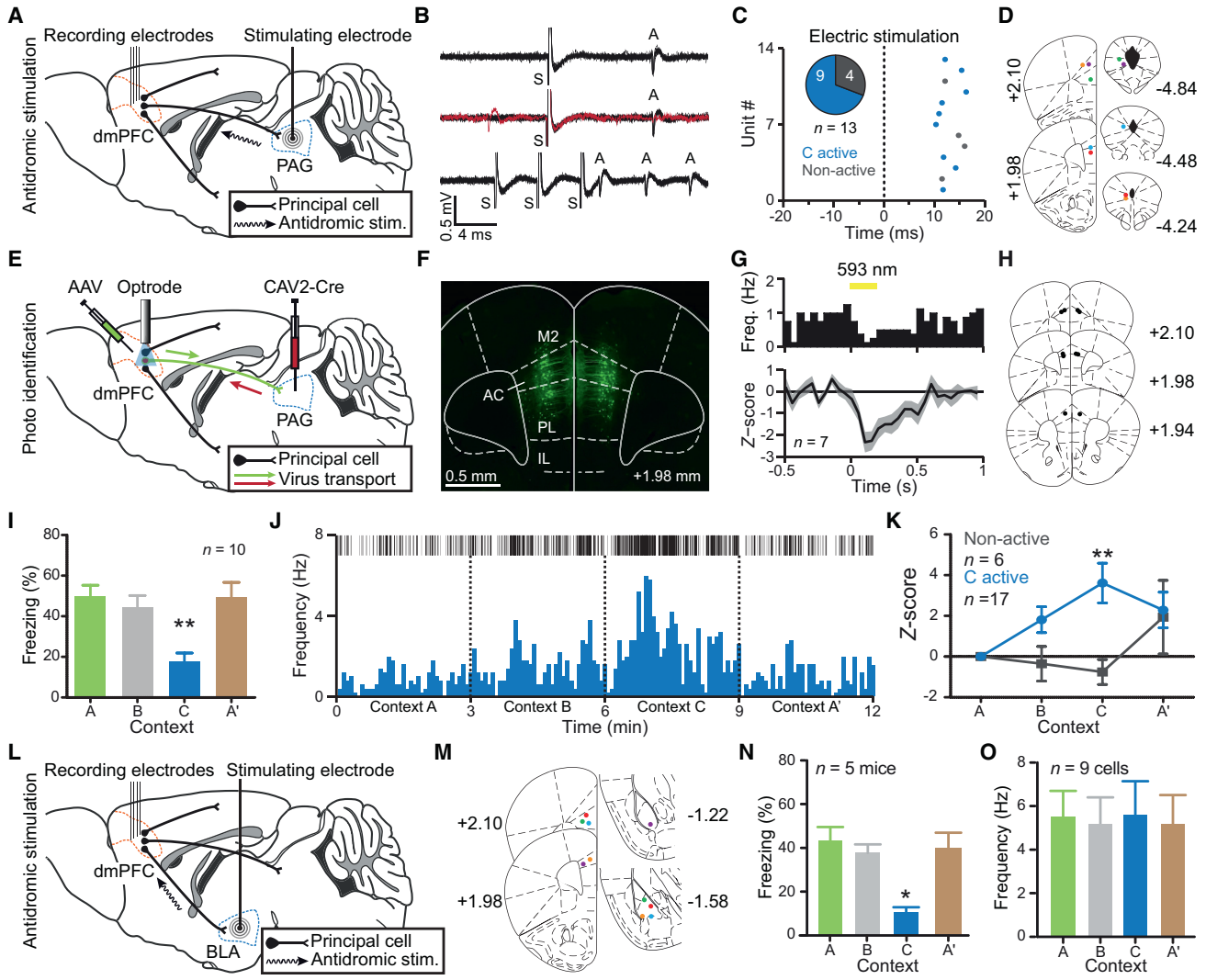

Figure 4. Identification of the dmPFC-l/vlPAG Pathway Activated during Contextual Fear Discrimination

(A) A schematic of electric antidromic stimulation method used to identify dmPFC-l/vlPAG-projecting neurons.

(B) Top and middle: antidromic spikes recorded in the dmPFC following stimulation in the l/vlPAG (10 superimposed traces) demonstrating fixed latency and high fidelity. S, stimulation artifact; A, antidromic spike. The red trace illustrates a collision between a spontaneously occurring and an antidromic spike. Bottom: antidromic spikes were recorded in the dmPFC following high-frequency stimulation (250 Hz) in the l/vlPAG (10 superimposed traces).

(C) Distribution of spike latencies for antidromically identified dmPFC-l/vlPAG units. Inset: pie chart illustrates the proportion of antidromically identified dmPFC-l/vlPAG units that were context C active (C active) and not active in context C (non-active).

(D) Left: schematic of electrolytic lesion sites of dmPFC recordings in mice (n = 5) with antidromically identified neurons. Right: lesion sites of antidromically stimulated sites in the l/vlPAG are shown. Corresponding recording sites in the dmPFC and lesion sites in the l/vlPAG are color coded. Numbered labels indicate distance (mm) relative to bregma.

(E) A schematic of the intersectional infection strategy for photo-identification.

(F) Expression of GFP in dmPFC-l/vlPAG-projecting neurons using the intersectional infection strategy.

(G) Top: representative peristimulus time histogram (PSTH) of light-evoked inhibition of a dmPFC-l/vlPAG unit. Bottom: averaged PSTH (*Z* score) of dmPFC-l/vlPAG units inhibited during 200 ms of yellow light stimulation is shown (n = 7 neurons, bin size = 50 ms).

(H) Termination sites of optic fiber tips for photo-identification of dmPFC neuron experiments. All optrodes (n = 5) were implanted in the left hemisphere. Numbered labels indicate distance (mm) relative to bregma.

(I) Average freezing behavior during configuration ABCA' in mice used for electric and photo-identification. Mice showed contextual fear discrimination in context C compared to contexts A, B, and A' (n = 10 mice; one-way RM ANOVA, $F_{(3, 27)} = 8.820$, $p < 0.001$, Bonferroni multiple comparison post hoc test).

(J) Representative dmPFC photo-identified PN that was active during context C (bin size = 5 s). At the top is a raster of the firing rate.

(K) Among the photo- and antidromically identified dmPFC-l/vlPAG-projecting neurons, the majority (n = 17/23) displayed significantly elevated firing during context C (Wilcoxon rank-sum tests, $p < 0.001$, Bonferroni multiple comparison post hoc test).

(L) A schematic of electric antidromic stimulation method used to identify dmPFC-BLA-projecting neurons.

(legend continued on next page)

revealed that the network state during non-freezing periods in context C was associated with a 2-fold increase in Mahalanobis distance compared to that in contexts A/B (Figure 3D). Moreover, firing rates during non-freezing periods for PNs significantly activated in context C were significantly elevated compared to non-freezing periods in contexts A, B, and A', as well as to neurons not significantly activated in context C (Figure 3E). These data indicate that contextual fear discrimination is represented in the population activity of dmPFC PNs significantly activated in context C. All together our results strongly suggest that a subset of dmPFC PNs mediates contextual fear discrimination through a sharp increase in their firing activity.

A Subpopulation of dmPFC Units Active during Context Fear Discrimination Project to the l/vlPAG

We next used two complementary strategies to evaluate the connectivity of dmPFC neurons significantly activated in context C to the l/vlPAG and the BLA, two structures critical for fear expression (Floyd et al., 2000; Mcdonald et al., 1996; Vertes, 2004; Vianna and Brandão, 2003). In one group of mice, we antidromically activated dmPFC efferents using electrical extracellular stimulation of l/vlPAG in anesthetized mice, following the completion of behavior (Figures 4A–4D). In a second group, we used an intersectional infection strategy to photo-identify dmPFC-l/vlPAG-projecting neurons. For this purpose, mice were injected with a retrogradely transported canine adenovirus type 2 expressing Cre-recombinase (CAV2-Cre) in the l/vlPAG. Mice were then injected with a conditional adeno-associated viral vector (AAV) encoding for archaerhodopsin (ArchT) locally into the dmPFC such that opsin expression was restricted to dmPFC PNs projecting to l/vlPAG (Figures 4E–4H, S5A, S6A, and S6B). In these animals, optrodes for simultaneous single-unit recording and optogenetic identification were implanted in the dmPFC. We found that the vast majority of dmPFC PNs projecting to the l/vlPAG that were identified using antidromic stimulation of the l/vlPAG or photo-identification approaches (n = 17/23, 73.91%; 9 PNs using antidromic stimulation and 8 PNs using photo-identification approaches) displayed a significantly higher firing activity in context C when freezing levels were low (Figures 4I–4K), a phenomenon that was absent from dmPFC PNs projecting to the BLA (Figures 4L–4O). Together, these data indicate that dmPFC PNs active during contextual fear discrimination preferentially project to the l/vlPAG, where they could directly regulate conditioned fear responses.

Optogenetic Manipulation of the dmPFC-to-l/vlPAG Circuit Alters Context Fear Discrimination

To evaluate if the changes in the firing activity of dmPFC-l/vlPAG-projecting neurons were causally related to contextual fear discrimination, CaMKIIα-Cre mice received intra-dmPFC injections of a conditional AAV encoding for ArchT or channelrhodopsin-2 (ChR2), and optic fibers were placed dorsal of the l/vlPAG (Figures 5A, S5C, S5D, and 6A). In a subset of injected CaMKIIα-Cre mice in which optrodes were implanted in the l/vlPAG, we observed that photoactivated and inhibited l/vlPAG neurons displayed homogeneous electrophysiological properties (Figures 5B–5E). Moreover, optogenetic inhibition or activation of dmPFC inputs to the l/vlPAG was associated with a decrease and increase of l/vlPAG unit firing activity, respectively (Figures 5F and 5G). These results thereby confirmed that our optogenetic strategy was efficient in blocking or facilitating dmPFC excitatory inputs to the l/vlPAG. Optogenetic inhibition or activation of dmPFC inputs to the l/vlPAG before contextual fear conditioning did not produce any light-induced changes in freezing or locomotor behavior in comparison to GFP control animals (Figures 6B, 6C, 6E, and S5E–S5G). Moreover, opsin-expressing and control mice displayed similar levels of freezing behavior during conditioning to context A (Figures S5H and S5I). Interestingly, photo-inhibition of dmPFC inputs to the l/vlPAG applied during exposure to context C, 24 hr following conditioning, prevented contextual fear discrimination when compared to GFP controls (Figure 6D). Conversely, optical activation of dmPFC inputs to the l/vlPAG when mice were exposed to the threatening contexts A or B reduced contextual fear behavior (Figures 6F, S5J, and S5K).

To control that optogenetic manipulations within the midbrain were specific to the l/vlPAG, and not due to activation of *en passant* dmPFC fibers, we used an intersectional strategy in which mice were injected with CAV2-Cre in the l/vlPAG and a Cre-dependent AAV encoding either ArchT or ChR2 in the dmPFC, and later optic fibers were implanted in the dmPFC (Figures S6A–S6C). Our results indicated that specific inhibition of the dmPFC-l/vlPAG pathway prevented contextual fear discrimination, whereas optical activation reduced contextual freezing (Figure S6D). Moreover, to evaluate whether these findings were specific to our contextual discrimination paradigm, we performed optogenetic activation or inhibition of the dmPFC-l/vlPAG pathway in a classical auditory fear-conditioning and extinction paradigm associated with high- and low-freezing levels. Following conditioning, optogenetic activation of the dmPFC-l/vlPAG pathway did not reduce freezing levels. Conversely, following extinction learning, optogenetic inhibition of the dmPFC-l/vlPAG pathway did not increase freezing levels (Figures S6E and S6F). Finally, to control that reduced freezing behavior upon light activation of dmPFC PNs in context B did not simply generate escape or avoidance fear behavior, mice were submitted to a place avoidance task in which they could actively avoid the compartment in which they received optical stimulation of dmPFC PNs projecting to the l/vlPAG. Our analyses revealed that optogenetic stimulation did not produce place aversion (Figures S6G–S6J), indicating that reduced freezing upon light activation of dmPFC PNs projecting to the l/vlPAG in

(M) Left: location of recording sites in the dmPFC for BLA antidromic stimulation (n = 5 mice). Right: lesions of antidromically stimulated sites in the BLA are shown. Numbered labels indicate distance from bregma (mm). Recording and corresponding antidromic stimulation sites are color coded.
(N) Freezing behavior during configuration ABCA' of mice submitted to the antidromic identification of dmPFC-BLA-projecting neurons revealed fear discrimination during context C (one-way ANOVA, $F_{(3, 12)} = 5.886$, $p < 0.05$, Bonferroni multiple comparison post hoc test difference between context C versus A and A').
(O) The firing rates of identified dmPFC-BLA-projecting neurons (n = 9 cells) were similar in contexts A, B, C, and A' (one-way ANOVA, $F_{(3, 24)} = 0.375$, $p > 0.05$).
Data are expressed as mean ± SEM (*$p < 0.05$ and **$p < 0.01$).

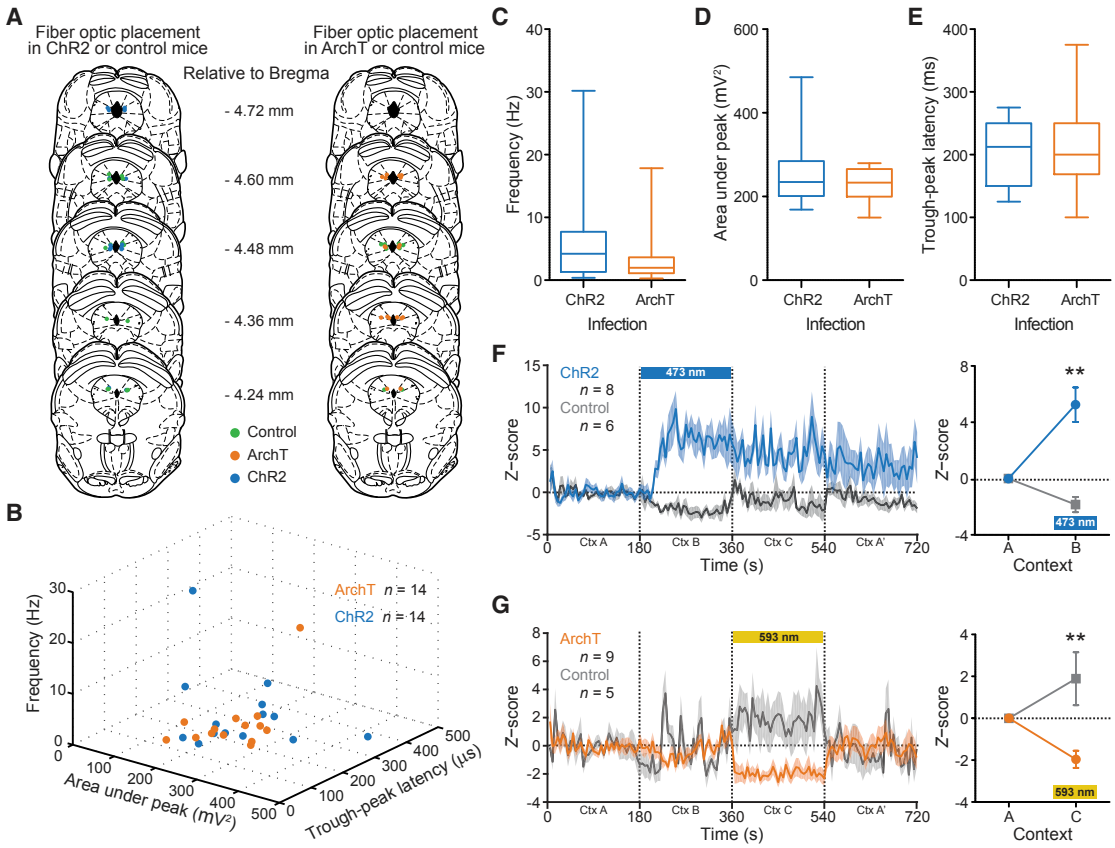

Figure 5. Photo-Stimulation of dmPFC Axon Terminals in l/vlPAG Modulates Unit Activity

(A) Left: placement of fiber optic tips in mice expressing ChR2 or GFP controls in the dmPFC-l/vlPAG pathway. Right: placement of fiber optic tips in mice expressing ArchT or GFP controls in the dmPFC-l/vlPAG pathway is shown.

(B) A subset of mice expressing ArchT or ChR2 in the dmPFC-l/vlPAG pathway was implanted with optrodes, and l/vlPAG single units were recorded. Units recorded were plotted based on the following extracellular electrophysiological properties: firing frequency, trough-peak latency, and the area under the peak of the spike waveform.

(C) No significant differences were observed in the firing frequency of l/vlPAG units recorded in ArchT- or ChR2-expressing mice (Wilcoxon rank-sum test, $p > 0.05$).

(D) Comparison of area under the peak revealed no difference between ChR2- and ArchT-expressing mice (unpaired t test, $t_{(26)} = 1.17$, $p > 0.05$).

(E) Trough-peak latency was compared between ChR2- and ArchT-expressing mice and no differences were found (unpaired t test, $t_{(26)} = 0.0787$, $p > 0.05$).

(F) Left: over half (8/14, 57%) of l/vlPAG units were excited during pre-synaptic 473-nm photo-stimulation (bin size = 5 s, baseline to context A). Right: blue light photo-stimulation significantly increased l/vlPAG unit activity in a subset of light-activated cells compared to non-light-activated cells (Wilcoxon rank-sum test, $p < 0.01$, Bonferroni multiple comparison post hoc test).

(G) Left: mice implanted with optrodes in the l/vlPAG and expressing ArchT in the dmPFC-l/vlPAG pathway received 593 nm photo-stimulation. Over half of l/vlPAG units (9/14, 64%) were inhibited following yellow light (bin size = 5 s, baseline to context A). Right: yellow light stimulation to pre-synaptic terminals significantly reduced l/vlPAG unit activity in a subset of light-inhibited cells compared to non-light-inhibited cells (Wilcoxon rank-sum test, $p < 0.01$, Bonferroni multiple comparison post hoc test). Box-and-whisker plots represent the median, interquartile range, and extreme values; other data are expressed as mean ± SEM (**$p < 0.01$).

context A or B was not due to augmented escape or avoidance behavior. All together, these results demonstrate that the increased activity of dmPFC PNs projecting to the l/vlPAG is a necessary and sufficient condition to drive the expression of contextual fear discrimination.

DISCUSSION

A dmPFC-to-l/vlPAG Circuit for Context Fear Discrimination

Using single-unit recordings and optogenetic manipulations in a novel behavioral paradigm, we demonstrated that contextual fear discrimination is dynamically represented in the firing activity of a subpopulation of dmPFC neurons projecting to the l/vlPAG. Moreover, our results indicate that the elevated firing activity of this neuronal subpopulation is both a necessary and sufficient condition for contextual fear discrimination. In classical contextual fear generalization and discrimination studies, animals are usually conditioned in a given context and subsequently transferred to variant contexts, which precludes investigating the precise neuronal changes occurring during contextual transitions. Our behavioral paradigm goes beyond these limitations by manipulating contextual features while the rodent remains in the same physical environment.

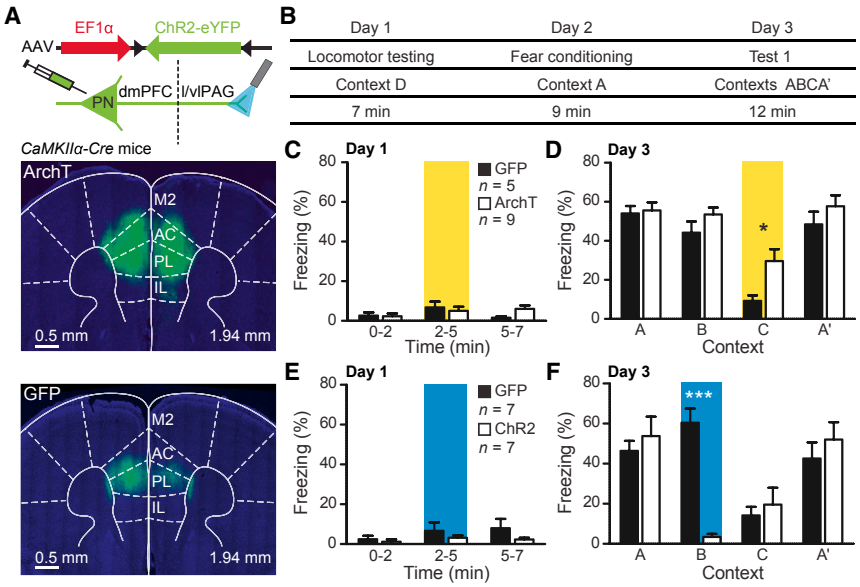

Figure 6. Optogenetic Manipulation of dmPFC-l/vlPAG Neurons Controls Contextual Fear Expression

(A) Top: schematic describing infection and optogenetic strategy. Middle and bottom: images of GFP labeling in the dmPFC of a CaMKIIα-Cre mouse expressing ArchT (middle) or GFP (bottom).

(B) Experimental protocol.

(C) Freezing behavior during yellow light activation before fear conditioning in control (GFP, n = 5) and ArchT-expressing (n = 9) mice (two-way RM ANOVA, $F_{(2, 24)} = 3.00$, $p > 0.05$).

(D) Freezing behavior of the same mice following yellow light activation during context C 24 hr following conditioning (two-way RM ANOVA for context, $F_{(3, 36)} = 25.61$, $p < 0.0001$, Bonferroni multiple comparison post hoc test).

(E) Freezing behavior during blue light activation before fear conditioning in GFP control (n = 7) and ChR2-expressing (n = 7) mice (Wilcoxon rank-sum tests, $p > 0.05$).

(F) Freezing behavior of the same mice following blue light activation during context B 24 hr following conditioning (two-way RM ANOVA, $F_{(3, 36)} = 19.47$, $p < 0.0001$, Bonferroni multiple comparison post hoc test). Data are expressed as mean + SEM (*$p < 0.05$ and ***$p < 0.001$).

This model allowed us to investigate the changes in dmPFC firing activity during contextual transitions, and it revealed that the overall changes in firing activity of dmPFC neurons precedes behavioral expression of context-dependent high- and low-fear states, independently of transition directionality. Importantly, our results also indicated that the increased activity of dmPFC-l/vlPAG-projecting PNs is highly specific of contextual fear discrimination, as it was not influenced by locomotor activity, sensory elements, order, or timing effect of the context presentations.

An alternative hypothesis is that this elevated activity is simply suppressing freezing behavior. However, several pieces of evidence suggest that this was not the case. First, when considering non-freezing intervals in all contexts, we observed that the neuronal representation of context C was significantly different from other contexts, and this was also accompanied by a significant increase in firing rate during non-freezing periods, compared to other contexts (Figures 3D and 3E). Moreover, when the optogenetic manipulation of the dmPFC-l/vlPAG pathway was performed in high- or low-fear conditions in behavioral paradigms different from our contextual fear discrimination paradigm, we failed to observe any effect of the stimulation (Figures S6E and S6F). This strongly suggests that (1) the effect we observed upon optogenetic activation or inhibition of the dmPFC-l/vlPAG pathway is specific to our contextual fear discrimination paradigm and (2) our findings are specifically related to contextual fear discrimination as opposed to the suppression of fear behavior. Additionally, we also observed that, within the entire dmPFC population, elevated PN activity was not concomitant with low fear behavior (Figure 3A) but rather could also reflect the passage of time (Hyman et al., 2012; MacDonald et al., 2011; Manns et al., 2007; Naya and Suzuki, 2011), as observed in both A and ABCA' groups.

Our experiments used a 3 min context exposure to assess fear conditioning. Accordingly, optogenetic manipulations investigating the necessity of the dmPFC-l/vlPAG pathway in context fear discrimination were temporally identical. However, appropriate caution is warranted when using prolonged light administration for photosilencing (Mahn et al., 2016). Our study did not assess intracellular activity during yellow light delivery; therefore, we cannot exclude the possibility that mice expressing ArchT had elevated presynaptic excitatory postsynaptic current (EPSC) activity. However, our photo-inhibition of dmPFC CaMKII+ cells led to reduced firing activity of postsynaptic l/vlPAG single units (Figure 5), suggesting that our silencing protocol was effective.

Comparisons to Other Fear-Conditioning Paradigms

Interestingly, whereas classical cued fear-conditioning studies reported elevated dmPFC neuronal activity during fear expression (Burgos-Robles et al., 2009; Chang et al., 2010; Courtin et al., 2014; Fitzgerald et al., 2014), our data revealed increased activity of dmPFC projections to the l/vlPAG, but not BLA, concurrent with low-fear expression during discrimination in context C. These data suggest that dmPFC projections targeting the l/vlPAG or BLA are differentially recruited during cued or contextual fear expression. Previous studies examining the dmPFC during fear behavior have correlated PN activity with conditioned auditory stimuli (CSs) (Courtin et al., 2014; Likhtik et al., 2014), but they did not examine the physiology of CS-responsive units during contextual fear behavior. This leaves the open question of whether separate circuits exist in the dmPFC that are responsive to auditory CSs and that support context fear discrimination.

Previous studies examining fear discrimination between auditory CSs have also found engagement of the dmPFC. For example, when mice were fear-conditioned to discriminate

between CS^+ and CS^- auditory cues, a selective synchrony of theta oscillations was observed between the dmPFC and BLA in mice that were able to discriminate between CSs (Likhtik et al., 2014). Interestingly, similar engagement of the BLA was observed in non-human primates during discrimination tasks (Resnik and Paz, 2015). In contrast to the abovementioned reports, our data did not identify a dmPFC-to-BLA circuit that was preferentially engaged during context fear discrimination. However, the absence of dmPFC-BLA engagement during our paradigm could be attributed to several factors. As discussed earlier, it remains to be resolved whether separate dmPFC circuits support the expression of freezing following cue and context fear conditioning. Additionally, differential context fear conditioning was not used in the present fear discrimination paradigm. Therefore, mice were never conditioned to context C in the absence of electric shock, which would preclude a safety learning framework for the interpretation of our results.

To date, the mechanisms leading to the activation of dmPFC-l/vlPAG-projecting neurons during fear discrimination are unclear but could be related to excitatory hippocampal or thalamic inputs (Knierim and Neunuebel, 2016; Rudy and O'Reilly, 2001; Xu and Südhof, 2013; Yassa and Stark, 2011). Alternatively, disinhibitory mechanisms, which have been previously found in the cortex (Courtin et al., 2014; Letzkus et al., 2011; Pi et al., 2013), could also lead to dmPFC activation during context fear discrimination, although in this study we did not observe preferential activity of cortical interneurons during fear discrimination. Moreover, it will be important in future studies to investigate how dmPFC PNs interact with l/vlPAG microcircuits during contextual fear discrimination and whether this circuit overlaps with central amygdala (CeA)-PAG circuits mediating cued fear behavior (Tovote et al., 2016). It is, however, very likely that contextual fear conditioning and discrimination recruit different neuronal circuits compared to those recruited during cued fear expression, as recently suggested (Tovote et al., 2016; Xu et al., 2016).

Synaptic Targets of dmPFC Units in the l/vlPAG

Currently, the synaptic targets within the l/vlPAG of dmPFC units active during fear discrimination are unknown. Nevertheless, previous studies investigating the microcircuity within the PAG (Tovote et al., 2016) reveal that defensive behavior is governed by two major cell types expressing glutamate decarboxylase 2 (Gad2+) and vesicular glutamate transporter 2 (Vglut2+). The existence of these two cell types in the l/vlPAG suggests several hypotheses that could explain how activation of the dmPFC-l/vlPAG pathway leads to low-fear states during contextual fear discrimination. A likely possibility is that inhibitory CeA and excitatory dmPFC afferents impinge upon the very same Gad2+ neurons in the l/vlPAG. Thus, activation of CeA inhibitory inputs during cued fear expression would lead to fear responses, as already documented (Tovote et al., 2016), whereas the activation of dmPFC excitatory inputs would induce the opposite effect, that is, a low-fear state. Alternatively, it is still possible that dmPFC excitatory inputs could also project onto Vglut2+ cells in the l/vlPAG directly involved in the reduction of fear behavior, although, to date, the activation of Vglut2+ cells in the l/vlPAG has only been linked to fear expression (Tovote et al., 2016).

In summary, our findings together indicate that the dmPFC encodes contextual changes and becomes active during switching between emotional states. Moreover, specific manipulation of dmPFC-l/vlPAG-projecting neurons is a necessary and sufficient condition to produce context fear discrimination. Future studies investigating this pathway could consider targeting this circuit for therapeutic strategies to treat contextual fear generalization, a core symptom of anxiety disorders.

STAR★METHODS

Detailed methods are provided in the online version of this paper and include the following:

- KEY RESOURCES TABLE
- CONTACT FOR REAGENT AND RESOURCE SHARING
- EXPERIMENTAL MODEL AND SUBJECT DETAILS
- METHOD DETAILS
  - Behavior
  - Surgery and recordings
  - Single unit analyses
  - Virus injections and optogenetics
  - Histological analyses
- QUANTIFICATION AND STATISTICAL ANALYSIS
- DATA AND SOFTWARE AVAILABILITY

SUPPLEMENTAL INFORMATION

Supplemental Information includes six figures and can be found with this article online at https://doi.org/10.1016/j.neuron.2017.12.044.

ACKNOWLEDGMENTS

We thank the members of the Herry laboratory for lively discussions and critical comments on the manuscript. We thank B. Frank for graphic design assistance, T.C.M. Bienvenu and H. Wurtz for histological guidance, A. Thomazeau and F. Dolbeault for technical assistance, and K. Deisseroth and E. Boyden for generously sharing materials. Microscopy was done in the Bordeaux Imaging Center of the CNRS-INSERM and Bordeaux University, member of France BioImaging. This work was supported by grants from the French National Research Agency (ANR-10-EQPX-08 OPTOPATH and LABEX BRAIN ANR 10-LABX-43), the Foundation for Medical Research (FRM, DEQ20170336748), the NRJ Foundation (R15021GG), and the European Research Council (ERC) under the European Union's Seventh Framework Program (FP7/2007-2013)/ERC grant agreement 281168.

AUTHOR CONTRIBUTIONS

C.H., D.J., N.K., and R.R.R. analyzed the behavioral and electrophysiological data. F.C., R.R.R., and S.K. performed behavioral experiments. D.G., F.C., N.W., and R.R.R. performed histology. C.H. and R.R.R. designed the experiments and wrote the paper.

DECLARATION OF INTERESTS

The authors declare no competing interests.

Received: September 14, 2017
Revised: December 7, 2017
Accepted: December 27, 2017
Published: February 1, 2018

REFERENCES

Antoniadis, E.A., and McDonald, R.J. (2006). Fornix, medial prefrontal cortex, nucleus accumbens, and mediodorsal thalamic nucleus: roles in a fear-based context discrimination task. Neurobiol. Learn. Mem. *85*, 71–85.

Blanchard, R.J., and Blanchard, D.C. (1969). Crouching as an index of fear. J. Comp. Physiol. Psychol. *67*, 370–375.

Bonne, O., Grillon, C., Vythilingam, M., Neumeister, A., and Charney, D.S. (2004). Adaptive and maladaptive psychobiological responses to severe psychological stress: implications for the discovery of novel pharmacotherapy. Neurosci. Biobehav. Rev. *28*, 65–94.

Bukalo, O., Pinard, C.R., Silverstein, S., Brehm, C., Hartley, N.D., Whittle, N., Colacicco, G., Busch, E., Patel, S., Singewald, N., and Holmes, A. (2015). Prefrontal inputs to the amygdala instruct fear extinction memory formation. Sci. Adv. *1*, e1500251.

Burgess, N., Becker, S., King, J.A., and O'Keefe, J. (2001). Memory for events and their spatial context: models and experiments. Philos. Trans. R. Soc. Lond. B Biol. Sci. *356*, 1493–1503.

Burgos-Robles, A., Vidal-Gonzalez, I., and Quirk, G.J. (2009). Sustained conditioned responses in prelimbic prefrontal neurons are correlated with fear expression and extinction failure. J. Neurosci. *29*, 8474–8482.

Cenquizca, L.A., and Swanson, L.W. (2007). Spatial organization of direct hippocampal field CA1 axonal projections to the rest of the cerebral cortex. Brain Res. Brain Res. Rev. *56*, 1–26.

Chang, C.H., Berke, J.D., and Maren, S. (2010). Single-unit activity in the medial prefrontal cortex during immediate and delayed extinction of fear in rats. PLoS ONE *5*, e11971.

Courtin, J., Chaudun, F., Rozeske, R.R., Karalis, N., Gonzalez-Campo, C., Wurtz, H., Abdi, A., Baufreton, J., Bienvenu, T.C., and Herry, C. (2014). Prefrontal parvalbumin interneurons shape neuronal activity to drive fear expression. Nature *505*, 92–96.

Cunningham, J.P., and Yu, B.M. (2014). Dimensionality reduction for large-scale neural recordings. Nat. Neurosci. *17*, 1500–1509.

De Oca, B.M., DeCola, J.P., Maren, S., and Fanselow, M.S. (1998). Distinct regions of the periaqueductal gray are involved in the acquisition and expression of defensive responses. J. Neurosci. *18*, 3426–3432.

Dejean, C., Courtin, J., Karalis, N., Chaudun, F., Wurtz, H., Bienvenu, T.C., and Herry, C. (2016). Prefrontal neuronal assemblies temporally control fear behaviour. Nature *535*, 420–424.

Del Arco, A., Park, J., Wood, J., Kim, Y., and Moghaddam, B. (2017). Adaptive encoding of outcome prediction by prefrontal cortex ensembles supports behavioral flexibility. J. Neurosci. *37*, 8363–8373.

Fitzgerald, P.J., Whittle, N., Flynn, S.M., Graybeal, C., Pinard, C.R., Gunduz-Cinar, O., Kravitz, A.V., Singewald, N., and Holmes, A. (2014). Prefrontal single-unit firing associated with deficient extinction in mice. Neurobiol. Learn. Mem. *113*, 69–81.

Floyd, N.S., Price, J.L., Ferry, A.T., Keay, K.A., and Bandler, R. (2000). Orbitomedial prefrontal cortical projections to distinct longitudinal columns of the periaqueductal gray in the rat. J. Comp. Neurol. *422*, 556–578.

Frankland, P.W., Cestari, V., Filipkowski, R.K., McDonald, R.J., and Silva, A.J. (1998). The dorsal hippocampus is essential for context discrimination but not for contextual conditioning. Behav. Neurosci. *112*, 863–874.

González, F., Quinn, J.J., and Fanselow, M.S. (2003). Differential effects of adding and removing components of a context on the generalization of conditional freezing. J. Exp. Psychol. Anim. Behav. Process. *29*, 78–83.

Hoover, W.B., and Vertes, R.P. (2007). Anatomical analysis of afferent projections to the medial prefrontal cortex in the rat. Brain Struct. Funct. *212*, 149–179.

Hyman, J.M., Ma, L., Balaguer-Ballester, E., Durstewitz, D., and Seamans, J.K. (2012). Contextual encoding by ensembles of medial prefrontal cortex neurons. Proc. Natl. Acad. Sci. USA *109*, 5086–5091.

Jackson, A., and Fetz, E.E. (2007). Compact movable microwire array for long-term chronic unit recording in cerebral cortex of primates. J. Neurophysiol. *98*, 3109–3118.

Jay, T.M., and Witter, M.P. (1991). Distribution of hippocampal CA1 and subicular efferents in the prefrontal cortex of the rat studied by means of anterograde transport of Phaseolus vulgaris-leucoagglutinin. J. Comp. Neurol. *313*, 574–586.

Karlsson, M.P., Tervo, D.G., and Karpova, A.Y. (2012). Network resets in medial prefrontal cortex mark the onset of behavioral uncertainty. Science *338*, 135–139.

Kim, J.J., Rison, R.A., and Fanselow, M.S. (1993). Effects of amygdala, hippocampus, and periaqueductal gray lesions on short- and long-term contextual fear. Behav. Neurosci. *107*, 1093–1098.

Knierim, J.J., and Neunuebel, J.P. (2016). Tracking the flow of hippocampal computation: Pattern separation, pattern completion, and attractor dynamics. Neurobiol. Learn. Mem. *129*, 38–49.

LeDoux, J.E. (2000). Emotion circuits in the brain. Annu. Rev. Neurosci. *23*, 155–184.

Legendre, P., and Legendre, L. (1998). Numerical ecology. In Developments in Environmental Modelling (Elsevier).

Letzkus, J.J., Wolff, S.B.E., Meyer, E.M.M., Tovote, P., Courtin, J., Herry, C., and Lüthi, A. (2011). A disinhibitory microcircuit for associative fear learning in the auditory cortex. Nature *480*, 331–335.

Likhtik, E., Stujenske, J.M., Topiwala, M.A., Harris, A.Z., and Gordon, J.A. (2014). Prefrontal entrainment of amygdala activity signals safety in learned fear and innate anxiety. Nat. Neurosci. *17*, 106–113.

Lipski, J. (1981). Antidromic activation of neurones as an analytic tool in the study of the central nervous system. J. Neurosci. Methods *4*, 1–32.

Livneh, U., and Paz, R. (2012). Amygdala-prefrontal synchronization underlies resistance to extinction of aversive memories. Neuron *75*, 133–142.

Ma, L., Hyman, J.M., Durstewitz, D., Phillips, A.G., and Seamans, J.K. (2016). A quantitative analysis of context-dependent remapping of medial frontal cortex neurons and ensembles. J. Neurosci. *36*, 8258–8272.

MacDonald, C.J., Lepage, K.Q., Eden, U.T., and Eichenbaum, H. (2011). Hippocampal "time cells" bridge the gap in memory for discontiguous events. Neuron *71*, 737–749.

Mahn, M., Prigge, M., Ron, S., Levy, R., and Yizhar, O. (2016). Biophysical constraints of optogenetic inhibition at presynaptic terminals. Nat. Neurosci. *19*, 554–556.

Manns, J.R., Howard, M.W., and Eichenbaum, H. (2007). Gradual changes in hippocampal activity support remembering the order of events. Neuron *56*, 530–540.

Maren, S. (2001). Neurobiology of Pavlovian fear conditioning. Annu. Rev. Neurosci. *24*, 897–931.

Maren, S., Phan, K.L., and Liberzon, I. (2013). The contextual brain: implications for fear conditioning, extinction and psychopathology. Nat. Rev. Neurosci. *14*, 417–428.

McCullough, K.M., Morrison, F.G., and Ressler, K.J. (2016). Bridging the gap: towards a cell-type specific understanding of neural circuits underlying fear behaviors. Neurobiol. Learn. Mem. *135*, 27–39.

Mcdonald, A.J., Mascagni, F., and Guo, L. (1996). Projections of the medial and lateral prefrontal cortices to the amygdala: a Phaseolus vulgaris leucoagglutinin study in the rat. Neuroscience *71*, 55–75.

Milad, M.R., and Quirk, G.J. (2002). Neurons in medial prefrontal cortex signal memory for fear extinction. Nature *420*, 70–74.

Mobbs, D., Petrovic, P., Marchant, J.L., Hassabis, D., Weiskopf, N., Seymour, B., Dolan, R.J., and Frith, C.D. (2007). When fear is near: threat imminence elicits prefrontal-periaqueductal gray shifts in humans. Science *317*, 1079–1083.

Motzkin, J.C., Philippi, C.L., Wolf, R.C., Baskaya, M.K., and Koenigs, M. (2015). Ventromedial prefrontal cortex is critical for the regulation of amygdala activity in humans. Biol. Psychiatry *77*, 276–284.

Nadel, L. (1991). The hippocampus and space revisited. Hippocampus *1*, 221–229.

Nader, K., Majidishad, P., Amorapanth, P., and LeDoux, J.E. (2001). Damage to the lateral and central, but not other, amygdaloid nuclei prevents the acquisition of auditory fear conditioning. Learn. Mem. *8*, 156–163.

Naya, Y., and Suzuki, W.A. (2011). Integrating what and when across the primate medial temporal lobe. Science *333*, 773–776.

Pi, H.J., Hangya, B., Kvitsiani, D., Sanders, J.I., Huang, Z.J., and Kepecs, A. (2013). Cortical interneurons that specialize in disinhibitory control. Nature *503*, 521–524.

Resnik, J., and Paz, R. (2015). Fear generalization in the primate amygdala. Nat. Neurosci. *18*, 188–190.

Rosen, J.B., and Schulkin, J. (1998). From normal fear to pathological anxiety. Psychol. Rev. *105*, 325–350.

Rozeske, R.R., Valerio, S., Chaudun, F., and Herry, C. (2015). Prefrontal neuronal circuits of contextual fear conditioning. Genes Brain Behav. *14*, 22–36.

Rudy, J.W., and O'Reilly, R.C. (2001). Conjunctive representations, the hippocampus, and contextual fear conditioning. Cogn. Affect. Behav. Neurosci. *1*, 66–82.

Sharpe, M., and Killcross, S. (2015). The prelimbic cortex uses contextual cues to modulate responding towards predictive stimuli during fear renewal. Neurobiol. Learn. Mem. *118*, 20–29.

Sotres-Bayon, F., and Quirk, G.J. (2010). Prefrontal control of fear: more than just extinction. Curr. Opin. Neurobiol. *20*, 231–235.

Tallone, T., Malin, S., Samuelsson, A., Wilbertz, J., Miyahara, M., Okamoto, K., Poellinger, L., Philipson, L., and Pettersson, S. (2001). A mouse model for adenovirus gene delivery. Proc. Natl. Acad. Sci. USA *98*, 7910–7915.

Tovote, P., Esposito, M.S., Botta, P., Chaudun, F., Fadok, J.P., Markovic, M., Wolff, S.B., Ramakrishnan, C., Fenno, L., Deisseroth, K., et al. (2016). Midbrain circuits for defensive behaviour. Nature *534*, 206–212.

Vertes, R.P. (2004). Differential projections of the infralimbic and prelimbic cortex in the rat. Synapse *51*, 32–58.

Vianna, D.M., and Brandão, M.L. (2003). Anatomical connections of the periaqueductal gray: specific neural substrates for different kinds of fear. Braz. J. Med. Biol. Res. *36*, 557–566.

Vianna, D.M., Graeff, F.G., Brandão, M.L., and Landeira-Fernandez, J. (2001). Defensive freezing evoked by electrical stimulation of the periaqueductal gray: comparison between dorsolateral and ventrolateral regions. Neuroreport *12*, 4109–4112.

Xu, W., and Südhof, T.C. (2013). A neural circuit for memory specificity and generalization. Science *339*, 1290–1295.

Xu, C., Krabbe, S., Grundemann, J., Botta, P., Fadok, J.P., Osakada, F., Saur, D., Grewe, B.F., Schnitzer, M.J., Callaway, E.M., and Lüthi, A. (2016). Distinct hippocampal pathways mediate dissociable roles of context in memory retrieval. Cell *167*, 961–972.e16.

Yassa, M.A., and Stark, C.E. (2011). Pattern separation in the hippocampus. Trends Neurosci. *34*, 515–525.

Yoshida, W., and Ishii, S. (2006). Resolution of uncertainty in prefrontal cortex. Neuron *50*, 781–789.

STAR★METHODS

KEY RESOURCES TABLE

REAGENT or RESOURCE	SOURCE	IDENTIFIER
Antibodies		
CaMKII mouse monoclonal antibody	Abcam	Cat# ab22609, RRID:AB_447192
Alexa 647-conjugated goat anti-mouse antibody	Invitrogen	Cat# A32728, RRID:AB_2633277
Chemicals, Peptides, and Recombinant Proteins		
AAV9-FLEX-ArchT-GFP	UNC Vector Core	Cat# AAV9-FLEX-ArchT-GFP
AAV5-EF1a-DIO-hChR2(H134R)-EYFP	UNC Vector Core	Cat# AAV5-EF1a-DIO-hChR2(H134R)-EYFP
CAV2-Cre retrograde virus	Montpellier Vector Platform	Cat# CAV2-Cre retrograde virus
AAV5-hSyn-mCherry	UNC vector core	Cat# AAV5-hSyn-mCherry
AAV5-FLEX-GFP	UNC Vector Core	Cat# AAV5-FLEX-GFP
Experimental Models: Organisms/Strains		
C57BL6/J wild type mice	C57BL6/J	C57BL6/J mice
B6.Cg-Tg(CaMk2A-cre)T29-1Stl/J mice	Jackson Laboratory	Cat# 005359, RRID: IMSR_JAX:005359
CAV human coxsackie adenovirus receptor mice	Copenhagen University	Cat# Hcar mice
Software and Algorithms		
MATLAB	MathWorks	https://www.mathworks.com/products/matlab.html
Neuroexplorer	Nex Technologies	http://www.neuroexplorer.com/purchase/
GraphPad Prism	GraphPad Software	https://www.graphpad.com/scientific-software/prism/
Offline Sorter	Plexon	https://plexon.com/products/offline-sorter/
Other		
Omnetics 18 pin connectors	Omnetics	Cat# A79042-001
Optic fibers	Thorlabs	Cat# FT200EMT
Custom built optrodes	C. Herry, INSERM, Bordeaux (Courtin et al., 2014)	N/A
593 nm solid state laser	CNI Laser, China	Cat# MGL-FN-593.5
473 nm solid state laser	CNI Laser, China	Cat# MBL-FN-473
1 × 2 fiber optic rotary joint	Doric Lenses	Cat# FRJ_1x2i_FC-2FC_0.22
Omniplex D	Plexon	https://plexon.com/products/omniplex-d-neural-data-acquisition-system-1/
Shuttle box	Imetronic	http://www.imetronic.com/devices/shuttle-box-2/
Morphing context fear conditioning	Imetronic	http://www.imetronic.com/devices/morphing-context-fear-conditioning-3/
Precision animal shocker	Coulbourn Instruments	Cat# H13-15

CONTACT FOR REAGENT AND RESOURCE SHARING

Further information and requests for resources and reagents should be directed to and will be fulfilled by the Lead Contact, Cyril Herry (cyril.herry@inserm.fr).

EXPERIMENTAL MODEL AND SUBJECT DETAILS

Male C57BL6/J mice (3 months old, Janvier), CaMKIIα-Cre mice (3 months old, Jackson Laboratory, B6.Cg-Tg(CaMk2A-cre) T29-1Stl/J), and hCAR mice expressing the CAV human coxsackie adenovirus receptor (hCAR) under the control of a ubiquitous promoter (Tallone et al., 2001) (3 months old) were individually housed for at least 7 days before all experiments, under a 12 h light–dark

cycle, and provided with food and water *ad libitum*. All procedures were performed in accordance with standard ethical guidelines (European Communities Directive 86/60-EEC) and were approved by the committee on Animal Health and Care of Institut National de la Santé et de la Recherche Médicale and French Ministry of Agriculture and Forestry (agreement #A3312001).

METHOD DETAILS

Behavior

Context fear discrimination

Mice were habituated to handling for at least 3 days before experimentation began. Mice that were implanted with recording electrodes in the dmPFC were submitted to the following procedure (Figures 1A–1D). On day 1, a subset of mice were placed in context D (25 × 25 cm square arena) for 5 min to record baseline behavior and neuronal activity. Testing chambers were cleaned with 70% ethanol following all behavioral procedures. On day 2 mice were conditioned to context A (24 × 24 cm diameter cylinder) with 5 scrambled foot shocks delivered via a grid floor (inter-trial interval 60-120 s) lasting 1 s each at an intensity of 0.7 mA (Imetronic). Context A contained tonic white noise (85 dB), vaporized lime odor (3%, Aroma-Zone) delivered via a port located in the floor of the testing chamber, and house lights (53 lux). Behavioral data were automatically collected using infrared beams spaced 1 cm apart in the x and y planes, located at the floor of the testing chamber. Freezing behavior was recorded following the cessation of movement for at least 2 s. Mice were tested in context A or configuration ABCA' on day 3. Mice assigned to configuration ABCA' underwent a suite of four contexts presented for 3 min each, sequentially, while left undisturbed in the testing chamber. Context B was identical to context A, except the lime odor was aspirated from the chamber. Context C was identical to context B, except the tonic white noise was turned off (72 dB), and the house lights dimmed to ambient levels (3 lux), and context A' was identical to context A. We incrementally subtracted sensory elements from the conditioning context as this is the most effective method to produce fear discrimination (González et al., 2003). Mice exposed to context A for 12 min served as controls. Additionally, to control for novelty-associated behavioral phenomena during configuration ABCA', mice were exposed to either configuration ABCA' or context A on day 4. Lastly, to control for timing effects, mice were exposed to configuration CAC'A' or context A on day 7. Context C' was identical to context C. These data were collected in four distinct replicates. An additional experiment was designed to investigate pre- and post-conditioning exposure to configuration ABCA'. Mice were exposed to configuration ABCA' on day 1. The following day mice were conditioned to context A as described above. On day 3 mice were tested in configuration ABCA'. Lastly, to assess the associability of context C with foot shock, mice were fear conditioned to context C with an identical shock protocol as mice conditioned to context A. The following day mice were tested in context C for fear expression.

For optogenetic studies, mice underwent locomotor testing in context D on day 1. Testing on day 1 lasted 7 min with 2-5 min containing photo stimulation. Three minutes of light exposure was chosen as this is the length of a single context exposure during ABCA' testing. Mice were conditioned to context A on day 2, as previously described. On day 3 mice were submitted to configuration ABCA' as previously described. Mice infected with channelrhodopsin-2 (ChR2) and green fluorescent protein (GFP) controls received 10 Hz photo stimulation during context B. Mice infected with archaerhodopsin (ArchT) and GFP controls received 3 min constant photo stimulation during context C. These data were collected in 2 distinct replicates. To control for the generality of the behavioral consequences of photo stimulation of ChR2, mice were submitted to a 9 min exposure to context A and received 10 Hz photo stimulation during 3-6 min. Additionally, to assess the specificity of 10 Hz stimulation, mice infected with ChR2 were tested in configuration ABCA' and received 5 Hz stimulation during context B.

Auditory fear conditioning

A discriminative auditory fear conditioning paradigm was used as previously described (Courtin et al., 2014). On Day 1, mice received 5 CS^+ presentations (30 s, 50 ms pips at 0.9 Hz repeated 27 times, 2 ms rise and fall, pip frequency 7.5 kHz, 80 dB) paired with a US (1 s foot-shock, 0.6 mA). The onset of the US coincided with the offset of the CS^+. The CS^- was presented after each CS^+-US association but was never reinforced (5 CS^- presentations, 30 s, 50 ms pips at 0.9 Hz repeated 27 times, 2 ms rise and fall, pip frequency white noise, 80 dB). The following day, in a different context from that of conditioning, mice were presented with blocks of 4 CS^- and CS^+. Extinction to auditory CS^+ was tested on day 3, where one block of CS^- was presented, followed by 3 blocks of CS^+.

Avoidance behavior

To control that photo stimulation of ChR2 was not producing aversion or escape behavior mice underwent testing in a closed-loop light stimulation avoidance paradigm. Mice underwent 15 min of baseline testing in the avoidance apparatus comprised of 2 compartments (20 × 10 × 14 cm, each) that contained either gray smooth or clear diamond studded plastic flooring (Imetronic). The time spent in each compartment was automatically recorded with infrared beams located near the floor of the testing chamber and mice were assigned to receive photo stimulation in one of the two compartments in a counterbalanced manner. On day 2, mice were tested for 15 min in the avoidance apparatus. The infrared beams detected the location of the mouse and upon complete entry into the photo stimulation-assigned compartment 10 Hz of 473 nm light stimulation was delivered until the mouse completely exited the compartment. On day 3 mice were tested in the avoidance apparatus for 15 min with no photo stimulation.

Locomotion

Locomotor behavior was calculated using beam break counts automatically acquired from infrared beams spaced 1 cm apart in the x and y planes, located at the bottom of the testing chamber. For correlational analysis of single unit activity and locomotion during day 1 baseline and day 3 testing in configuration ABCA', PN spike trains and beam breaks were binned at 2 s (based upon

the criteria for freezing behavior) and correlated over the course of 3 min (Figures S4F and S4G). In the optogenetic manipulations (Figures S5F and S5G) locomotion was assessed by dividing the number of beam breaks per bin by the number of beam breaks during the entire 7 min habituation session. Data were plotted (bin size = 1 min) to illustrate locomotor dynamics, but analyses were performed by the experimental blocks of pre-light stimulation (0-2 min), light stimulation (2-5 min), and post-light stimulation (5-7 min).

Surgery and recordings

Mice were anaesthetized with isoflurane (induction 3%, maintenance 1.75%) in O_2. Body temperature was maintained at 37 °C with a temperature controller system (FHC) and eyes were hydrated with Lacrigel (Europhta Laboratories). Mice were placed in a stereotaxic frame (Kopf Instruments) and 3 stainless steel screws were attached to the skull. Following craniotomy, mice were unilaterally implanted in the left dmPFC with an electrode array at the following coordinates relative to bregma: +1.98 mm AP; −0.35 mm ML; and −1.50 mm DV from dura. The electrode arrays consisted of 16 or 32 individually insulated nichrome wires (13 μm diameter, impedance 30–100 KΩ; Kanthal) fixed to an electrode guide. Depending on the array, the electrode bundle was attached to either one or two 18-pin connectors (Omnetics). Connectors were referenced/grounded via a silver wire (127 μm diameter, A-M Systems) placed above the cerebellum. All implants were secured using Super-Bond cement (Sun Medical). During surgery long- and short-lasting analgesic agents were injected (Metacam, Boehringer; Lurocaïne, Vetoquinol). After surgery mice were allowed to recover for at least 7 days. Electrodes were connected to a headstage (Plexon) containing sixteen unity-gain operational amplifiers. Each headstage was connected to a 16-channel PBX preamplifier (gain 1000 × , Plexon) with bandpass filters at 300 Hz and 8 kHz. Spiking activity was digitized at 40 kHz and isolated by time-amplitude window discrimination and template matching using an Omniplex system (Plexon). At the conclusion of the experiment, electrolytic lesions were administered before transcardial perfusion to verify electrode tip location using standard histological techniques.

Single unit analyses

Single-unit spike sorting was performed using Offline Sorter software (Plexon) and analyzed using Neuroexplorer (Nex Technologies) and MATLAB (MathWorks) for all behavioral sessions. Waveforms were manually defined while visualizing in a three-dimensional space using principal components, timing, and voltage features of the waveforms. A single unit was defined as a cluster of waveforms that formed a discrete, isolated, cluster in the feature space, and did not contain spikes with a refractory period less than 1 ms, based upon auto-correlation analyses. Additionally, multivariate ANOVA and J3 statistics were used to quantify separation of clusters in the principal component space. Cross-correlation analyses were performed to control that a single unit was not recorded on multiple channels. Target neurons that displayed a peak of activity when the reference neuron fired were considered duplicates and only a single neuron was considered for analysis. Units that met these criteria were separated into putative inhibitory interneurons (INs) and putative excitatory principal neurons (PNs) using a hierarchical cluster algorithm based on Ward's method. Briefly, the Euclidian distance was calculated between all unit pairs based on the three-dimensional space defined by each neuron's average trough to peak latency, firing rate, and the area under the peak of the spike waveform. An iterative agglomerative procedure was then used to combine neurons into groups based on the matrix of distances in the feature space so that the total number of groups was reduced to produce the minimal within-group sum of square deviation. Comparisons of firing rate among ABCA' and context A groups on day 3 was normalized to the first 3 minutes of testing as both experimental groups were in context A during that period. Firing rates during non-freezing periods were obtained by calculating the minimum duration of ''non-freezing'' across contexts for each mouse. For each context and each mouse, random 2 s samples (1,000 repetitions) from non-freezing periods, for a total duration of the minimum non-freezing duration, were selected. The random sampling produced an empirical distribution of the non-freezing firing rates and the average firing rate across these samples was calculated for each unit. This procedure controlled for the variable duration of non-freezing periods and allowed direct comparison of the firing rate of units across contexts and animals. To assess unit stability between baseline (day1) and fear expression (day 3) recordings, the waveforms recorded on each day were averaged and then correlated. Correlations with r values greater than 0.97 were considered stable units (Jackson and Fetz, 2007).

Antidromic identification

Following behavioral testing in configuration ABCA', mice were anesthetized with urethane (1.4 g kg^{-1}) and secured in a stereotaxic frame. Concentric stimulating electrodes (FHC) were lowered in the PAG at the following coordinates relative to bregma, −4.55 mm AP; −0.60 mm ML; −1.45 to −1.80 mm DV from dura and into the BLA, −1.70 mm AP; −3.10 mm ML; −3.80 to −4.60 mm DV from dura. During electric identification the stimulation electrodes were advanced in steps of 2 μm by a motorized micromanipulator (FHC) and evoked responses were recorded in the dmPFC. Stimulation-induced and spontaneous spikes were recorded and sorted as described in ''Surgery and recordings'' and ''Single unit analyses.'' To ensure the same neurons were recorded during ABCA' behavior and electric identification, waveforms were averaged during behavior and anesthesia and correlated as previously described. To be classified as antidromic, evoked-responses had to meet at least two out of three criteria (Lipski, 1981): stable latency (< 0.3 ms jitter), collision with spontaneously occurring spikes, and follow high-frequency stimulation (250 Hz). At the end of the experiments, stimulating sites were marked with electrolytic lesions before perfusion, and electrode locations were verified as described in ''Histological analyses.''

Context responsive unit identification

A bootstrap resampling method was used to identify units that were significantly excited or suppressed during a particular context (Figures S4A and S4B). For each unit, we considered the number of spikes that occurred in each context following ABCA' presentation. We then created a surrogate distribution of expected spike counts for each context by shuffling the inter-spike intervals from the original spike train (10,000 repetitions). Units that fell outside of the surrogate distribution ($p < 0.01$) were considered to be context responsive. This method identifies units that are exclusively modulated during a single context and units that may be modulated during one or more contexts. All analyses (except Figures S4C and S4D) considered units that may be significantly modulated during one or more contexts.

Population analyses

To investigate dmPFC neuronal activity during context fear discrimination we performed population analyses. This approach was suitable for our paradigm as mice were tested during a single-trial with a broad timescale containing few controlled stimuli (Cunningham and Yu, 2014; Hyman et al., 2012). Additionally, although the variability of freezing behavior within each context was minimal (Figure 1E), freezing epochs throughout contexts and during transitions were heterogeneous among mice (Figure 2H) and therefore averaging neuronal activity across subjects at fixed time points may not produce easily interpretable results. Spike train activity from units recorded in all mice were compiled for population analyses. For each unit the instantaneous spike count was temporally smoothed with a sliding-window of 2 s (0.1 s steps) and normalized by *z*-score. The instantaneous population vector (*iPV(t)*) was formed by pooling the individual instantaneous *z*-scores at time *t* (Figure 2C). Therefore, the activity of the dmPFC ensemble recorded for a particular time point is represented by a vector with a dimension equal to the total number of units. A 2-dimensional projection of the *iPV* obtained using principal component analysis (PCA) was used for data visualization purposes in a low dimensional space. To assess how the population varied among different contexts, we measured the distance between the clusters formed by the *iPV* during the different context exposures. The 20 s after a context transition were excluded from this analysis to minimize the impact of the transitions between contexts. We used the Mahalanobis generalized distance (Legendre and Legendre, 1998) as a way to assess whether dmPFC population activity was uniform across context presentations. The generalized Mahalanobis distance between *iPV* in contexts *C1* and *C2* was defined as:

$$D_{Mah}(iPV(C1), iPV(C2)) = \sqrt{\left(\overline{iPV(C1)} - \overline{iPV(C2)}\right) S^{-1} \left(\overline{iPV(C1)} - \overline{iPV(C2)}\right)^{T}},$$

where each column of the matrix *iPV(Ck)* contains the instantaneous population vector for time bins (*n* bins) defined in context *k*, whereas $\overline{iPV(Ck)}$ is the mean of the *iPV* for the different *n* bins in context *k*, and S^{-1} is the inverse of the pooled covariance matrix, defined as:

$$S = \frac{1}{(nC1 + nC2 - 2)} \left((nC1 - 1)\, Cov(iPV(C1)) + (nC2 - 1)\, Cov(iPV(C2))\right), \text{ where } Cov(iPV(Ck))$$

refers to the covariance matrix of $iPV(Ck)$. In order to compare the Mahalanobis generalized distance between pre- and post-conditioning exposure to configuration ABCA' (n = 285) we randomly sampled (10,000 repetitions) the same number of neurons as in the pre-conditioning ABCA' exposure (n = 60) (Figure 2F). We used an identical method for comparing the Mahalanobis generalized distance between configuration ABCA' (n = 285) and the 12 min exposure to context A (n = 141) (Figures S3A and S3B). This resampling method was used given the differences in subject number and neurons recorded between experiments, as the Mahalanobis distance can expand as dimensions increase, preventing direct comparisons among groups. To estimate the number of units required to realize an iPV that formed discretized context clusters during ABCA' exposure (Figures S3C–S3E) a resampling procedure was used. Units were randomly sampled with replacement (10,000 repetitions) from post-conditioning exposure to ABCA' (n = 285) or pre-conditioning exposure to ABCA' (n = 60). This resampling procedure was performed at increments of 5 units and the mean Mahalanobis distance was calculated for each iteration. When the pre-conditioning and post-conditioning curves diverged, this represented an estimate of the number of units hypothetically required to differentiate the dmPFC representation of contexts ABCA' after conditioning. Lastly, to control that a single mouse did not inordinately contribute to the fear conditioning-induced expansion of the context clusters formed by the iPV, a jackknife procedure was used (Figure S3F).

Context transitions

To compare the dynamics of freezing behavior and the dmPFC population during context transitions (A/B, B/C, C/A'), we used sliding windows of 5 s (0.5 s step) during 20 s before and after each transition time. First, freezing probability (Figure 2H, S3G, and S3K) was calculated by the presence of freezing divided by the number of mice for each bin (bin size = 0.1 ms). Second, we computed the difference of the Euclidean distance between the iPV and the centroid of the previous context and the distance to the following context (see schematic Figure 2G). The 95% confidence interval of the centroid distances was calculated by randomly sampling with replacement (10,000 repetitions) from the total number of neurons recorded during the particular behavioral session. To determine when context transitions altered freezing behavior and dmPFC population activity we calculated from the previous context the values for significant (mean ± 5 s.d.) alteration in freezing and iPV values.

Virus injections and optogenetics

For optical control of CaMKIIα-expressing neurons, conditional AAV encoding ChR2 (AAV5-EF1a-DIO-hChR2(H134R)-EYFP, UNC Vector Core Facility) or ArchT (AAV9-FLEX-ArchT-GFP, UNC Vector Core Facility) were bilaterally injected into the dmPFC of CaMKIIα-Cre mice from glass pipettes (tip diameter 10-20 μm) connected to a picospritzer (Parker Hannifin Corporation; ~0.4 μL per hemisphere) at the following coordinates relative to bregma: +1.98 mm AP; +0.35 mm ML; −1.35 mm DV from dura. At least 3 weeks after the injection mice were implanted bilaterally with custom-built optic fibers (diameter: 200 μm; numerical aperture: 0.39; Thorlabs) above the l/vlPAG at the following coordinates relative to bregma: −4.50 mm AP; ± 0.90 mm ML; −1.90 mm DV from dura; lowered at an angle of 10°. A subset of mice were also implanted in the left hemisphere of the l/vlPAG with a custom-built optrode consisting of a 16-wire electrode bundle, as described in "Surgery and recordings," attached to an optic fiber to record l/vlPAG unit activity during presynaptic photo stimulation. Due to the known functional heterogeneity of the PAG (Tovote et al., 2016) mice with optic fibers terminating in the dPAG were excluded from optogenetic experiments due to photo stimulation-induced locomotor effects. Control experiments were performed using an AAV containing the construct for only GFP (AAV5-FLEX-GFP, UNC Vector Core Facility). All implants were secured using 3 stainless steel screws and Super-Bond cement. Behavioral and recording experiments were performed at least 1 week post-implantation.

Light delivery in l/vlPAG

Blue light of 473 nm (~8 mW at fiber tip) was bilaterally delivered from a diode-pumped solid state laser (CNI Laser) to the mice via two fiber-optic patch cords (diameter: 200 μm, Doric Lenses), connected to a rotary joint (1 × 2 fiber-optic rotary joint, Doric Lenses) that allowed mice to freely move during behavioral testing. Similarly, yellow light of 593 nm (~6 mW at fiber tip) was delivered from a diode-pumping solid state laser (CNI Laser). For optogenetic manipulation of ArchT-expressing CaMKIIα neurons, and matched GFP controls, we delivered 180 s of continuous light. Mice expressing ChR2 in CaMKIIα neurons, and matched GFP controls, all received 5 ms light pulses delivered at 10 Hz (except Figure S5K). Single unit activity in the l/vlPAG was recorded during ABCA' behavior on days 3 and 4 to maximize the number units, owing to the low yield in this brain region (Tovote et al., 2016). Recorded l/vlPAG units were analyzed as described in "Single unit analyses." To determine whether presynaptic photo stimulation modulated l/vlPAG unit activity, firing activity was *z*-scored (bin size = 5 s), normalized to context A, and the average *z*-score was calculated for the 3 min of photo stimulation. Due to the poor temporal precision of presynaptic photo stimulation on unit firing, units with a positive *z*-score averaged during blue light delivery, or negative *z*-score averaged during yellow light delivery, were considered to be photo responsive. This criterion, albeit broad, was adopted to survey general neuronal activity in the l/vlPAG and would otherwise be inadequate for dissection of mono-synaptic circuits in the midbrain.

Light delivery in dmPFC

For pathway specific photo manipulation of the dmPFC-l/vlPAG pathway during behavior or photo identification we used both C57BL6/J wild-type (n = 11) and hCAR mice (n = 6). Mice were bilaterally injected (~0.4 μL per hemisphere) with a cocktail of CAV2-Cre retrograde virus (Montpellier Vector Platform) and AAV-hSyn-mCherry in the l/vlPAG at the following coordinates relative to bregma: −4.50 mm AP; ± 0.55 ML; −1.55 DV from dura, and AAV9-FLEX-ArchT-GFP or AAV5-EF1a-DIO-hChR2(H134R)-EYFP in the dmPFC relative to bregma: +1.98 mm AP; ± 0.40 ML; −1.35 DV from dura. Importantly, virus recombination using this intersectional infection strategy (Figures S6A–S6C) and behavior during contexts ABCA' (Figures 4I and S5B) between wild-type and hCAR mice was similar. Following 4 weeks of recovery from injections, mice were implanted with a custom-built optrode consisting of 32-wire electrode, as described in "Surgery and recordings," attached to an optic fiber at the following coordinates relative to bregma: +1.98 mm AP; ± 0.60 mm ML; −1.50 mm DV from dura; lowered at an angle of 10°. For mice tested during auditory fear behavior (Figures S6E and S6F), only optical fibers were implanted in the dmPFC. Optogenetic stimulation during CS^+ consisted of 10 Hz blue light delivery for 500 ms at CS^+ pip onset. Alternatively, photo inhibition consisted of constant yellow light during CS^+ presentation for 500 ms at CS^+ pip onset.

Mice implanted with optrodes for photo identification were given pulses of yellow light (~8 mW at the tip) lasting 200 ms (Figure 4G) or 300 ms (Figure S5A). To avoid false-positive photo identification due to recurrent network excitation with stimulation of ChR2, we opted for photo inhibition in ArchT infected mice. Units were classified as photo responsive if they displayed at least one significant bin with a *z*-score value below −1.65 within the stimulation period. Although inhibition-mediated photo identification of a low firing frequency neuronal population has temporal limitations, among the 10 cells photo identified, 8 displayed significant inhibition within 100 ms of light delivery and 8 of 10 began inhibition within 50 ms of light onset. Additionally, to confirm our photo identification results we complemented these studies with classical electric antidromic identification and observed analogous results. Due to the low yield of units identified with photo and antidromic techniques, units demonstrating a maximal firing rate during context C were classified as context C active. After behavioral and recording experiments, mice were perfused and histological analysis was performed.

Histological analyses

Mice were administered a lethal dose of isoflurane and underwent transcardial perfusions via the left ventricle with 4% w/v paraformaldehyde (PFA) in 0.1 M PB. Following dissection, brains were post-fixed for 24 h at 4°C in 4% PFA. Brain sections of 60 μm-thick were cut on a vibratome, mounted on gelatin-coated microscope slides, and dried. To identify electrolytic lesions sections were stained with toluidine blue, dehydrated, mounted, and verified using conventional transmission light microscopy. Only electrodes terminating in the anterior cingulate, prelimbic, and l/vlPAG were included in our analyses. For verification of viral injections and optic fiber location in dmPFC and l/vlPAG, serial 60 μm-thick slices containing the regions of interest were mounted in VectaShield

(Vector Laboratories) and were imaged using an epifluorescence system (Leica DM 5000) fitted with a 10x dry objective. For imaging of slices at different wavelength (Figure 6A), we always started imaging the higher wavelength (green) and then the lowest one (blue). In some cases, the microscope setting was not optimum and revealed stripes on the acquired images (Figures 6A and S6B). The location and the extent of the injections/infections were visually controlled. Only infections accurately targeted to the dmPFC and optic fibers terminating in the anterior cingulate, prelimbic cortex, and dorsal to the l/vlPAG were considered for behavioral and electrophysiological analyses.

The specificity of CaMKIIα neuron infection was assessed with immunofluorescence to visualize colocalization of CaMKII-positive neurons and GFP expression. Two naive CaMKIIα-Cre mice were injected with AAV5-FLEX-GFP to avoid confounding effects of brain damage associated with optic fiber implantation. Mice were given a lethal dose of isoflurane and perfused with PB (pH 7.4), and fixed with 4% PFA at 4°C (TAAB, pH 7.3). Following post-fixation, 50 μm-thick coronal sections were cut and kept in 0.1 M PB. All reagents were diluted in 0.1 M PB containing Triton X-100 0.3% v/v. Free-floating sections were blocked in 20% normal goat serum (NGS, Vector laboratories) for 2 h at room temperature and incubated at 4°C for 2 days in 1:500 anti-CaMKII mouse monocolonal antibody (Abcam ab22609) with 2% NGS. Sections were washed and incubated at 4°C overnight in 1:500 Alexa 647-conjugated goat anti-mouse (Invitrogen) with 2% NGS. After extensive washes, sections were mounted in Vectashield (Vector Laboratories). Two confocal image stacks (1 μm steps, slice thickness 1 Airy unit) were acquired (Leica DM2500 TCS SPE 40x oil immersion 1.3 NA objective) for each animal, from different sections of dmPFC, close to the virus injection sites. Immunoreactivity of cell bodies for GFP was assessed independently for each stack (n = 231 GFP^+ cells). Cells were then marked as $CaMKII^+/GFP^+$ or $CaMKII^-/GFP^+$ with Leica Application Suite Advanced Fluorescence Lite (Leica Microsystems CMS GmbH). Specificity was calculated as (number of $CaMKII^+/GFP^+$ cells / total number of GFP^+ cells).

QUANTIFICATION AND STATISTICAL ANALYSIS

For all datasets normality was tested using the Kolmogorov–Smirnov test ($\alpha < 0.05$) and homogeneity of variance with Levene's test ($\alpha < 0.05$) to determine whether parametric or non-parametric analyses were required. Parametric analyses included t tests and one- and two-way repeated-measures ANOVA followed by Bonferroni's multiple comparison post hoc test if a significant main effect or interaction was observed. If either homogeneity of variance or normality assumptions were not met, non-parametric analyses were used. When required, non-parametric Wilcoxon rank sum, Wilcoxon signed rank, or Friedman's rank tests were used. If significance was observed, these non-parametric analyses were followed by Bonferroni's or Dunn's multiple comparison post hoc tests to protect from false positive errors. For frequency data analyzed in the bootstrap resampling procedure to identify context responsive units, binomial probabilities were calculated by approximating to a normal distribution, owing to the large sample size. To analyze the significance of the number of context responsive units we considered the number of *k* units that were modulated by a particular context divided by the sum of *n* instances that a unit was significantly modulated by any context. Therefore in the calculations of binomial probabilities *n* is larger than the number of units recorded for a particular experiment (except Figures S4C and S4D). Chance level was calculated based upon the null hypothesis that PNs selected by the bootstrap method would be equally distributed among the 4 contexts. Analyses of this frequency data are reported as the number of context responsive units. All tests were two-tailed and data are expressed as either mean ± s.e.m.; median, interquartile range, and extreme values; or mean ± 95% confidence interval. Sample sizes were determined based upon previous publications. Analyses were performed with MATLAB and Prism (GraphPad Software). Apart from t tests, the asterisks in the figures represent the *P*-values of post hoc tests corresponding to the following values $^*p < 0.05$; $^{**}p < 0.01$; $^{***}p < 0.001$ based on mean ± s.e.m. The pound signs represent significance levels $^{\#}p < 0.05$ and $^{\#\#}p < 0.01$ based upon mean ± 95% confidence interval.

DATA AND SOFTWARE AVAILABILITY

The data presented in this manuscript is available upon request to the Lead Contact.

nature neuroscience

4-Hz oscillations synchronize prefrontal–amygdala circuits during fear behavior

Nikolaos Karalis[1–3,6], Cyril Dejean[1,2,6], Fabrice Chaudun[1,2,6], Suzana Khoder[1,2], Robert R Rozeske[1,2], Hélène Wurtz[1,2], Sophie Bagur[4], Karim Benchenane[4], Anton Sirota[3], Julien Courtin[1,2,5,7] & Cyril Herry[1,2,7]

Fear expression relies on the coordinated activity of prefrontal and amygdala circuits, yet the mechanisms allowing long-range network synchronization during fear remain unknown. Using a combination of extracellular recordings, pharmacological and optogenetic manipulations, we found that freezing, a behavioral expression of fear, temporally coincided with the development of sustained, internally generated 4-Hz oscillations in prefrontal–amygdala circuits. 4-Hz oscillations predict freezing onset and offset and synchronize prefrontal–amygdala circuits. Optogenetic induction of prefrontal 4-Hz oscillations coordinates prefrontal–amygdala activity and elicits fear behavior. These results unravel a sustained oscillatory mechanism mediating prefrontal–amygdala coupling during fear behavior.

Long-range neuronal synchronization among groups of neurons is an effective mechanism that promotes the transmission of information between neural structures[1–4]. This form of neuronal communication has been largely described in sensory and motor systems[5–8] and more recently between neural structures involved in the processing of emotions such as fear-related information[9–12]. Fear behavior is known to depend on the interaction between the dorsal medial prefrontal cortex (dmPFC) and the basolateral amygdala (BLA), and recent data indicate that local or distant synchronization of neuronal activity in this dmPFC–BLA network strongly correlates with fear behavior[9–12]. In particular, synchronization of spiking activity between dmPFC and BLA has been associated with resistance to extinction learning, whereas fear discrimination has been associated with transient, sensory-driven dmPFC–BLA synchronization[10,11]. However, the precise neuronal mechanisms mediating long-range network synchronization during fear behavior remain unknown. Furthermore, a causal role of neuronal synchrony among dmPFC and BLA circuits in driving fear behavior has not yet been demonstrated.

RESULTS

Internally generated freezing behavior

To address these questions, we performed single-unit and local field potential (LFP) recordings in the dmPFC and BLA of freely behaving mice subjected to auditory fear conditioning (**Fig. 1a**). Twenty-four hours after conditioning, re-exposure to the conditioned auditory stimulus (CS^+) but not to the control auditory stimulus (CS^-) induced conditioned freezing behavior, which we used as readout of fear memory acquired upon associative learning (**Fig. 1b**). Quantification of freezing episodes occurring during or between CS^+ presentations indicated that mice froze more often between CS^+ presentations (**Fig. 1c**). Moreover, evaluation of freezing-period onset distribution during or between CS^+ presentations indicated that a large fraction of freezing periods ($41.8 \pm 0.03\%$) were initiated outside of CS^+ presentations (**Fig. 1d**). Finally, cross-correlation analysis performed between freezing and CS^+ onset revealed that the freezing period onset was delayed by 1.5 s with respect to CS^+ onset (**Fig. 1e**). These observations indicate, that in addition to freezing episodes driven by auditory inputs, internally generated mechanisms can initiate and maintain freezing episodes following CS^+ presentations.

dmPFC and BLA 4-Hz oscillations predict freezing behavior

Analysis of dmPFC LFPs recorded throughout the behavioral sessions revealed a prominent and sustained 2–6 Hz oscillation with a peak frequency at 4 Hz (hereafter referred to as 4-Hz oscillations), which strongly correlated with episodes of freezing behavior following conditioning (**Fig. 2a–d** and **Supplementary Fig. 1a**,**b**). These oscillations were not present when animals were passively immobile during the habituation session (**Fig. 2a** and **Fig. 3a–c**). Moreover, the duration and power of 4-Hz oscillations in the dmPFC was strongly correlated with the length of freezing episodes (**Fig. 3d**).

To evaluate whether 4-Hz oscillations could predict freezing behavior, we first computed freezing-triggered spectrograms centered on the onset and offset of freezing episodes (**Fig. 3e**). Statistical analyses for the temporal progression of significant changes of 4-Hz power indicated that 4-Hz oscillations in the dmPFC emerged and terminated significantly earlier than freezing behavior. These results strongly suggest that 4-Hz oscillations are an accurate predictor of freezing onset and offset, rather than a consequence of freezing

[1]INSERM, Neurocentre Magendie, U862, Bordeaux, France. [2]Univ. Bordeaux, Neurocentre Magendie, U862, Bordeaux, France. [3]Bernstein Center for Computational Neuroscience Munich, Munich Cluster of Systems Neurology (SyNergy), Faculty of Medicine, Ludwig-Maximilians Universität München, Planegg-Martinsried, Germany. [4]Team Memory, Oscillations and Brain states (MOBs), Brain Plasticity Unit, CNRS UMR 8249, ESPCI ParisTech, Ecole Supérieure de Physique et de Chimie Industrielles de la Ville de Paris, Paris, France. [5]Friedrich Miescher Institute for Biomedical Research, Basel, Switzerland. [6]These authors contributed equally to this work. [7]These authors jointly directed this work. Correspondence should be addressed to C.H. (cyril.herry@inserm.fr) or N.K. (karalis@bio.lmu.de).

Received 23 October 2015; accepted 22 January 2016; published online 15 February 2016; doi:10.1038/nn.4251

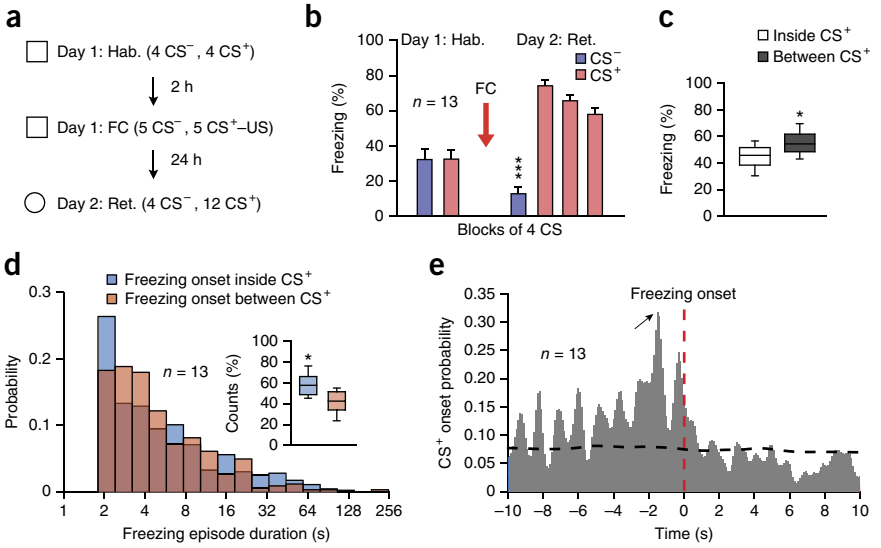

Figure 1 Freezing behavior is triggered by internally generated mechanisms. (**a**) Experimental protocol. Hab., habituation; FC, fear conditioning; Ret., retrieval; US, unconditioned stimulus. (**b**) Behavioral results. During habituation, mice ($n = 13$) exhibited low freezing during the CS^- and CS^+. After conditioning (day 2: retrieval), the CS^+ (CS^+ 1–12, grouped in blocks of four) induced higher freezing than CS^- (paired t-tests, CS^- versus each CS^+ block: $t(12) = -11.929$; $t(12) = -11.929$; $t(12) = -8.442$; all $^{***}P < 0.001$). (**c**) Percentage of freezing exhibited during and between CS^+ presentations (paired t-test, freezing inside versus between CS^+: $t(12) = -2.480$, $^{*}P = 0.029$). (**d**) Distribution probability for freezing episode duration as a function of whether freezing was initiated inside or between CS^+ presentations. Inset, percentage of freezing episodes initiated inside or between CS^+ presentations ($n = 13$ mice, paired t-test, $t(12) = 2.762$, $^{*}P = 0.016$). (**e**) Cross-correlation analysis performed between freezing and CS^+ onset ($n = 13$ mice, 100-ms bins). Red vertical dotted line represents freezing onset. Black horizontal dotted line represents significance level. Black arrow indicates the highest probability for CS^+ onset at 1.5 s before freezing onset. Error bars, mean ± s.e.m. For box plots, the middle, bottom and top lines correspond to the median, bottom quartile and top quartile, and whiskers to lower and upper extremes minus bottom quartile and top quartile, respectively.

behavior. This observation was further supported by analyses using supervised learning models, which allowed us to successfully predict freezing behavior on a trial-by-trial basis using the 4-Hz dmPFC signal-to-noise ratio (SNR) (**Fig. 3f,g**). 4-Hz oscillations developed during auditory fear conditioning (**Supplementary Fig. 2**) and dmPFC 4-Hz oscillations were also observed during freezing episodes in mice submitted to contextual fear conditioning, indicating that 4-Hz oscillations might correspond to a general physiological signature of freezing behavior (**Supplementary Fig. 3**). A similar but less prominent phenomenon was observed in the BLA, although the coupling between 4-Hz oscillations and freezing behavior was stronger in the dmPFC, likely because of the different laminar anatomical organization of the two structures and putative localization of the source of the 4-Hz oscillation in the prefrontal circuits (**Fig. 4** and **Supplementary Figs. 1c,d** and **4a–e**).

To evaluate whether 4-Hz oscillations were the mere consequence of freezing-, motor- or respiratory-related behavior, we performed further recordings in the ventrolateral periaqueductal gray (vlPAG),

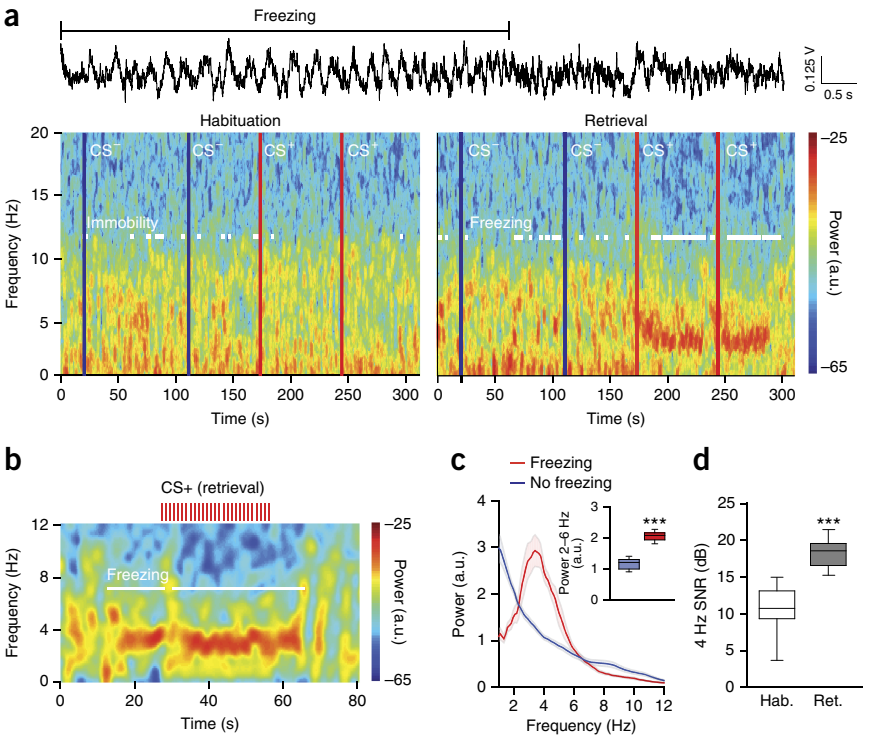

Figure 2 Emergence of dmPFC 4-Hz oscillations during freezing behavior. (**a**) Top, representative dmPFC raw LFP traces recorded during retrieval. 4-Hz oscillatory activity is prominent during freezing behavior. Bottom, representative spectrograms of dmPFC LFPs during habituation and retrieval sessions during CS^- and CS^+ presentations (blue lines, CS^- onset; red lines, CS^+ onset; habituation, recording during CS^- 3 and 4; retrieval, recording during CS^+ 1 and 2). White lines on the spectrogram indicate immobility or freezing episodes. (**b**) Representative spectrogram of dmPFC LFPs at a finer time resolution before, during and after presentation of a CS^+ during retrieval. Each red tick represents a single CS^+ pip. White lines on the spectrogram indicate freezing episodes. a.u., arbitrary units. (**c**) Averaged power spectra of dmPFC LFPs recorded during retrieval for freezing and no-freezing periods ($n = 13$ mice). Inset, averaged dmPFC 2–6 Hz power during retrieval for freezing and no-freezing periods (paired t-test, freezing versus no freezing: $t(12) = -14.884$, $^{***}P < 0.001$). (**d**) Averaged SNR of 4-Hz oscillation (2–6 Hz) during habituation (Hab.) and retrieval (Ret.) ($n = 12$ mice, paired t-tests, habituation versus retrieval: dmPFC: $t(11) = -6.805$, $^{***}P < 0.001$). Shaded areas, mean ± s.e.m. For box plots, the middle, bottom and top lines correspond to the median, bottom quartile and top quartile, and whiskers to lower and upper extremes minus bottom quartile and top quartile, respectively. For representative examples (**a**,**b**), similar traces were observed for the 13 animals used in these experiments.

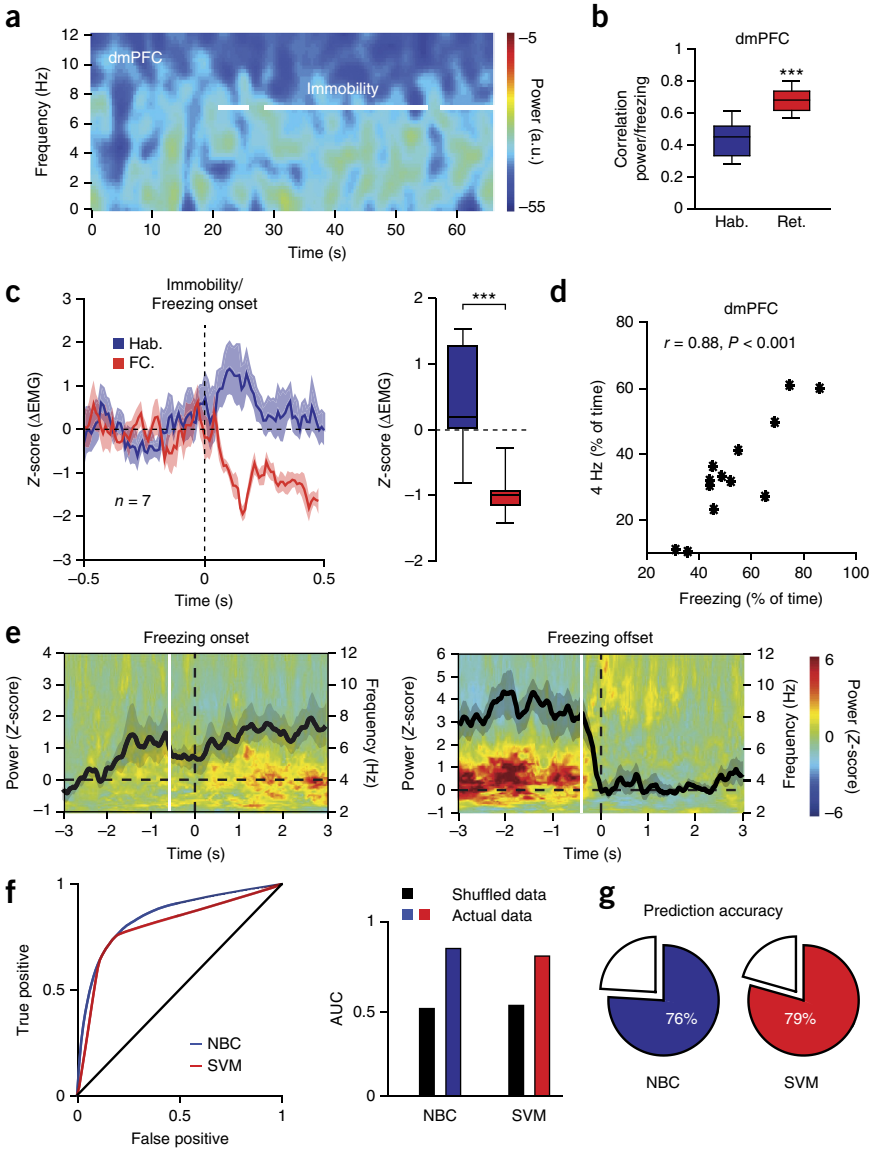

Figure 3 dmPFC 4 Hz oscillations predict freezing. (**a**) Spectrograms of dmPFC LFP during habituation. White lines indicate immobility. (**b**) Correlation between dmPFC 4-Hz power and freezing during habituation and retrieval ($n = 13$ mice, paired t-tests: $t(12) = 6.134$, $^{***}P < 0.001$). (**c**) Left, mean Z-score for neck electromyography (EMG) during immobility or freezing ($n = 7$ mice) for CS^+ presentations. Right, averaged EMG (0–500 ms after CS^+, Mann-Whitney U test, habituation (Hab.) versus fear conditioning (FC): $U = 0$, $^{***}P < 0.001$). (**d**) Correlation between freezing and dmPFC 4 Hz ($n = 13$ mice; Pearson's $r = 0.88$, $P < 0.001$). (**e**) Averaged freezing onset-triggered (left) and offset-triggered (right) Z-scored spectrograms of dmPFC LFPs ($n = 13$ mice; black lines, averaged Z-scored power envelope; white lines, first significant bin of 4-Hz power changes (increase, -0.53 ± 0.31 s; decrease, -0.39 ± 0.10 s; one-sample t-test: first significant bin versus hypothetical mean = 0, increase: $t(12) = 19.207$, $P < 0.001$; decrease: $t(12) = 16.615$, $P < 0.001$)). (**f**) Left, receiver operating characteristics analysis performed on a naive Bayes classifier (NBC) and support vector machine (SVM) classifier trained on dmPFC 4-Hz SNR during freezing. Right, averaged area under the curve for both classifiers versus shuffled data. (**g**) Accuracy of both classifiers at predicting freezing; a.u., arbitrary units. Power in log scale. Shaded areas, mean ± s.e.m. For box plots, the middle, bottom and top lines correspond to the median, bottom and top quartile, and whiskers to lower and upper extremes minus bottom quartile and top quartile, respectively. For the representative example in **a**, similar traces were observed for the 13 animals used in these experiments.

a neuronal structure involved in the genesis of freezing behavior and the control of breathing during emotional load[13–16]. Power spectrum analyses performed on vlPAG recordings did not reveal significant 4-Hz oscillations during freezing episodes, which strongly suggests that 4-Hz oscillations do not reflect freezing-, motor- or respiratory-related activity (**Supplementary Fig. 4f**,**g**).

4-Hz oscillations are distinct from theta oscillations

To evaluate whether dmPFC 4-Hz oscillations could correspond to hippocampus-dependent low theta oscillations observed previously during conditioned stimulus presentations[10,12,17,18], we inactivated the medial septum, a neuronal structure known to be involved in the genesis of theta oscillations[19]. Targeted, reversible inactivation of the medial septum with muscimol, which is known to reduce theta power in the dorsal hippocampus[19], impaired dmPFC theta but had no effect on dmPFC 4-Hz oscillations (**Supplementary Fig. 5a–e**). In addition, this manipulation had no effects on the percentage of dmPFC neurons phase-locked to 4-Hz oscillations but reduced the number of dmPFC neurons phase-locked to theta oscillations (**Supplementary Fig. 5f**). Furthermore, in contrast to transient dmPFC local theta oscillations, which displayed CS^+-evoked phase resetting and were short-lasting (~300 ms)[9,10], the sustained dmPFC 4-Hz oscillations were not modulated by CS^+ presentations, did not display CS^+-evoked phase resetting (**Supplementary Fig. 6**) and could be maintained over long periods of freezing behavior even between CS^+ presentations (**Figs. 2a**,**b**, **3d** and **4a**,**b**), suggesting that the two phenomena are generated independently. Together these data indicate that the development of hippocampus-independent, internally generated 4-Hz oscillations in dmPFC–BLA circuits precede and therefore predict freezing behavior.

dmPFC 4-Hz oscillations drive BLA during freezing

Analyses of moment-to-moment covariations in oscillatory power and phase between structures revealed that during freezing episodes 4-Hz oscillations in the dmPFC and BLA were strongly synchronized (**Fig. 5a**,**b** and **Supplementary Fig. 7**). Consequently, coherence between dmPFC and BLA LFPs was significantly enhanced during freezing behavior (**Fig. 5c** and **Supplementary Fig. 7**). Moreover, a series of statistical directionality measures, in both the phase and the amplitude domains, revealed that dmPFC 4-Hz oscillations led BLA LFPs during freezing episodes but not during locomotor activity (**Fig. 5b–d** and **Supplementary Fig. 7**). Together, these data demonstrate that conditioned freezing behavior is associated with a preferential dmPFC-to-BLA phase coupling of 4-Hz LFP oscillations.

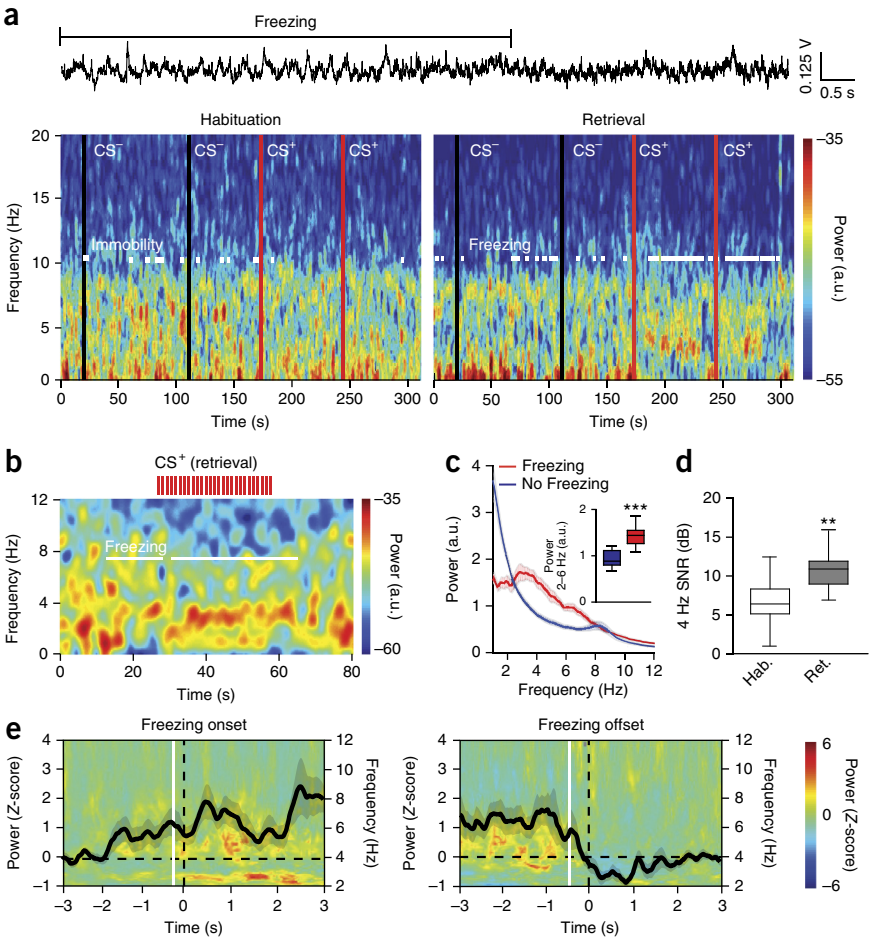

Figure 4 BLA 4-Hz oscillations emerge during freezing. (**a**) Top, representative BLA LFP traces recorded during retrieval. Bottom, spectrograms of BLA LFPs during habituation and retrieval during CS$^-$ and CS$^+$ (black lines, CS$^-$ onset; red lines, CS$^+$ onset). White lines indicate immobility or freezing. (**b**) Spectrogram of BLA LFPs before, during and after presentation of a CS$^+$ during retrieval. Red ticks represent single CS$^+$ pips. White lines indicate freezing. (**c**) Averaged power spectrum of BLA LFPs recorded during retrieval for freezing and no freezing ($n = 13$ mice). Inset, averaged BLA 2–6 Hz power during retrieval for freezing and no freezing (paired t-test, freezing versus no freezing: $t(12) = 6.077$, $^{***}P < 0.001$). (**d**) Averaged 4-Hz SNR during habituation (Hab.) and retrieval (Ret.) ($n = 12$ mice, paired t-tests, habituation versus retrieval: BLA, $t(11) = 3.334$, $^{**}P = 0.003$). (**e**) Averaged freezing onset-triggered (left) and offset-triggered (right) Z-scored spectrograms of BLA LFPs ($n = 13$ mice; black lines, averaged Z-scored power envelope; white lines, first significant bin of 4-Hz power changes (increase, -0.27 ± 0.20 s; decrease, -0.46 ± 0.22 s; one-sample t-test: first significant bin versus hypothetical mean = 0, increase: $t(12) = 10.976$, $P < 0.001$; decrease: $t(12) = 34.372$, $P < 0.001$)); a.u., arbitrary units. Spectral power in log scale. Shaded areas, mean ± s.e.m. For box plots, the middle, bottom and top lines correspond to the median, bottom and top quartile, and whiskers to lower and upper extremes minus bottom quartile and top quartile, respectively. For representative examples (**a**,**b**), similar traces were observed for the 13 animals used in these experiments.

4-Hz oscillations organize dmPFC and BLA firing activity

To evaluate the consequences of synchronized 4-Hz oscillatory activity for individual dmPFC and BLA putative excitatory principal neurons ($n = 92$ and $n = 72$, respectively) and putative inhibitory interneurons ($n = 35$ and $n = 15$, respectively) (**Supplementary Fig. 8**), we measured the phase-locking to dmPFC 4-Hz oscillations and changes in firing frequency of dmPFC and BLA neurons during fear behavior. These analyses revealed that a large proportion of principal neurons and interneurons in both structures were significantly phase-locked to dmPFC 4-Hz oscillations during freezing episodes, among which the vast majority exhibited 4-Hz-related oscillatory activity (**Fig. 6**). Moreover, freezing episodes were associated with a global increase in the firing rate of principal neurons compared to the rate during no-freezing periods in both the dmPFC and the BLA (**Supplementary Fig. 8**). Correlation and co-firing analyses of pairwise spiking activity performed between neurons recorded in the dmPFC and neurons recorded in the BLA indicated that phase-locked pairs of principal neurons were more co-activated during freezing episodes as compared to both no-freezing periods and non-phase-locked neurons (**Fig. 6c**,**h**). Together, these data indicate that dmPFC and BLA principal neurons synchronize their firing activity to 4-Hz oscillations during freezing behavior.

Optogenetic induction of dmPFC 4 Hz drives fear behavior

To further evaluate the causal role of 4-Hz oscillations in synchronizing dmPFC–BLA principal neurons firing activity during fear behavior, we artificially induced 4-Hz oscillations in the dmPFC of naive animals by analog optogenetic modulation of dmPFC interneurons, which contribute to the emergence of dmPFC 4-Hz oscillations (**Supplementary Fig. 9**). In particular, we manipulated parvalbumin-expressing cells, which is an efficient approach for inducing rhythmic inhibition of cortical principal neurons at low frequencies[20–22]. These genetically identified cells were predominantly phase-locked to 4-Hz oscillations and displayed 4-Hz oscillatory activity (**Supplementary Fig. 9d–j**). Rhythmically driving parvalbumin-expressing interneurons at 4 Hz resulted in prominent 2–6 Hz oscillations in the dmPFC and induced persistent fear behavior (**Fig. 7a–c** and **Supplementary Fig. 10a**,**b**). Freezing behavior was frequency and structure specific, as dmPFC rhythmic stimulation using a number of different control frequencies and BLA or motor cortex stimulation at 4 Hz were inefficient at inducing fear responses (**Fig. 7d**,**e** and **Supplementary Fig. 10c**,**d**). Furthermore, the artificial induction of dmPFC 4-Hz oscillations synchronized dmPFC and BLA spiking activity during freezing episodes (**Fig. 7f** and **Supplementary Fig. 10g–i**).

Given the emergence of 4-Hz oscillations during fear conditioning and retrieval of contextual fear memory (**Supplementary Figs. 2** and **3**), we retested the mice 24 h later in the context in which they received artificial induction of 4-Hz oscillations. In these conditions, mice exhibited more contextual fear behavior than GFP control animals (**Fig. 7c** and **Supplementary Fig. 10a**,**b**). Furthermore, mice exhibited low freezing levels when tested in a neutral context 24 h later, indicating that fear behavior was specific to the context where the optogenetic stimulation occurred (**Supplementary Fig. 10b**).

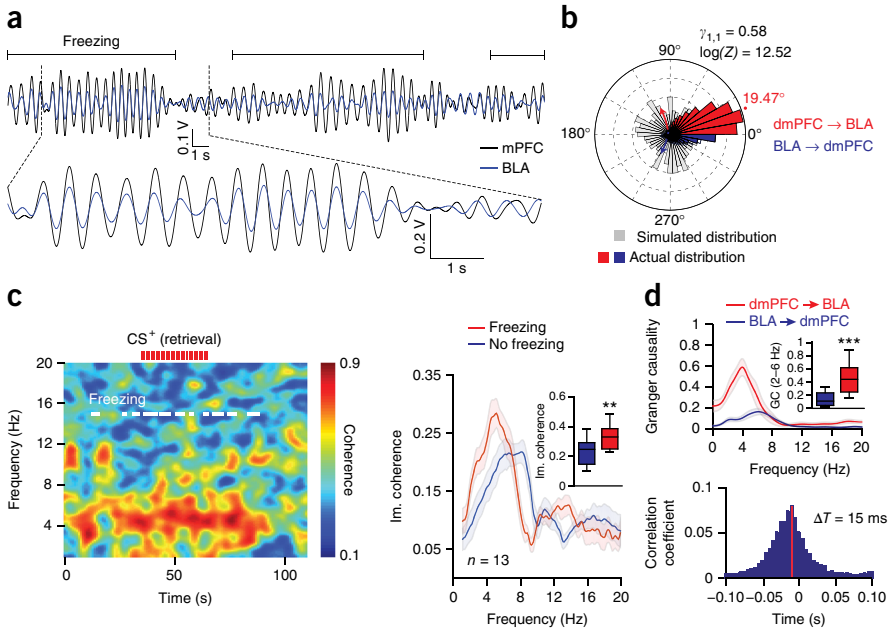

Figure 5 Synchronization of dmPFC and BLA 4-Hz oscillations during freezing. (**a**) Overlaid filtered (2–6 Hz) dmPFC and BLA LFP traces illustrating synchronized 4 Hz during freezing. (**b**) Circular distribution of the phase differences between dmPFC and BLA LFPs recorded for freezing during retrieval compared to a control bootstrap-simulated phase distribution ($n = 13$ mice). (**c**) Left, representative coherogram for dmPFC and BLA LFPs recorded during retrieval during CS$^+$. Red ticks represent individual CS$^+$ pips. White lines indicate freezing. Right, averaged dmPFC and BLA LFPs imaginary coherence (Im. coherence) for freezing and no freezing during retrieval ($n = 13$ mice). Inset, averaged peak of imaginary coherence for freezing and no freezing during retrieval (paired t-test, freezing versus no freezing: $t(12) = 3.933$, $^{**}P = 0.002$). (**d**) Top, Granger causality (GC) analysis performed between dmPFC and BLA LFPs during freezing ($n = 13$ mice). Inset, averaged GC (2–6 Hz) between dmPFC and BLA LFPs during freezing (retrieval, paired t-test, dmPFC → BLA versus BLA → dmPFC: $t(12) = -5.940$, $^{***}P < 0.001$). Bottom, averaged cross-correlogram performed between dmPFC and BLA LFPs (2–6 Hz). The peak (red bar) and negative skewness of the distribution indicate that dmPFC 4-Hz oscillations lead the BLA oscillatory activity by 15 ms ($n = 13$ mice). Shaded area, mean ± s.e.m. For box plots, the middle, bottom and top lines correspond to the median, bottom and top quartile, and whiskers to lower and upper extremes minus bottom quartile and top quartile, respectively. For representative examples (**a**,**c**), similar traces were observed for the 13 animals used in these experiments.

Together, these results indicate that freezing behavior upon artificial induction of dmPFC 4-Hz oscillations cannot be explained by motor impairments and further suggest that 4-Hz oscillations are causally involved in the synchronization of dmPFC–BLA spiking activity and the expression of aversive fear memories. Finally, post-training optogenetic silencing of BLA neurons during CS$^+$ presentations reduced fear behavior, indicating that the BLA is necessary for the full expression of conditioned fear behavior (**Supplementary Fig. 10e**,**f**).

DISCUSSION

In this study, we demonstrated that expression of conditioned fear memories is associated with prominent synchronous 4-Hz oscillations in dmPFC–BLA circuits, which organize the spiking activity of local neuronal populations. Furthermore, both dmPFC and BLA 4-Hz oscillations develop specifically during fear conditioning and predict the onset and offset of freezing episodes. The length of freezing episodes was also strongly correlated with the duration and power of dmPFC 4-Hz oscillations, a phenomenon not observed in the BLA. This could be due to the different laminar anatomical organization of the two structures. Aligned pyramidal cells in the cortex form spatially coherent dipoles. The resulting summation of field potentials allows the detection of high-SNR oscillations in the extracellular space[23]. The BLA, by contrast, is a nuclear structure with no clear anatomical organization (dipoles are distributed uniformly and not aligned). Consequently, the SNR of extracellularly recorded LFP oscillations is expected to be lower than in the dmPFC. Nonetheless, spike trains of a number of BLA neurons present both intrinsic 4-Hz oscillations and phase-locking to dmPFC 4 Hz, whether under physiological conditions or during light stimulation. Moreover, the presence of 4-Hz oscillations in LFP is indicative of the underlying synaptic activity; however, differences in the absolute power to SNR ratio between the two structures cannot be interpreted as a stronger involvement of the dmPFC. Again, because of the radically different neuronal organization between the two structures, synaptic inputs are differentially filtered by the biophysical properties of the BLA neural tissue[24,25].

Our data indicate that internally generated freezing-related 4-Hz dmPFC oscillations constitute a specific oscillatory mechanism, distinct from the CS$^+$-evoked dmPFC theta resetting observed previously[9,10,12]. These previously published studies[9,10] evaluated transient sensory-evoked theta oscillations in the dmPFC, which lasted around 300 ms and have been linked to sensory-driven processes during fear behavior or fear discrimination[9,10]. In contrast, the 4-Hz oscillatory phenomenon correlated not only with long periods of freezing behavior observed during CS$^+$ presentations, but also with spontaneously occurring freezing episodes. Functionally this implies that spontaneously occurring freezing periods are internally maintained or generated and not directly driven by sensory stimulations. To our knowledge, this is the first report of a sustained brain state (4-Hz oscillations) that predicts and temporally coincides with freezing episodes. The freezing responses observed between CS presentations are unlikely to have been triggered by the context for several reasons. First, mice were tested in a context distinct from the one used for the conditioning session. Second, freezing levels during CS$^-$ presentations during retrieval were very low, indicating that the retrieval context was not aversive *per se* (**Fig. 1b**; 13.19% freezing on CS$^-$ presentations). Our interpretation that freezing episodes occur between CS presentations relies on the induction of a fearful state after the initial CS-induced retrieval of the fear memory and thus the emergence of non-CS-related spontaneous freezing episodes.

Our data and analyses suggest that the 4-Hz oscillations represent a mechanism for the initiation and maintenance of freezing episodes, inside and outside of CS presentations. The data also confirm published observations that CS$^+$ onset is associated with a transient resetting of the phase of theta oscillations[9,10], which is, however, specific for oscillations in the 8–12 Hz range and is associated with transient increases in theta power, but is not observed for the 4-Hz oscillations (**Supplementary Fig. 6**). Hence, these observations

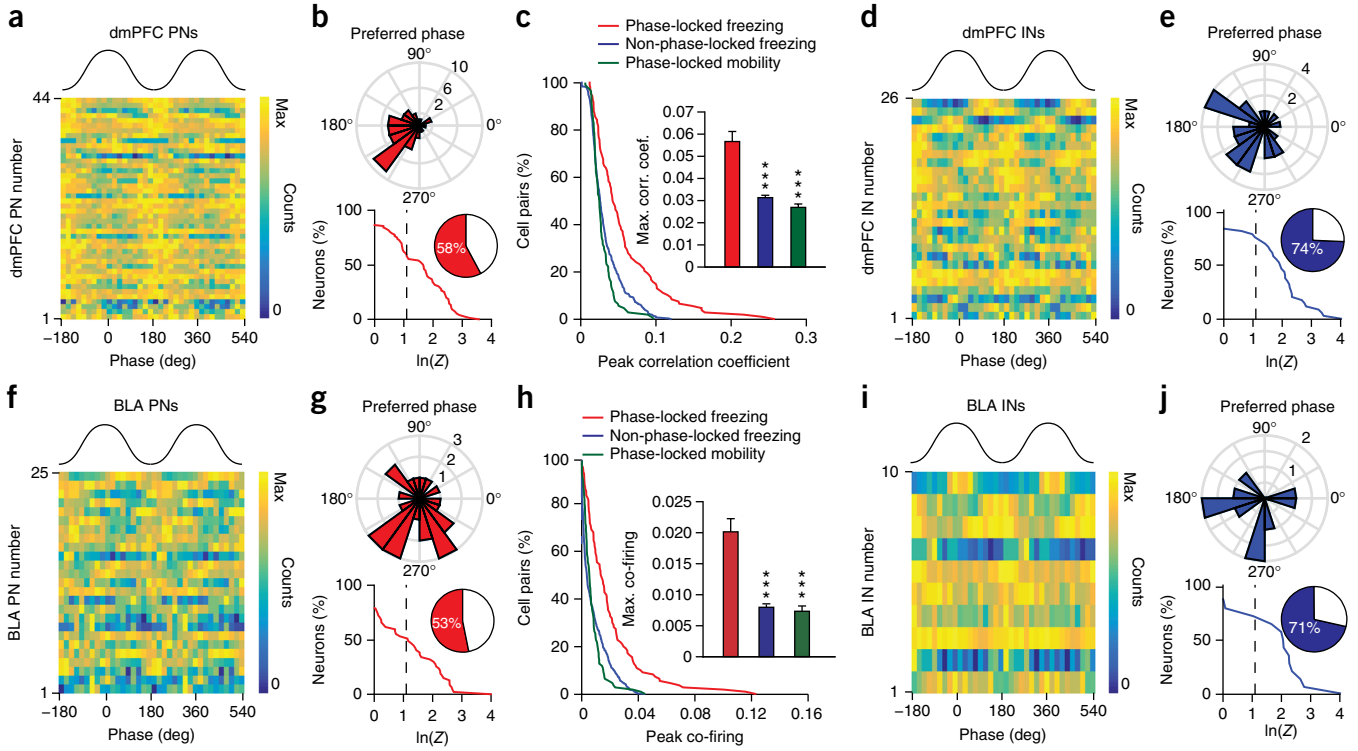

Figure 6 4-Hz oscillations synchronize dmPFC–BLA spiking activity. (**a**,**d**,**f**,**i**) Phase distribution relative to 4-Hz oscillations for dmPFC (**a**,**d**) and BLA (**f**,**i**) putative excitatory principal neurons (PN) (**a**,**f**) or putative inhibitory interneurons (IN) (**d**,**i**). (**b**,**g**,**e**,**j**) Circular distribution of the 4-Hz preferred phase for populations of dmPFC (**b**,**e**, top) and BLA (**g**,**j**, top) phase-locked PNs (**b**,**g**) and INs (**e**,**j**) during freezing (dmPFC: 44 PNs and 26 INs; BLA: 25 PNS and 10 INs) and cumulative distribution of log-transformed Rayleigh's test Z of dmPFC (**b**,**e**, bottom) and BLA (**g**,**j**, bottom) PNs (**b**,**g**) and INs (**e**,**j**). Inset, percentage of dmPFC and BLA neurons significantly phase-locked to 4-Hz oscillations. Dashed line, significant 4-Hz phase-locking threshold ($\ln(Z) = 1.097$, $^{*}P < 0.05$, dmPFC: 44 of 92 PNs and 26 of 35 INs; BLA: 25 of 72 PNs and 10 of 15 PNs). (**c**,**h**) Cumulative distribution of peak correlation coefficient (**c**) and co-firing index (**h**) for pairs of dmPFC and BLA phase-locked and non-phase-locked neurons during freezing and mobility. Insets, maximum correlation coefficient (**c**) and co-firing index (**h**) for all pairs of recorded dmPFC and BLA neurons (phase-locked pairs, $n = 180$; non-phase-locked pairs, $n = 911$; Mann-Whitney U test, top and bottom, phase-locked pairs during freezing versus mobility or non-phase-locked pairs: $U = 50{,}313$, 7,893, 16,200, 9,413, $^{**}P < 0.001$, $^{***}P < 0.001$). Error bars, mean ± s.e.m.

indicate that sustained 4-Hz oscillations described in the present manuscript do not correspond to sensory-driven transient theta oscillations previously observed[9,10]. Taken together, these results have important functional consequences, as they indicate the existence of distinct and independent dmPFC neuronal oscillations involved in the regulation of different aspects of fear behavior, such as stimulus-evoked attention processes related to the presentation of a salient CS, fear discrimination or the expression of freezing behavior. Notably, all of these findings were observed in mice, further studies are required to evaluate whether these oscillations also occurs in different species.

Our data also indicate that stationary dmPFC 4-Hz oscillations do not correspond to hippocampus-mediated dmPFC theta oscillations observed previously[17], as muscimol inactivation of the medial septum blocked hippocampal theta recorded in the dmFFC without affecting prefrontal 4-Hz oscillations, nor the percentage of dmPFC neurons phase-locked to 4-Hz oscillations. Our observation of BLA 4-Hz oscillatory activity during freezing behavior is consistent with previous recordings of slow theta oscillations in the lateral amygdala during fear behavior, which correlate with dorsal hippocampal theta oscillations[17,18], although in these studies the temporal relation between CS^{+} onset, 4-Hz oscillatory activity and freezing onset and offset were not clearly established. A recent observation of power increase for 4–7.5 Hz oscillations in the cingulate cortex during a hippocampus-dependent trace fear-conditioning procedure is also partly consistent with our observation[26]. Indeed, the authors observed that in some conditioning trials, 4–7.5 Hz power increased during the interval separating the conditioned stimulus from the footshock. In that study, however, the neuronal interaction between the cingulate cortex and the BLA, the precise temporal relation between slow oscillation and freezing behavior, and the causal role of prefrontal 4-Hz oscillations were not established. These data nevertheless suggest that prefrontal 4-Hz oscillations might be a general mechanism of fear expression encompassing classical auditory and contextual fear conditioning.

A key finding of our study comes from the demonstration that, during freezing behavior, dmPFC 4-Hz oscillations entrain BLA oscillatory activity and synchronize spiking activity between dmPFC and BLA neurons. Recent publications have highlighted neuronal co-firing between prefrontal cortex and amygdala during resistance to extinction behavior[11], LFP coherence between dmPFC and BLA after CS^{+} onset during fear discrimination, and amygdala neurons phase-locked to dmPFC theta oscillations during fear discrimination[10]. To our knowledge, our data provide the first mechanistic demonstration of a 4-Hz-mediated long-range synchronization of spiking activity between dmPFC and BLA during freezing behavior. Moreover, our findings also indicate that dmPFC activity leads the BLA one during freezing behavior.

Accordingly, we found that the optogenetically mediated artificial induction of 4-Hz oscillations in dmPFC synchronizes dmPFC and BLA neuronal activity and increases freezing behavior in a persistent manner, which demonstrates that internally generated

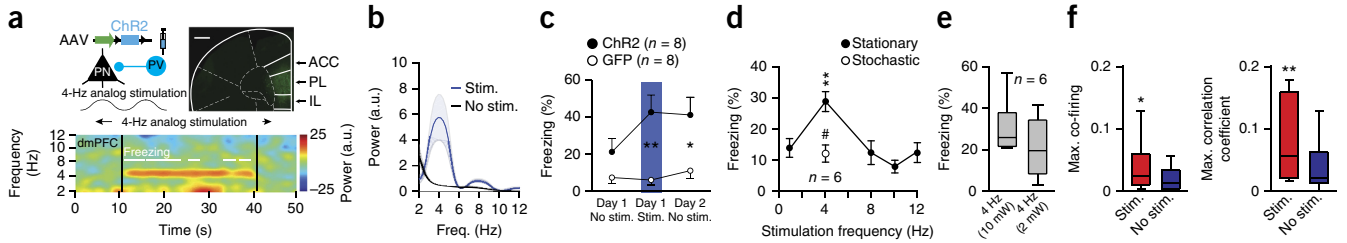

Figure 7 Optogenetic induction of dmPFC 4-Hz oscillations drives freezing. (**a**) Top left, strategy used to activate parvalbumin-expressing (PV) interneurons. Top right, coronal dmPFC micrograph from a PV-IRES-Cre mouse expressing channelrhodopsin2 (ChR2). Solid and dashed lines represent the boundaries between the cingulate cortex (ACC), the prelimbic (PL) and infralimbic (IL) areas, and other cortical structures. Scale bar, 0.5 mm. Bottom, spectrogram during 4-Hz analog stimulation. (**b**) Averaged normalized LFP power spectra of dmPFC LFPs during (Stim.) and outside (No stim.) stimulation ($n = 8$). (**c**) Percentage of freezing for ChR2 ($n = 8$) or GFP ($n = 8$) mice before, during and after 4-Hz induction (two-way ANOVA repeated measures; group: $F(1,14) = 0.868$, $P = 0.367$, time $F(1,2) = 8.926$, $P = 0.001$, group × time $F(1,28) = 6.925$, $P = 0.0036$); unpaired t-tests: day 1: Stim. $t(14) = 3.712$, $^{**}P = 0.002$; day 2: No stim., $t(14) = 2.758$, $^{*}P = 0.013$). (**d**) Percentage of freezing for ChR2 mice ($n = 6$) during analog stimulation at 1, 4, 8, 10, 12 Hz (Stationary) or using a 4-Hz stochastic waveform (stationary: one-way repeated measures ANOVA: $F(5,4) = 8.618$, $P < 0.001$; Bonferroni-corrected paired t-tests: 4 versus 1 Hz: $t(5) = 5.927$, $^{**}P = 0.0019$; 4 versus 8 Hz: $t(5) = 4.712$, $^{**}P = 0.0053$; 4 versus 10 Hz: $t(5) = 7.632$, $^{***}P < 0.001$; 4 versus 12 Hz: $t(5) = 4.009$, $^{**}P = 0.01$; paired t-test: 4-Hz stationary versus stochastic: $t(5) = 3.533$, $^{\#}P < 0.016$). (**e**) Percentage of freezing for ChR2 ($n = 6$) mice during dmPFC 4-Hz analog stimulation at 2 or 10 mW (paired t-test: $t(5) = 0.951$, $P = 0.385$). (**f**) Maximum correlation and co-firing index for pairs of dmPFC and BLA neurons during and outside stimulation ($n = 31$ pairs, Mann-Whitney, $U = 326$ and 278, $^{*}P = 0.03$; $^{**}P = 0.004$). a.u., arbitrary units. Power in log scale. Shaded area and error bars, mean ± s.e.m. For box plots, the middle, bottom and top lines correspond to the median, bottom and top quartiles, and whiskers to lower and upper extremes minus bottom quartile and top quartile, respectively. For representative examples (**a**), similar images and traces were observed for the 16 (top, 8 ChR2 and 8 GFP mice) and 8 (bottom, 8 ChR2 mice) animals used in these experiments.

oscillations drive behavior. Neuronal synchronization between dmPFC and BLA has been classically evaluated using powerful correlational analyses[10,11,18], but never causally demonstrated. Our data indicate that the genesis of 4-Hz oscillations in the dmPFC is sufficient to synchronize neuronal activity between dmPFC and BLA and further drive the expression of freezing responses. Moreover, this effect was frequency and structure specific, as dmPFC manipulation at other frequencies or 4-Hz induction in the motor cortex and BLA did not induce any behavioral effects. However, our data indicate that when freezing behavior is induced following auditory fear conditioning, the BLA is necessary for its full expression. Together these data strongly suggest that dmPFC 4-Hz oscillations are instrumental for dmPFC–BLA synchronization of neuronal activities during fear behavior and that the synchronized firing activity of BLA neurons triggers fear responses (**Supplementary Fig. 11**).

The dmPFC 4-Hz analog optogenetic stimulation induced freezing behavior not only during the stimulation but also 24 h later in the context in which the mice were stimulated. This observation suggests that the artificial induction of dmPFC 4-Hz oscillations might be involved in the formation of associative fear memories. Another possibility could be that this artificial induction might lead to nonspecific anxiety behavior. However, it is unlikely that a sudden inactivation or rhythmic inhibition of prefrontal areas could lead to nonspecific anxiety behavior for at least two reasons. Optogenetic inactivation of the cingulate cortex during remote contextual memory retrieval results in a reduction of contextual fear behavior, an observation not consistent with a general increase in anxiety levels[27]. Furthermore, in our optogenetic experiments (**Fig. 7**), dmPFC 4-Hz induction induced freezing in a context-specific manner, which is also an observation not consistent with a general increase in anxiety. Furthermore, while it is possible that induction of 4-Hz oscillations leads to the formation of associative fear memories, an alternative interpretation is that the contextual fear memory observed 24 h after optogenetic stimulation is a direct consequence of the association between contextual elements and the aversive state induced by 4-Hz oscillations. This interpretation is consistent with the notion that dmPFC–BLA 4-Hz oscillations are causally involved in the expression of freezing behavior.

Although our data indicate that dmPFC 4-Hz oscillations are causally involved in the neuronal synchronization of spiking activity between dmPFC and BLA during freezing behavior, it is conceivable that this mechanism could be involved in other emotional processes, such as avoidance, flight responses, sensory processes or cognitive tasks. For instance, recent reports have observed 4-Hz oscillations in the whisker barrel cortex during respiration[28] and in the rat dmPFC under working memory load during locomotor behavior[29]. Another important question is the source of the 4-Hz oscillations. Although our data indicate that these oscillations do not originate from the hippocampus and are localized in dmPFC circuits, more work will be required to address this question and unequivocally identify the source of the 4-Hz oscillations. In summary, our data reveal a specific 4-Hz oscillatory mechanism allowing the expression of fear memories by long-range synchronization of neuronal activity between dmPFC and BLA neuronal circuits.

METHODS

Methods and any associated references are available in the online version of the paper.

Note: Any Supplementary Information and Source Data files are available in the online version of the paper.

ACKNOWLEDGMENTS

We thank the members of the Herry laboratory for discussions and comments on the manuscript and K. Deisseroth (Stanford University) and E. Boyden (Massachusetts Institute of Technology) for generously sharing material. This work was supported by grants from the French National Research Agency (ANR-2010-BLAN-1442-01; ANR-10-EQPX-08 OPTOPATH; LABEX BRAIN ANR 10-LABX-43, LABEX TRAIL ANR 10-LABX-57), the European Research Council (ERC) under the European Union's Seventh Framework Program (FP7/2007-2013)/ERC grant agreement no. 281168, the Conseil Regional d'Aquitaine (C.H.), the Fondation pour la Recherche Médicale (FRM) (F.C.), the CNRS ATIP program (2014) and the city of Paris (Grant Emergence 2014), the French National Research Agency (ANR-10-LABX-54 MEMO LIFE; ANR-11-IDEX-0001-02 PSL) (K.B.), Munich Cluster for Systems Neurology (SyNergy, EXC 1010), Deutsche Forschungsgemeinschaft Priority Program 1665 and 1392 and Bundesministerium für Bildung und Forschung via grant no. 01GQ0440 (Bernstein Centre for Computational Neuroscience Munich) (A.S.) and a scholarship from the Erasmus Mundus program Neurasmus (N.K.).

AUTHOR CONTRIBUTIONS
S.B., K.B., F.C., J.C., C.D., N.K., S.K., R.R.R., A.S. and H.W. performed the experiments and analyzed the data. J.C., C.D., N.K. and C.H. designed the experiments. C.H. wrote the paper.

COMPETING FINANCIAL INTERESTS
The authors declare no competing financial interests.

Reprints and permissions information is available online at http://www.nature.com/reprints/index.html.

1. Bosman, C.A. *et al.* Attentional stimulus selection through selective synchronization between monkey visual areas. *Neuron* **75**, 875–888 (2012).
2. Siegel, M., Donner, T.H., Oostenveld, R., Fries, P. & Engel, A.K. Neuronal synchronization along the dorsal visual pathway reflects the focus of spatial attention. *Neuron* **60**, 709–719 (2008).
3. Rodriguez, E. *et al.* Perception's shadow: long-distance synchronization of human brain activity. *Nature* **397**, 430–433 (1999).
4. Hipp, J.F., Engel, A.K. & Siegel, M. Oscillatory synchronization in large-scale cortical networks predicts perception. *Neuron* **69**, 387–396 (2011).
5. Friedrich, R.W., Habermann, C.J. & Laurent, G. Multiplexing using synchrony in the zebrafish olfactory bulb. *Nat. Neurosci.* **7**, 862–871 (2004).
6. Riehle, A., Grün, S., Diesmann, M. & Aertsen, A. Spike synchronization and rate modulation differentially involved in motor cortical function. *Science* **278**, 1950–1953 (1997).
7. Benchenane, K. *et al.* Coherent theta oscillations and reorganization of spike timing in the hippocampal- prefrontal network upon learning. *Neuron* **66**, 921–936 (2010).
8. Gregoriou, G.G., Gotts, S.J., Zhou, H. & Desimone, R. High-frequency, long-range coupling between prefrontal and visual cortex during attention. *Science* **324**, 1207–1210 (2009).
9. Courtin, J. *et al.* Prefrontal parvalbumin interneurons shape neuronal activity to drive fear expression. *Nature* **505**, 92–96 (2014).
10. Likhtik, E., Stujenske, J.M., Topiwala, M.A., Harris, A.Z. & Gordon, J.A. Prefrontal entrainment of amygdala activity signals safety in learned fear and innate anxiety. *Nat. Neurosci.* **17**, 106–113 (2014).
11. Livneh, U. & Paz, R. Amygdala-prefrontal synchronization underlies resistance to extinction of aversive memories. *Neuron* **75**, 133–142 (2012).
12. Stujenske, J.M., Likhtik, E., Topiwala, M.A. & Gordon, J.A. Fear and safety engage competing patterns of theta-gamma coupling in the basolateral amygdala. *Neuron* **83**, 919–933 (2014).
13. Gabbott, P.L., Warner, T.A., Jays, P.R., Salway, P. & Busby, S.J. Prefrontal cortex in the rat: projections to subcortical autonomic, motor, and limbic centers. *J. Comp. Neurol.* **492**, 145–177 (2005).
14. Holstege, G. The periaqueductal gray controls brainstem emotional motor systems including respiration. *Prog. Brain Res.* **209**, 379–405 (2014).
15. Subramanian, H.H., Balnave, R.J. & Holstege, G. The midbrain periaqueductal gray control of respiration. *J. Neurosci.* **28**, 12274–12283 (2008).
16. Vianna, D.M., Landeira-Fernandez, J. & Brandão, M.L. Dorsolateral and ventral regions of the periaqueductal gray matter are involved in distinct types of fear. *Neurosci. Biobehav. Rev.* **25**, 711–719 (2001).
17. Lesting, J. *et al.* Patterns of coupled theta activity in amygdala-hippocampal-prefrontal cortical circuits during fear extinction. *PLoS One* **6**, e21714 (2011).
18. Seidenbecher, T., Laxmi, T.R., Stork, O. & Pape, H.C. Amygdalar and hippocampal theta rhythm synchronization during fear memory retrieval. *Science* **301**, 846–850 (2003).
19. Yoder, R.M. & Pang, K.C. Involvement of GABAergic and cholinergic medial septal neurons in hippocampal theta rhythm. *Hippocampus* **15**, 381–392 (2005).
20. Stark, E. *et al.* Inhibition-induced theta resonance in cortical circuits. *Neuron* **80**, 1263–1276 (2013).
21. Siegle, J.H. & Wilson, M.A. Enhancement of encoding and retrieval functions through theta phase-specific manipulation of hippocampus. *eLife* **3**, e03061 (2014).
22. Atallah, B.V., Bruns, W., Carandini, M. & Scanziani, M. Parvalbumin-expressing interneurons linearly transform cortical responses to visual stimuli. *Neuron* **73**, 159–170 (2012).
23. Nunez, P.L. & Srinivasan, R. *Electric Fields of the Brain: The Neurophysics of EEG* 2nd edn. (Oxford Univ. Press, 2006).
24. Magee, J.C. Dendritic integration of excitatory synaptic input. *Nat. Rev. Neurosci.* **1**, 181–190 (2000).
25. Vaidya, S.P. & Johnston, D. Temporal synchrony and gamma-to-theta power conversion in the dendrites of CA1 pyramidal neurons. *Nat. Neurosci.* **16**, 1812–1820 (2013).
26. Steenland, H.W., Li, X.Y. & Zhuo, M. Predicting aversive events and terminating fear in the mouse anterior cingulate cortex during trace fear conditioning. *J. Neurosci.* **32**, 1082–1095 (2012).
27. Goshen, I. *et al.* Dynamics of retrieval strategies for remote memories. *Cell* **147**, 678–689 (2011).
28. Ito, J. *et al.* Whisker barrel cortex delta oscillations and gamma power in the awake mouse are linked to respiration. *Nat. Commun.* **5**, 3572 (2014).
29. Fujisawa, S. & Buzsáki, G. A 4 Hz oscillation adaptively synchronizes prefrontal, VTA, and hippocampal activities. *Neuron* **72**, 153–165 (2011).

ONLINE METHODS

Animals. Naive male C57BL6/J mice (3 months old, Janvier) and PV-IRES-Cre mice (3 months old, Jackson Laboratory, B6;129P2-*Pvalb*$^{tm1(cre)Arbr}$/J) were individually housed for at least 7 d before all experiments, under a 12-h light–dark cycle, and provided with food and water *ad libitum*. Experiments were performed during the light phase. All procedures were performed in accordance with standard ethical guidelines (European Communities Directive 86/60-EEC) and were approved by the committee on Animal Health and Care of Institut National de la Santé et de la Recherche Médicale and French Ministry of Agriculture and Forestry (authorization A3312001).

Behavior. Auditory fear conditioning and testing took place in two different contexts (context A and B). The conditioning and testing boxes were cleaned with 70% ethanol and 1% acetic acid before and after each session, respectively. To score freezing behavior independently of the experimenter, an automated infrared beam detection system located on the bottom of the experimental chambers was used (Coulbourn Instruments). Because the detection of our dependent variable (freezing) was independent of the experimenter, we did not use a blinding process for group allocation or behavior scoring. The animals were considered to be freezing if no movement was detected for 2 s. On day 1, C57BL6/J mice were subjected to a habituation session in context A, in which they received four presentations of the CS$^+$ and of the CS$^-$ (total CS duration, 30 s; consisting of 50-ms pips at 0.9 Hz repeated 27 times, 2 ms rise and fall, pip frequency, 7.5 kHz, or white-noise, 80 dB sound pressure level).

Discriminative fear conditioning was performed on the same day by pairing the CS$^+$ with a US (1 s foot-shock, 0.6 mA, 5 CS$^+$–US pairings, inter-trial intervals 20–180 s). The onset of the US coincided with the offset of the CS$^+$. The CS$^-$ was presented after each CS$^+$–US association but was never reinforced (five CS$^-$ presentations; inter-trial intervals, 20–180 s). The frequencies used for CS$^+$ and CS$^-$ were counterbalanced across animals and randomization of CS$^-$ and CS$^+$ allocation was performed using an online randomization algorithm (http://www.randomization.com/).

On day 2, conditioned mice were submitted to a testing session (retrieval session) in context B during which they received 4 and 12 presentations of the CS$^-$ and CS$^+$, respectively. Thirteen naive C57BL6/J mice recorded simultaneously in the dmPFC and BLA were included in this experiment and the data collected in two distinct replicates. Five additional naive C57BL6/J mice recorded in the vlPAG were fear conditioned using the same protocol. Contextual fear conditioning took place in contexts A and B as describe above. On day 1, C57BL6/J mice were subjected for 5 min to a habituation session in context A. Contextual fear conditioning was performed 24 h later by pairing context B with a US. The next day, mice were subjected for 12 min to a testing session (retrieval) in context B. Six naive C57BL6/J mice were included in this experiment and the data collected in two distinct replicates. For neck muscle EMG recordings, C57BL6/J mice were exposed to 20 CS$^+$ presentations in context B as describe above and auditory fear conditioning was performed on the same day by pairing the CS$^+$ with a US. Seven naive C57BL6/J mice were included in this experiment and the data collected in two distinct replicates.

For optogenetic experiments using channelrhodopsin, PV-IRES-Cre mice and GPF controls were exposed on day 1 to context A as described above. During the session, four blue-light 4-Hz rhythmic analog (2 or 10 mW, 30 s) stimulations were delivered in the dmPFC to activate parvalbumin-expressing interneurons. On days 2 and 3, mice were exposed to the same context as day 1 or to the neutral context B as described above, without any stimulation, respectively. To test for the frequency and structure specificity of the stimulation, other groups of naive PV-IRES-Cre mice were submitted to four blue-light rhythmic analog dmPFC stimulations at different frequencies (1, 8, 10 and 12 Hz, stochastic 4 Hz composed of 2–12 Hz frequency with an average at 4 Hz, 10 mW, 30 s, $n = 6$ mice) or to four blue-light rhythmic analog stimulations at 4 Hz of the motor cortex ($n = 4$ mice) or the BLA ($n = 5$ mice). These five mice infected in the BLA were also submitted to auditory fear conditioning as described above and tested 24 and 48 h later to evaluate the effect of BLA silencing during fear behavior. Randomization of group allocation (ChR2 versus GFP controls) was performed using an online randomization algorithm (http://www.randomization.com/).

For pharmacological experiments, C57BL6/J mice were submitted to a fear conditioning paradigm consisting of CS$^+$ and US pairings in context A as described above. On days 2, 3 and 4, conditioned mice were tested in context B, during which they received four presentations of the CS$^+$ before muscimol injections (day 2, test 1), 5 min after muscimol injections (day 3, Inac.) and 24 h after muscimol injections (day 4, test 2). Six naive C57BL6/J mice were included in this experiment and the data collected in two distinct replicates.

Surgery and recordings. Mice were anaesthetized with isoflurane (induction 3%, maintenance 1.5%) in O_2. Body temperature was maintained at 37 °C with a temperature controller system (FHC). Mice were secured in a stereotaxic frame and unilaterally implanted in the left dorsomedial prefrontal cortex (dmPFC) with a multi-wire electrode array aimed at the following coordinates: 2.0 mm anterior to the bregma, 0.3 mm lateral to the midline and 0.8 to 1.4 mm ventral to the cortical surface. They were implanted in the left basolateral amygdala (BLA) with a multi-wire electrode array aimed at the following coordinates: 1.7 mm posterior to the bregma, 3 mm lateral to the midline and 4 mm ventral to the cortical surface.

Another group of mice was implanted only in the ventrolateral periaqueductal gray at the following coordinates: −4.30 mm anterior to the bregma, 0.55 mm lateral to the midline and 2.20 mm ventral to the cortical surface. For contextual fear conditioning experiments, mice were implanted only in the dmPFC. For electromyographic (EMG) recording experiments, Teflon-coated stainless steel electrodes (AM Systems) were sutured into the right and left nuchal muscles. Wires were connected to a multi-wire electrode array connector attached to the skull.

For pharmacological experiments, animals were implanted in the dmPFC at the same coordinate as above and in dorsal hippocampus at the following coordinates: 2 mm posterior to bregma, 1.2 mm lateral to midline and 1.2 to 1.4 mm ventral to the cortical surface. The electrodes consisted of 16 individually insulated nichrome wires (13 µm inner diameter, impedance 30–100 KΩ; Kanthal) contained in a 26-gauge stainless steel guide cannula. The wires were attached to an 18-pin connector (Omnetics) and two connectors were used for each mouse. All implants were secured using Super-Bond cement (Sun Medical). After surgery, mice were allowed to recover for 7 d and were habituated to handling. Analgesia was applied before and 1 d after surgery (Metacam, Boehringer). Electrodes were connected to a headstage (Plexon) containing 16 unity-gain operational amplifiers. The headstage was connected to a 16-channel preamplifier (gain 100×, bandpass filter from 150 Hz to 9 kHz for unit activity; Plexon). Spiking activity was digitized at 40 kHz and bandpass filtered from 250 Hz to 8 kHz, and isolated by time-amplitude window discrimination and template matching using a Multichannel Acquisition Processor system (Plexon). At the conclusion of the experiment, recording sites were marked with electrolytic lesions before perfusion, and electrode tip locations were reconstructed with standard histological techniques.

Single-unit analyses. Single-unit spike sorting was performed using Off-Line Spike Sorter (OFSS, Plexon) for all behavioral sessions. Principal component scores were calculated for unsorted waveforms and plotted in a three-dimensional principal component space; clusters containing similar valid waveforms were manually defined. A group of waveforms were considered to be generated from a single neuron if the waveforms formed a discrete, isolated cluster in the principal component space and did not contain a refractory period less than 1 ms, as assessed using autocorrelogram analyses. To avoid analysis of the same neuron recorded on different channels, we computed cross-correlation histograms. If a target neuron presented a peak of activity at a time that the reference neuron fired, only one of the two neurons was considered for further analysis.

To separate putative inhibitory interneurons from putative excitatory principal neurons, we used an unsupervised clustering algorithm based on Ward's method. In brief, the Euclidian distance was calculated between all neuron pairs on the basis of the three-dimensional space defined by each neuron's average half-spike width (measured from trough to peak), the firing rate and the area under the hyperpolarization phase of the spike. An iterative agglomerative procedure was then used to combine neurons into groups based on the matrix of distances such that the total number of groups was reduced to give the smallest possible increase in within-group sum of squares deviation.

For the detection of interactions between units recorded in the dmPFC and BLA, the spike trains of each simultaneously recorded pair were binned (10 ms bin size), the cross-correlation of the binned histograms was calculated over multiple lags (maximum lag, ± 500 ms) and the peak cross-correlation coefficient for each pair was determined. For the detection of co-firing property for unit pairs,

spike trains were binned as before and the co-firing index was calculated as the ratio of co-occurring (common) spikes to the total number of spikes for the two units. This provides a simple yet direct measure of the co-occurrence of unit spikes on multiple levels of temporal resolution. For the determination of the bin size and the robustness of the method, different bin sizes were tested; they all gave qualitatively similar results. Among those tested, 10 ms was selected because it allows the identification of potentially monosynaptic interactions. To evaluate whether neurons were oscillating at 4 Hz, we used Gabor functions, which are commonly used to fit autocorrelation (AC) histograms of nonstationary rhythmic biological time series such as neuronal spiking activity[30–32]. Gabor functions are damped sine waves with two components: first, the sine wave frequency (f_o); second, a damping frequency (f_d) that modulates the amplitude of the sine wave. The Gabor functions served as a predicted AC (pAC) that was used to fit the actual AC of the frequencies of interest. We constructed a set of Gabor functions as follows[32]:

$$\mathrm{pAC}_{\mathrm{fofd}} = \cos\left(2\pi x f_o\right) \times \exp\left(Cx^2 f_d\right)$$

with f_o and f_d both ranging from 1 to 25 Hz, hence creating 100 × 100 predicted ACs. The quality of the fit of each predicted AC was then assessed by its correlation (Spearman's ρ) with the actual AC of specific frequency bands (calculated for lags t of 0–500 ms), and this correlation score was plotted for each f_0, f_d pair. Points showing the highest correlation thus represent candidate f_0, f_d pairs capable of predicting oscillations.

Local field potential and EMG analyses. Local field potentials were analyzed using custom-written Matlab programs. Raw LFP traces were filtered between 0.7 Hz and 400 Hz and downsampled to 1 kHz. All signals were filtered using zero-phase-distortion sixth-order Butterworth filters. For phase analyses, the signal was filtered in the desired frequency band (2–6 Hz for the 4-Hz oscillation) and the complex-valued analytic signal was calculated using the Hilbert transform as below.

$$\rho(t)e^{-i\varphi(t)}$$

The vector length and the arctangent of the vector angle provide the estimation of the instantaneous amplitude and instantaneous phase of the signal, respectively, at every time point. All analyses were performed during freezing episodes and, where indicated, during subsampled non-freezing epochs. A phase of 0° corresponds to the peak of prefrontal–amygdala oscillations. LFP power spectrum and LFP–LFP coherence estimations were, unless otherwise noted, performed using the multitaper method[33]. Briefly, data were multiplied by a set of 2–5 orthogonal taper functions (discrete prolate spheroidal sequences), Fourier transformed using a window size of 2 s and averaged to obtain a direct multitaper spectral estimate.

Signal to noise ratio (SNR) for 4-Hz power was calculated as the ratio of the mean power in the 2–6 Hz band to the mean power outside this band. Because one mouse did not show immobility behavior during habituation, it was excluded from SNR analyses. For coherence analyses, a method based on imaginary coherence was employed[34]. Imaginary coherence was calculated as

$$\mathrm{iCoh} = \frac{\left|\mathrm{Im}\left(\sum_{\mathrm{bins}} S_{xy}\right)\right|}{\sqrt{\sum_{\mathrm{bins}} S_{xx} \times \sum_{\mathrm{bins}} S_{yy}}}$$

where S_{xy} is the cross-spectrum, S_{xx} and S_{yy} are the auto-spectra and summation takes place over the spectrogram bins corresponding to the quantified state. By keeping the imaginary part of the normalized cross-spectrum, coherence value is weighted inversely proportionally to the time lag between the two signals. Consequently, it is sensitive only to time-lagged signals, whereas the effect of absolutely synchronous signals is eliminated. Given the very synchronous nature of the oscillation examined here and the small phase lag, imaginary coherence is expected to underestimate the strength of the interaction. However, we opted for this conservative variety of coherence analysis to avoid any influence of volume-conducted currents or artifacts that can artificially boost coherence values.

To investigate any potential causal interaction between the oscillations recorded in the two structures, spectrally resolved Granger causality was calculated for the unfiltered LFP signals. Granger causality is a statistical measure of the predictive power of one variable over another. Linear trends were removed from the LFP signals and signals were normalized before the analysis. For these analyses, the MVGC multivariate Granger causality toolbox[35] was used to fit a higher order vector autoregressive model to the processes. Data were tested for stability in time and model order was determined using the Akaike information criterion. To identify directionality and quantify the lag between the two signals in terms of phase and amplitude, a point process was defined consisting of the peaks of the bandpass-filtered LFP signal for each of the two structures. The lag of the peak of the cross-correlation of these point processes identifies the time lag of the oscillation in the two structures and the directionality of their potential interaction. To avoid any potential bias due to phase asymmetry, the same procedure was tested for the troughs, giving identical results. To investigate this relationship throughout the oscillation cycle, the phase of each analytical signal was extracted using the Hilbert transform and the distribution of the phase differences between the two structures was characterized for deviation from uniformity using circular statistics and Monte Carlo simulations. To evaluate the specific role of phase, amplitude and their interplay on the directionality and causality measures for the LFP data, a procedure was devised for the selective perturbation of phase and amplitude of the signals. Signals were converted in the spectral domain using a discrete Fourier transform and the phase (or amplitude) component of the signal was permuted, leaving the amplitude (or phase) intact. The modified signal was converted back to the time domain using the inverse Fourier transform. For the power comodulation analysis, the power profile for each frequency bin in each structure was calculated and the correlation coefficient of every pair was calculated[36].

To compare the impact of CS^+ during freezing on local theta and 4-Hz phase resetting, we used a multitaper analysis of LFP signals for frequencies ranging from 2 to 12 Hz and computed a stimulus-triggered spectrogram. For the CS^+-triggered theta and 4-Hz phase overlays, signals were filtered in the corresponding range (theta, 8–12 Hz; 4-Hz, 2–6 Hz) and phases were extracted from the analytic signal as described above. To quantify phase stability across all CS^+ pips during freezing episodes, we calculated the mean resultant length for all time–frequency pairs. To evaluate the predictive value of 4-Hz power for freezing behavior, we used wavelet analysis, which in some instances allows a higher temporal resolution, to quantify the spectral content of the signal for frequencies between 2 and 12 Hz and computed freezing-triggered spectrograms. To evaluate the latency to freeze in response to the CS^+, individual tone onsets and freezing period onsets for individual mice were binned (100 ms bin size), smoothed and averaged, and cross-correlation analysis was performed on these data taking freezing onset epochs as the reference event (**Fig. 1e**). In these conditions, negative lags indicate that conditioned stimuli precede freezing events. Statistical significance was evaluated using two different approaches and then combined. We first simulated 1,000 instances of a uniform distribution of freezing episodes and recomputed the cross-correlation analysis. We next shuffled 1,000 times the freezing ISIs of the actual freezing episodes to preserve the first-order statistics of freezing behavior but perturb its relation to CS^+ and recomputed the cross-correlation analysis. The results of the two analyses were averaged to produce a more robust significance threshold. However, each individual result was not qualitatively and quantitatively different from the final average. One interesting characteristic of the cross-correlation is its oscillatory nature, which is due to the rhythmic repetition of CS^+ (27 pips delivered at 1.1 Hz) and the tendency of elicited freezing to occur in response to these events (**Fig. 1e**).

For correlation analyses between freezing behavior and 4-Hz oscillations (**Fig. 3d** and **Supplementary Fig. 2e**), we first evaluated the percentage of time individual animals spent frozen during the entire recording session. For 4-Hz quantification, 4-Hz oscillation periods were evaluated as periods of significant 4-Hz SNR, as compared to baseline (a 2-min period before the first CS presentation). 4 Hz expressed as the percentage of total time corresponds to the ratio of the total duration of 4-Hz episodes to the recording session duration. For electromyographic recordings, unilateral EMG signals were band-pass filtered (100–1,000 Hz), rectified and integrated (convolution with 100-ms Gaussian kernel). The ΔEMG signal was calculated as the differential EMG recorded in the left and right nuchal muscle[37]. The absolute value of ΔEMG was then Z-score transformed and averaged around freezing onsets (−500 ms to 500 ms) occurring during CS^+ presentation, during both habituation and fear conditioning.

doi:10.1038/nn.4251

Phase-locking analyses. For phase modulation analysis, the variance-stabilized ln(Z) ($Z = R^2/n$, R being the resultant length and n the sample size) statistics for the Rayleigh test for uniformity against the von Mises distribution were calculated[38,39]. To partially account for the sample size bias of the resultant length, only units with at least 100 spikes during freezing behavior were taken into consideration. All results were corroborated using the pairwise phase consistency method, a bias-free estimate of neuronal synchronization based on the average pairwise circular distance

$$D = \frac{2}{N(N-1)} \sum_{i=1}^{N-1} \sum_{j=(i+1)}^{N} \left| \theta_i - \theta_j \right| \bmod \pi$$

with θ_i and θ_j being the phases from two different spikes. This method is analytically equivalent to the squared phase-locking value[40]. To calculate the statistics for each unit, bootstrap analyses and Monte Carlo simulations were performed. In the Monte Carlo simulations, the Y_{sim} value, indicating the expected value for a uniform prior distribution, was calculated for each sample size. Units for which the Y_{unit} exceeded the 95% percentile of the simulated Y_{sim} estimate were considered phase-locked. For the bootstrap statistics, in order to take into account the higher-order statistics of the spike trains, for each unit the inter-spike intervals were shuffled randomly and the potentially nonuniform prior distribution was calculated.

Phases for both dmPFC and BLA spikes were extracted using the dmPFC 4-Hz oscillation phase that exhibits the highest SNR and allows direct comparison of the phase-locking statistics. For the statistical evaluations, before the phase extraction, the prior distribution of phases of the 4-Hz oscillation was examined, and, as is the case for other neuronal slow oscillations, this prior distribution deviated from the uniform distribution. This bias can alter the phase-locking statistics and produce false positives[38,39]. To account for this potential bias, the phases of the LFPs were transformed using the inverse of the empirical cumulative density function to return a signal with uniform prior distribution. Following this transformation, the spike phases were drawn from a uniform distribution, allowing the application of circular statistics for detecting deviations from uniformity. For normalized averaged phase density analyses, the circular histogram for each neuron was normalized to the maximum and the averaged circular histogram was computed.

Supervised learning algorithms. To establish the predictive value of dmPFC and BLA 4-Hz oscillations for the animal's behavioral state ("freezing" or "not freezing"), we used two distinct machine learning approaches. Specifically, we used the 4-Hz signal-to-noise ratio (SNR) of the two structures as features to train a naive Bayes classifier and a support vector machine (SVM). On the basis of the time-resolved spectral decomposition of the signals (spectrograms), we calculated the mean 4-Hz SNR across three consecutive time bins (with a bin size of 150 ms) and assigned a binary value based on the behavioral state of the animal during the corresponding time (450 ms: freezing = 1; mobility = 0). Each formed SNR–binary value pair constitutes a single data point used as an input to the classifier.

For this analysis, we considered the total duration of the recordings; that is, all time bins were used in this analysis. SVM projects data into a higher dimensional space and estimates a hyperplane that best separates the data points belonging to distinct classes[41]. Naive Bayes classifiers assume independence of the probability distributions of the features and classify the test data on the basis of the maximal posterior probability of class assignment[42]. The data set was randomly split into a training data set containing 70% of the data points, which was used to train the classifiers, and a test data set containing the remaining 30% of data points, that was used to test the accuracy of the algorithms. To estimate the stability of the algorithms and confidence intervals of the accuracy and receiver operating characteristics (ROC) curves of the classifiers, we implemented a Monte Carlo procedure whereby the data set was randomly split 1,000 times in mutually exclusive training and test data sets and the algorithms were trained and tested on the respective data sets. The accuracy, defined as

$$\text{accuracy} = \frac{\text{number of true positives} + \text{number of true negatives}}{\text{number of datapoints}}$$

and the area under the curve (AUC) of the ROC curve were used to characterize the performance of the classifiers and were compared with the same algorithms trained on shuffled data using the exact same Monte Carlo procedure.

Statistical analyses. For each statistical analysis provided in the manuscript, the Kolmogorov–Smirnov normality test was first performed on the data to determine whether parametric or non-parametric tests were required. When multiple statistical tests were performed, Bonferroni corrections were applied. Two different approaches were used to calculate the sample size. For studies in which we had sufficient information on response variables, power analyses were carried out to determine the number of mice needed. For studies in which the behavioral effect of the manipulation could not be prespecified, such as optogenetic experiments, we used a sequential stopping rule (SSR). In essence, this method enables null-hypothesis tests to be used in sequential stages by analyzing the data at several experimental points using t-tests. Usually the experiment started by testing only a few animals, and if the P value was below 0.05, the investigator declared the effect significant and stopped testing. If the P value was greater than 0.36, the investigator stopped the experiment and retained the null hypothesis.

For sample-size estimation using power analyses, we used a power analysis calculator (G*Power3). For each analysis, sample size was determined using a power >0.9 and α error = 0.05. All tests were two-sided. Power analyses were computed for matched pairs (cued and contextual fear conditioning protocol (**Fig. 1** and **Supplementary Fig. 4**) and pharmacological experiments (**Supplementary Fig. 5**)). In our behavioral experiments, a critical parameter is freezing percentage, and the numerical endpoint typically ranged between 50% and 70% freezing for CS^+ presentations immediately following auditory fear conditioning and between 10% and 30% freezing for CS^- presentations. A minimum biologically significant difference in the mean values between CS^- and CS^+ conditions for cued fear conditioning (**Fig. 1**) or between habituation and test sessions for contextual fear conditioning (**Supplementary Fig. 4**) is 1.5-fold. If we assume a s.d. of 1.5 for a mean value of 60% freezing for CS^+ test session and 20% freezing for CS^- habituation (which are realistic numbers), then a minimum $n = 6$ is needed to reject the null hypothesis with 90% probability. Sample size determination using SSR analyses was used for optogenetic experiments, in which it was not possible to determine a priori the effect of the optical manipulation. We used P values of 0.05 and 0.36 for the lower and upper criteria.

Muscimol inactivation. Mice were unilaterally implanted with a stainless steel guide cannula (26 gauge; Plastics One) aimed at the medial septum using an angle of 10° and recording electrodes were implanted in the dmPFC and the dorsal hippocampus as described in the section "Surgery and recordings.". To target the medial septum, we used the following coordinates: 1 mm anterior to bregma; 0.7 mm lateral to midline and 3.0 to 3.3 mm ventral to the cortical surface with an angle of 10° in the coronal plane. The cannula was secured using Super-Bond cement (Sun Medical). On the injection day, muscimol (muscimol-bodipy-TMR-X conjugate, Invitrogen; 0.8 mM in PBS 0.1 M) was infused at a rate of 0.2 µL/min over 2 min (total volume of 0.4 µL). On the injection day, muscimol was infused 15 min before the behavioral test. After the end of the experiment, muscimol was again infused with the same parameters to control for drug diffusion in the medial septum and mice were perfused. Brains were collected for histological analyses as described below.

Anatomical analysis. Mice were euthanized with isoflurane and perfused through the left ventricle with 4% w/v paraformaldehyde (PFA) in 0.1 M PBS. Brains were dissected out and postfixed for 24 h at 4 °C in the same solution. 60-µm-thick sections were cut, mounted on gelatin-coated microscope slides and dried. Sections were stained with toluidine blue, dehydrated and mounted. Electrolytic lesions were identified with conventional transmission light microscopy. Only recordings with confirmed lesions in cingulate or prelimbic areas of dmPFC and basolateral amygdala (BLA) were included in our analyses. For verification of muscimol injections in the medial septum and viral injections in dmPFC, BLA or motor cortex, serial 80-µm-thick slices were imaged using an epifluorescence system (Leica DM 5000) fitted with a 10× dry objective. The location and the extent of the injections or infections were visually controlled. All included muscimol injections were targeted and limited to the medial septum. Similarly, only infections accurately targeting the region of interest were considered for behavioral and electrophysiological analyses.

Virus injections and optogenetics. For optical identification of parvalbumin-expressing interneurons, conditional AAV encoding ChR2 (AAV-EF1a-DIO-hChR2(H134R)-EYFP, serotype 5, Vector Core, University of North Carolina)

or ArchT (AAV-FLEX-ArchT-GFP, serotype 5, Vector Core, University of North Carolina) were bilaterally injected into the dmPFC of PV-IRES-Cre mice ($n = 12$ mice) from glass pipettes (tip diameter 10–20 µm) connected to a Picospritzer (Parker Hannifin Corporation; approximately 0.4 µL per hemisphere) at the following coordinates: dmPFC: 2.0 mm anterior to bregma, 0.4 mm lateral to midline and 0.9 to 1.2 mm ventral to the cortical surface. One to 2 weeks after the injection, mice were implanted bilaterally with optic fibers (diameter, 200 µm; numerical aperture, 0.37; flat tip; Doric Lenses) at the same coordinates. All implants were secured using Super-Bond cement (Sun Medical). For experiments using optogenetic stimulation coupled to single-unit and LFP recordings, one of the two optic fibers was combined to the array of 16 or 32 individually insulated nichrome wires. Single-unit recordings during the manipulation of PV interneurons were performed as described in the section "Surgery and recordings."

Behavioral and recording experiments were performed 3–5 weeks after injection. The light (approximately 2 or 10 mW per implanted fiber) was bilaterally conducted from the laser (OptoDuet 473/593 nm, Ikecool) to the mouse via two fiber-optic patch cords (diameter, 200 µm, Doric Lenses) connected to a rotary joint (1 × 2 fiber-optic rotary joint, Doric Lenses) that allowed mice to freely move in the behavioral apparatus. For optical control of parvalbumin-expressing interneurons, conditional AAV encoding ChR2 (AAV-EF1a-DIO-hChR2(H134R)-EYFP, serotype 5, Vector Core, University of North Carolina) was bilaterally injected into the dmPFC or the BLA at the same coordinates as above or into the motor cortex of PV-IRES-Cre mice at the following coordinates: 2.0 mm anterior to bregma, 1.5 mm lateral to midline and 1.3 mm ventral to the cortical surface. Control experiments were performed using an AAV containing the DNA construct for GFP alone (AAV-FLEX-GFP, Vector Core, University of North Carolina).

For optogenetic manipulation of PV interneurons during behavior, we used a 30-s analog dmPFC stimulation delivered at 1, 4, 8, 10 or 12 Hz. As a control we also used a stochastic 4-Hz analog dmPFC stimulation generated by an oscillator with a randomly time-modulated frequency drawn from a Gaussian distribution centered on 4 Hz. The power spectrum of the signal displayed a broad peak around 4 Hz, but the duration of each cycle varied randomly from 0.15 to 0.6 s, thereby destroying the regularity of the population activity. For motor cortex experiments, we used a 4-Hz analog stimulation. For BLA silencing experiments, a continuous pulse of blue light was applied during CS^+ presentations 24 h after fear conditioning. After behavioral and recording experiments, mice were perfused and histological analysis was performed.

A **Supplementary Methods Checklist** is available.

30. Engel, A.K., König, P., Gray, C.M. & Singer, W. Stimulus-dependent neuronal oscillations in cat visual cortex: inter-columnar interaction as determined by cross-correlation analysis. *Eur. J. Neurosci.* **2**, 588–606 (1990).
31. Gray, C.M., König, P., Engel, A.K. & Singer, W. Oscillatory responses in cat visual cortex exhibit inter-columnar synchronization which reflects global stimulus properties. *Nature* **338**, 334–337 (1989).
32. Young, M.P., Tanaka, K. & Yamane, S. On oscillating neuronal responses in the visual cortex of the monkey. *J. Neurophysiol.* **67**, 1464–1474 (1992).
33. Mitra, P.P. & Pesaran, B. Analysis of dynamic brain imaging data. *Biophys. J.* **76**, 691–708 (1999).
34. Nolte, G. *et al.* Identifying true brain interaction from EEG data using the imaginary part of coherency. *Clin. Neurophysiol.* **115**, 2292–2307 (2004).
35. Barnett, L. & Seth, A.K. The MVGC multivariate Granger causality toolbox: a new approach to Granger-causal inference. *J. Neurosci. Methods* **223**, 50–68 (2014).
36. Buzsáki, G. *et al.* Hippocampal network patterns of activity in the mouse. *Neuroscience* **116**, 201–211 (2003).
37. Steenland, H.W. & Zhuo, M. Neck electromyography is an effective measure of fear behavior. *J. Neurosci. Methods* **177**, 355–360 (2009).
38. Siapas, A.G., Lubenov, E.V. & Wilson, M.A. Prefrontal phase locking to hippocampal theta oscillations. *Neuron* **46**, 141–151 (2005).
39. Sirota, A. *et al.* Entrainment of neocortical neurons and gamma oscillations by the hippocampal theta rhythm. *Neuron* **60**, 683–697 (2008).
40. Vinck, M., van Wingerden, M., Womelsdorf, T., Fries, P. & Pennartz, C.M. The pairwise phase consistency: a bias-free measure of rhythmic neuronal synchronization. *Neuroimage* **51**, 112–122 (2010).
41. Cortes, C. & Vapnik, V. Support-vector networks. *Mach. Learn.* **20**, 273–297 (1995).
42. Bishop, C.M. *Pattern Recognition and Machine Learning* (eds. Jordan, M., Kleinberg J. & Schölkopf, B.) (Springer, 2006).

doi:10.1038/nn.4251

Résumé prolongé

La peur, une réaction permettant à un organisme de s'adapter à son environnement, est présente chez un grand nombre d'espèces allant des invertébrés jusqu'aux mammifères. La peur est une réaction transitoire qui s'arrête dès que la menace est éliminée et doit ainsi être distinguée de l'anxiété qui elle persiste même en l'absence de toute menace. L'un des modèles les plus utilisés au laboratoire pour l'étude des réponses de peur est le rongeur et plus spécifiquement la souris. La peur est définie comme étant une réaction transitoire face à un danger imminent et peut se manifester sous différentes formes en fonction de plusieurs facteurs environnementaux notamment la proximité du danger et la présence ou non d'une voie d'échappement de la menace. Ainsi une souris face à un danger exprime une réponse d'immobilisation totale excepté les mouvements liés à la respiration (réponse de freezing), une réponse d'évitement permettant d'esquiver toute confrontation avec le danger ou une réponse de confrontation physique au danger. De ce fait, une des questions essentielles adressée en neurosciences consiste à identifier les structures et circuits neuronaux impliqués dans l'acquisition et l'expression du freezing et/ou de l'évitement de peur. Des recherches précédentes ont démontrés que la réponse de peur freezing qualifiée comme passive ainsi que la réponse active d'évitement de peur engagent toute les deux trois structures cérébrales principales : le cortex préfrontal médian (mPFC), l'amygdale ainsi que la substance grise périaqueducale. De ce fait, les circuits neuronaux qui sous-tendent les différentes phases d'acquisition, d'expression et d'extinction de freezing sont maintenant bien connus. Cependant, les circuits neuronaux qui interviennent dans l'acquisition et l'expression de la réponse d'évitement restent controversés. En effet, en fonction de la tâche comportementale utilisée différentes sous-régions du mPFC semblent être impliquées. Des chercheurs utilisant une tâche d'évitement actif d'un son aversif (Bravo-Rivera, et al., 2014 ; Diehl, et al., 2018) par la fuite vers une plateforme ont démontré que le cortex préfrontal dorso-médian (dmPFC) est engagé lors de l'expression de la réponse d'évitement de peur. Alors que d'autres recherches (Moscarello and LeDoux, 2013 ; LeDoux, 2017) ont démontré que l'évitement actif d'un son aversif est accompagné d'une activation du cortex préfrontal ventro-médian (vmPFC).

Ainsi l'objectif de ma thèse consiste à déterminer la/les sous-région(s) du cortex préfrontal médian (mPFC) impliqué dans l'expression des réponses passive (freezing) et active (évitement) de peur ainsi que d'identifier l'implication de projections entre le cortex préfrontal médian et la substance grise périaqueducale dans l'acquisition et l'expression des réponses de freezing et d'évitement de peur.

Dans le but d'adresser ces questions, dans un premier temps, nous avons développé au laboratoire une tâche comportementale pendant laquelle une souris exprime un comportement actif de peur: l'évitement ou un comportement passif: le freezing en fonction du contexte. Les souris sont entrainées à associer un son (CS^+ : Stimulus Conditionnel aversif) à un stimulus aversif (US : Stimulus Inconditionnel ; un choc électrique de faible intensité) dans une ‘'shuttle-box ‘' : boite à 2 compartiments identiques séparés par une porte ; lors de l'ouverture de la porte entre les 2 compartiments le comportement d'évitement est rendu possible. Un second son neutre (CS^-: Stimulus Conditionnel neutre) est utilisé en tant que control interne. En fonction de leur taux de freezing et d'évitement 2 groupes de souris sont identifiés : -«Good avoiders» : présentent des taux élevés de freezing en condition porte fermée, et des taux élevés d'évitement en condition porte ouverte ainsi qu'une bonne discrimination entre le CS^+ et le CS^-.
–«Bad avoiders» : présentent des taux élevés de freezing en condition porte fermée mais n'évitent pas lors de l'ouverture de la porte séparant les 2 compartiments de la shuttle-box. Ces souris discriminent aussi les 2 sons en terme de comportement de freezing.

Les «Bad avoiders» ne montrent pas de différence concernant le temps d'immobilité comparés aux «Good avoiders» dans un test de nage forcée, utilisé comme un test comportemental pour identifier des phénotypes de dépression chez les rongeurs. Ainsi le manque d'évitement chez les «Bad avoiders» ne serait pas lié à un phénotype de dépression chez les «Bad avoiders».

Dans un second temps, nous avons utilisé un marqueur d'activation neuronale, la protéine c-Fos, codée par un gène à expression précoce immédiate. L'expression de la protéine c-Fos étant directement corrélée à l'expression d'un comportement tel que le freezing ou l'évitement, nous avons constaté que l'évitement est associé à une augmentation de l'expression de la protéine c-Fos dans le dmPFC ainsi que

dans la région dorso-latérale de la substance grise périaqueducale (dlPAG) chez les «Good avoiders». Ainsi, nous avons déterminé que dans notre tâche comportementale l'expression du comportement d'évitement de peur est corrélée avec une activation du dmPFC et du dlPAG.

Par la suite, des enregistrements extracellulaires des neurones du cortex préfrontal dorso-médian (dmPFC) au cours de la tâche comportementale ont abouti à l'identification de 2 populations neuronales principales : une population de neurones excités (21%) ainsi qu'une population de neurones inhibés (25%) pendant le comportement d'évitement. La majorité des neurones activés pendant l'évitement ne sont pas modulés par le comportement de freezing alors que la moitié des neurones inhibés pendant l'évitement sont aussi freezing activés. Pour déterminer laquelle de ces populations neuronales projette du cortex préfrontal vers la substance grise périaqueducale (PAG), structure essentielle dans l'encodage du comportement d'évitement comme démontré avec l'étude c-Fos, des stimulations antidromiques dans le dorso-latéral PAG (dlPAG) ont été réalisées au cours des enregistrements extracellulaires dans le dmPFC. Nos résultats indiquent que les neurones du dmPFC activés pendant l'évitement et ne répondant pas électrophysiologiquement pendant le freezing projettent vers le dlPAG. L'augmentation de l'activité de cette population de neurones projettant du dmPFC vers le dlPAG au cours de l'évitement n'est corrélée avec l'augmentation de la vitesse de l'animal. Ainsi la modulation de l'activité des neurones projetant du dmPFC vers le dlPAG pendant l'évitement n'est pas liée à la modification de la locomotion.

Des manipulations optogénétiques de la voie dmPFC vers le dorso-latéral ainsi que latéral PAG dl/lPAG ont permis de déterminer que l'inhibition de cette voie empêche l'acquisition mais pas l'expression des réponses d'évitement de peur. Ainsi moyennant l'optogénétique nous avons démontré que la voie projetant du dmPFC vers le dl/lPAG est nécessaire pour l'acquisition des réponses d'évitement de peur. De plus, l'activation optogénétique de la voie dmPFC-dl/lPAG chez les «Bad avoiders» induit un comportement d'évitement du CS^+ mais pas du CS^-. Ceci indique que l'activation de la voie dmPFC-dl/lPAG est suffisante pour l'acquisition du comportement d'évitement de peur.

Finalement, nous avons utilisé des enregistrements de patch-clamp in-vitro nous permettant de démontrer que le passage d'un phénotype «Bad avoider» à un phénotype «Good avoider» est rendu possible grâce à une potentiation au niveau des synapses du dlPAG provenant du dmPFC. De plus, nos recherches ont permis de démontrer que ces synapses contactent aussi bien les cellules glutamatergiques que GABAergiques du dlPAG.

Dans leur ensemble ces résultats démontrent pour la première fois que la plasticité dépendante de l'activité des neurones du dmPFC projetant sur le dl/lPAG contrôle l'apprentissage de l'évitement de peur.